



The role of the planar cell polarity pathway in branching morphogenesis

A thesis presented for the degree of Doctor of Philosophy (D.Phil)
University of Oxford

Laura Yates

Mammalian Genetics Unit, Medical Research Council Harwell

Department of Biochemistry, University of Oxford

Supervisors: Dr. Charlotte Dean and Prof. Penny Handford

Michaelmas Term 2010

Abstract

The development of organs such as the lung and kidney occurs by branching morphogenesis. Changes in the cytoskeletal architecture, cell-cell adhesion and cell polarity are necessary for the formation of new branches. Interactions and reciprocal signalling between epithelial and mesenchymal cells mediate these organised cell movements that give rise to a complex system of tubes suitable for the transport of gas or fluids. Mutations that disrupt formation of either the correct number, or shape of epithelial branches, affect lung function. This, in turn, can lead to congenital abnormalities such as cystadenomatoid malformations, pulmonary hypertension or lung hypoplasia. Defects in lung architecture are also associated with adult lung disease, particularly in cases of idiopathic lung fibrosis. Identifying the signalling pathways that drive epithelial tube formation will likely shed light on both congenital and adult lung disease.

This study shows that mutations in the planar cell polarity (PCP) genes: Celsr1; Vangl2 and Scribble, lead to disrupted lung development and defects in lung architecture. Examination of Vangl2 mutant kidneys reveals similar impairment of branching morphogenesis. Detailed histological and immunocytochemical analysis reveals that lungs from *Celsr1*$^{Crsh/Crsh}$, *Vangl2*$^{Lp/Lp}$ and *Scribble*$^{Crc/Crc}$ mice are small and misshapen with fewer branches, and by late gestation exhibit thickened interstitial mesenchyme and defective saccular formation. Moreover, epithelial integrity is disrupted, cytoskeletal remodelling perturbed and mutant endoderm does not branch normally in response to the chemoattractant FGF10. In *ex-vivo* culture, inhibition of Rho kinase, an important downstream effector of the PCP signalling pathway, can mimic the branching defects observed in these three mouse mutants. Furthermore all three proteins are present in restricted spatial domains within lung epithelium. *Scribble*$^{Crc/Crc}$ lungs, the most severely affected line, exhibit additional defects in components of the tight and adherens junctions; this in turn affects lumen diameter.

These findings show that components of the PCP pathway: Celsr1; Vangl2 and Scribble are required for normal foetal lung development, thereby revealing a novel signalling pathway critical for this process.

Examination of postnatal mice was not possible as homozygous mutations result in embryonic lethality. However, an assessment of *Vangl2*$^{Lp/+}$ mice reveals that loss of a single copy of Vangl2 is enough to cause defects in embryonic lung development that persist into adult life, affecting lung function. Similarly, *Vangl2*$^{Lp/+}$ mice show a small but significant reduction in kidney glomeruli.

Acknowledgments

Firstly I would like to thank my supervisor Dr. Charlotte Dean for all her support and guidance throughout my time at MRC Harwell and for making my PhD experience both challenging but very enjoyable. I am grateful to Charlotte for reading my thesis so efficiently and would like to extend this to Dr. Andy Greenfield who in addition to reading sections of my thesis has been implemental in helping me secure a postdoc position in Australia. I would also like to thank my Oxford Supervisor Prof. Penny Handford for many helpful conversations over lunch at St. Catherine's college.

I would like to thank all the members of the developmental genetics lab who have provided useful advice and comments during lab meetings. In particular I would like to thank Jonathan Stevens for showing me the ropes when I first arrived and Paraskevi Goggliodou for being my unofficial postdoc and teaching me the basics of Real time PCR. I am also grateful to many other scientists within the core facilities at MRC Harwell, without whom this project would not have been possible. In particular Sara Wells, Jackie Harrision, Michelle Stewart and Liz Pears in the MLC; Debbie Williams in the microarray facility; Rosario Romero and Helen Hilton in Proteomics for the Westerns they have run for me. Thanks to Jim Humphreys, Kate Vowell and especially Dave Shipston in necropsy as well as everyone in histology who have provided protocols, advice and have spent many hours cutting sections for me, for which I am very grateful.

I would like to thank Caroline Formstone for use of her Celsr1 antibody and Mirelle Montcuoquiol for the use of her Vangl2 antibody. To Adrian Woolf, Jenny Papakrivopoulou and David Long for their expertise in kidney development and disease and for a very enjoyable and educational collaboration resulting in a successful publication in HMG.

My thanks goes to all the students who have been both supportive, helpful and for making the atmosphere in the student office a fun place to work. I would especially like to thank Chris Church, Octavio Espinosa and Laura Pastarelli for their friendship and support and for the many fun and eventful nights out! Working with both Fiona McMurray and Lauren Chessum in Charlotte's lab was a pleasure and I wish them both well with their current PhDs.

Lastly, but by no means least I would like to thank all my friends and family. In particular Joanne Safo, Francesca Lodej, Vicky Staples, Kiran laxman, Vicki Dyer and Fleur Mason, for making me laugh and keeping me sane throughout my PhD. I'd especially like to thank Laura Eccles for her friendship, her unending support and for the fun we've had over the past four years! I wish her all the best in her postodoc position in New York City! A special thank you goes to Cassiano Sala for our fun adventures both past and future, and for helping me to remember what I'm grateful for. Most importantly, I would like to thank my parents Angela and Dave and my brother Matt for their constant love, support and encouragment in whatever I do.

Table of Contents

1 Chapter One: Introduction 14

1.1 Branching Morphogenesis; An Overview 2
1.1.1 The Junctional complex 2
1.1.2 Actin- myosin cytoskeleton 4
1.1.3 Cell types 6
1.1.4 Bud elongation 8
1.1.5 Branching morphogenesis and human disease 8
1.2 Lung development and branching morphogenesis 9
1.2.1 Pseudoglandular phase of lung development 10
1.2.2 Modes of lung branching 11
1.2.3 Canalicular stage of lung development 13
1.2.4 Saccular phase of lung development 15
1.2.5 Lumen formation 16
1.2.6 Lumen formation in the lung 17
1.2.7 Embryonic lung development and adult disease 21
1.3 Kidney Development and branching morphogenesis 22
1.3.1 Formation of specialised Kidney structures 24
1.3.2 Glomeruli 26
1.4 The role of Scribble in apical-basal and planar polarity 28
1.5 Planar Cell Polarity 32
1.5.1 Drosophila PCP 33
1.5.2 Asymmetric localisation of PCP proteins 35
1.5.3 Mammalian PCP 37
1.5.4 PCP signalling and kidney development 39
1.5.5 PCP signalling; differences between *Drosophila* and mammals 42
1.6 Concluding remarks and Outline of thesis 43

2 Chapter Two : Experimental Procedures 45

2.1 Genomic DNA preparation for PCR 46
2.2 Mouse strains and Genotyping 46
2.3 Gel Electrophoresis 50
2.4 Dissections 50
2.5 Antibodies and Immunostaining 50
2.5.1 Fixation and Embedding 50
2.5.2 Haematoxylin & Eosin, Periodic-Acid Schiff Staining and Martius Scarlet Blue trichrome staining. 51
2.5.3 Immunohistochemistry and Immunofluorescence 52
2.5.4 Antigen Retrieval 53
2.5.5 Primary Antibodies 53
2.5.6 Secondary Antibodies 53
2.5.7 Whole Lung Immunostaining 54
2.5.8 Whole Kidney Immunostaining 55
2.6 Western Blotting 55
2.7 Protein extraction and quantification 55
2.8 Immunoblotting 56
2.9 Culture Experiments 58
2.9.1 Lung Explant cultures 58
2.9.2 Kidney Explant Cultures 59
2.9.3 59

2.9.4 Organotypic Cultures 59
2.9.5 Scribble morpholino knock-down and organotypic cultures 60
2.10 Lung Function Analysis 60
2.10.1 Whole body unrestrained plethysmograph (Buxco) with Methacholine challenge 60
2.10.2 Jugular Bleeds 61
2.10.3 Bronchioalveolar Lavage 61
2.10.4 Cytospin and Diff quick stain 62
2.10.5 Haemoanalyser measurement of immune cells in blood and BALF samples 62
2.11 Kidney Function analysis 62
2.11.1 Murine Micro-albuminuria ELISA 63
2.11.2 Retinol Binding Protein 4 ELISA 64
2.12 Glomerular Counts 65
2.13 Statistical analysis 65
2.14 Microscopy 66
2.14.1 Leica TCS SP5 66

3 Chapter Three: The PCP genes *Celsr1* and *Vangl2* are required for normal branching morphogenesis 68

3.1 Introduction 69
3.1.1 Aims 74
3.2 Results 74
3.2.1 Branching morphogenesis is disrupted in Celsr1$^{Crsh/Crsh}$ and Vangl2$^{Lp/Lp}$ mutants 74
3.2.2 Lung morphogenesis is disrupted in Celsr1$^{Crsh/Crsh}$ and Vangl2$^{Lp/Lp}$ mutants 77
3.2.3 Cell differentiation, proliferation and apoptosis are not affected in Celsr1$^{Crsh/Crsh}$ or Vangl2$^{Lp/Lp}$ mutants 80
3.2.4 Branching morphogenesis defects in Celsr1$^{Crsh/Crsh}$ and Vangl2$^{Lp/Lp}$ ex vivo lung culture 84
3.2.5 Celsr1 and Vangl2 are required for all three modes of lung branching 86
3.2.6 Celsr1$^{Crsh/Crsh}$ and Vangl2$^{Lp/Lp}$ mutant lungs phenocopy lungs treated with Rho kinase inhibitor and Rho activation partially rescues the branching defect in Crsh 88
3.2.7 Mutations in Celsr1$^{Crsh/Crsh}$ and Vangl2$^{Lp/Lp}$ lead to disrupted cytoskeletal organisation and disordered epithelial airways 91
3.2.8 Apical-basal polarity remains intact in Celsr1$^{Crsh/Crsh}$ and Vangl2$^{Lp/Lp}$ mutants 94
3.2.9 Lung endoderm from Celsr1$^{Crsh/Crsh}$ and Vangl2$^{Lp/Lp}$ mutants responds to the chemoattractant FGF10 but is unable to branch 96
3.2.10 Celsr1 and Vangl2 proteins are spatially restricted and differentially expressed in lung epithelia 98
3.2.11 Celsr1 co-localises with the basement membrane component laminin 101
3.2.12 Celsr1 and Vangl2 expression is enriched in highly specific regions of the branching lung epithelium 104
3.2.13 Loss of Vangl2$^{Lp/Lp}$ results in kidney branching defects 106
3.2.14 The late gestation Vangl2$^{Lp/Lp}$ kidney has poor cortico-medullary definition, a hypoplastic medulla and mildly dysmorphic tubules 109
3.2.15 Looptail heterozygous kidneys have fewer glomeruli but do not display functional defects when compared to wildtype littermates 112
3.3 Discussion 115
3.3.1 Mutations in PCP genes disrupt lung branching morphogenesis and cytoskeletal organisation 115
3.3.2 The expression patterns of Celsr1 and Vangl2 suggest both common and differential roles for these proteins in lung branching morphogenesis 117

3.3.3 Celsr1 is required for bud bifurcation 118
3.3.4 Vangl2 is required for normal kidney development 119
3.4 Conclusion 124

4 Chapter Four: Scribble is required to maintain the airway lumen 125

4.1 Introduction 126
4.1.1 Aims 130
4.2 Results 130
4.2.1 Scribble is required for normal lung development 130
4.2.2 Differentiation, proliferation and apoptosis are unaffected in Scribble$^{Crc/Crc}$ lungs 133
4.2.3 Epithelial tube formation is perturbed in Scribble$^{Crc/Crc}$ mutants 138
4.2.4 Scrib1 is expressed in tight junctions 140
4.2.5 Loss of Scrib1 leads to specific tight junction disruption 142
4.2.6 Scribble is expressed towards the luminal surface in a 3D model of active branching 145
4.2.7 Scribble signals via the PCP pathway downstream effector, Rho kinase 147
4.2.8 Scribble$^{Crc/Crc}$ lung epithelia displayed cytoskeletal defects 149
4.2.9 Apical-basal polarity appears unaffected in Scribble$^{Crc/Crc}$ lungs 151
4.2.10 Scribble is required for epithelial cell organisation necessary for the formation of new airways 153
4.2.11 Scribble modulates localisation of the core PCP proteins Celsr1 and Vangl2 in lung epithelium 154
4.3 Discussion 157
4.3.1 Scribble$^{Crc/Crc}$ lungs display branching morphogenesis and cytoskeletal defects 157
4.3.2 Scribble appears to operate via the PCP pathway 157
4.3.3 Scrib1 is not required for apical basal polarity in the lung 158
4.3.4 Scrib1 is required to maintain airway lumina 158
4.3.5 Cross talk between PCP and A/B polarity pathways 160
4.3.6 A more severe phenotype is observed in Scribble$^{Crc/Crc}$ lungs compared to those of either Celsr1$^{Crsh/Crsh}$ or Vangl2$^{Lp/Lp}$ mouse mutants 161

5 Chapter Five: Preliminary analysis of lung phenotype and function in *Vangl2*$^{Lp/+}$ mice 163

5.1 Introduction 164
5.1.1 Aims 169
5.2 Results 169
5.2.1 Vangl2 heterozygotes have reduced numbers of airways and display localised tissue disruption in the lung. 169
5.2.2 Differentiation, proliferation and apoptosis are unaffected in Vangl2$^{Lp/+}$ lungs 172
5.2.3 Mild disruption to actin-myosin cytoskeleton is observed in Vangl2$^{Lp/+}$ lungs .. 174
5.2.4 Adult Vangl2$^{Lp/+}$ display histological defects 176
5.2.5 Adult heterozygotes have an intrinsic lung function defect 179
5.3 Discussion 181
5.3.1 Vangl2 heterozygous mice display embryonic lung defects 181
5.3.2 Adult Vangl2$^{Lp/+}$ mice have histological defects 182
5.3.3 *Vangl2*$^{Lp/+}$ mice have an activated immune system with a consistent increase in Penh at baseline, but no significant elevation in Penh is observed following administration of methacholine. 183
5.3.4 Advantages and disadvantages of using Penh to determine lung function 184

6 Discussion 189

6.1 Overall findings of this study 189
6.2 Future work 190
6.2.1 Embryonic analysis 190
6.2.2 Adult analysis 193
6.3 Conclusion 194

7 References 196

8 Appendix; Publications arising from this work 222

Figures and Tables

Figure 1.1: Schematic drawing of the mammalian epithelial junctional complex... **14**

Figure 1.2: Schematic diagram of the contractile assemblies in nonmuscle cells... **16**

Figure 1.3: Schematic diagram of the categorisation of epithelia based on the shapes of individual epithelial cells and the number and relative arrangement of cell layers ... **17**

Figure 1.4: The three modes of embryonic lung branching ... **21**

Figure 1.5: Budding; the process of lung lumen formation. ... **26**

Figure 1.6: Schematic diagram of a glomeruli ... **34**

Figure 1.7: Asymmetric localisation and transport of PCP proteins ... **38**

Figure 2.1: Example of Pyrogram trace results for genotyping *Scribble*^{Crc} ... **52**

Figure 3.1: The planar cell polarity signal transduction pathway... **71**

Figure 3.2: Branching morphogenesis is disrupted in *Celsr1*$^{Crsh/Crsh}$ and *Vangl2*$^{Lp/Lp}$ mutants ... **75**

Figure 3.3: Disruption of Celsr1 or Vangl2 causes lung morphogenesis defects ... **78**

Figure 3.4: Immunohistochemical analysis of lung epithelial cell differentiation in *Celsr1*$^{Crsh/Crsh}$ and *Vangl2*$^{Lp/Lp}$ compared to wildtype... **78**

Figure 3.5: Proliferation and apoptosis are unaffected in *Celsr1*$^{Crsh/Crsh}$ and *Vangl2*$^{Lp/Lp}$ mutants ... **78**

Figure 3.6: *Celsr1*$^{Crsh/Crsh}$ and *Vangl2*$^{Lp/Lp}$ mutant lungs display branching defects in *ex vivo* lung culture ... **78**

Figure 3.7: Celsr1 and Vangl2 are expressed in all modes of branching ... **78**

Figure 3.8: *Ex-vivo* lung cultures reveal that mutations in *Celsr1* and *Vangl2* phenocopy treatment with Rho kinase inhibitor and Rho kinase activation partially rescues the branching defect in *Crsh/Crsh*.... **78**

Figure 3.9: Mutant lungs display aberrant cell architecture ... **78**

Figure 3.10: *Celsr1*$^{Crsh/Crsh}$ and *Vangl2*$^{Lp/Lp}$ mutant lungs display normal apical-basal polarity ... **78**

Figure 3.11: Mutant lung endoderm responds to FGF10 but is unable to undergo branching ... **78**

Figure 3.12: Celsr1 and Vangl2 proteins are spatially restricted and differentially expressed in lung epithelia ... **78**

Figure 3.13: Celsr1 colocalises with laminin a component of the basement membrane... **78**

Figure 3.14: Differential expression of Celsr1 and Vangl2 is observed in branching lung endoderm explants ... **78**

Figure 3.15: Loss of Vangl2 leads to defects in kidney branching morphogenesis ... **78**

Figure 3.16: Histology of E18.5 looptail kidney sections ... **78**

Figure 3.17: Vangl2 heterozygote kidneys have fewer glomeruli but have normal renal function ... **78**

Figure 4.1: Scrib1 is required for normal lung development ... **78**

Figure 4.2: Differentiation is unaffected in *Scribble*$^{Crc/Crc}$ lungs ... **78**

Figure 4.3: Proliferation and apoptosis are unaffected in *Scribble*$^{Crc/Crc}$ lungs ... **78**

Figure 4.4: *Ex vivo* cultures of *Scribble*$^{Crc/Crc}$ lungs have fewer buds that appear broader and far denser than wildtype littermates ... **78**

Figure 4.5: Scrib1 is expressed in tight junctions ... **78**

Figure 4.6: Specific tight junction proteins are disrupted in *Scribble*$^{Crc/Crc}$ lungs ... **78**

Figure 4.7: Immunostaining of an active 3D model of branching with Scrib1 and Phalloidin ... **78**

Figure 4.8: Levels of Total and Active RhoA are reduced in *Scribble*$^{Crc/Crc}$ lungs ... **78**

Figure 4.9: Actin-myosin cytoskeleton is disrupted in *Scribble*$^{Crc/Crc}$ lungs ... **78**

Figure 4.10: Apical-basal polarity appears unaffected in *Scribble*$^{Crc/Crc}$ lungs ... **78**

Figure 4.11: Morpholino knockdown of Scribble prevents normal epithelial cyst formation in organotypic culture ... **78**

Figure 4.12: Scrib1 is required for Celsr1 localisation in the basement membrane ... **78**

Figure 5.1: Calculation of enhanced pause (Penh) ... **78**

Figure 5.2: Changes in chamber pressure waveform after methacholine challenge **78**

Figure 5.3: *Vangl2*$^{Lp/+}$ mice display mild histological lung defects with reduced branching **78**

Figure 5.4: Differentiation, proliferation and apoptosis are unaffected in *Vangl2*$^{Lp/+}$ lungs **78**

Figure 5.5: Mild disruption to the actin-myosin cytoskeleton is observed in *Vangl2*$^{Lp/+}$ lungs **78**

Figure 5.6: Histological analysis of 10 week old adult *Vangl2*$^{Lp/+}$ lungs **78**

Figure 5.7: No significant difference in Penh was observed between *Vangl2*$^{Lp/+}$ and wildtype mice **78**

Abbreviations

aPKC	atypical protein kinase C
Aqp5	Aquaporin-5
BALF	Bronchioalveolar lavage fluid
BMP	Bone morphogenetic protein
BSA	Bovine serum albumin
Baz	Bazooka
CAKUT	Congenital abnormalities of the kidney and urinary tract
CC-10	Clara Cell – 10
cDNA	complimentary DNA
COPD	Chronic obstructive pulmonary disease
CL	Lung compliance
CNF-1	*Escherichia coli* cytotoxic necrotizing factor-1
Crc	Circletail
Crsh	Crash
Crb	Crumbs
DAB	3,3'-diaminobenzidine
Dlg	Discs Large
Dpc	days post coitum
ECM	Extracellular Matrix
FGF	Fibroblast growth factor
H&E	Haematoxylin and Eosin
IHC	Immunohistochemistry
IPA	Isopropyl alcoho
ITS	Insulin-transferrin-sodium selenite
MET	Mesenchymal to Epithelial transition
MGU	Mammalian Genetics Unit
MM	Metenephric mesenchyme
MSB	Martius Scarlett Blue
μl	microlitre
mls	milliters
mg	milligram

mRNA	messenger RNA
ng	nanogram
Lgl	Lethal giant larve
Lp	Looptail
PBS	Phosphate buffered Saline
PCP	Planar cell polarity
PCT	Proximal convoluted tubule
PCR	Polymerase chain reaction
PK	Proteinase K
Pro-SpC	Pro-surfactant protein C
RCD	Renal cystic diseases
RNAi	RNA interferance
RT	Room temperature
RT-PCR	Reverse transcription polymerase chain reaction
RL	Lung resistance
SJs	Septate junctions
SOX9	Sry-related transcription factor 9
SP5	5 SpectroPhotometer channels of Leica Confocal Microscope
TBS	Tris buffered saline
TCS	True Confocal Scanner
UB	Ureteric bud
UGR	Urogenital ridge
UP	Unrestrained plethysmograph
WBP	Whole body plethysmograph
FWBP	Flow whole body plethsmograph
PWBP	Pressure whole body plethysmograph
uWBP	Buxco unrestrained whole body plethysmograph
WNT	wingless-related gene
WT1	Wilms' tumour suppressor 1
Z	Lung input impedance

Declaration

All the work detailed in this thesis was performed by myself, with the help of the other members of the Development Department and core facilities at MRC Harwell as detailed in my acknowledgements.

1 Chapter One: Introduction

1.1 Branching Morphogenesis; An Overview

Branching morphogenesis is the mechanism by which many glands and organs develop, including the vasculature, lung, kidney, mammary, lacrimal and salivary glands. The branching process results in a specialised structure with a large surface area to allow for efficient function, e.g. gas exchange in the lungs or fluid exchange in the kidney. The molecular mechanisms that drive the process and patterning of branched organs are largely unknown. However, it is known that epithelial cells, that exhibit apical-basal polarity (A/B), a uniformly orientated cytoskeleton and highly elaborate cell junctions, organise into new branches, each of which contains a centrally located lumen. (Affolter et al., 2009; Andrew and Ewald, 2009; Chung and Andrew, 2008; Hogan and Kolodziej, 2002; Lubarsky and Krasnow, 2003). The epithelial tubes are surrounded by a complex mixture of supporting cells, or stroma and extracellular matrix (ECM). Together these supporting cells along with the epithelial tubes comprise the entire organ. During the development of epithelial tubes cell-cell contacts, adhesion, apical-basal polarity and remodelling of the basement membrane or basal lamina are independently modulated to allow the growth and development of the complex tubular structure, such that the cellular organisation of a specific organ early on in development can have dramatic effects on the structure of the adult organ (Andrew and Ewald, 2010).

1.1.1 The Junctional complex

Interspecies differences are observed in epithelial organisation (Knust and Bossinger, 2002). One of the main differences observed is in the organisation and location of the junctional complexes, which provide a barrier to the inside of cells. The mammalian epithelial junctional complex (Fig. 1.1.1) is comprised of tight junctions or *zonula*

occludens, adherens junctions and desmosomes (Farquhar and Palade, 1963). These junctional complexes completely surround the cell resulting in a continuous belt that interconnects neighbouring cells. In mammalian epithelial cells, tight junctions are the most apical component of the junctional complex, with the adherens junctions located just below, followed by the desmosomes. The junctional complex provides a semi-permeable barrier that is capable of finely regulating the movement of ions, solutes and cells through the paracellular space according to the size and charge of migrating particles/molecules (Steed et al., 2009). Size selective paracellular diffusion of small hydrophilic molecules requires the dynamic properties of tight junctions and the Rho-regulated actin-myosin cytoskeleton (Matter and Balda, 2003). In addition the junctional complex also plays a role in the maintenance of apical-basal polarity (Matter and Balda, 2003).

The *Drosophila* septate junctions (SJs) while simpler than their mammalian counterparts have the same functional role; to maintain the paracellular permeability (Knust and Bossinger, 2002). Recent studies have revealed claudins to localise to and be required for the formation of the SJs (Behr et al., 2003; Wu et al., 2004). In *Drosophila*, the SJs sit basal to the adherens junctions and contain conserved proteins including the tumour suppressors Scribble (Scrib), Discs Large (Dlg) and Lethal Giant Larvae (Lgl), which also localise to the basolateral regions in vertebrate cells (Bilder and Perrimon, 2000; Strand et al., 1994; Woods and Bryant, 1991) (discussed in more detail below and in Chapter 4). Whereas, in mammals, the tight or occludins junctions sit apical to the adherens junctions (Steed et al., 2010).

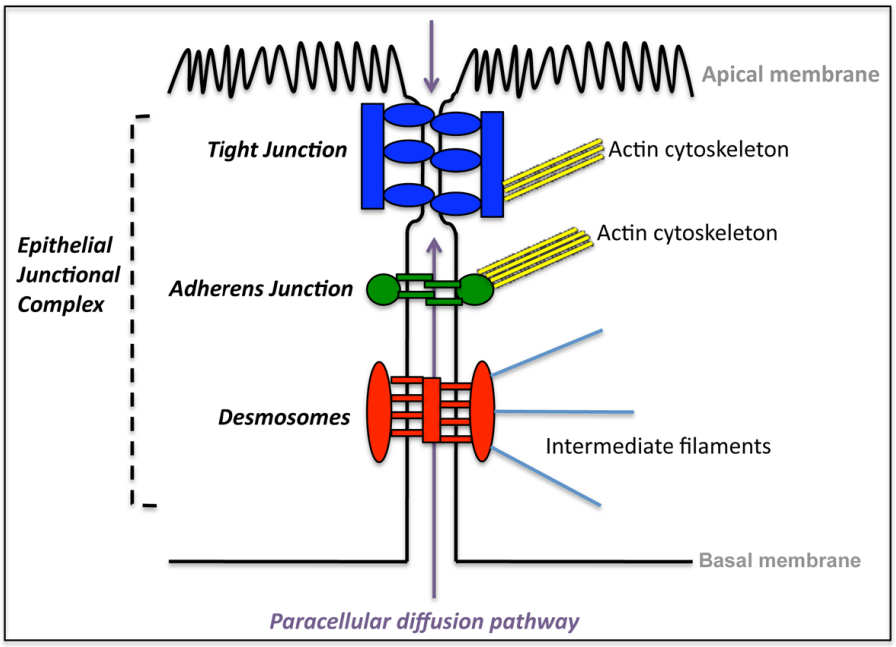


Figure 1.1.1 Schematic drawing of the mammalian epithelial junctional complex. The tight junctions are highlighted in blue, with the adherens just below in green and the desmosomes located below these highlighted in red. The purple arrows indicate the paracellular route for the diffusion of ions and hydrophilic solutes. (Adapted from (Steed et al., 2010).

1.1.2 Actin-myosin cytoskeleton

Morphogenesis of epithelial tissues involves various forms of reshaping of cell layers, such as invagination or bending, convergent extension, and epithelial–mesenchymal transition. At the cellular level, these processes include changes in the shape, position, and assembly pattern of groups of cells. The actin cytoskeleton provides a structural framework around which cell shape and polarity are defined, in addition its dynamic properties the cytoskeleton provides the mechanical force required for cells to move and to divide. Actin filaments, in association with myosin are responsible for many of these types of cell movements. Myosin is the prototype molecular motor—a protein that converts chemical energy (ATP) to mechanical energy, thus generating force and

movement. Contractile assemblies of actin and myosin in non-muscle cells which arise as a result of Rho activation (Hall, 1998) are small-scale versions of muscle fibers. As in muscle, the actin filaments in these contractile assemblies are interdigited with bipolar filaments of myosin II, consisting of 15 to 20 myosin II molecules, which produce contraction by sliding the actin filaments over one another (Fig. 1.1.2). Two examples of contractile assemblies in non-muscle cells, are stress fibers and adhesion belts. The contraction of stress fibers produces tension across the cell, allowing the cell to pull on a substrate (e.g., the extracellular matrix) to which it is anchored. The contraction of adhesion belts alters the shape of epithelial cell sheets, a process that is particularly important when sheets of epithelial cells fold into structures such as tubes (discussed below in section 1.2.2).

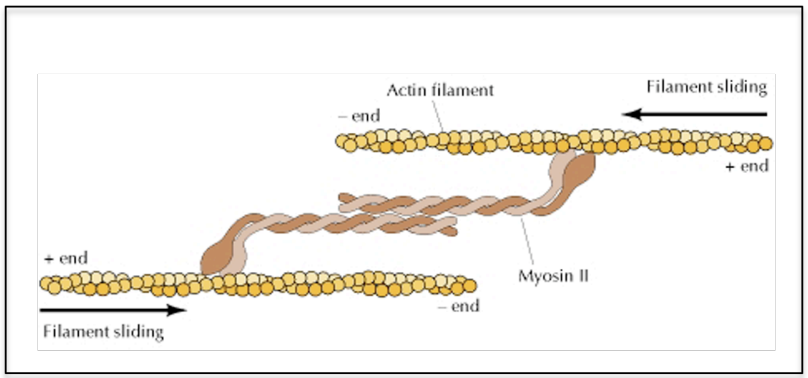


Figure 1.1.2 Schematic diagram of the contractile assemblies in non-muscle cells. Adapted from (Cooper, 2001).

1.1.3 Cell types

Differences in epithelia are observed between specific organs such that each organ has specifically differentiated epithelia that is architecturally organised for that organ's specific function. Epithelia can be divided in to several sub-types (Fig. 1.1.3); single layered epithelia are referred to as simple with multilayered epithelia termed stratified. If the nuclei occupies more than one layer but all cells remain in contact with the basement membrane the epithelia is referred to as pseudo-stratified. If the epithelia display more than one type of organisation, it is considered to be a transitional epithelium. Depending on the epithelial cells' shape, the epithelia can be classified further, for example; cells with similar height to width ratio are termed cuboidal and those with a greater height to width ratio are columnar, and finally those with a greater width than height are squamous. Secretory epithelia are associated with another layer of cells that express muscle markers such as α-smooth muscle actin. The location of these cells determines their terminology; those located between the epithelial cells and basement membrane are myoepithelial cells whereas those located outside the basement membrane are myofibroblasts.

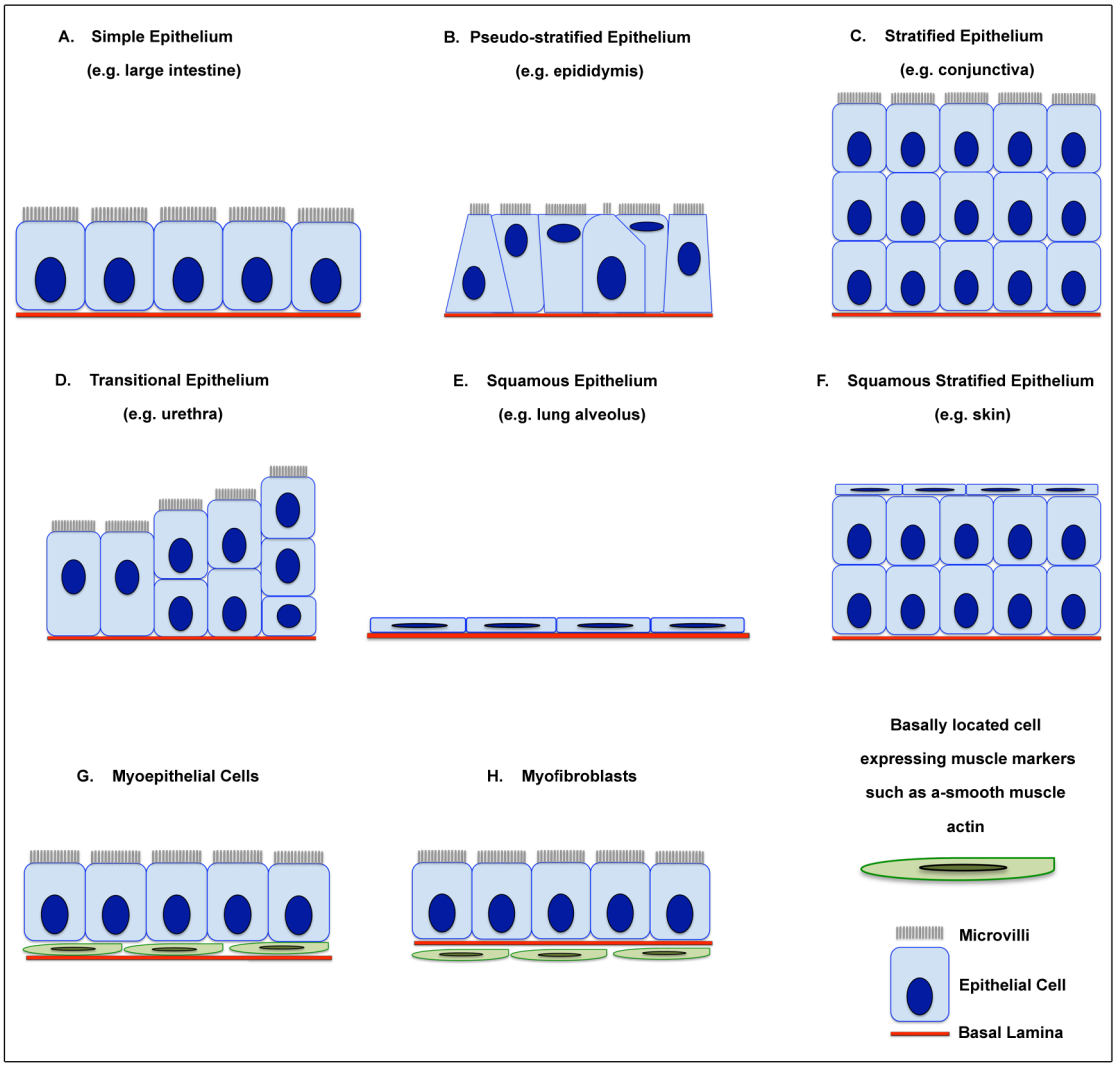


Figure 1.1.3 Schematic diagram of the categorisation of epithelia based on the shapes of individual epithelial cells and the number and relative arrangement of cell layers. Apical surfaces of epithelial cells often contain microvilli, actin-rich finger like structures that protrude from the apical membrane into the lumen. In some cases epithelial tubes are comprised of an inner epithelial layer and an outer "muscle" cell layer that is either in direct contact with the epithelial cells or is separated by the basal lamina. (Adapted from (Andrew and Ewald, 2010).

The mesenchyme is less 'organised' in comparison to epithelia and is predominantly characterised by single cells dispersed through an extensive ECM. Within the mesenchyme, integrin-based cell-matrix adhesion is more common than the cadherin-based intercellular adhesion observed in epithelia. Epithelial and mesenchymal cells can be interchangeable such that epithelial cells can undergo an epithelial-to-mesenchyme transition (EMT), an example of this includes the vertebrate neural crest during gastrulation. Mesenchymal-to epithelial transition (MET) can also occur, for example, the condensation of mesenchymal cells at branch tips in the developing kidney.

1.1.4 Bud elongation

Branching morphogenesis requires elongation and elaboration of epithelial tubes. Three mechanisms exist for tube elaboration; the distal tip of a tube can split, with further elongation in both directions, this is termed bifurcation. New tubes can initiate at distinct sites along the length of an existing branch, termed side branching, both of these mechanisms are common in lung and kidney branching. Finally the tube can separate and exchange cell-cell contacts for cell-matrix contacts without significant elongation, a process referred to as clefting. New branches are formed by clefting in the submandicular gland and studies have revealed components of the basement membrane Laminin alpha 5 to be expressed at these cleft points (Rebustini et al., 2007).

1.1.5 Branching morphogenesis and human disease

An understanding of the molecular and cellular events that underlie the development of branched organs and tube formation e.g. how epithelial cells develop and coordinate their polarity, is essential for understanding both normal development

and human disease. Defects in lung development can result in a number of lung diseases such as cystadenomatoid malformations, pulmonary hypertension and agenesis or hypoplasia of the lung (Jancelewicz et al., 2008; Thebaud and Abman, 2007; Whitsett et al., 2004). It is also important to note that post-natal lung function is highly dependant on normal cell and tissue architecture being formed *in utero* (Whitsett et al., 2004). Adult diseases such as idiopathic pulmonary fibrosis and adult respiratory distress syndrome result in abnormal tissue structure and fibrosis leading to impaired gas/air exchange and respiratory dysfunction (Chapman, 2004). Many of the most common adult diseases in other systems including atherosclerosis and polycystic kidney disease arise as a result of defective tissue organisation and tubular architecture e.g. abnormally broad or narrow lumina (Chung and Andrew, 2008; Lubarsky and Krasnow, 2003). In addition epithelial carcinomas frequently display disrupted tubular architecture, loss of apical-basal polarity, loss of differentiation and excessive proliferation. It is widely acknowledged that decreased apical-basal polarity and decreased differentiation correlates with advanced tumour progression and poorer patient prognosis (Nguyen et al., 2009; Nguyen and Massague, 2007). A current working hypothesis is that the normal developmental program for a specific organ may be recapitulated during cancer progression. Therefore a molecular understanding of branching morphogenesis could lead to new ways of diagnosing and treating many different human diseases.

1.2 Lung development and branching morphogenesis

The lung is essential to life, yet relatively little is known about how its development is controlled at the molecular and cellular level. However, a number of studies, using

mouse genetics, have begun to unravel the important molecular pathways required for normal lung branching morphogenesis.

1.2.1 Pseudoglandular phase of lung development

Mouse lung development begins with the appearance of the primary bud that first appears around embryonic day (E) 9.5 in the ventral-lateral aspect of the foregut in response to localised Nkx2.1 (also known as (Titf1) expression (Minoo et al., 1995). This epithelial bud soon becomes two primordial buds and simultaneously the foregut tube, just anterior of the lung buds begins to separate in two, to form a dorsal oesophagus that leads into the stomach and a ventral trachea that connects to the lung buds. These primary lung buds give rise to the future main steam bronchi. They extend into the surrounding splanchnic mesenchyme in response to FGF10 (Min et al., 1998) which signals to Fgfr2 in the endoderm (De Moerlooze et al., 2000), initiating the process of branching morphogenesis. The localised expression of Fgf10 in the surrounding mesenchyme is crucial for lung development to continue as mutants lacking *Fgf10*, do not undergo branching, although the trachea development is normal (Min et al., 1998; Sekine et al., 1999). Retinoic acid receptors (RARs) (Mendelsohn et al., 1994) are also key players during early lung development, depletion of multiple RARs causes severe tracheal and lung malformations, including lung hypoplasia and agenesis (Mendelsohn et al., 1994). SHH is produced by endodermally derived cells that activate the Ptch/Smo/Gli pathway in the pulmonary mesenchyme (Pepicelli et al., 1998). *Shh*$^{-/-}$ mice display tracheoesophageal fistula (an abnormal connection between the oesophagus and trachea) and simple cyst-like lung sacs that fail to branch (Litingtung et al., 1998; Pepicelli et al., 1998). E9.5 – E16.5 is referred to as

the pseudoglandular stage, when pulmonary blood vessels are produced by vasculogenesis and angiogenesis (deMello et al., 1997).

1.2.2 Modes of lung branching

The primary buds undergo sixteen rounds of stereotypical branching to give rise to a complex tree-like structure ending in thousands of terminal tubules. Metzger et al., recently undertook morphometric analysis of fixed lungs at different developmental stages, from this work, he described three modes of branching that occur in the lung (Metzger et al., 2008). The three distinct modes are: domain branching; orthogonal branching and planar branching (Fig. 1.1).

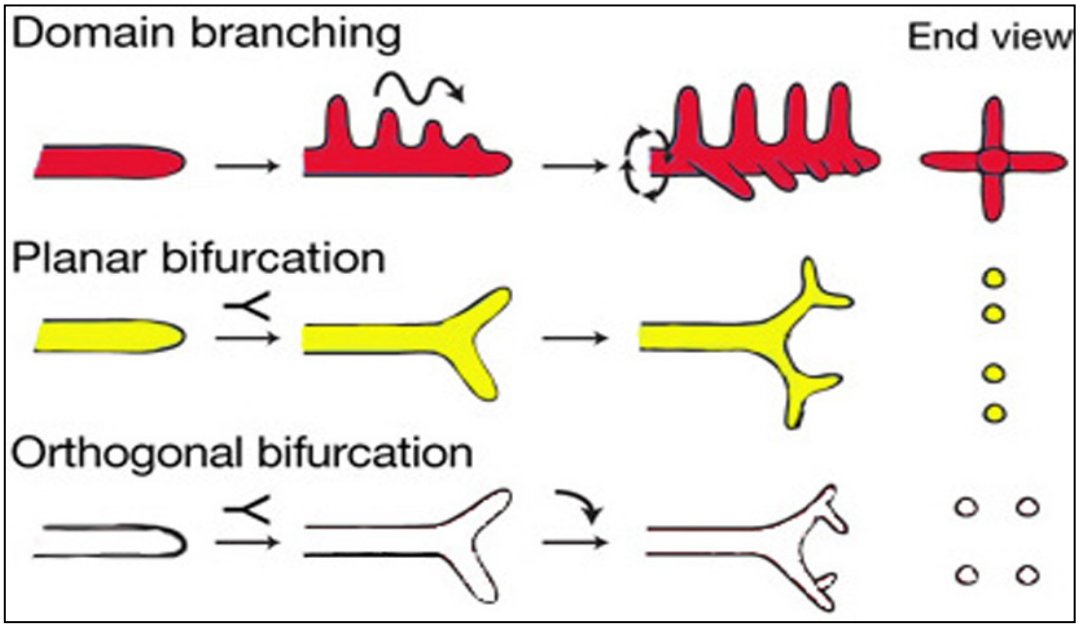


Figure 1.2.1 The three modes of embryonic lung branching. Lung branching begins with domain branching (red), and progresses into planar branching (yellow) and/or orthogonal branching (white) (adapted from Metzger et al. 2008).

Domain branching is the sprouting of new buds at specific distances along the length of a single stalk. The branches sprout around the circumference of the stalk either in the dorsal/ventral or medial/lateral axis relative to the parent stalk. This branching mode establishes the main structure of the respiratory tree that consists of five lobes in the mouse, one left and the four right lobes (cranial, medial, caudal and accessory lobes). Orthogonal and planar branching occur at the tips, planar branching occurs when the tip splits into two buds within a single plane, and orthogonal branching involves the formation of new buds orthogonal to the parent stalk.

During branching morphogenesis the lung buds undergo repetitive cycles of four processes: bud elongation, cessation of outgrowth, expansion of the tip and bifurcation (either planar or orthogonal) (Metzger et al., 2008). These processes are associated with dynamic changes in the localisation of FGF10 transcripts in the mesoderm, in the expression level of genes such as Bmp4 in the endoderm, and in the deposition of extracellular matrix molecules. Much of our current understanding of the cellular mechanisms involved in bud morphogenesis, comes from studies in other branches organs such as the kidney where convergent extension and changes in the plane of cell division modulate the length of epithelial tubules at different stages (Karner et al., 2009; Rebustini et al., 2007; Yu et al., 2009). Studies in the salivary gland indicate a role for the basement membrane protein Laminin α5 in clefting of one branch into two (Rebustini, Patel et al. 2007).

1.2.3 Canalicular stage of lung development

From E16.5-E17.5 the mechanism of lung development changes from branching morphogenesis into the canalicular stage whereby terminal buds begin to narrow (Chung and Andrew, 2008). Up until this point the epithelial cells lining the trachea,

bronchi and bronchioles are relatively undifferentiated. By adulthood however the lungs comprise a large number of diverse cell types which include squamous basal, ciliated, brush, goblet, noncilitaed/secretory cells (also termed Clara cells), intermediate and neuroepithelial cells, and the cuboidal cells located in the bronchioalveolar duct junctions (BADJ cells). There are significant differences between the cellular composition and organisation of the airway epithelium of mouse and human lungs. In the mouse lung, the epithelium is either cuboidal or columnar and a pseudostratified layer is found only in the trachea and main stem bronchi. Whereas in humans the lung epithelium is mostly pseudostratified with the smallest most distal tubes lined by a simple epithelium. The mechanisms determining the complex patterning of differentiated cell types lining the airways is poorly understood, but they are influenced by autocrine-paracrine signalling that control cell differentiation (Morrisey and Hogan, 2010). TTF-1, NF-1β, GATA-6 along with other transcription factors including RB, ETS, SOX and FOX family members play roles in cell specific differentiation and gene expression in the conducting airways (Maeda et al., 2007).

β-Catenin plays a critical role in establishing proximal versus distal cell fate in the respiratory epithelium. A number of Wnt ligands and components of the Wnt/β-Catenin signalling pathway are expressed in various pulmonary cells throughout lung morphogenesis (Tebar et al., 2001; Weidenfeld et al., 2002). β-Catenin is expressed in both proximal and distal regions of the lungs in both epithelial and mesenchymal cells. Studies have shown deletion of β-catenin in respiratory epithelial cells impaired branching morphogenesis and cell differentiation *in vivo* (Mucenski et al., 2005; Shu et al., 2005). Further studies in mammalian systems confirmed the role of Wnt signalling and the β-catenin/TCF/LEF pathway in regulating branching

morphogenesis and airway epithelial differentiation (Duan et al., 1999; Mucenski et al., 2005; Okubo and Hogan, 2004; Shu et al., 2005; Tebar et al., 2001). It is important to note that reciprocal signalling occurs between the epithelium and mesenchyme and β-catenin is expressed in both, therefore fully understanding its function is complex. Studies in the lung and lacrimal gland have revealed a complete loss of β-catenin in the epithelium alone resulted in a reduction in the number of branches that formed. Whereas simultaneous morpholino knockdown of β-catenin in both epithelial and mesenchymal tissue revealed an increase in the number of branches (Dean et al., 2005).

1.2.4 Saccular phase of lung development

By E18.5 small sacs, the precursors of alveoli start to develop at the bud tips; this is referred to as the saccular stage. The blood vessels that have been developing in parallel with the airways become closely associated with the epithelium to enable gas exchange, this is essential for efficient lung function after birth. The lungs continue to increase in size after birth as a result of increases in the length and diameter of the airways that have formed *in utero,* and the subdivision of the immature alveoli into smaller subunits (Bourbon et al., 2009; Kauffman, 1980). The timing of alveolar development varies between species, e.g. in mice it occurs between postnatal day 5-30, whereas in humans some alveoli form before birth and continue for many months afterwards. During the saccular-alveolar period is when the foetus is born and the lungs move from a fluid-filled to an air-filled system. At birth, pulmonary vascular resistance falls, pulmonary blood flow increases, lung fluid is reabsorbed and pulmonary surfactant is secreted into the peripheral saccules of the lung, thus reducing surface tension and preventing alveolar collapse once the lung is filled with

air. Lack of surfactant results in respiratory distress syndrome in preterm infants, an important cause of morbidity and mortality in new-borns need to put some refs in here.

1.2.5 Lumen formation

Despite tubular organs varying in size and shape as well as ranging from highly intricate networks of branched tubules to simple cylinders, they all comprise a polarised epithelium that surrounds a central lumen. The apical surface of each epithelial cell faces into the lumen whereas the basal surface faces the surrounding tissues. The lateral surface of each cell forms contacts with neighbouring cells via elaborate and specialised junctions comprised of adherens and tight junctions that anchor the epithelial cells to one another and provide a barrier from the external environment. Branched organs form lumen via several mechanisms. Branched organs that develop from an already polarised primordium establish their lumen via one of two mechanisms, wrapping or budding. In both processes the primordium folds inward to create a cup-like structure. Wrapping results in the final tube being parallel to the plane of epithelial origin and the new tube is eventually completely separated from the surrounding non-tube epithelia by fusion of the epithelial folds at the edges of the tube primordium. An example of wrapping is the development of the neural tube from the neural plate in birds and mammals (Andrew and Ewald, 2010).

In the lung, epithelial cells are already polarised and lumen formation occurs by budding, and only requires a change in cell shape and/or organisation (discussed in more detail below, see Fig 1.2.1) (Chung and Andrew, 2008; Lubarsky and Krasnow, 2003). Epithelial tubes can also establish lumen from unpolarized rudiments that polarise and create a lumen via one of three separate mechanisms; cord hollowing,

cell hollowing or cavitation (Lubarsky and Krasnow, 2003).

1.2.5.1 Cord hollowing

Cord hollowing requires cells to polarize and create small lumenal spaces at sites of apical membrane contact, these spaces subsequently join together into a single common lumen e.g in MDCK cells grown 3D matrices (Martin-Belmonte et al., 2008), secondary neurulation in mouse and chick (Schoenwolf, 1984; Schoenwolf and Delongo, 1980) gut formation in zebrafish (Bagnat et al., 2007).

1.2.5.2 Cell hollowing

Individual cells form large apical vesicles, which eventually fuse with each other and the plasma membrane to form a large common lumen. Lumen formation in the *C.elegans'* single excretory cell (kidney) (Buechner, 2002), *Drosophila* tracheoles (Guillemin et al., 1996) and zebrafish blood vessels (Blum et al., 2008; Kamei et al., 2006) all form lumen via cell hollowing.

1.2.5.3 Cavitation

Cells on the periphery of the primordium will form the epithelial tube lining and cells in the center either die by apoptosis or intercalate into the periphery and contribute to the tube lining (Andrew and Ewald, 2010). Mammary (MCF-10A) cells grown in 3D matrices (Debnath et al., 2002) use cavitation to form lumina. In addition, apoptosis has also been observed *in vivo* during lumen formation of the mammalian mammary and salivary glands (Humphreys et al., 1996; Jaskoll and Melnick, 1999).

1.2.6 Lumen formation in the lung

Correct lumen formation and precise maintenance of lumen diameter is essential for lung function, and disruption of lumen diameter lies at the heart of a number of

human diseases such as polycystic kidney disease, hypertension and ischemic injury. In the lung understanding how lumen diameter is regulated may shed light on the pathogenesis of cystadenomatoid malformations, pulmonary hypertension and even asthma where narrowing of the upper airways occur. *In vitro* studies have shown that apical-basal cell polarity, cell-cell adhesion and establishment of an apical membrane are pre-requisites for lumen formation. In the lung, when new buds form from existing branches, the new lumen remains contiguous with that from the original bud, thus generating a lumen for the new bud/tube (Hogan and Kolodziej, 2002; Lubarsky and Krasnow, 2003) (Fig. 1.2.1).

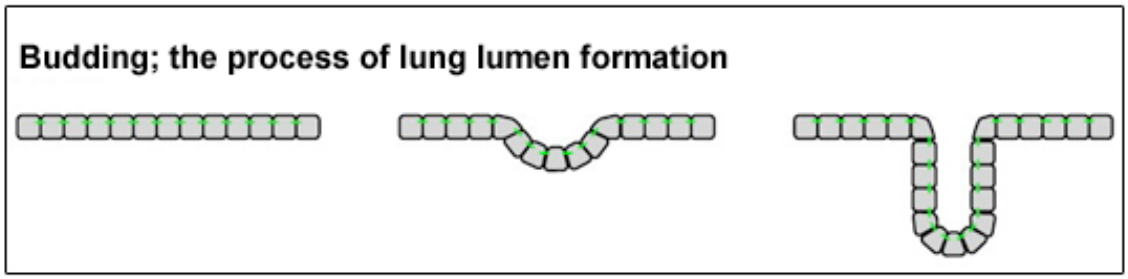


Figure 1.2.1. Lumen formation in the embryonic mouse lung occurs via a process known as budding. Apical restriction allows cells within a single plane to extend out orthogonal to the plane of the epithelium. The new tubule remains continuous with the surrounding epithelium.

Budding is driven in part by apical constriction, a cell shape change that promotes the inward bending of a polarised epithelium (Sawyer et al., 2010). Localised activation of Rho kinases at the apical surface is critical for apical constriction and is bought about by transcriptional activation of signalling cascades as well as the apical localisation of key actin binding proteins including Shroom3 in vertebrates and folded gastrulation and DRhoGEF2 in *Drosophila* (Barrett et al., 1997; Dawes-Hoang et al., 2005; Hacker and Perrimon, 1998; Haigo et al., 2003; Hildebrand, 2005; Kolsch et al., 2007; Nishimura and Takeichi, 2008; Sawyer et al., 2010). The localised Rho kinase (Rok in Drosophila and ROCK1 and ROCK2 in mammals) activity at the apical membrane results in the local accumulation and activation of non-muscle myosin. Myosin contractions result in apical constriction through the tethering of the actin-myosin cytoskeleton to the circumferential apical adherens junctions. This mechanism has been referred to as the "purse-string" whereby apical constriction is driven by a continuous purse-string like contraction of the actin-myosin belt underlying the adherens junctions (Rodriguez-Diaz et al., 2008). However live imaging studies carried out by Martin et al., revealed in *Drosophila* mesoderm formation apical restriction appears to occur via a ratcheting mechanism (Martin et al., 2009). This involves repeated asynchronous myosin contractions at the medial apical cortex that pulls the adherens junction's inwards. The constrictions are maintained by the actin-myosin belt underlying the adherens junctions, such that the apical area reduces with every contraction thus driving cell shape changes required for remodelling of epithelial tubes (Martin et al., 2009).

1.2.7 Embryonic lung development and adult disease

During embryonic lung development there are many factors that can affect the overall function of the lung post birth. These include human prematurity, oxygen exposure, corticosteroid exposure, incorrect amounts of growth factor such as platelet-derived growth factor, FGF, vascular endothelial growth factor (VEGF), transforming growth factor (TGF)-β signalling, abnormal regulation or injury of the pulmonary capillary vasculature, all of which can result in hypoplasia of the alveolar surface, leading to insufficient gas exchange, especially during stesses such as exercise or low oxygen environments (Warburton et al., 2006).

Later in adult life, during ageing, progressive involution or degeneration of the lung occurs, which can be accelerated by environmental factors such as tobacco smoke, smog, industrial pollutants, toxic inhalants and infectious agents. As a result of these environmental factors increasing within industrialised societies chronic obstructive pulmonary disease (COPD) has become one of the leading causes of death worldwide. COPD is a multi-factorial disease that encompasses chronic bronchitis and pulmonary emphysema. The molecular and cellular events that result in COPD are poorly understood but are known to involve aberrant differentiation, inflammation, structural damage in the distal lung with enlargement of the alveolar spaces and tissue remodelling. While COPD has been extensively linked with cigarette smoke, only 15% of smokers develop emphysema thus suggesting there must be some genetic factors contributing to this disease (Sharafkhaneh et al., 2008; Shi et al., 2009; Siafakas and Tzortzaki, 2002; Warburton et al., 2006). Microarray profiling and genome-wide association studies in both human patients and animal models have revealed genes previously associated with developmental processes to be implicated in COPD. Identified pathways include Sonic hedgehog, Notch, Retinoic acid signalling

and Tgfβ. Therefore recent studies have begun focusing on understanding whether these developmental regulators become re-activated during lung-injury, or whether subtle changes during development such as altered differentiation of progenitor cells, predispose individuals to COPD or influence the severity of the disease once triggered by environmental factors (Shi et al., 2009).

1.3 Kidney Development and branching morphogenesis

Kidney development in the mouse begins when the ureteric bud (UB) emerges from the wolfian duct at E10.5 and invades the surrounding meteneprhic mesenchyme (MM). The UB undergoes a complex process of growth, branching and remodelling, to eventually give rise to the entire urinary collecting systems, including the collecting ducts, calyces, pelvis and ureter (Costantini, 2006; Ishibe et al., 2009). These early events in renal branching morphogenesis have been studied in the mouse by observing kidney development in organ cultures using the transgenic strain that expresses eGFP specifically in the UB epithelium under the Hoxb7 promoter and time-lapse imaging (Caruana et al., 2006; Srinivas et al., 1999; Watanabe and Costantini, 2004). When explanted at E11.5 and cultured on a filter at an air-medium interface, the kidney will grow for about 7 days, during which the early stages of UB branching morphogenesis and nephrogenesis occur in a similar, but slower way to that *in vivo* (Costantini, 2006). These studies revealed the tip of the UB branch first forms a swollen rounded ampulla, which is gradually remodelled into a laterally elongated structure that then gives rise to two new branches. Recent data by Shakya et al., suggests the UB trunk as well as the ampulla contributes to the next generation of branches (Shakya et al., 2005).

Trifid branching also occurs in the kidney, more frequently in the second round of branching, instead of the ampulla giving rise to two new branches it gives rise to three new branches. Only some of these trifid branch points are maintained throughout development, in most cases, these will remodel to form bifid branch points indicating these branch points are transient structures. Lateral branching also occurs in the kidney in a similar manner to domain branching in the lung, instead of an ampulla forming a new branch instead it is generated from the side of an existing branch (Watanabe and Costantini, 2004).

The cellular events responsible for subsequent ureteric bud branching during development of the kidney are not well known. Orientated cell division, changes in cell shape (Meyer et al., 2004) or cell movements within the epithelium (Chi et al., 2009) may contribute to ureteric bud branching but their role in early stages of kidney branching and ureteric bud initiation remains unclear. However at later stages of kidney branching, when narrowing of the collecting ducts occurs, the cellular events are better understood. Postnatal elongation of the medullary collecting ducts is driven by cell division in a single, uniform orientation along the long axis of the duct, this planar polarised cell division, is thought to be a form of planar cell polarity (Fischer et al., 2006). Since little cell migration occurs at this stage, the longitudinally orientated cell division leads to elongation of the collecting ducts without altering their diameter. Interestingly orientated cell division is disrupted in the kidneys of a number of mouse mutants e.g. Fat4 and Wnt9b and this results in a progressive increase in ductal diameter (Fischer et al., 2006) (Saburi et al., 2008) (Karner et al., 2009). In addition to its role in orientated cell division Karner et al. also showed Wnt9b to be involved in convergent extension movements that allow the collecting ducts to elongate and become narrower as cells intercalate along the

trunk of the duct. By E15.5 most collecting duct cells are elongated with their long axes perpendicular to the long axis of the duct, however collecting duct cells in the Wnt9b hypermorph were randomly organised and ductal diameter increased, thus concluding that Wnt9b appears to act at different stages to regulate orientated cell division and intercalative cell movements (Karner et al., 2009).

1.3.1 Formation of specialised Kidney structures

Reciprocal signalling between the ureteric bud and the metenephric mesenchyme results in elaborate branching of the ureteric bud and induces MM cells to condense around the UB tips at E11.5. Mesenchymal to epithelial transformations (MET) induced at the tip of these ureteric bud branches form the nephrons, the glomeruli, proximal tubules, loop of Henle and distal tubules (Costantini, 2006; Saxen and Sariola, 1987). The final outcome of the interplay between the UB and MM determines the final nephron number and ensures correct development of the kidney (Ishibe et al., 2009). Many in vitro studies have shown a number of factors to be involved in this process by either stimulating (Gdnf, Fgf2, Fgf7, Fgf10, Hgf, Egf and pleitropin) or inhibiting (Bmp4, activin A and semaphorinchck sp.) ureteric branching (Bates, 2007; Costantini, 2006; Ishibe et al., 2009; Sainio et al., 1997; Sakurai et al., 2001; Tufro et al., 2008).

The continuation of UB branching requires proliferation and cell migration at the UB tip along with alterations in tissue morphology that create the branch point. Pollack et al., modelled this process by growing renal epithelial cells in cysts *in vitro* and stimulating them with factors that promote branching morphogenesis resulting in the formation of new branches from the cysts grown in culture (Pollack et al., 1998). In the developing kidney, PI 3-kinase, Pkc, Plc, Src, Fak and Jak/Stat, are some

of the downstream signalling pathways which are crucial for cytoskeletal remodelling and cell-cell junction reshaping in kidney branching morphogenesis (Ishibe et al., 2006; Ishibe et al., 2004; Ishibe et al., 2003; Karihaloo et al., 2005; Liu et al., 2002; O'Brien et al., 2004; Ponzetto et al., 1994; Rosario and Birchmeier, 2004; Weidner et al., 1993; Woolf et al., 1995).

Differentiation within the kidney is an integral part of its development, with correct proximal and distal patterning essential for its correct formation. The kidney forms in a proximal to distal fashion, with the internal medullary epithelia forming first and is thus the most undifferentiated, whilst the outer cortical epithelia is formed later and as a result is the least differentiated (Marose et al., 2008). The mesenchymal cells that condense at the tips of the ureteric bud branches express a unique combination of markers including Six2, Gdnf, Cited1 which define a stem cell population. Mesenchymal to epithelial transformations begin with cap mesenchyme polarising into a primitive epithelial sphere known as the renal vesicle, in response to the expression of addition markers such as Wnt4 and Pax8. Cells in the metanephric mesenchyme that do not aggregate at the bud tips express Foxd1 and the retinoic receptors (RARs) and mark the stromal population. The renal vesicle fuses to the ureteric stalk, which forms the collecting ducts, and generates an S portion of the S-shaped body with a proximal and distal cleft. The proximal cleft is infiltrated by endothelial cells and forms the glomerular tuft. The proximal portion of the S-shaped body activates the notch pathway, as seen by the presence of the cleaved Notch intracellular domain. The nephron begins to take shape as glomerular development proceeds and the more proximal tubules elongate and grow towards the medulla to form the descending and ascending limbs of the loop of henle. Notch signalling is

essential for the proximodistal patterning of the nephron, as Notch2 mutations delete all proximal cell types and structures. (Cheng et al., 2007; Dressler, 2009)

1.3.2 Glomeruli

The glomerulus is the most proximal component of the nephron and is responsible for ultrafiltration of plasma through its barrier wall, which consists of a capillary loop bound by mesangialcheck spelling cells, enveloped in podocytes, and enclosed by bowmens capsule. The filtrate flows from the glomerular space through the neprhon tubule, consisting, in sequence, of the proximal tubule, loop of henle and distal tubule which joins a collecting duct (CD). The collecting system itself is made up of the cortical and medullary collecting ducts, calyces, papilla and ureter.

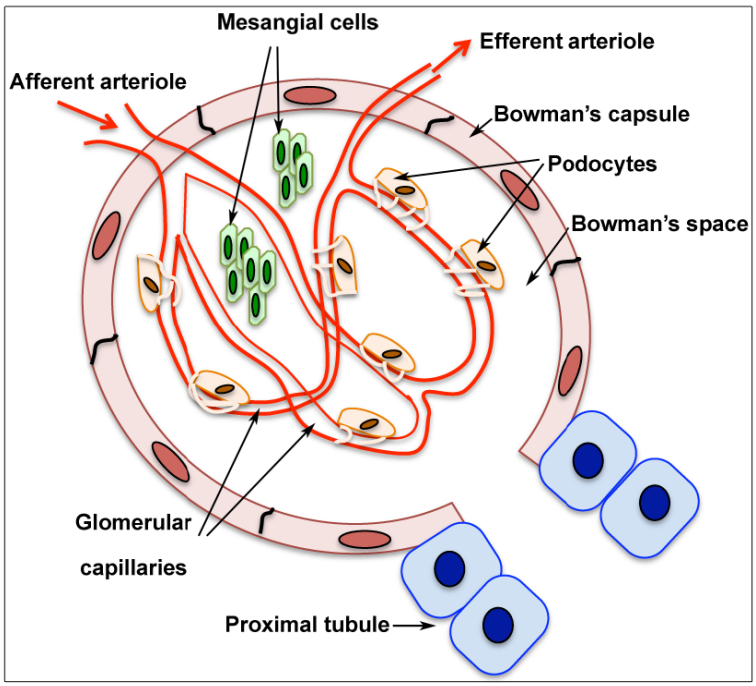


Fig 1.3.1 Schematic diagram of a glomeruli. The glomeruli consists of a the bowmans capsule which encases a capillary loop, that associates with the highly specialised epithelial cells, the podocytes that are required for the filtration of plasma molecules.

Plasma molecules such as water, sugars, electrolytes and small proteins are sieved through the glomerular barrier wall based on their size, and possibly also by their charge as well (Goldberg et al., 2009; Haraldsson et al., 2008; Harvey et al., 2007; Quaggin and Kreidberg, 2008). All three layers of the glomurular capillary wall are required for correct function in the filtering process (Patrakka and Tryggvason, 2009). Podocytes are highly specialised epithelial cells that are important for proper glomerular filtration to occur. Many kidney disorders arise as a result of mutations in genes that encode proteins with highly specialised functions in podocytes, such as α-actinin-4 (Kaplan et al., 2000), nephrin (Kestila et al., 1998), the phospholipase C epsilon gene (Hinkes et al., 2006) and podocin (Boute et al., 2000). These are important in maintaining the protein barrier, thus preventing a massive loss of proteins from the circulation (a process known as the nephritic syndrome). Mutations in these genes cause disruption of the filtration barrier as a result of rearrangement of the actin cytoskeleton. In addition, other genes involved in regulating plasticity of the podocyte actin cytoskeleton such as synaptopodin (Asanuma et al., 2005; Asanuma et al., 2006) are also crucial in maintaining the protein barrier (Faul et al., 2007).

1.4 The role of Scribble in apical-basal and planar polarity

Vertebrate epithelial tissue exhibits two types of polarity 1. Apical basal polarity (A/B polarity) perpendicular to the epithelial plane and 2. Planar polarity as described below. Both are required for the correct structuring and organisation of most if not all tissues and organs and defects in either polarity can result in a number of genetic disorders (Courbard et al., 2009; Simons and Mlodzik, 2008). Apical-basal polarity allows organs such as the lung, kidney and vasculature to form organised lumen

critical for their functions. The epithelial plasma membrane has an apical surface facing the lumen and a basolateral surface, which contacts adjacent cells and the underlying extracellular matrix. The apical and basal membranes are composed of different proteins and lipids that are specialised for the varying functions of the two membranes. For example in recent years studies have shown phosphoinositides to be key markers of membrane identity. In mammalian epithelial cells phosphatidylinositol 4,5-bisphosphate (*PtdIns*(*4,5*)*p2*) is a key determinant of the apical surface whereas phosphotidylinositol 3,4,5 triphosphate (*PtdIns*(*3,4,5*)*p3*) is a key determinant of the basolateral membrane (Di Paolo and De Camilli, 2006; Gassama-Diagne et al., 2006; Martin-Belmonte et al., 2007; Martin-Belmonte and Mostov, 2008). Apical and basal membranes are separated by cellular junctions such as tight and adherens junctions in vertebrates and septate junctions in invertebrates, which prevent the crossing of proteins and lipids between the two surfaces.

Three protein complexes have been identified that play a major role in establishing and maintaining A/B polarity; the crumbs (Crb) complex comprised of Crb, Stardust (Sdt) and Patj; the Par3/Bazooka (Baz) complex, comprised of Baz, Par6 and atypical protein kinase C (aPKC); and finally the Scribble complex, consisting of Scrib, Lethal giant larve (Lgl) and Discs Large (Dlg) (Assemat et al., 2008; Humbert et al., 2008). Work in *Drosophila* has shown the Crumbs complex to be most apically localised followed by the Par3/Baz complex, which is associated with the apical junctional areas, and the Scribble complex is localised to the septate junctions just basal to the adherens junction. Many of the proteins that comprise these complexes contain PDZ-protein-protein interaction domains, with Sdt, dPatj, Baz Dlg along with Scribble having multiple PDZ domains. The Par complex plays a role in polarity and spatial organisation in almost all metazoan cells whereas the Crumbs complex

appears more specific to epithelial cells. The three complexes interact to define the apical and basolateral surfaces of epithelial cells in *Drosophila* (Bilder et al., 2003; Tanentzapf and Tepass, 2003). The Par3/Par6/aPKC complex is crucial in regulating polarity (Munro, 2006) and Par3 in mammals localises to (Izumi et al., 1998) and functions in the assembly of the tight junctions (Chen and Macara, 2005) at the apical/lateral boundary whereas Par6/aPKC are required to maintain the apical domain (Martin-Belmonte et al., 2007). Par6 acts as a targeting subunit for aPKC which in turn recruits both the Crumbs (Hurd et al., 2003; Lemmers et al., 2004) and Scribble complex as substrates (Betschinger et al., 2005).

While studies in recent years have revealed more about how these complexes operate our understanding is still incomplete in more than one way, for example it is still not clear how phosphoinositides are connected to the polarity complexes. It is thought that the small GTPase Cdc42 may have a connecting role between phophoinositides and the polarity complexes as it is well known that *PtdIns*(*3,4,5*)*P3* and *PtdIns*(*4,5*)*P2* can function in positive feed back loops with Rho family GTPases such that recruitment and activation of these GTPases to the plasma membrane occurs where they modulate actin dynamics in various cell types (Etienne-Manneville and Hall, 2002; Yin and Janmey, 2003). Studies in both *Drosophila* and the 3D MDCK cell model reveal *PtdIns*(*4,5*)*P2* can induce the recruitment of Cdc42 (Martin-Belmonte and Mostov, 2007). Cdc42 is also known to bind the Crib domain of Par6 and is necessary for the correct localisation of Par6/aPKC as well as for normal apico-basal polarisation of *Drosophila* neuroblasts and epithelial cells (Atwood et al., 2007; Hutterer et al., 2004).

Much of the work investigating the function of Scribble to date, has been carried out in *Drosophila* where this protein is required for apical-basal polarity (as

mentioned above). Whereas, in vertebrates, Scribble is required for planar cell polarity (see below). (Metais et al., 2005; Montcouquiol et al., 2003; Murdoch et al., 2003; Nakagawa and Huibregtse, 2000).

Components of the Scribble complex, Scribble itself, Discs Large (Dlg) and Lethal Giant Larvae (Lgl) were originally identified in *Drosophila* whereby homozygous mutants in all of these genes resulted in a loss of apical-basal polarity and neoplastic tissue overgrowth (Bilder and Perrimon, 2000; Mechler et al., 1985; Woods and Bryant, 1989). As a result of their similar mutant phenotypes and genetic interactions it was concluded that these were operating within the same pathway to regulate the establishment of apical-basal polarity in epithelial cells (Bilder et al., 2000). There is only one known Scribble gene in the mouse, whereas there are four Dlgs, Dlg1, Dlg2, Dlg3 and Dlg4 and two Lgls, Lgl1, and Lgl2 (Dow et al., 2007; Humbert et al., 2006; Martin-Belmonte and Mostov, 2008).

Scribble is a large cytoplasmic protein and member of the LAP and PDZ protein family (Kallay et al., 2006). Scribble contains 16 leucine rich-repeats (LRR) and four PSD-95, ZO-1 and Discs large (PDZ) domains (reviewed by (Bryant and Huwe, 2000; Santoni et al., 2002). In *Drosophila* epithelial cells, Scribble localises to the cortex, basal to the adherens junctions, at the septate (basolateral) junctions (Bilder and Perrimon, 2000). In mammalian cells Scribble has shown to be localised basally with overlapping expression at the adherens junctions (Dow et al., 2003; Navarro et al., 2005). Studies have shown the LRR region and PDZ regions of *Drosophila* Scribble to be highly important for its localisation and stability at the plasma membrane (Albertson et al., 2004; Zeitler et al., 2004). In addition it appears the LRR domain is evolutionary conserved as point mutations in this domain in both mouse and worm (*Caenorhabditis elegans*) result in mislocalisation of the protein

(Dow et al., 2007; Legouis et al., 2003; Zarbalis et al., 2004). Even in humans, structure-function analysis suggests both the LRR and PDZ domains are required for its correct localisation (Nagasaka et al., 2006; Navarro et al., 2005).

The discovery of Scribble's role in planar cell polarity (PCP) in mammals along with other genes such as PTK7 suggest as organisms became evolutionarily more complex additional proteins are necessary for the correct establishment of PCP (Wang and Nathans, 2007). PTK7 and Scribble mutants exhibit classic PCP phenotypes and moreover show genetic interactions with Vangl2 (Lu et al., 2004; Murdoch et al., 2001b). The frizzled ligands Wnt11 (Zhou et al., 2007b) and Wnt5a (Qian et al., 2007) have also been shown to function in the regulation of PCP.

Scribble$^{Crc/Crc}$ mouse mutants display craniachichisis, the most severe form of failed neural tube closure (Murdoch et al., 2003) as well as disruption to the polarity of inner ear hair cells (Montcouquiol et al., 2003), classic PCP mutant phenotypes. Vangl2 a core component of the PCP pathway and Scribble show colocalised expression patterns and have strong genetic interactions. As discussed above, in addition to its role in planar cell polarity Scribble is expressed in the tight junctions of epithelial cells that are located just below the apical surface. Knockdown of Scribble has been shown to affect apical-basal polarity in *Drosophila* and some mammalian systems. Therefore it is thought Scribble may act as an important link to couple the two polarities; Planar polarity and apical-basal polarity (Courbard et al., 2009).

1.5 Planar Cell Polarity

The planar cell polarity (PCP) pathway is best known for directing polarisation of cells orthogonal to the axis of apical-basal polarity within the plane of an epithelium. PCP signalling has been shown to control the polarity of numerous epithelia in both

Drosophila and vertebrates (Jones and Chen, 2007; Klein and Mlodzik, 2005; Wang and Nathans, 2007; Zallen, 2007).

1.5.1 Drosophila PCP

The PCP genes were initially identified as a result of spontaneous mutations that caused disruption to the organisation of wing hair cells, bristles on the abdomen and photoreceptors in the eye of *Drosophila melangaster* (McNeill). The genes were named according to the pattern of disorganisation they caused once mutated; *dishevelled* (*dsh*) and *frizzled* (*fz*) (Gubb and Garcia-Bellido, 1982), van gogh (vang, also known as *strabismus*) (Taylor et al., 1998) and starry night (stan also known as *flamingo* [*fmi*]) (Chae et al., 1999). These along with prickle (pk), and diego (dgo) (Feiguin et al., 2001) comprise the core PCP genes. Genetic analysis suggests these genes work together to establish PCP in all tissues and form part of what is now referred to as the non-canonical Wnt or planar cell polarity signalling pathway. Wnts have long been thought to play a role in PCP signalling as Frizzled, a seven-transmembrane receptor functions as a receptor for Wingless (Wg) and Dishevelled is a cytoplasmic transducer of the Wg pathway. While direct loss of Wg does not lead to disrupted PCP it was hypothesized that a Wnt activated morphogen gradient could direct PCP establishment. However, despite extensive work investigating the role of a number of Wnts in PCP signalling, neither over expression nor loss of function resultes in disrupted PCP in the wing (McNeill). Despite Wnts seemingly unimportant role in establishing PCP in *Drosophila*, studies in vertebrates suggest Wnts may have permissive roles in establishing PCP.

During early *Drosophila* development, the core PCP proteins initially localise to the apical junctions (Axelrod, 2001; Bastock et al., 2003; Das et al., 2004; Jenny et al.,

2003; Strutt and Strutt, 2002; Tree et al., 2002), but by the pupal stage, they redistribute and localise asymmetrically in the cell. Fz, Dsh and Dgo all localise to the distal side of each cell in the wing, at the site where the hair will eventually emerge. Vang and Pk localise to the proximal side of the cell, whilst Fmi is expressed at both proximal and distal ends. A similar polarized localisation of the core PCP proteins is observed in the eye, however as the eye is a more complex system the pattern of localisation is therefore more complex. Studies have revealed direct protein-protein interactions between core PCP proteins: Diego and Pk bind Dsh (Jenny et al., 2003; Tree et al., 2002); Fmi binds Vang (Wu and Mlodzik, 2008) and Fz (Chen et al., 2008); and Vang binds Pk and Dsh, which is the likely reason for the asymmetric localisation of these proteins within the cell.

1.5.1.1 The Fat/Ds/Fj PCP cassette

The Fat/Ds/Fj PCP cassette (Casal et al., 2002; Matakatsu and Blair, 2004; Rawls et al., 2002; Simon, 2004; Yang et al., 2002; Zeidler et al., 1999) comprises another group of PCP genes that includes the large cadherins, Fat and Dachsous (Ds) and the golgi-associated kinase Four-jointed (Fj). These genes have also been shown to regulate PCP in all tissues in *Drosophila* but do not asymmetrically localise in the cell, like the core PCP genes. Instead Fat and Ds expression is graded accross the tissue, e.g. in the *Drosophila* wing Ds is highly expressed in the proximal region and is absent from the distal region. Fj however is expressed in the opposite formation; high levels are observed in the distal region with decreasing expression further towards the proximal regions. Fat is expressed evenly throughout the wing. The Fat/Ds/Fj cassette is thought to establish PCP by direct protein-protein binding of the individual components. Ds binds Fat to inhibit Fat PCP activity (Ma et al., 2003; Yang et al.,

2002) and Fat regulates the expression of Fj by binding directly to the transcriptional repressor Atrophin (Fanto et al., 2003). The Fat/Ds/Fj cassette was initially thought to act upstream of Frizzled in PCP signalling (Ma et al., 2003; Yang et al., 2002) although some studies now suggest Fat and Ds function in parallel to Frizzled PCP signalling (Casal et al., 2006).

1.5.2 Asymmetric localisation of PCP proteins

Core PCP proteins have been shown to asymmetrically localise to the apical cell surface. At the apical surface, further asymmetric localisation of PCP proteins occurs so that the Celsr1-Vang-prickle proteins form a complex and colocalise to the proximal side of the cell while the Fzd-Dvl-Celsr1 complex localises to the opposite (distal) side of the cell (refs in here). *Drosophila* work has shown that this polarity is initiated by a gradient of Fat and Ds in the cell. Fat and Ds localise to opposite sides of the cell and form heterodimers to allow cell-cell communication (Axelrod, 2009). This first cue of planar polarity leads to the alignment of the microtubules at the apical side of the cell in a – to + orientation towards the distal side of the cell where Ds is localised. Loss of Ds leads to random polarisation of the microtubule. At the proximal side of the cell Celsr1-Vang-Pk complex competes with the Celsr1-Fzd-DVL complex, resulting in the packaging of the Celsr1 fzd dvl complex into vesicles that travel on the microtubules to the proximal side of the cell, thus establishing the polarized localisation of the core PCP proteins (Axelrod, 2009) (see Fig. 1.4.1).

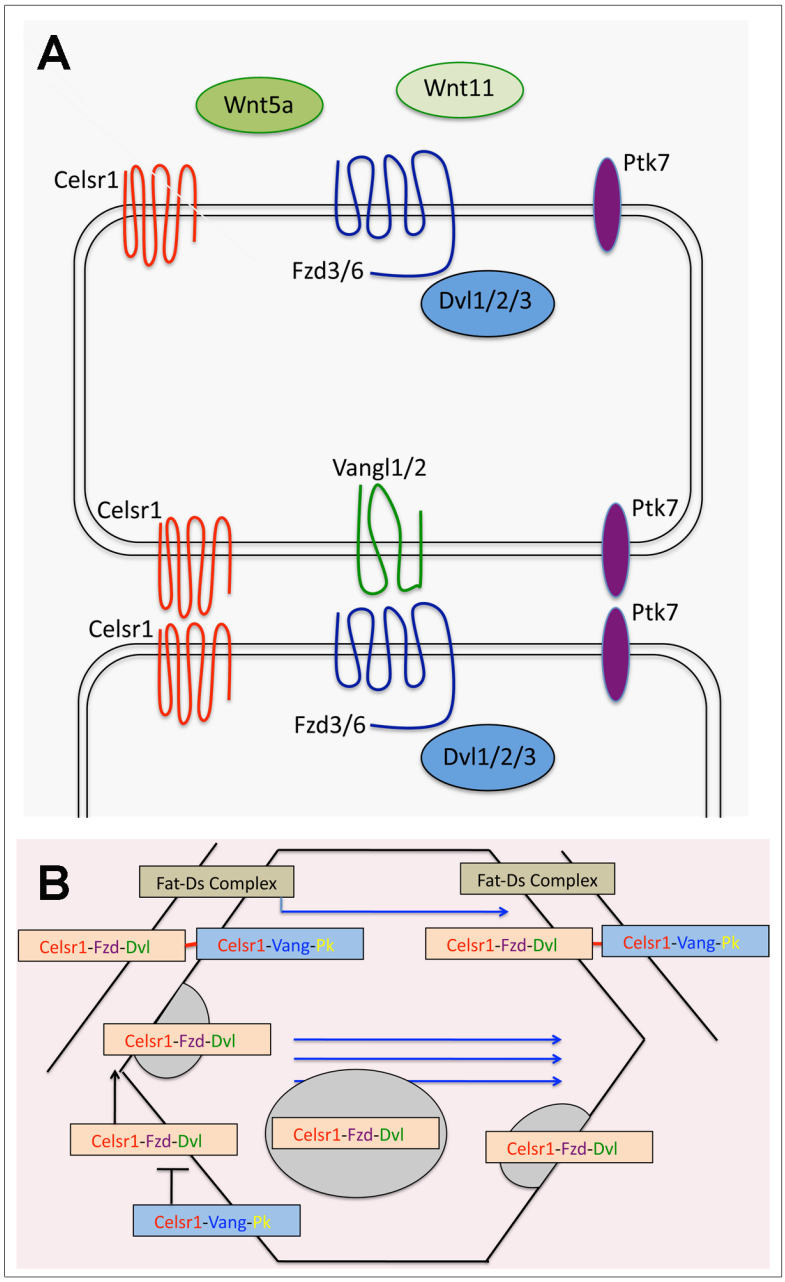


Figure 1.4.1 Asymmetric localisation and transport of PCP proteins. (A) The core PCP proteins; Vangl1, 2, Fzd3, 6, Dvl1, 2,3 and Celsr1, are asymmetrically localised on the apical cell membrane. (B) The Fat-Dachous (Ds) complex is known to position the majority of the apical microtubules in one direction. The Celsr1-Vang-Pk complex blocks the Celsr1-Fzd-Dvl complex on the proximal side of cells. The Celsr1-Fzd-Dvl complex then gets recruited to the distal side of cells by vesicle transport on the microtubules, thus establishing planar polarity.

1.5.3 Mammalian PCP

Planar cell polarity is also required to correctly pattern mammalian systems. Many studies over recent years have documented similar roles for *Drosophila* core PCP homologs in mammals, suggesting this pathway is evolutionary well conserved.

Loss of *Fzd6*, (*mammalian ortholog of Drosophila frizzled*) *Vangl2* (homolog of *van gogh/strabismus)* or *Celsr1* (a homolog of *Fmi/Stan*) leads to disorganised fur on the back of a mouse with swirls that are reminiscent of those observed on the wing of a fly with mutations in PCP genes (Devenport and Fuchs, 2008; Guo et al., 2004). Mutations in *Vangl2*, *Celsr1*, *Fzd3/6* and *Dvl1/2* (orthologs of *Drosophila dsh*) result in disrupted orientation of the sensory hair cells in the organ of Corti in the mouse inner ear (Curtin et al., 2003; Montcouquiol et al., 2003), defects which result in deafness. While there are similarities between the function of the core PCP genes in *Drosophila* and mammals there are some very striking differences. The extent to which PCP signalling operates between flies and vertebrates has not been fully investigated, in part because many *Drosophila* PCP components have yet to be examined in vertebrates, but also because analysis of the PCP pathway in mammals is complicated further by the existance of multiple family members of many PCP genes in mammals leading to a much more complex system.

1.5.3.1 Ceslr1

Ceslr1 (*Drosophila* homologue stan (starry night) or flamingo) is part of a family of proteins known as Celsr/flamingo all of which are seven-pass transmembrane atypical cadherins. The seven transmembrane domain is homologous to the second largest family of G-protein-coupled receptors (GPCR); the secretin family or Family B (Strader et al., 1995) which is coupled to a large extracellular region containing a

number of conserved motifs including extracellular EGF-like (Davis, 1990) and Laminin-G domains (Timpl et al., 2000) as well as nine protocadherin repeats capable of homeophilic interaction (Devenport and Fuchs, 2008; Shima et al., 2007; Shima et al., 2004; Usui et al., 1999; Witzel et al., 2006; Yagi and Takeichi, 2000). This unique combination of domains within the Celsr/Flamingo family allows these proteins to signal directly following self-recognition across neighbouring cell interfaces as well as via heterophilic ligand/receptor interactions(refs). Flamingo is the *Drosophila* seven transmembrane cadherin and along with the three mammalian orthologous Celsr1, Celsr2 and Celsr3 comprise the Celsr/Flamingo family (Formstone and Little, 2001; Shima et al., 2002). Flamingo is believed to act at the top of the PCP pathway hierarchy in *Drosophila*, and as such, is thought to be required for the correct localisation of other PCP proteins (Seifert and Mlodzik, 2007; Strutt, 2001). All three Celsr genes in the mouse, Ceslr1, 2 and 3 have been associated with brain and neural tube development in mice (Curtin et al., 2003; Tissir et al., 2002a; Tissir and Goffinet, 2006; Zhou et al., 2007a). Two independent ENU-generated mutant mouse alleles of Celsr1, *crash* (*Crsh*) and *spin-cycle* (*Scy*) display characteristic PCP defects such as misorientation of sensory hair cells within the inner ear along with the most severe neurulation defect craniorachischisis (Curtin et al., 2003). Interestingly a recent study by Formstone et al., demonstrated a novel distribution of Celsr1 to the extreme basal domain of neuroepithelial cells both within the early neural tube and in a population of cells at the dorsal ventral midline of the developing spinal cord, an absence of this expression is observed in the Celsr1 mouse mutant *Crsh* (Formstone et al., 2010a) indicating a novel role for this protein.

1.5.3.2 Vangl2

Vangl2 is the homologue of *Drosophila* strabismus/van gogh. Both mammalian and *Drosophila* Vangl2 contain two putative transmembrane domains and a PDZ-binding domain consistent with conserved functional properties. The mouse has two Vangl genes, Vangl1 and 2, which share ~70% homology. Relatively little is known about the role of Vangl1, but like Celsr1, Vangl2 has been studied in detail, with respect to its role in PCP and convergent extension (Kibar et al., 2007; Montcouquiol et al., 2006; Torban et al., 2007; Ybot-Gonzalez et al., 2007). Studies have shown human missense mutations in both Vangl1 and Vangl2 result in neural tube defects (Kibar et al., 2009; Lei et al., 2010). Recently, Torban et al, generated a mouse mutant bearing an inactivating mutation at Vangl1 (Vangl (gt)). *Vangl1*$^{gt/+}$ heterozygotes and *Vangl1*$^{gt/gt}$ homozygotes were viable and fertile, although *Vangl1*$^{gt/gt}$ displayed subtle defects in planar polarity e.g. alterations in the polarity of inner hair cells of the cochlea. Interestingly *Vangl1*$^{gt/+}$*; Vangl*$^{Lp/+}$ double heterozygotes showed severe developmental defects that included; severe craniorachischisis, disorganization of the stereociliary bundles of hair cells of the organ of Corti, and cardiac abnormality, despite *Vangl1*$^{gt/+}$ being healthy. Thus providing evidence that genetic interactions between Vangl1 and Vangl2 result in aberrant planar polarity and subsequent developmental defects (Torban et al., 2008).

1.5.4 PCP signalling and kidney development

PCP genes such as *Vangl2* (Montcouquiol et al., 2003; Qian et al., 2007; Torban et al., 2008) and *Celsr1* (Curtin et al., 2003) are known to be required for correct patterning and extension of the complex organ of Corti within the cochlea. As a result of early work carried out in *Xenopus* and *Zebrafish*, it was discovered PCP genes were also

required for convergent extension (Djiane et al., 2000; Heisenberg et al., 2000; Wallingford et al., 2000). This in turn lead to the discovery that core PCP genes are required to regulate the polarised cell movements during development such as convergent extension in mammals e.g. in neural tube closure (Curtin et al., 2003; Goto and Keller, 2002; Kibar et al., 2001b; Murdoch et al., 2003; Wang et al., 2005). It has also been shown that these PCP genes can mediate directed movement of groups of cells and are required for female reproductive tract development, cardiac outflow tract formation and kidney tubule development (Bastock and Strutt, 2007; Henderson et al., 2006; Karner et al., 2009; Lawrence et al., 2004; Vandenberg and Sassoon, 2009).

Studies showing mutations in the Dgo homolog inversin in *Zebrafish* were the first indication of PCP functioning in the kidney; disruption of this gene can lead to cystic kidney disease (Otto et al., 2003). Interestingly, Inversin is a micro-tubule-associated protein essential for cilia morphogenesis (Watanabe et al., 2003) and this is not the first ciliary protein to be associated with PCP signalling or kidney dysfunction. Bardet-Biedl syndrome protein 4 (BBS4) is also implicated in planar polarity and convergent extension (Park et al., 2006; Ross et al., 2005).

In addition to its requirement for cilia morphogenesis, Simons et al., also showed inversin to control the balance between canonical and non-canonical Wnt (PCP) signalling (Simons et al., 2005). Another recent publication showed an interesting link between one particular Wnt ligand, Wnt9b, and non-canonical PCP signalling in both kidney development and polycystic kidney disease (Karner et al., 2009). During normal embryonic development, kidney tubule diameter dramatically reduces from a diameter of 11 cells/tubule at E15.5 to approximately 4 cells/tubule at P0 (Bacallao and McNeill, 2009). Karner et al. showed that loss of Wnt9b results in

disorganised epithelial cells, that resulted in broader tubes and cyst formation, whereas wildtype epithelial cells were organised such that they were perpendicular to the axis of the tubule which had elongated and narrowed (Karner et al., 2009). This is reminiscent of cells undergoing convergent extension, suggesting cell intercalation may be one mechanism underlying tubule elongation in the kidney.

As a result of studies in flies, showing loss of orientated cell division (Bellaiche et al., 2001; Garoia et al., 2000; Gho and Schweisguth, 1998) and a failure of convergent extension (Djiane et al., 2000; Heisenberg et al., 2000; Wallingford et al., 2000) in PCP mutants, it was hypothesised that defects in PCP gave rise to cystic kidney disease as a result of disrupted oriented cell division and a failure of convergent extension in kidney tubules.

This hypothesis was strengthened further by Saburi et al., and their observations of the Fat4 mouse mutant. Fat4 is an ortholog of *Drosophila* Fat which localises to the primary cilium, an organelle which has already been associated with PCP signalling. The Fat4 mouse mutants display classic PCP phenotypes such as defects in elongation of the cochlea and a broadening of the neural tube (Saburi et al., 2008). $Fat4^{-/-}$ kidneys were significantly smaller than wild-type littermates and displayed cystic dilations as early as E16, which increased in severity with age. Kidney tubules were short and broad and showed randomised spindle orientation leading to disrupted orientated cell division. Loss of Fat in the *Drosophila* wing leads to loss of orientated cell division suggesting the role of fat in controlling cell division is conserved (Baena-Lopez et al., 2005). In fact the Fat/Ds/Fj cassette appears to function in the same way in mammals as in flies, as in $Fat4^{-/-}$, Fjx1, the fj ortholog is transcriptionally up-regulated, as it is in flies. It has also been shown that the cystic phenotype in $Fat4^{-/-}$ is enhanced by loss of Fj ortholog Fjx1 as well as by loss of one or

more copies of *Vangl2*, further supporting the hypothesis that loss of PCP signalling leads to cyst formation (Saburi et al., 2008).

Interestingly Saburi et al., showed Fat4 and Vangl2 both localise to the basal body of the primary cilium in cultured cells (Saburi et al., 2008), an organelle already implicated in polycystic kidney disease and in vertebrate PCP signalling. Recent studies have begun to unravel the relationship between PCP signalling and cilia. (Corbit et al., 2005; Ross et al., 2005; Simons et al., 2005). Loss of the PCP effector genes Fuzzy and Inturned leads to disruption of the cytoskeleton and defects in cilia formation (Park et al., 2006). Park et al., also showed by interfering with Dsh, bronchial epithelial cells lose their cilia as a result of basal body docking disruption (Park et al., 2006). Loss of cilia also leads to defects in convergent extension of the cochlea (Jones et al., 2008). The exact role of cilia in PCP signalling is still largely unknown, recent studies in the cochlea suggest cilia act downstream of PCP signalling as loss of cilia does not affect the asymmetric localisation of the core PCP proteins (Jones et al., 2008).

1.5.5 PCP signalling; differences between *Drosophila* and mammals

Few cells in *Drosophila* are ciliated and cilia have no role in the control of PCP in the wing or eye, suggesting the role of cilia in PCP and cystic kidney disease is specific to vertebrates. Also a number of Wnts in vertebrates appear to regulate non-canonical signalling, e.g. hair cells of the cochlea are misorientated in the Wnt5a mutant mice (Qian et al., 2007) and both Wnt5a and Wnt11 are required for convergent extension in *Xenopus* and *Zebrafish* (Heisenberg et al., 2000; Kilian et al., 2003; Tada and Smith, 2000). Regulation of PCP in vertebrates appears more complicated as recent studies suggest that the ability of a specific Wnt to signal via

canonical versus non-canonical pathways may be caused by the presence of specific co-receptors or additional kinases (Hikasa et al., 2002; Lu et al., 2004; Yamamoto et al., 2008). The receptor tyrosine kinase PTK7, has recently been shown to function in vertebrate PCP as mutants display a failure of neural tube closure and disruption to the inner ear (Lu et al., 2004), interestingly the *Drosophila* homolog Otk has no PCP defects in either the eye or wing (Winberg et al., 2001) again highlighting the differences between the PCP signalling pathway in *Drosophila* and mammals.

1.6 Concluding remarks and Outline of thesis

From the literature it is clear that components of the planar cell polarity pathway are required to modulate normal kidney development. As the kidney is a branched organ and develops in a similar manner to the lung it would be interesting to investigate whether components of the PCP pathway were also required for lung branching morphogenesis. In addition, many of the requirements for a branched organ to develop correctly such as the reorganisation of the actin-myosin cytoskeleton are impacted on by the PCP pathway. Taken together this suggests a potential role of the PCP pathway in lung development. Therefore the main aim of this thesis was to determine the role of three polarity genes, Vangl2, Celsr1 and Scribble in lung branching morphogenesis by studying the well characterised PCP mouse mutants Looptail ($Vangl2^{Lp}$), Crash ($Celsr1^{Crsh}$) and Circletail ($Scribble^{Crc}$).

In addition to understanding the role of Vangl2 in lung development this project aimed to further delineate the role of Vangl2 in kidney development to understand whether common mechanisms exist between different branched structures..

Finally, a further aim of this thesis, was to determine whether Vangl2 was important for adult lung function.

2 Chapter Two : Experimental Procedures

2.1 Genomic DNA preparation for PCR

Ear biopsies taken from adult mice at 28 days post partum (dpp) were digested with 200μl of 10mg/ml Proteinase K (PK) in lysis buffer (50mM Tris HCL, pH 8.5 (from 1M stock), ImM EDTA, 0.5% EDTA, 0.5% Tween 20, from 10% stock) and placed in a water bath at 50-55°C o/n. PK stock solution was prepared by adding 10mg/ml Proteinase K to 50mM Tris-HCL pH 8 (from 1M stock), 5mM $Cacl_2$ (from 100mM stock), 50% v/v Glycerol and ddH_2O. PK was inactivated by heating samples at 95°C for 15 mins.

2.2 Mouse strains and Genotyping

Vangl2^{Lp} mice of the LPT/Le strain were obtained from Jackson Labs (Bar Harbour, USA) and maintained on C3H/HeH background. *Vangl2*^{Lp} mice carry a single nucleotide mutation in the *Vangl2* gene (kibar 2001 and Murdoch 2001). The mutation results in a serine to asparagine substitution resulting in malfunction of the protein product. Homozygotes were identified by the craniorachischisis phenotype and heterozygotes were distinguished by their looped tails. Wildtype littermates were used as control embryos. *Vangl2*^{Lp} mice were also occasionally genotyped for the mutation using a pyrosequencing assay to amplify the mutation directly (For: 5'Biotin-GTCCTGGCGCTTCAAGAGGA, Rev: NNNGGCCAAACAGTGGACCTTGG, Seq: CAGTGGACCTTGGTGA).

Pyrosequencing involves the hybridisation of the primer to a single stranded PCR amplicon that serves as a template, incubated with the enzymes DNA polymerase, ATP sulfurylase, luciferase and apyrase as well as the substrates adenosine 5' phosphosulfate (APS) and luciferin. The first deoxribonucleotide triphosphate (dNTP) is added to the reaction. DNA polymerase catalyses the

incorporation of the deoxyribo-nucleotide triphosphate into the DNA strand, if it is complementary to the base in the template strand. Each incorporation event is accompanied by release of pyrophosphate (PPi) in a quantity equimolar to the amount of incorporated nucleotide. ATP sulfurylase converts PPi to ATP in the presence of adenosine 5' phosphosulfate (APS). This ATP drives the luciferase-mediated conversion of luciferin to oxyluciferin that generates visible light in amounts that are proportional to the amount of ATP. The light produced in the luciferase-catalysed reaction is detected by a charge coupled device (CCD) chip and seen as a peak in the raw data output (Pyrogram). The height of each peak (light signal) is proportional to the number of nucleotides incorporated. Apyrase, a nucleotide-degrading enzyme, continuously degrades unincorporated nucleotides and ATP. When degradation is complete, another nucleotide is added. Addition of dNTPs is performed sequentially. As the process continues, the complementary DNA strand is built up and the nucleotide sequence is determined from the signal peaks in the Pyrogram trace. For all pyrosequencng assays 10μl thermoscientific master mix (AB-0575/DC/LD/A) was added to 8μl H_2O, 0.5μl forward primer (10μM), 0.5μl reverse primer (10μM) and 1ul DNA (5ng/μl) to give a total reaction volume of 20μl. PCR cycling conditions were as follows;

Step 1	95 °C	5 min
Step 2	95°C	15 sec
Step 3	62 °C	30 sec
Step 4	72 °C	15 sec
Step 5	go to step 2 X 38	
Step 6	72 °C	5 min
Step 7	4 °C	hold
Step 8	end	

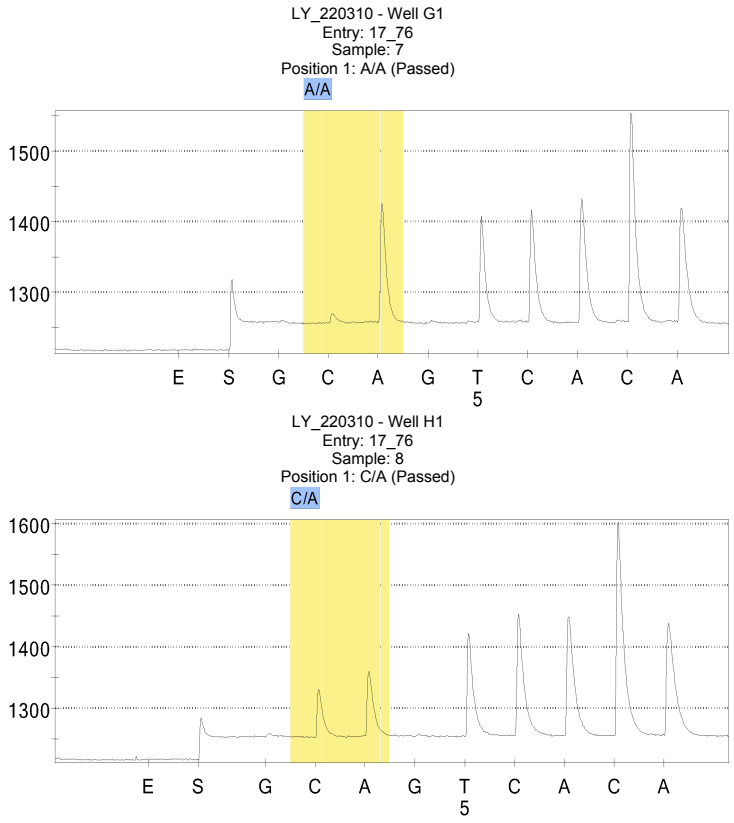


Figure 2.1 Example of Pyrogram trace results for genotyping *Scribble*^{Crc}.

Sample 7 displays a wildtype sample with two copies of adenine. Sample 8 displays a *Scribble*^{Crc} heterozygote with one copy of cytosine and one copy of adenine.

The mouse mutant Circletail (*Crc*) contains a single base insertion that creates a frame shift leading to truncation of the Scrib1 protein that lacks two of its four PDZ domains (Murdoch et al., 2003). *Scribble*^{Crc} mice on a C57BL/6 background, were genotyped by PCR amplification of a 10bp fragment containing the mutation and subsequent sequencing of this fragment (Murdoch et al., 2003) using the following primers, For: GTGGGGTATAGAGGGGGCTA, Rev: GAAAGGCTGTGTACTTCGTTCTG. All primers were synthesized by Eurogentec and thermocycling reactions were carried out on either a Tetrad (MJ Research) or a G-storm (Greiner bio-one) thermocycler.

Celsr1^{Crsh} mice were originally reported in (Curtin et al., 2003) and maintained on BALB/C or C3H/HeH background. *Celsr1*^{Crsh} mice carry a single point mutation that substitutes aspartate for glycine within the highly conserved extracellular domain. The mutation is within the eight cadherin repeat and is likely to reduce extracellular structural integrity of the protein product. *Celsr1*^{Crsh} mice and embryos were genotyped for the mutation itself by using a pyrosequencing assay to amplify the mutation directly (For: NNNGAGAACAGCCCTGTGGGTTCA, Rev: 5'BiotinCATTGCCCTCCACGATCTGA, Seq: GAATAAGGGCCAACG). *Scribble*^{Crc} mice, originally described in (Rachel et al., 2000) and were maintained on a C3H/HeH background or out crossed onto C57BL/6. Genotyping of *Scribble*^{Crc} mice on a C3H/HeH background was carried out by PCR amplification of flanking SNPs at 74.88 (For: NNNCATTGGAAAACATGGGGAGGA, Rev: 5'BiotinAGCATCAGGGACAGGCAAGG, Seq:AAAACATGGGGAGGAC, and 76Mb For: 5'BiotinGACAGTGGGCAAGGCTGACA, Rev:NNNGGCTGCACTTGTCGCTCAGA, Seq: GCTCAGAGGACTCTCATC, annealing temperature 62°C and 38 cycles, followed by pyrosequencing.

2.3 Gel Electrophoresis

The presence of DNA bands after the PCR reaction, before pyrosequencing was carried out by agarose gel electrophoresis. 1% TBE gels were used containing SYBR® Safe (Invitrogen, 10,000X SYBR® Safe DNA gel stain diluted 1:10,000 in agarose gel buffer). Gels were visulaised using an Ultra Violet (UV) gel doc system (Biorad). DNA was mixed with 10% Orange G loading buffer prior to loading, mix 1/5th volume of loading dye to DNA solutions. Band sizes were gauged by comparison to DNA ladder (100-10000bp from Fermentas).

2.4 Dissections

Mouse embryos were harvested between embryonic (E) 11.5 – 18.5 post coitum, with E0.5 being noon on the day of visualisation of the vaginal plug. Lungs and kidneys were micro-dissected in either PBS for subsequent embedding (see below) or in L15 media (Sigma) for explant culture (see below).

2.5 Antibodies and Immunostaining

2.5.1 Fixation and Embedding

Paraffin sections for Haematoxylin and Eosin (H&E) or Periodic-Acid Schiff (PA) staining, and immunohistochemistry were prepared by fixing whole tissue in 4% PFA o/n at 4°C, followed by 2x 30min washes in PBS, and then dehydrated through 25%, 50%, 75%, 100% ethanol for 30mins each at RT. Tissue was then embedded in the desired orientation in parrafin wax and 4μm sections were cut. Cryosections for immunostaining were prepared by fixing whole lungs in 4% PFA for 1h on ice, or whole kidneys for 2h at RT followed by extensive washing in PBS and then placed in in 30% sucrose o/n at 4°C until the tissue had sunk to the bottom of the container.

Tissue was then washed to remove excess sucrose, embedded in OCT, snap frozen and sectioned. Adult kidneys were formalin fixed for 48hours. Adult lungs were inflation fixed with ~ 1.5ml (2ml/40g mouse) formalin for 48hours. Samples were processed for either paraffin embedding or cryopreserved as described above. Longitudinal sections were obtained from the left and accessory lung lobes and transverse sections were obtained from the remaining right lobes. Kidneys were sectioned in Longitudinally.

2.5.2 Haematoxylin & Eosin, Periodic-Acid Schiff Staining and Martius Scarlet Blue trichrome staining.

E14.5, E17.5 and E18.5 lung and kidney paraffin wax sections were deparaffinised in Xylene x2 10mins followed by a graded series of ethanol: 100%, 75%, 50%, 25% (all diluted in water). For H&E staining, sections were immersed in haematoxylin solution to highlight cell nuclei for 6mins rinsed in distilled water and immersed in eosin to highlight the cytoplasm for 90secs, rinsed in tap water and mounted in crystal mount (Invitrogen).

For PAS staining, slides were immersed in Periodic-Acid solution 5mins RT, rinsed x3 in distilled water, immersed in Schiff's reagent 15mins RT, washed under running tap water 5mins and counter stained with haematoxylin solution 90secs, rinsed in running tap water and mounted in Crystal mount (Invitrogen).

For M.S.B trichrome staining sections were washed well in tap water, followed by dehydration in 70% and 100% ethanol. Slides were stained with Weigerts haematoxylin (iron) haematoxylin 20-30mins, washed well in tap water and differentiated in 1% acid alcohol. Weigerts haematoxylin (iron) solution was prepares as follos; a) dilute 1g haematoxylin in 100 ml of 95% alcohol. b) dilute 2mls

60% aqueous ferric chloride in 97 ml of distilled water. Add 1ml concentrated hydrochloric acid. For a working solution mix equal volumes of (a) and (b) prior to use. Slides were rinsed in 95% ethanol and stained with 0.5% martius yellow solution in 2% phosphotunstic acid in 95% alcohol for 10mins. Martius yellow, a small molecule dye, together with phosphotungstic acid in alcoholic solution stains red cells. Early fibrin deposits may be coloured, but the phosphotungstic acid blocks the staining of muscle, collagen and connective tissue fibres. Slides were rinsed in distilled water then stained with 1% brilliant scarlet 6R in 2.5% acetic acid for 10mins then rinsed in distilled water before treating with phosphotunstic acid for 5mins. Brilliant crystal scarlet, a medium sized molecule, stains muscle and mature fibrin. Phosphotungstic acid removes any red stain from the collagen. Slides were again washed in distilled water and stained with 0.5% aniline (soluble) blue in 1% acetic acid for 2mins. The large molecule dye aniline blue stains the collagen and old fibrin. Slides are then rinsed in distilled water and rapidly dehydrating through graded ethanols to isopropyl alcohol (IPA) and immediately mounted in clearium (Surgipath). Nuclei are stained blue/black.

2.5.3 Immunohistochemistry and Immunofluorescence

Wax sections were deparaffinised through a xylene series (see above) and re-hydrated through 100%, 75%, 50% and 25% to deionised water. Cryosections were air-dried for 1h at RT prior to staining.

For rabbit anti-Vangl2 (a gift from M. Montcouquiol) staining, sections were washed in 0.1% Triton X-100 (Sigma) 10mins RT, blocked and primary antibody diluted 1:500 in 10% goat serum (Sigma) containing 0.1% Triton X-100 in PBS. For immunostiaing with all remaining antibodies, sections and wholemounts were

blocked and primary antibodies diluted in PBSBT [PBS containing 1% BSA (Sigma) and 0.2% Triton X-100) and washed in PBS.

2.5.4 Antigen Retrieval

For goat anti-CC10 antibody, antigen retrieval was required to unmask antigens prior to immunodetection. De-waxed slides were heated 2x in 0.01M sodium citrate buffer (stock 100mM 14.7g/500ml ph6, 1:10 dilution in milliQ water) at 60% power in a microwave oven for 6mins, buffer was topped up as necessary. Slides were then cooled to RT and washed in PBS for 2min prior to blocking.

2.5.5 Primary Antibodies

Primary antibodies were diluted as follows: rabbit anti-Celsr1 1:1000, gift from C.Formstone (Formstone et al., 2010b), rabbit anti-Scrib 1:200 Santa Cruz 28737; rhodamine phalloidin 1:20 45 min RT or 1:40 o/n 4°C, Invitrogen R415; mouse anti-Vimentin 1:50, Sigma V630; mouse anti-pan-cytokeratin 1:500, Sigma C2931; rabbit anti-pro-SP-C 1:1000, Chemicon AB3428; rabbit anti-aquaporin-5 1:400, Santa Cruz sc-9890; mouse anti-alpha smooth muscle actin 1:1000, Lab Vision RB-9010 and goat anti-CC-10 1:1000 using antigen retrieval, Santa Cruz sc-9772, rabbit anti-phosphoERK1/2 1:500, Biosource 44-680G; rabbit anti-non-muscle myosin IIA 1:1200, Sigma M8064; rabbit anti-β-catenin 1:500, Sigma C2206; rabbit anti-phospho-histone H3 (pH3) 1:500, Upstate cell signalling 06-570; rabbit anti-cleaved caspase-3 (D175) 1:1000, Cell Signalling 9661S; rat anti-Laminin A chain 1:500, Chemicon MAB1905;.

2.5.6 Secondary Antibodies

Antibodies were detected by incubation for 45min at RT with either: anti-mouse Alexa Fluor 488 or 594, anti-rabbit Alexa Fluor 488 or 594, anti-rat Alexa 488 or 594,

anti-goat Alexa Fluor 488 or 594 all from Invitrogen. All fluorescent secondaries were diluted 1:500 in PBSBT unless otherwise stated.

rabbit anti-Pro-SpC, rabbit anti-aquaporin-5 and mouse anti-smooth muscle actin were revealed using a peroxidase VECTASTAIN Elite ABC universal kit (Vector labs), goat anti-CC-10 was revealed using a peroxidase VECTASTAIN Elite ABC goat kit (Vector labs) according to manufacturers protocol. Briefly, prior to blocking and primary antibody incubation slides were incubated in 3% H_2O_2 to quench endogenous peroxidase activity for 5mins at RT. After incubation with primary antibody o/n 4°C, slides were washed x3 PBS 5mins and incubated in a biotinylated secondary antibody (5μl biotinylated secondary antibody + 15μl normal serum in 1ml PBS) thus linking numerous biotins onto the primary antibody. Slides were then washed x3 PBS 5mins and incubated in the avidin:biotin complex (ABC), which binds to the biotinylated secondary antibody, for 30mins RT (20μl of solution A was added to 1ml PBS followed by addition of 20μl solution B – this must be prepared 30mins prior to use). Slides were washed x3 PBS 5mins and incubated in 3,3'-diaminobenzidine (DAB) peroxidase substrate solution (2 drops of DAB was added to 1ml of buffer) until staining was visible. As a control, identical sections were immunostained without primary antibody and DAB was added for the same time as the sections incubated with primary antibody.

2.5.7 Whole Lung Immunostaining

E12.5 and E14.5 wildtype and *Celsr1*^{Crsh} and *Vangl2*^{Lp} lungs were fixed in 4% PFA at 4°C for 1h. Lungs were then washed in PBS + 0.1% Triton X-100 (Sigma) 10mins RT, rinsed in PBS, and incubated overnight at 4C in blocking solution (5% FCS/PBS/0.1% Triton X-100) containing either rabbit anti-Celsr1 1:1000 or rabbit anti-Vangl2 1:500

and mouse anti-pan-Cytokeratin 1:500, washed x3 PBS 5mins, before detection with either α-rabbit alexa fluor 594 1:500 Invitrogen or α-mouse alexa 488 fluor Invitrogen 1:500 45 mins RT. Lungs were washed 3x 5mins PBS, mounted in vectashield containing DAPI (Vector Labs).

2.5.8 Whole Kidney Immunostaining

E11.5 + 48h kidney explant cultures and E13.5 kidneys were fixed in 4% PFA for 15min or 1h respectively, washed in PBS/0.5% triton for 30mins, rinsed in PBS and blocked in PBS/10% FCS/0.1% triton for 1 hour RT. Kidneys were incubated o/n with mouse anti-pan-Cytokeratin 1:500 and/or rabbit anti-WT1 (Wilms tumour 1 protein) 1:100 overnight at 4°C. Kidneys were subsequently washed 3x PBS 5mins and primary antibodies were detected with either α-mouse alexa fluor 488 Invitrogen 1:500 or α-rabbit alexa fluor 594 1:500 Invitrogen 45mins RT. Finally, kidneys were washed 3x PBS 5mins, mounted in vectashield containing DAPI.

2.6 Western Blotting

2.7 Protein extraction and quantification

Lung tissue was micro-dissected and placed in 100μl lysis buffer (NP40/Igepal 1%, Nacl 150mM, Tris Ph8 50mM) and 4μl of proteinase inhibitor before homogenising with a pestle in a 1.5ml eppendorf. Samples were centrifuged at 13,000rpm, for 30mins at 4°C, the supernatant was removed and protein concentration quantified (see below). Phosphatase inhibitors were added to protein samples prior to Western blot with phospho-ERK1/2 antibody. 1mM Sodium Vanadate (Biolabs PO7585) plus 100μl Phospho stop tablet dissolved in 1ml PBS pH 7.0, was added to 1ml NP40 lysis buffer prior to addition of protease inhibitors. This cocktail of phosphatase inhibitors

inhibit a broad range of phophatases such as acid and alkaline phosphatses as well as serine/threonine (PP1, PP2A and PP2B) and tyrosine phosphatises (PTP), thus protecting the tissue against dephosphorylation. Protein concentration was determined using the Bradford method. The assay is based on the observation that the absorbance maximum for an acidic dye (Coomassie Brilliant Blue) shifts from 465 nm to 595 nm when binding to protein occurs. Both hydrophobic and ionic interactions stabilise the anionic form of the dye, causing a visible color change. The assay is useful since the extinction coefficient of a dye-albumin complex solution is constant over a 10-fold concentration range. The Bradford protein assay (Bio-rad) was used as follows; 1.5mg/ml BSA (Sigma) stock was used to make up protein standards as shown in table below.

BSA μl/μg	0	0.25	0.5	0.75	1	1.25	1.5
Vol. BSA μl	-	2.5	5	7.5	10	12.5	15
Vol ddH_2O μl	15	12.5	10	7.5	5	2.5	-
Total Volume	15	15	15	15	15	15	15

Protein standards and samples were added to a 96 well plate. 20μl reagent S was added to reagent A to give solution A', 25μl of solution A' was added to each well, followed by 200μl Reagent B to each well and left at RT for 15mins. Absorbance was measured at 595nm.

2.8 Immunoblotting

Invitrogen NuPAGE pre-cast gels were used, following the manufacture's instructions. 3-8% Tris-Acetate gels were run in Tris-Acetate running buffer (Invitrogen), 4-12%

Bis-Tris gels were run in either MOPS running (Invitrogen) buffer or MES running buffer (Invitrogen).Following electrophoresis, the gels were transferred to a nitrocellulose membrane using the iBLOT system (Invitrogen), using standard techniques; Remove membrane from blotter and block in blocking solution (5% (w/v) dried skimmed milk powder and 0.1% Tween 20 in PBS, unless stated otherwise) either for 1 h at room temperature or overnight at 4°C. Add primary antibody (concentration antibody dependent) diluted in blocking solution and incubate overnight at 4°C. The following day, wash membrane 3 times for 10 minutes in PBS and 0.1% Tween 20. Add secondary antibody conjugated to horseradish peroxidase (HRP) diluted in blocking solution for 1 hour at room temperature. Wash membrane 3 times for 10 minutes in PBS and 0.1% Tween 20. Remove membrane from wash solution and briefly blot on blue roll before transferring to a clean petri dish, do not allow it to dry out. Add ECL solution to the membrane (type antibody dependent) and incubate for 5mins - ensure the solution covers the membrane fully. Briefly blot membrane onto blue roll and position in hypercassette. Expose to ECL hyperfilm (Amersham Bioscience) and develop using the Xograph developer.

Immunoblotting for ERK proteins was performed using either 18μg/lane of E12.5 wildtype and *Vangl2*$^{Lp/Lp}$ or 7μg/lane of E13.5 wildtype and *Celsr1*$^{Crsh/Crsh}$ whole lung protein extract with antibodies to total ERK 1:500 (Biosource)., phosphoERK1/2 1:1000, (Biosource). Immunoblotting for Rho proteins was performed using 10μg/lane of E13.5 wildtype and *Scribble*$^{Crc/Crc}$ whole lung protein extract with antibodies to anti-Active RhoA (NewEast Biosciences, 26904), 1:500, 5% advance blocking agent in TBS + 0.1% Tween 20, anti-Total RhoA (Cell Signaling, 2117), 1:1000, 5% milk in TBS + 0.1% Tween 20. Immunoblotting for tight and adherens junctions markers was carried out using 10μg/lane of E13.5 wildtype and

Scribble$^{Crc/Crc}$ whole lung protein extract with antibodies to rabbit anti-ZO-1 (Invitrogen, 61-7300), 1:125, goat anti-ZO-2, (Santa Cruz Biotechnology, 8148), 1:1000, 5% milk in TBS + 0.1% Tween 20. Anti-β-Catenin (Sigma, C 2206), used at 1:4000, rabbit anti-E-Cadherin (Cell Signaling, 24E10), 1:2000, rabbit anti-Claudin-18 (Zymed Laboratories, 38-8000), 1:150, 5% Advance blocking agent in TBS + 0.1% Tween 20, anti-GAPDH-HRP, 1:3000 and anti-β tubulin, used at 1:10000.

2.9 Culture Experiments

2.9.1 Lung Explant cultures

Left lung lobes were micro dissected at E11.5 (wild-type tissue was obtained from FVB/N, CD1 or C3H/HeH mice) and cultured for 48h in 1:1 DMEM:F12 containing 50μg/ml Penicillin-streptomycin (Sigma), 0.2mg/ml ascorbic acid (Sigma) and 0.01% BSA (Sigma) at 37°C in a 5% CO_2/air atmosphere. The medium was changed every 24 h. In some cases the media was supplemented with FGF-10 (400ng/ml, R&D systems), Rho kinase inhibitor Y-27632 (Uehata et al., 1997) (10-30mM), or Rho kinase activator CNF-1 (20ng/ml, gift from K. Aktories and G. Schmidt). Following culture, explants were fixed in 4% PFA o/n at 4°C, washed in PBS and photographed using a Leica digital camera and imaging software on a Leica MZ12 microscope. Explants of lung endoderm were prepared essentially as described (Bellusci et al., 1997) E11.5 left lung lobes were isolated and placed in 0.2% trypsin in tyrodes ringer saline (Sigma) on ice for 45mins. Using tungsten needles the mesenchyme was removed and the remaining endoderm were cultured in growth factor reduced matrigel (BD Biosciences) at 37°C in a 5% CO_2/air atmosphere. Explants were photographed at t=0h, t=24h and t=48h; medium was changed every 24h. At 48h endoderm explants were

fixed with 4% PFA for 30mins on ice and released from matrigel using matrigel recovery solution (BD Biosciences) prior to counting the number of terminal buds.

2.9.2 Kidney Explant Cultures

E11.5 and E12.5 mesenephroi were dissected in ice-cold PBS. Tissues were placed on 0.4 um cellulose filters placed in 24 well plates in the presence of 1:1 DMEM:F12 (Invitrogen) supplemented with 5% Insulin-transferrin-sodium selenite (ITS) (Sigma) and antifungal and antibiotic mixture (Sigma). Explants were cultured at 37°C in a 5% CO_2/air atmosphere for up to 72 h, and the medium was changed every 24 h. At 72 h explants were fixed with 4% PFA for 30mins on ice and the number of tubules counted.

2.9.3 Organotypic Cultures

E12.5 lungs were dissected in L15 media, individual lobes were separated and digested in 2mls 0.3% trypsin for 45mins 37°C. Lungs were transferred into 2mls 1:1 DMEM:F12 (Invitrogen), 10% foetal bovine serum (FBS) (Sigma), non-essential amino acids (Sigma), 200mM glutamine (Sigma) + 50μg/ml Penicillin-streptomycin (Sigma). Lung tissue was triturated by pipetting up and down until no large clumps of tissue remained, followed by further disassociation into a single cell suspension with a 23-gauge needle. 500μl medium was added and cells centrifuged at 1000rpm 5min. Media was removed carefully leaving behind the cell pellet, which was re-suspended in 100μl media. Cells were counted using a haemocytometer under a x10 objective and diluted 1:1 in Geltrex basement membrane (Sigma) and either plated at a density of x cells/ml, or in 20ul drops. in an 8 well slide chamber (Lab Tek II). Cells were grown for 48hr at 5% CO_2 37°C, in the presence of either control or Scribble morpholino, then fixed 4% PFA 15mins and stained with rhodamine phalloidin.

2.9.4 Scribble morpholino knock-down and organotypic cultures

Both Scribble-F (Gene Tools, GAGCGGGATGCACTTCAGCATGATG 3' fluorescein) and Control morpholino (Gene Tools Standard control oligo CCTCTTACCTCAgTTACAATTTATA) were supplied as lyophilised powder. Scribble morpholino was tagged on the 3' end with fluorescein the enable visualisation within the cells. Morpholinos were re-constituted to 100nM in water and then diluted 1:100 to obtain a 1mM working stock. Morpholino was added to the media 1:100 to a final concentration of 10μM .

2.10 Lung Function Analysis

2.10.1 Whole body unrestrained plethysmograph (Buxco) with Methacholine challenge

A whole body unrestrained plethysmograph (WBP) is an animal chamber used for detecting a breathing flow waveform. The unrestrained chamber allows conscious animals to move freely, eat, and drink. The single chamber plethysmograph utilizes a barometric analysis technique (Drorbaugh and Fenn, 1955) that compares the pressure difference between the animal chamber and a reference chamber to measure airway physiological parameters. Actual flows are calculated by Buxco software, taking into account temperature, humidity and pressure. Airway resistance in the WBP is determined by calculating the dimensionless parameter enhanced pause (PenH), an indicator of changes in airway resistance, as described by (Chong et al., 1998; DeLorme and Moss, 2002).

4 chambers were used to enable simultaneous measurement of multiple animals as well as direct comparison between wildtype and mutant lines. The chambers were

connected to a nebuliser to allow administration of an aerolised bronchochonstrictor such as methacholine.

Mice were placed in a whole body plethysmograph (Buxco) and allowed to acclimatise to their new environment for 5 mins before recording a baseline reading for 2mins. 50μl PBS was nebulised into each chamber for 2mins followed by a 3min rest period, breathing flow was measured throughout. 200μl of increasing concentration of methacholine (Sigma) (12.5mg/ml, 25mg/ml, 50mg/ml) were nebulised into each chamber for 2mins each followed by a 3min rest period for each concentration, PenH was measured throughout. If any mice appeared to be in distress or their PenH reached 6 or above the experiment was stopped and mice culled immediately. Once all mice had been through the plethysmograph protocol they were culled by overdose of anaesthetic.

2.10.2 Jugular Bleeds

Immediately after the heart stopped beating the jugular vein was cut and blood collected via capillary tube. Exactly 200μl was collected in EDTA containing tubes, placed on a rotor for 30mins RT, followed by analysis on haematology analyser. The remaining blood was collected, centrifuged 8°C, 10 mins 7,000rpm (5,000g). Plasma was removed carefully and put into a clean eppendorf and stored at -80°C ready for TNF-α ELIZA, Bradford assay and analysis of immune cell populations and numbers.

2.10.3 Bronchioalveolar Lavage

Following overdose of anaesthetic, tracheas of mice were exposed and a small incision made. A tracheal tube attached to 23 gauge needle and 1ml syringe was introduced carefully through the trachea and down into the lungs. 3x 1ml PBS was used to lavage the lungs. Bronchioalveolar lavage fluid was used for Bradford assays

to measure protein concentration and for measurement of immune cell types and numbers by cytospin or haemoanalyser.

2.10.4 Cytospin and Diff quick stain

500µl of BALF was pipetted into a Shandon single cytofunnel (Thermo Scientific 5991040) containing a slide and centrifuged at 1,000rpm 4mins RT, fixed in ice-cold methanol for 5mins and allowed to air dry. Slides were immersed in diff quick stain 'B' for 30seconds followed by 15-20seconds in diff quick stain 'C', washed briefly in water, pH 6.8 and left to air dry.

2.10.5 Haemoanalyser measurement of immune cells in blood and BALF samples

Haematology was performed on an Advia 2120 analyser (Siemens Diagnostics Ltd) using species-specific software settings suitable for the analysis of mouse blood and BALF. 200µl of whole blood or BALF was collected into EDTA coated tubes (Kabe Labortechnik, Germany) and processed for full blood count and differential analysis using on board reagents and the protocol reccommended by the manufacturer. Following collection samples were mixed on a rotary mixer for 30 minutes and then kept at RT until processed.

2.11 Kidney Function analysis

12 week old male *Vangl2*^{Lp} heterozygote and wildtype littermates were individually housed in Techniplast metabolic cages (Buggeggiate, Italy) for 24 hours and urine was collected from each individual throughout this time period. Urine samples were clarified by centrifugation at 3000rpm for 3-5 mins RT, supernatant was removed

and stored at -20°C before testing. Urine creatinine was measured on an Olympus AU400 analyser (Olympus UK), as described by (Hough et al., 2002).

2.11.1 Murine Micro-albuminuria ELISA

A mouse Albumin ELISA kit (Exocell, Albuwell M, Bethyl Laboratories Inc. E99-134) was used to determine the concentration of urine albumin using the manufacturers protocol as follows. Albuwell M plates were precoated and ready to use. Urine samples were collected and clarified as above. Sample dilutions were prepared by adding 120µl EIA diluent to 7 eppendorfs labelled 1-7. 120µl Murine Serum Albumin (MSA) 2-fold standard was added to tube 1 and mixed by aspirating and expelling the fluids 5 times. 120µl from tube 1 was added to tube 2 and mixed as before. This procedure was continued to tube 7. Tubes 1-6 contained dilutions of 10.0, 5.0, 2.5, 1.25, 0.625, 0.313 and 0.156µg/ml respectively. Urine samples were diluted 1:13 by adding 120µl EIA diluent followed by 10µl sample and vortexing briefly. 100µl of EIA diluent from stock bottle was added to well A1 and used as a negative control. 50µl of EIA diluent from stock bottle was added to well A2 and used as a positive control. Standards and samples were added to the plate in duplicate. 50µl anti-murine albumin was added to all wells except for negative control well and incubated RT 30mins. The plate was washed by removing all fluids and rinsing each well with 300µl tap water 10x, 100µl anti-rabbit HRP conjugate was then added to each well before incubating a further 30mins RT and washing as before. 100µl colour developer was added to each well and incubated RT 6mins, 100µl colour stopper was added to each well and absorbance measured at 450nM. The blank absorbance was subtracted from the readings for each standard and sample. A standard curve was plotted using the known concentration (Y) of standard versus the absorbance's (X) of standard and

the albumin concentration calculated by interpolation of the regression curve formula.

2.11.2 Retinol Binding Protein 4 ELISA

Urine RBP-4 levels were measured using a Mouse RBP-4 ELISA kit (ALPCO DIAGNOSTICS$_{TM}$) using the manufacturers protocol. ALPCO DIAGNOSTICS$_{TM}$ plates were precoated and ready to use. Urine samples were collected and clarified as above. 1x wash solution, 1x diluent, 1x detector and substrate solutions were prepared occording to manufacturers instructions. The working standards were prepared by briefly centrifuging the standard vial, adding 1ml deionised water to make a stock concentration of 24ng/ml and mixed well. 8 microcentrifuge tubes were labelled 0-7 and 300µl of 1x diluent was added to each. 300µl of the stock standard solution was added to tube number 7 and vortexed. Thus giving standard tube number 7 a concentration of 12ng/ml. Standards 6-1 were then prepared by performing serial dilutions of the preceding standard, without adding any to tube number 0. Sample QC was reconstituted with 1ml-deionised water as a negative control. Each urine sample was diluted 1:100 with 1x diluent and mixed well, 10µl was then taken and added to 990µl 1x diluent. 100µl of standard 0-7, the reconstituted QC sample and diluted urine sample was pipetted into the antibody-coated plate. Samples were incubated 37°C 1h, following which, the solution was removed and each well was washed 3x with 250µl 1x wash solution. 100µl secondary antibody was then added to each well and the plate was incubated at 37°C for 1h and washed as above. 100µl 1x detector was then added to each well before incubation at 37°C 1h. All solution was removed and each well was washed 5x 250µl 1x wash solution before adding 100µl substrate solution to each well and incubating at RT for 20min in the dark. Using a multichannel

pipette 100μl stop solution was added to each well. Absorbance was read at 450nM, the blank absorbance was subtracted from the readings for each standard and sample. A standard curve was plotted using the known concentration (Y) of standard versus the absorbances (X) of standard. The RBP4 concentrations of samples were calculated by interpolation of the regression curve formula. RBP4 concentrations were multiplied by dilution factor 2 to obtain the concentration from the undiluted samples.

2.12 Glomerular Counts

Vangl2^{Lp} heterozygote and wildtype littermates were harvested 4 weeks postnatally. The kidneys were dissected out and placed in 0.1M hydrochloric acid for 30mins at 37°C. The acid was removed and replaced with 1ml PBS (pH 7.4) and the tissue homogenised using a bench top homogeniser. 20μl of this was pippetted into a haemocytometer and,the number of glomeruli in the aliquot were counted using a 10x objective lens. This was repeated in triplicate for each sample and the three results averaged to determine the number of glomeruli in each sample and therefore each kidney (Welham et al., 2002).

2.13 Statistical analysis

All statistics were calculated using Excel and Graphpad software. Error bars represent standard error of mean (s.e.m.) and significance was scored using unpaired two-tailed t-tests.

2.14 Microscopy

2.14.1 Leica TCS SP5

TCS stands for True Confocal Scanner and SP5 for the 5 SpectroPhotometer channels this system is equipped with. The microscope is a Leica DMI 6000 CS inverted microscope with a motorized XY-stage and Z-drive motor focus on the microscope stand (100 nm step size) as well as a SuperZ Galvo stage (1500 µm travel range) for higher speed and accuracy. An incubator is fitted on the microscope stage and CO2 can be piped into this chamber for live cell imaging. The non-confocal illumination is provided by a long-life proprietary Leica EL6000 metal-halide fluorescence lamp with a fibre optic light guide. The TCS-SP5 confocal microscope and DMI 6000 inverted stand are controlled by proprietary LAS AF software (Leica Application Suite Advanced Fluorescence) version 2.1.0 build 4316. The computer is a Leica workstation GECOMP 24726, with Intel R coreTM2 2,13Ghz CPU and 1,98 G RAM, running Windows XP version 2002, service pack 3.

Objectives:

Type	Magnification/NA/imm	Working distance (mm)	Coverslip
HC PL APO CS	10x/0.4 dry	2.2	0.17
HC PL APO Lbd. Bl	20x/0.70 immersion	0.26 (water) - 0.17 (oil)	-
HCX PL APO CS	40x/1.25-0.75 oil	0.1	0.17
HCX PL APO Lbd. Bl	63x/1.4-0.6 oil	0.1	0.17
HCX PL APO CS	>63x/1.3 Glyc 21°C	0.28	0.14-0.18

Confocal Lasers:

50 mW diode 405 nm
100 mW Argon laser 458, 476, 488, 496

and 514 nm
10 mW DPSS 561 nm
2 mW HeNe 594 nm
10 mW HeNe 633 nm

The SP5 uses an acousto-optical tunable filter (AOTF) to control the excitation laser light and an acousto-optical beam splitter (AOBS) instead of filter blocks to send the excitation laser light to the sample and to reflect the emitted light from the sample into the scan head. This is a more light efficient way than using glass di- or multi-chroic mirrors and filters. Besides the 5 detectors for detection of fluorescence light there is one detector for the detection of transmitted light.

3 Chapter Three: The PCP genes *Celsr1* and *Vangl2* are required for normal branching morphogenesis

3.1 Introduction

Branching morphogenesis is the mechanism by which many organs including the lung and kidney develop from a single epithelial bud to a complex tree like system specialised for gas or fluid exchange. Cells that are epithelial in nature i.e. they exhibit apical-basal polarity, a uniformly orientated cytoskeleton and have highly elaborate cell junctions, associate and organise into new branches and tubes. Reciprocal signalling between epithelial and mesenchymal cells are required to direct the growth of newly formed epithelial buds in the lung. In addition, complex morphogenetic movements are required to precisely pattern the complex network of three-dimensional epithelial tubes within the lung. The complex morphogenetic movements required for the formation of new epithelial branches is modulated by the intracellular cytoskeletal network and by intercellular interactions such as cell adhesion. The signalling pathways that control this cytoskeletal organisation in the lung and kidney are not well known however, in the lung, it has been shown that Rho GTPases and Rho kinases can mediate cytoskeletal remodelling (Moore et al., 2005). Rho kinase is a downstream effector in a number of signalling pathways including the PCP pathway. Rho signalling has also been shown to modulate cell polarity and the organised re-structuring of epithelial tissue during development (Fig. 3.1).

PCP has been defined as the polarisation of cells within the plane of an epithelium, where the polarisation is orthogonal to the axis of apical basal polarity. This signalling pathway was originally shown to regulate the patterning of external epidermal structures, such as wing and abdominal hair cells in *Drosophila* (Adler, 2002), however new roles for this pathway have begun to emerge. These include modifying cellular direction and movement (Barrow, 2006; Jenny and Mlodzik, 2006;

Karner et al., 2006; Seifert and Mlodzik, 2007) and coordinating the movement of groups of cells (Bastock and Strutt, 2007).

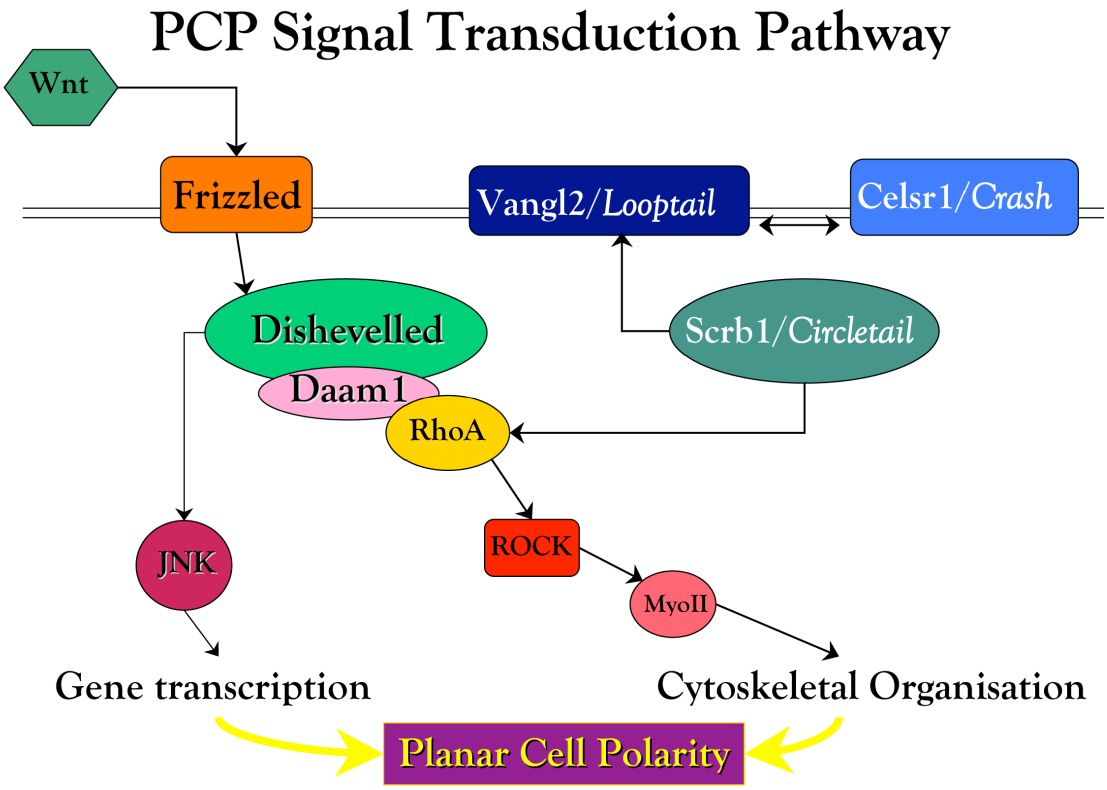


Figure 3.1 The planar cell polarity signal transduction pathway. This diagram depicts a simplified outline of the planar cell polarity signal transduction pathway. Vangl2, Celsr1 and Scribble interact with this pathway via Rho GTPases and Rho kinases to alter cytoskeletal organisation that allows cellular organisation and movement, enabling the formation of complex organs such as the lung.

Therefore the cellular arrangements necessary for lung and kidney epithelial tube formation could be coordinated in part by the PCP signalling pathway to regulate tissue morphogenesis. Previous studies have shown *Celsr1* and *Vangl2* to belong to the core PCP gene family (Copp et al., 2003; Jenny and Mlodzik, 2006; Karner et al., 2006) and mouse mutants of these genes display characteristic PCP defects such as craniorachischisis and disrupted orientation of stereo cilia in the mammalian cochlea (Jenny and Mlodzik, 2006; Karner et al., 2006).

Ceslr1 (*Drosophila* homologue stan (starry night) or flamingo) is a seven-pass transmembrane atypical cadherin, which has been proposed to act at the top of the PCP pathway hierarchy in *Drosophila*, and is thought to be required for the correct localisation of other PCP proteins to the cell membrane (Seifert and Mlodzik, 2007; Strutt, 2001). There are three known Celsr genes in the mouse, Ceslr1, 2 and 3. Ceslr1-3 have been associated with brain and neural tube development in mice as well as in regulating PCP (Crompton et al., 2007; Curtin et al., 2003; Tissir et al., 2002b; Tissir and Goffinet, 2006; Zhou et al., 2007a). In *Drosophila* PCP signalling is dependant on the apico-lateral distribution of Flamingo within individual epithelial cells followed by the stabilisation of Flamingo homodimers across neighbouring cell interfaces in response to an external (currently unknown) polarity cue (Usui et al., 1999). Celsr1 and its homolog in the chick (c-FMi1) are known to distribute in a similar manner during epidermal and inner ear development (Davies et al., 2005; Devenport and Fuchs, 2008). However, Formstone et al., recently demonstrated a novel distribution of Celsr1 to the extreme basal domain of neuroepithelial cells both within the early neural tube and in a population of cells at the dorsal ventral midline of the developing spinal cord, an absence of this expression is observed in the Celsr1 mouse mutant Crash (*Crsh*) (Formstone et al., 2010a). This finding is interesting

because, as mentioned above previous reports have shown Celsr1 to be localised to cell membranes when operating in PCP singalling. The spatial and temporal pattern of Celsr1 protein within the neuroepithelia suggests both novel and diverse functions for Celsr1 during neural development. The absence of Celsr1 enrichment to the extreme basal domain of *Crsh/Crsh* neuroepithelial cells indicates the importance of this novel protein distribution to Celsr1 function during neural development and suggests lack of this protein expression in *Crsh/Crsh* mutants may contribute to the mutant phenotype in the neural tube (Formstone et al., 2010b). Thus suggesting Celsr1 and potentially other PCP genes may have other more complex functions than those already documented in PCP signalling.

Vangl2 is the homologue of *Drosophila* strabismus/van gogh. Both mammalian and *Drosophila* Vangl2 contain two putative transmembrane domains and a PDZ-binding domain consistent with conserved functional properties. The mouse has two Vangl genes, Vangl1 and 2, which share ~70% homology. Vangl2, like Celsr1 and Scribble, has been studied in detail with respect to its role in PCP and convergent extension (Kibar et al., 2007; Montcouquiol et al., 2006; Torban et al., 2007; Ybot-Gonzalez et al., 2007). Less is known about the role of Vangl1, though recently Torban et al., identified a mutant embryonic stem cell line (*Vangl1*^{gt}) carrying a β-Geo gene-trap cassette (β-gal and neomycin phosphotransferase fusion) inserted into intron 3 of *Vangl1*, 237 nucleotides downstream of the exon 3 donor-splice. The transcript expressed by the targeted *Vangl1* allele is predicted to code for a severely truncated nonfunctional protein consisting of 63 amino acids of the N-terminal cytoplasmic portion fused to β-gal. Both Vangl1 (*gt/+*) heterozygotes and Vangl1 (*gt/gt*) homozygotes were viable and fertile, although Vangl1 (gt/gt) displayed subtle defects in planar polarity e.g. alterations in the polarity of inner hair cells of the cochlea.

Interestingly, although no phenotype was observed in Vangl1(*gt/+*) mice, Vangl1(*gt/+);*Vangl2(*Lp/+*) double heterozygotes showed severe developmental defects that included; craniorachischisis, disorganization of the stereociliary bundles in the organ of Corti, and cardiac abnormalities. These experiments provide evidence that genetic interactions between Vangl1 and Vangl2 result in aberrant planar polarity and subsequent developmental defects (Torban et al., 2008).

This chapter describes studies that were undertaken to determine the roles of *Celsr1* and *Vangl2*, in lung epithelial tube formation, and to a lesser extent in kidney tubule development, using mouse mutants containing loss of function mutations in *Celsr1 (Crash, Crsh*) and Vangl2 (*Loop-tail, Lp*) (Curtin et al., 2003; Kibar et al., 2001a; Kibar et al., 2001b; Murdoch et al., 2001a; Torban et al., 2004).

3.1.1 Aims

- To determine whether *Ceslr1* and/or *Vangl2* are required for branching morphogenesis
- To determine the role of *Ceslr1* and *Vangl2* in lung epithelial tube formation
- To characterise the phenotype of *Vangl2* mutant Kidneys

3.2 Results

3.2.1 Branching morphogenesis is disrupted in Celsr1$^{Crsh/Crsh}$ and Vangl2$^{Lp/Lp}$ mutants

Loss of *Celsr1* or *Vangl2* results in branching defects in a number of organs including the lungs, kidneys, salivary and lacrimal glands (Fig 3.2). Macroscopic analysis of E18.5 *Celsr1*$^{Crsh/crsh}$ and *Vangl2*$^{Lp/Lp}$ lungs and kidneys revealed them to be smaller, with fewer branches compared to wildtype littermates (Fig 3.2 A-E). All lung lobes

display abnormal morphology as do the kidneys of both mutants, suggesting that *Celsr1* and *Vangl2* are required to maintain the normal morphology of these branched organs. *Vangl2*$^{Lp/Lp}$ kidneys show a reduced anterior-posterior axis in comparison to wildtype controls and therefore calculation of the length to width ratio of *Vangl2*$^{Lp/Lp}$ kidneys revealed a significant reduction compared to wildtype littermates (Wildtype average ratio 1.475, n=3, Looptail average ratio 1.375, n=3 $p < 0.0002$) (Fig 3.2 D,E). Histological analysis of E18.5 H&E stained sections of *Vangl2*$^{Lp/Lp}$ salivary and lacrimal glands also revealed branching defects. Both were smaller with fewer branches in *Celsr1*$^{Crsh/Crsh}$ and *Vangl2*$^{Lp/Lp}$ mutants when compared to wildtype littermates (Fig 3.2 F-I and data not shown). While some variation in the phenotype could be observed between the two mutants, e.g. *Celsr1*$^{Crsh/Crsh}$ kidneys are smaller than *Vangl2*$^{Lp/Lp}$ kidneys and the morphology of the individual lung lobes are variable in both mutants, in general, all branched structures were smaller, abnormally shaped and contained fewer branches in both *Lp/Lp* and *Crsh/Crsh* mutants; consistent with *Celsr1* and *Vangl2* operating within the same signalling pathway.

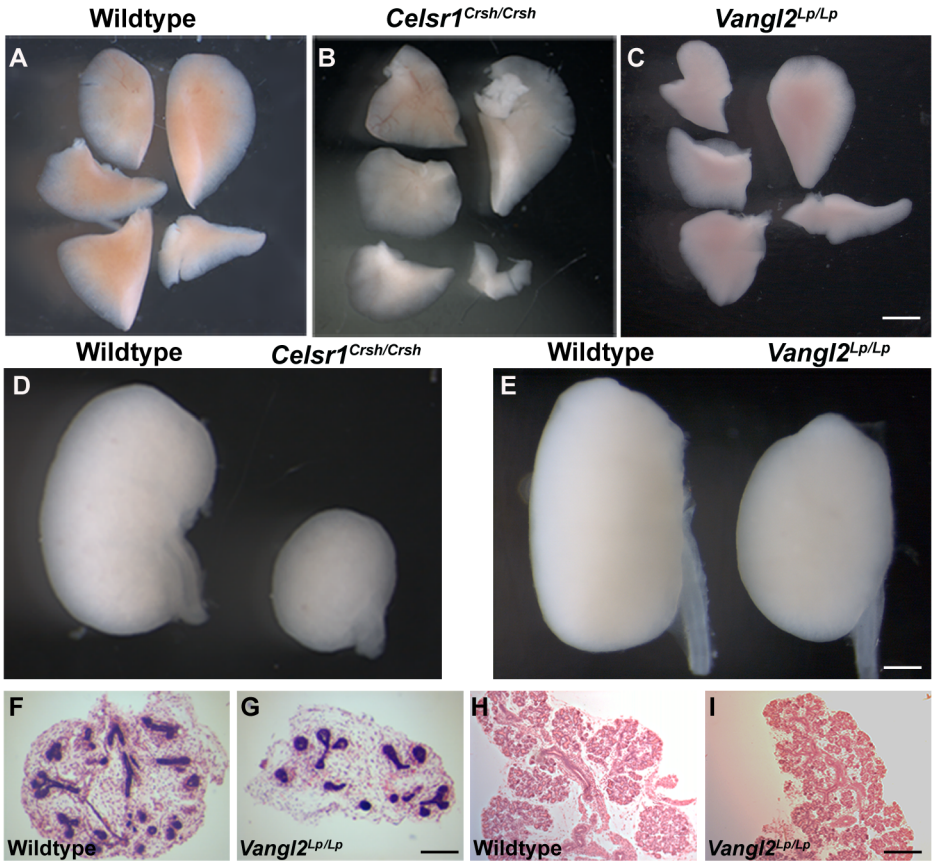


Figure 3.2 Branching morphogenesis is disrupted in *Celsr1*$^{Crsh/Crsh}$ and *Vangl2*$^{Lp/Lp}$ mutants. Analysis of E18.5 separated mouse embryonic lung lobes (A-C) reveals visibly misshapen lobes of *Celsr1*$^{Crsh/Crsh}$ (B) and *Vangl2*$^{Lp/Lp}$ (C) lungs compared to wildtype (A). Macroscopic analysis of E18.5 kidneys also reveal these to be smaller with fewer branches and overall disrupted morphology in both *Celsr1*$^{Crsh/Crsh}$ (D, Right) and *Vangl2*$^{Lp/Lp}$ (E, Right) mutants compared to wildtype littermates (D and E left). E18.5 H&E stained sections of wildtype (F) and *Vangl2*$^{Lp/Lp}$ (G) lacrimal glands and wildtype (H) and *Vangl2*$^{Lp/Lp}$ (I) salivary glands. Mutant glands (G,I) contain fewer branches compared to wildtype littermates (F,H) . Scale bars: (A-E) 62.5μM, (F-I) 50μM.

3.2.2 Lung morphogenesis is disrupted in Celsr1$^{Crsh/Crsh}$ and Vangl2$^{Lp/Lp}$ mutants

To further analyse the branching defects observed in the lungs of both, *Celsr1*$^{Crsh/Crsh}$ and *Vangl2*$^{Lp/Lp}$ mutants, E14.5 and E18.5 sections were H&E stained and histology analysed (Fig 3.3 A-F). Early in normal lung development airway lumina are narrow, surrounded by a multilayered, epithelium. As the lumina expand and widen, the surrounding epithelium subsequently reduces in thickness, resulting in a single layer of uniformly aligned epithelial cells surrounding an open, circular lumen. At E14.5 lumina are clearly visible in wildtype sections, surrounded by a single layer of organised epithelial cells (Fig 3.3 A). However, in both *Celsr1*$^{Crsh/Crsh}$ and *Vangl2*$^{Lp/Lp}$ mutants, the structure of the airway epithlium at E14.5 was highly disturbed, such that the lumina remained narrow, often with cells occupying the luminal space. Moreover, the surrounding epithelium appeared disorganised and multilayered (Fig 3.3 B-C). Whilst both mutant phenotypes appeared broadly similar, disorganisation was more severe in *Ceslr1*$^{Crsh/Crsh}$ airways, with more cells occupying the luminal space than in *Vangl2*$^{Lp/Lp}$.

At E18.5 disruption of both *Celsr1*$^{Crsh/Crsh}$ and *Vangl2*$^{Lp/Lp}$ mutant lungs was more obvious with clear evidence of hypoplasia and a lack of septation (the process by which epithelial cells branch out to form new airways) (Fig 3.3 E-F) compared to wildtype littermates (Fig 3.3 D). Quantification of the number of airways at both E14.5 and E18.5, revealed a significant reduction in both mutants compared to wildtype littermates (Fig 3.3 M-N). In addition the width of airways at E18.5 was also significantly reduced in both *Celsr1*$^{Crsh/Crsh}$ and *Vangl2*$^{Lp/Lp}$ mutants compared to littermate controls (Fig 3.3 M-O). This type of reduction in the number and width of

airways will likely have detrimental affects on post-natal lung function, however due to the embryonic lethality caused by these mutations (Murdoch et al., 2001a) this could not be investigated.

To further visualise the disorganised cellular arangements in both *Celsr1*$^{Crsh/Crsh}$ and *Vangl2*$^{Lp/Lp}$ mutant lungs, E14.5 sections were immunostained with pan-cytokeratin (Fig 3.3 G-I), an epithelial cell marker and DAPI to highlight the cell nuclei (Fig 3.3 J-L). Wildtype epithelial cells were clearly distinguishable from the mesenchyme by their organised structure; cell nuclei uniformly aligned in a single layer, surrounding visibly open lumen (Fig 3.3 G,J). Both *Celsr1*$^{Crsh/Crsh}$ and *Vangl2*$^{Lp/Lp}$ mutant epithelial cells were disorganised and randomly orientated around small, or in some cases, absent lumina (Fig 3.3 see inserts in H-I compared to insert in G). In most cases it was difficult to distinguish between epithelial cells from the mesenchyme by DAPI staining alone in mutants (Fig 3.3 K-L). *Celsr1*$^{Crsh/Crsh}$ airways were more severely affected than *Vangl2*$^{Lp/Lp}$ mutant lungs.

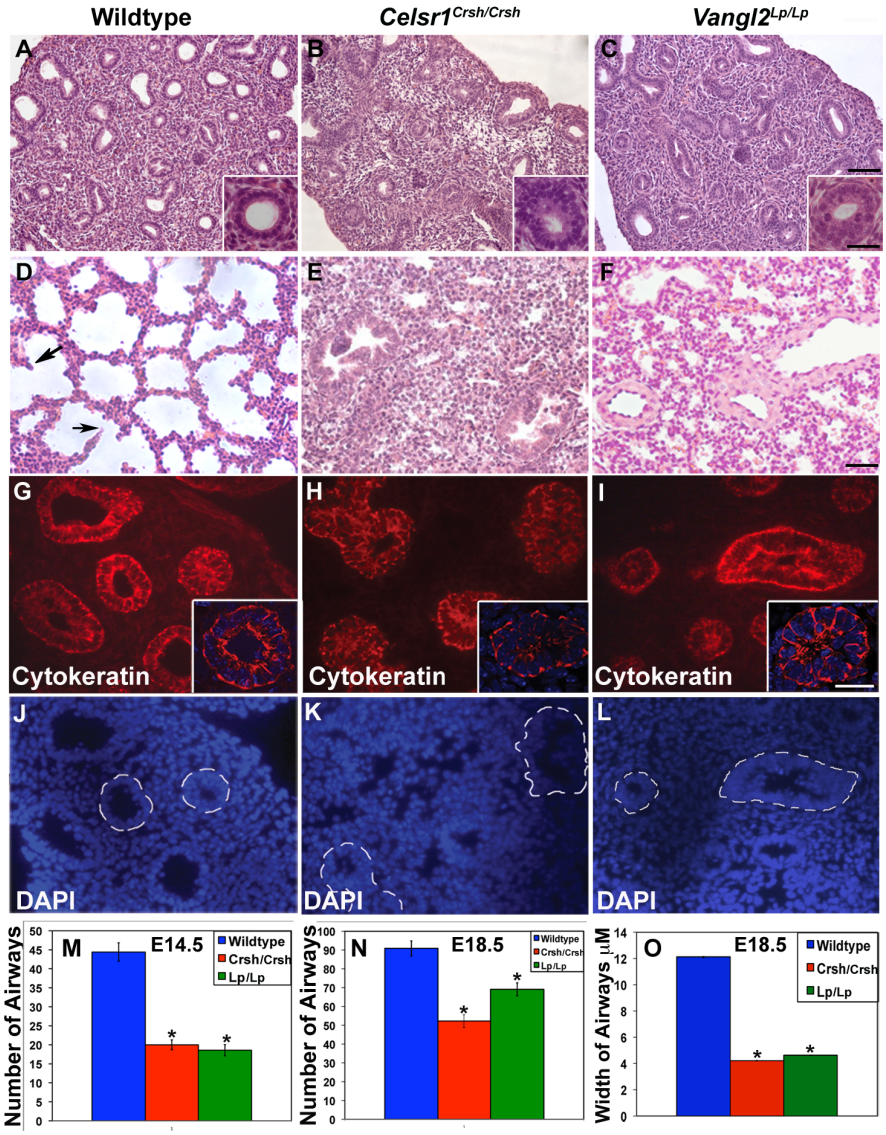


Figure 3.3 Disruption of Celsr1 or Vangl2 causes lung morphogenesis defects. H&E staining of sections of E14.5 *Celsr1*$^{Crsh/Crsh}$ (B) and *Vangl2*$^{Lp/Lp}$ (C) lungs compared to wildtype (A). (M) There was a significant reduction in the number of epithelial branches in both mutants at E14.5: wildtype 44.42, ±2.43, n=12; *Celsr1*$^{Crsh/Crsh}$ 20.00. ±1.3, n=12; *Vangl2*$^{Lp/Lp}$ 18.58, ±1.48, n =12. H&E sections from a minimum of three mutants for each genotype were used for counts. Airway lumina were narrow or absent in many *Crsh/Crsh and Lp/Lp* airways and epithelium had a multilayered morphology, in contrast to the wider lumina surrounded by single layered epithelium that predominates in wildtype. H&E staining of sections of E18.5 wildtype (D), *Celsr1*$^{Crsh/Crsh}$ (E), *Vangl2*$^{Lp/Lp}$ (F) lungs. Control lung sections display typical saccular structure and evidence of septation (arrows in D). In contrast, mutant lung sections (E,F) show no evidence of septation. Number (N) and width (O) of airways is dramatically reduced at E18.5. Number or width of airways was determined by counting airways visible in a complete section of E18.5 lungs from a minimum of two separate embryos (N) wildtype 90.89; ±3.97; *Celsr1*$^{Crsh/Crsh}$ 52.22, ±3.37; *Vangl2*$^{Lp/Lp}$ 69.11, ±3.43, n=9 for each genotype (O) wildtype 12.13, ±0.05, *Celsr1*$^{Crsh/Crsh}$ 4.21, ±0.03, *Vangl2*$^{Lp/Lp}$ 4.63, ±0.03 n=10 for each genotype. E14.5 cryosections immunostained for expression of pan-cytokeratin (G-I, inserts show airways at higher magnification), corresponding sections to G-I counterstained with DAPI (J-L), dashed lines outline cytokeratin positive cells (as seen in G-I) difficult to distinguish from surrounding cells in *Celsr1*$^{Crsh/Crsh}$ (K) and *Vangl2*$^{Lp/Lp}$ (L), airways are easily visualised in wildtype (J). Scale bars: A-C 50mM, D-L 12.5mM, inserts in A-C, G-I 5mM *P<0.05.

3.2.3 Cell differentiation, proliferation and apoptosis are not affected in *Celsr1*$^{Crsh/Crsh}$ or *Vangl2*$^{Lp/Lp}$ mutants

Analysis of cell differentiation, proliferation and apoptosis by immunohistochemistry was carried out to begin to determine the cause of lung tissue defects in *Celsr1*$^{Crsh/Crsh}$ and *Vangl2*$^{Lp/Lp}$ mutants (Fig 3.4). E18.5 *Crsh* and *Lp* homozygous lung sections were immunostained for α-smooth muscle actin (Fig 3.4 A-C), to highlight smooth muscle cells surrounding proximal airways, and pro-surfactant protein C (Pro-SpC) (Fig 3.4 D-F), a marker of alveolar type II cells in distal airways. Despite the disrupted tissue architecture in both mutants making direct comparison of Pro-SpC expression difficult, no difference was observed in the expression patterns of α-smooth muscle actin or Pro-SpC in either mutants compared to wildtype littermates (Fig 3.4 I). Immunostaining of two additional cell specific markers was carried out on *Lp* homozygous sections. Expression patterns of the distal alveolar type I cell marker, Aquaporin 5 (Fig 3.4 J-K) and the proximal Clara cell marker CC-10 (Fig 3.4 G-H) again showed no obvious differences when compared to wildtype littermates.

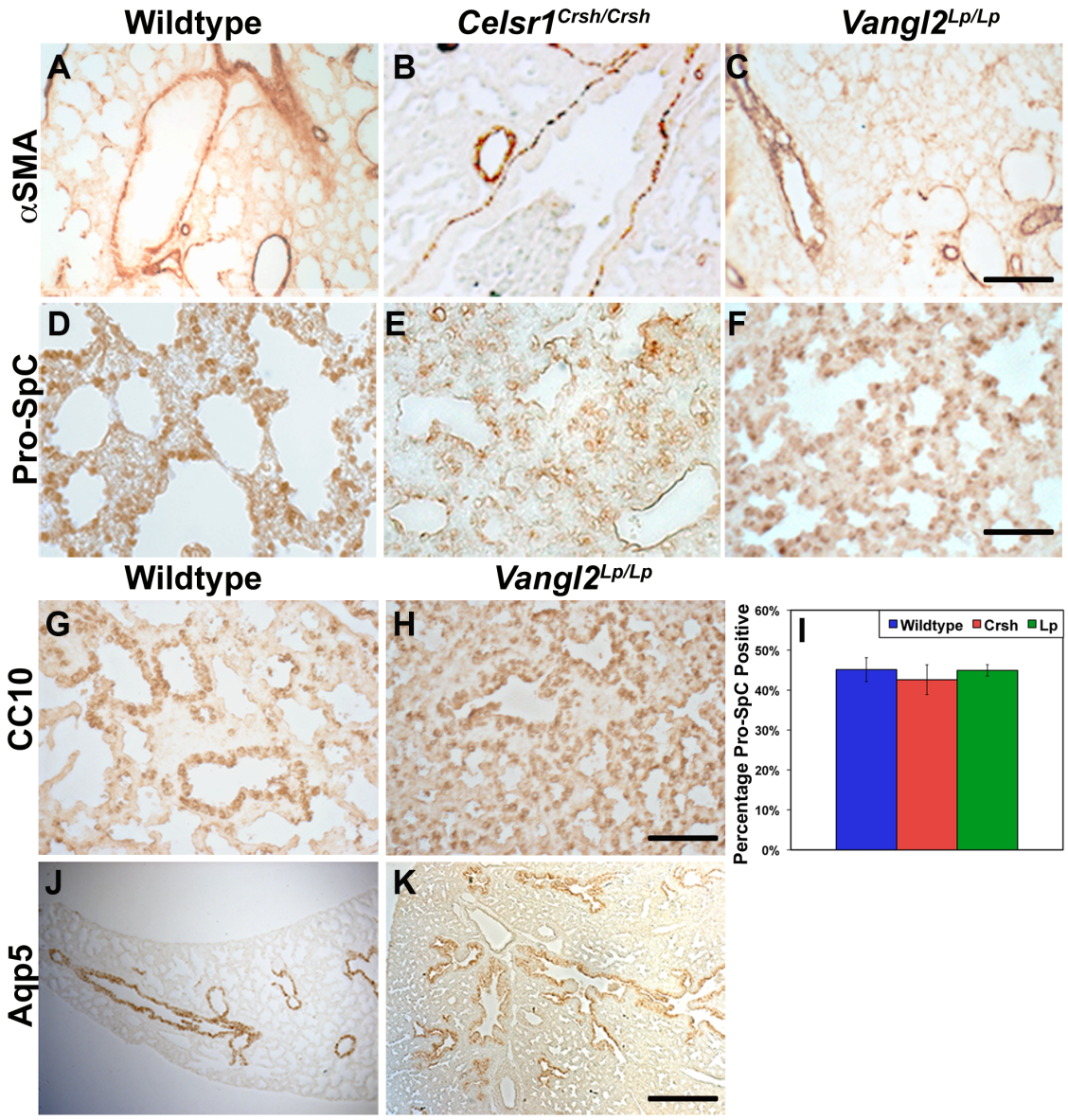


Figure 3.4 Immunohistochemical analysis of lung epithelial cell differentiation in *Celsr1*$^{Crsh/Crsh}$ and *Vangl2*$^{Lp/Lp}$ compared to wildtype. Comparison of E18.5 control lung sections (A,D) with *Celsr1*$^{Crsh/Crsh}$ (B,E), and *Vangl2*$^{Lp/Lp}$ (C,F) showed no apparent alteration in the expression of proximal airway marker, alpha smooth muscle actin (A-C) or distal airway marker, pro-surfactant C (D-F). Graphical comparison of the percentage of Pro-SP-C positive cells in wildtype and mutant lungs (I) confirmed no significant difference between control and *Celsr1*$^{Crsh/Crsh}$ or *Vangl2*$^{Lp/Lp}$ lungs, n=8 for each genotype. Counts were performed on sections of left lung lobe obtained from 3 mutants for each genotype, n=8 for each genotype. Wildtype 45.12%; ±3.00; *Celsr1*$^{Crsh/Crsh}$ 42.60%, ±3.72; *Vangl2*$^{Lp/Lp}$ 44.93%; ±1.43. Further comparison of E18.5 wildtype (G,J) lung sections with *Vangl2*$^{Lp/Lp}$ (H,K) sections also revealed no alteration in the expression of the distal airway marker CC10 (G,H) or αSMA (J,K) which highlights the proximal airways. Scale bars: A-H 12.5μM, J-K 25μM.

To determine whether the reduced number of airways observed in *Celsr1*$^{Crsh/Crsh}$ and *Vangl2*$^{Lp/Lp}$ mutants was caused by abnormal tissue growth, the percentage of proliferating cells in E14.5 wildtype and mutant lung sections was investigated (Fig 3.5 A-C, G) by immunostaining for anti-phospho histone H3 antibody. This antibody detects endogenous levels of histone H3 when phosphorylated at Ser28, which only occurs when cells are undergoing mitosis (Goto et al., 1999). No significant difference was observed in the percentage of proliferating cells in either *Celsr1*$^{Crsh/Crsh}$ or *Vangl2*$^{Lp/Lp}$ compared to wildtype littermates.

Similarly no difference was observed in the level of apoptosis in either mutant when compared to littermate controls (Fig 3.5 D-F), determined by immunostaining E14.5 sections for anti-cleaved caspase-3. Caspase-3 is a critical executioner of apoptosis, as it is either partially or totally responsible for the proteolytic cleavage of many key proteins (CPP-32, Apoptain, Yama, SCA-1). Cleaved caspase-3 (Asp175) antibody detects endogenous levels of the large fragment (17/19 kDa) of activated caspase-3 resulting from cleavage adjacent to Asp175, therefore is a useful maker of apoptosis.

From this data it can be concluded that the cellular disorganization observed in *Celsr1*$^{Crsh/Crsh}$ and *Vangl2*$^{Lp/Lp}$ mutants does not arise as a result of disrupted differentiation, proliferation or apoptosis and therefore is likely caused by impaired cell and/or tissue morphogenesis.

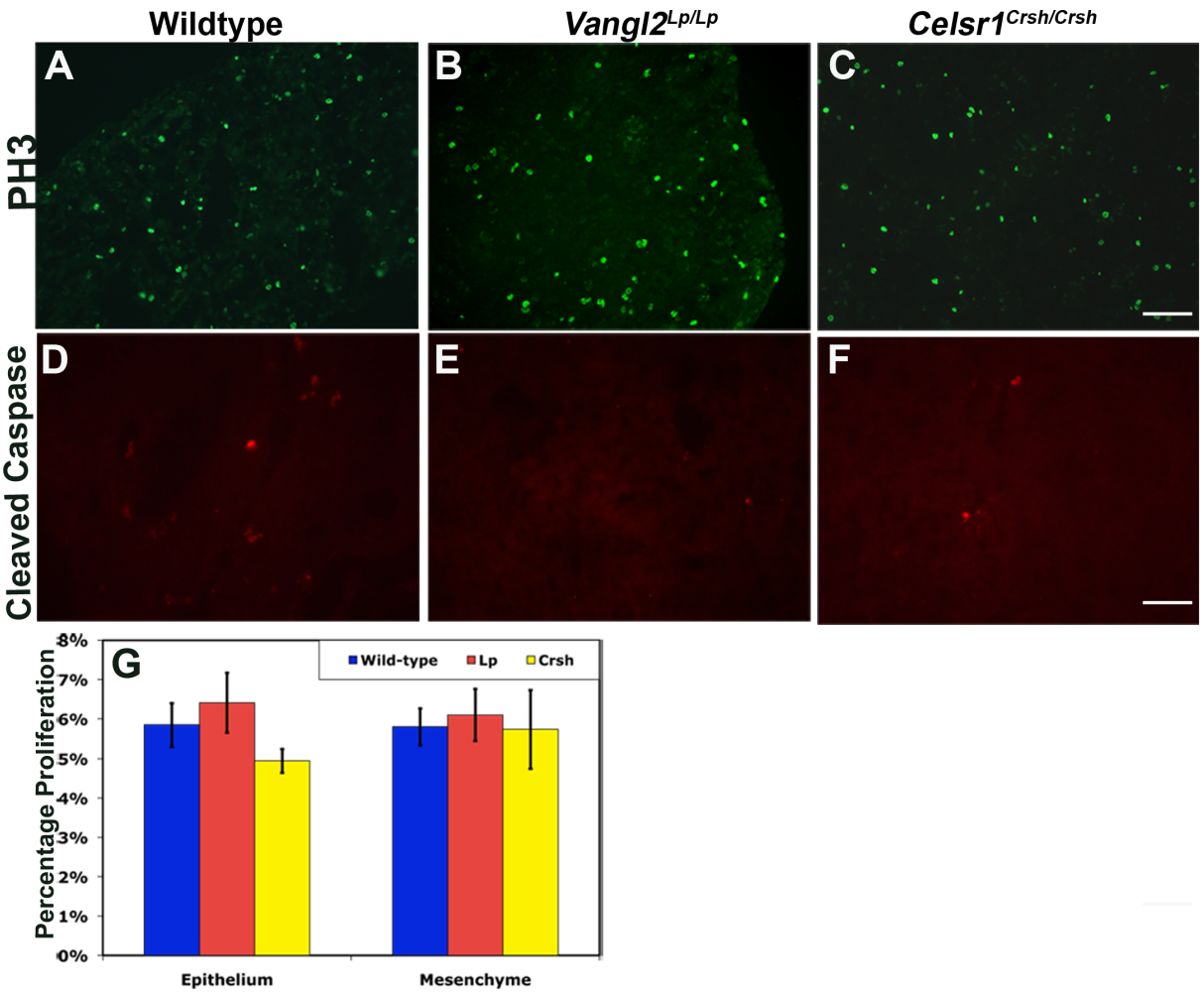


Figure 3.5 Proliferation and apoptosis are unaffected in *Celsr1*$^{Crsh/Crsh}$ and *Vangl2*$^{Lp/Lp}$ mutants Staining for phospho-histone H3 (PH3) of wildtype (A) *Vangl2*$^{Lp/Lp}$ (B) and *Celsr1*$^{Crsh/Crsh}$ (C). Analysis of E14.5 lung revealed no significant difference in proliferation. Anti-Cleaved caspase-3 staining of E14.5 wildtype (D), *Vangl2*$^{Lp/Lp}$ (E) and *Celsr1*$^{Crsh/Crsh}$ lung (F) showed no significant difference in apoptosis in mutant lungs compared to wildtype. Quantification of proliferation (G,H) or apoptosis (I) in both epithelium and mesenchyme of E11.5 (G,I) or E14.5 (H) lung sections reveals no significant difference between *Vangl2*$^{Lp/Lp}$ and *Celsr1*$^{Crsh/Crsh}$ compared to wildtype. Scale bars: A-F 25μM.

3.2.4 Branching morphogenesis defects in *Celsr1*$^{Crsh/Crsh}$ and *Vangl2*$^{Lp/Lp}$ *ex vivo* lung culture

As shown in section 3.3.2 there is a significant reduction in the number of airways in both *Celsr1*$^{Crsh/Crsh}$ and *Vangl2*$^{Lp/Lp}$ mutant lungs at E14.5 compared to wildtype littermates, suggesting both *Celsr1* and *Vangl2* are required for epithelial bud branching in the lung. The rostrocaudal axis of both *Crsh* and *Lp* homozygous mutants is significantly reduced as a result of disrupted convergent extension (Wang et al., 2006; Ybot-Gonzalez et al., 2007) yet neither *Crsh* nor *Lp* homozygous mutants display developmental delay as assessed by limb development. This shortened axis leads to reduced intrathoracic space which itself can impair lung development (Laudy and Wladimiroff, 2000). To ensure this reduced intrathoracic space was not the cause of the branching defects observed in these mutants, E11.5 homozygous mutant lungs were cultured *ex vivo* for 48h, in the absence of space restriction. No difference in the number of buds was observed at T0 between mutants and wildtype littermates (Fig 3.6 A-C), however by T48 a significant reduction in the number of terminal buds was seen in both *Celsr1*$^{Crsh/Crsh}$ and *Vangl2*$^{Lp/Lp}$ mutant lungs compared to wildtype littermates (Fig 3.6 D-E, G). In addition, the terminal buds were significantly enlarged (Fig 3.6 dashed lines in E, F compared with D and H) indicating a failure of normal branching morphogenesis. Therefore this data suggests that *Celsr1* and *Vangl2* are required for normal lung branching morphogenesis and the defects observed do not result from reduced intrathoracic space.

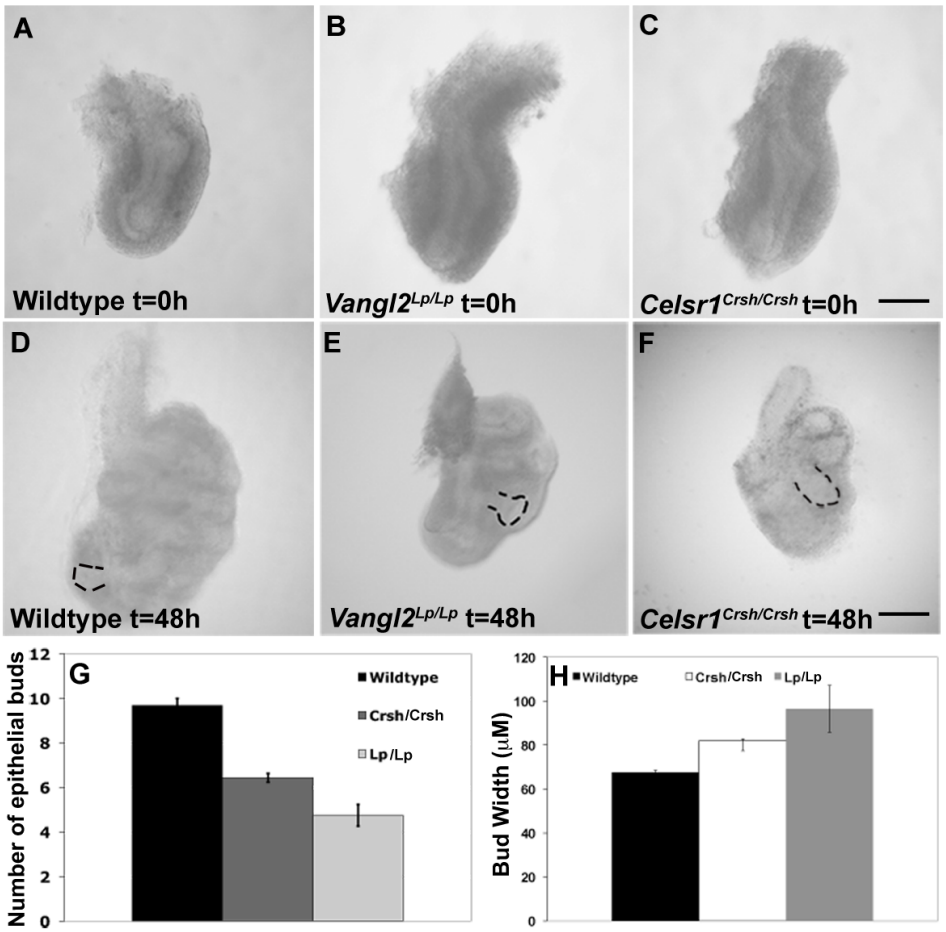


Figure 3.6 *Celsr1*$^{Crsh/Crsh}$ and *Vangl2*$^{Lp/Lp}$ mutant lungs display branching defects in *ex vivo* lung culture. E11.5 left lung lobes from wildtype (A,D); *Vangl2*$^{Lp/Lp}$ (B,E) and *Celsr1*$^{Crsh/Crsh}$ (C,F) were cultured for 48h. t=0 mutant lungs (B,C) were indistinguishable from wildtype lungs (A). t=48h wildtype lungs exhibited an increased number of terminal buds (D,G). A smaller increase in terminal buds was observed in *Vangl2*$^{Lp/Lp}$ (E,G) and *Celsr1*$^{Crsh/Crsh}$ (F,G) explants: wildtype 9.67, ±0.33, n=14; *Crsh* 6.43, ±0.48, n=8; *Lp* 4.75, ±0.2, n=6. Mutant lung buds are also expanded (E,F,H) relative to wildtype (D,H): wildtype 67.47, ±4.54 n=10; *Crsh* 81.85, ±4.34 n=16, *Lp* 96.5, ±10.6 n=8. Scale bars; A-F 63μM. *P<0.05.

3.2.5 Celsr1 and Vangl2 are required for all three modes of lung branching

To determine whether *Celsr1* or *Vangl2* affect lung branching as a whole, or whether they form part of a molecular mechanism that controls a specific mode of branching, we assessed whether all three modes of branching recently described by Metzger et al., were affected in mutant lungs compared to littermate controls. Domain branching occurs during the early stages of lung branching and involves the sprouting of new buds at specific distances along the length of a single stalk. Orthogonal and planar branching occur at the tips; planar branching happens when the tip splits into two buds within a single plane, and orthogonal branching involves the formation of new buds orthogonal to the parent stalk (Metzger et al., 2008).

Double immunostaining of E12.5 and E14.5 wildtype whole lungs with antibodies to either Celsr1 or Vangl2 and pan-cytokeratin to highlight epithelial cells, revealed both Celsr1 and Vangl2 expression in all modes of branching (Fig 3.7 red lines: domain branching, white lines: orthogonal branching, yellow lines: planar branching). In addition, all three modes of branching were observed in both *Celsr1*$^{Crsh/Crsh}$ and *Vangl2*$^{Lp/Lp}$ mutant lungs (Fig 3.7 C,D and data not shown) despite the defects already described. Thus suggesting Celsr1 and Vangl2 are part of the general mechanism of lung epithelial branching, rather than operating in one specific mode of branching.

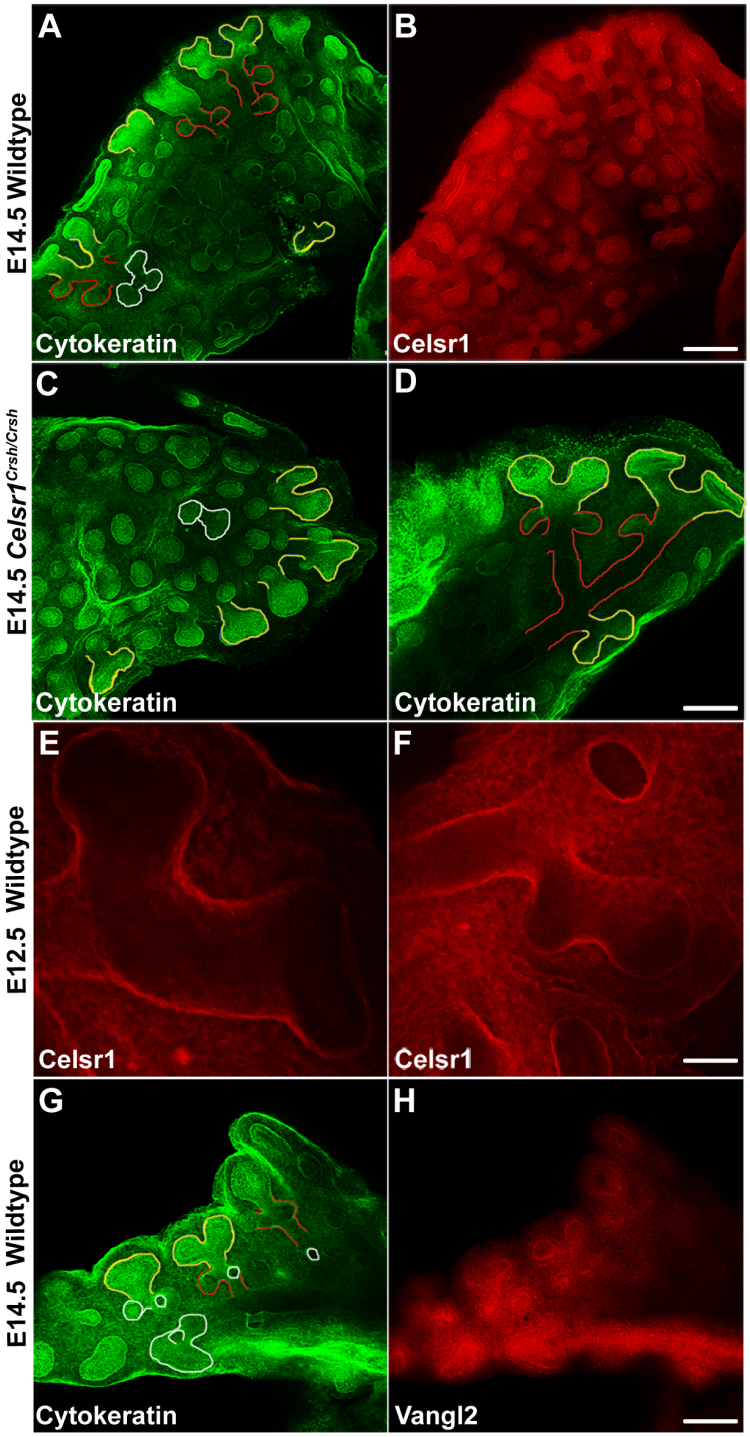


Figure 3.7 Celsr1 and Vangl2 are expressed in all modes of branching. Confocal images of wildtype E14.5 (A,B,G,H) and *Crsh/Crsh* (C,D) or E12.5 wildtype (E,F) whole lungs immunostained with anti-pan-cytokeratin (A,C,D,G), anti-Celsr1 (B,E,F) or anti-Vangl2 (H) antibodies. Pictures are slices showing a single layer from a z-stack. In wildtype lungs Celsr1 and Vangl2 are expressed in all three branching modes described by Metzger et al. 2008; examples of planar branching (yellow lines in A,C,D,G); domain branching (red lines in A,D,G) and orthogonal branching (white lines in A,C,G) are highlighted. All three modes are present in *Celsr1*$^{Crsh/Crsh}$ and *Vangl2*$^{Lp/Lp}$ lungs (C,D and data not shown) indicating that the defects are not restricted to a specific mode of branching. Scale bars A-B 125mM plus 1.2x zoom, C 125mM plus 1.2 x zoom, D 125μM plus 1.7 x zoom. E-F 125μM plus x6.3 zoom, G-H 125μM plus 1.7 x zoom.

3.2.6 *Celsr1*$^{Crsh/Crsh}$ and *Vangl2*$^{Lp/Lp}$ mutant lungs phenocopy lungs treated with Rho kinase inhibitor and Rho activation partially rescues the branching defect in Crsh

Rho kinases are important downstream effectors of a number of signalling pathways including the PCP pathway (Komiya and Habas, 2008; Maddala et al., 2003; Marlow et al., 2002; Schlessinger et al., 2009) These molecules directly impact upon cytoskeletal remodelling (Moore et al., 2002; Moore et al., 2005), by regulating the phosphorylation of non-muscle myosin II isoforms (Sandquist et al., 2006) and are essential for cellular morphogenesis and normal lung branching morphogenesis (Fanto et al., 2000; Moore et al., 2002; Wei et al., 2001). To determine whether rho kinases are required to control lung branching morphogenesis downstream of *Celsr1* and *Vangl2* in the PCP pathway, E11.5 left lung lobes were cultured *ex vivo* in the presence of a Rho kinase inhibitor (Y27632) (Uehata et al., 1997; Ybot-Gonzalez et al., 2007) for 48h. A dose dependant inhibition of branching was observed along with enlarged terminal buds (Fig 3.8 A,D) reminiscent of the phenotype observed in both *Celsr1*$^{Crsh/Crsh}$ and *Vangl2*$^{Lp/Lp}$ lungs in culture and *in vivo* (Fig 3.6 B,C).

Disruption to the cytoskeleton by addition of the cell permeable, potent inhibitor of actin polymerisation, Cytochalasin D to the culture medium, also resulted in a significantly reduction in the number of terminal buds that appeared broader than in control cultures (Fig 3.8 D,E). To confirm the role of Rho kinases downstream of Celsr1 and Vangl2, the rho activator, *Escherichia coli* cytotoxic necrotizing factor-1 (CNF-1) (Lerm et al., 1999) was added to wildtype E11.5 left lung lobes in culture, this lead to an increased number of terminal buds (Fig 3.8 F).

In a seperate experiment *Crsh/Crsh* left lung lobes were cultured in the presence of CNF-1 and the reduced number of terminal buds in *Crsh/Crsh* cultures

could be partially rescued. The rate of rescue was higher in *Crsh/Crsh* cultures compared to wildtypes when cultured in the presence of CNF-1 (24% increase in *Crsh/Crsh* lungs compared to 14% increase in wildtype lungs) (Fig 3.7 F). Taken together, this data is consistent with Celsr1 and Vangl2 signalling via the downstream PCP effectors Rho GTPases and Rho kinase, which can effect cytoskeletal organisation. Importantly, this discovery, suggests that the cellular disorganisation observed in the lungs of $Celsr1^{Crsh/Crsh}$ and $Vangl2^{Lp/Lp}$ mutants may be caused by defects in cytoskeletal organisation.

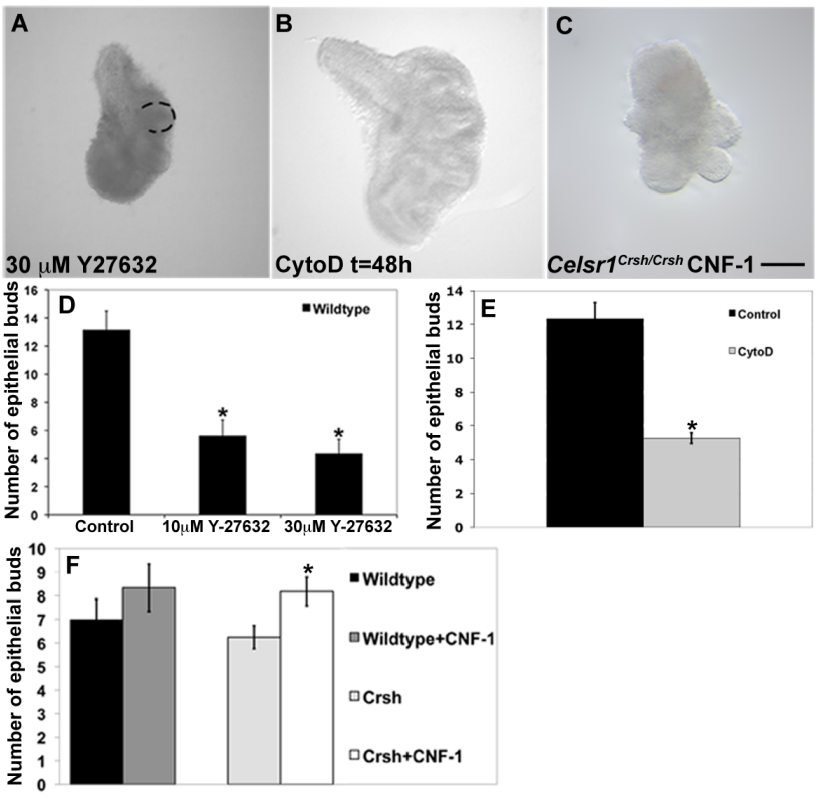


Figure 3.8 *Ex-vivo* lung cultures reveal that mutations in *Celsr1* and *Vangl2* phenocopy treatment with Rho kinase inhibitor and Rho kinase activation partially rescues the branching defect in *Crsh/Crsh*. Addition of Y27632 severely inhibits branching morphogenesis of a wildtype lung in a dose dependent manner (A,D): control 13.14, ±0.51, n=7; 10μM Y27632 5.60, ±0.51, n=5; 30μM Y27632 4.33, ±0.42, n=6. Disruption of the cytoskeleton with 100ng/ml Cytochalasin D also inhibits lung branching morphogenesis (B,E): wildtype 12.33, ±0.97, n=27; CytoD 5.28, ±0.32, n=18. Explants in A and B have broad branches and appear similar to those from *Vangl2*$^{Lp/Lp}$ (compare with Fig 3.6 B) and *Celsr1*$^{Crsh/Crsh}$ (compare with Fig 3.6 C). Wildtype lung explants treated with 20ng/ml CNF-1 show a small increase in number of epithelial buds formed (N): wildtype (untreated) 7, ±0.94, n=6; wildtype with CNF-1 8.33, ±1.13, n=9, two-tailed P value P=0.4819. This result was consistent though not statistically significant. Whereas in a separate set of experiments, treatment of *Crsh* homozygous lung explants with 20ng/ml CNF-1 results in a greater, statistically significant increase in bud numbers (C,F): *Crsh* (untreated) 6.25, ±0.52, n=8; *Crsh* with CNF-1 8.18, ±0.63, n=11. Explants were stage matched at t=0 to allow direct comparison of the number of end buds between control and treated or wildtype and mutant lungs within each experiment. Scale bars: A-C 63μM. *P<0.05.

3.2.7 Mutations in *Celsr1*$^{Crsh/Crsh}$ and *Vangl2*$^{Lp/Lp}$ lead to disrupted cytoskeletal organisation and disordered epithelial airways

The actin cytoskeleton provides a structural framework around which cell shape and polarity are defined, in addition its dynamic properties provide the driving force for cells to move and to divide (Hall, 1998). The assmebly of contractile actin-myosin filaments occurs as a result of Rho activation (Hall, 1998).

During morphogenesis epithelia will maintain their multicellular architecture, therefore they must be able to alter their spatial relationship with neighboruing cells without disrupting the junctions. The adherens junctions are required for the firm associations between cells, as disruption of them causes disorganisation of the epithelial architecture. They are composed of cadherin adhesion receptors and are associated with the actin-myosin cytoskeleton (Nishimura and Takeichi, 2009).

To determine whether defects in the cytoskeleton could be the cause of the cellular disruption and failure of morphogenesis observed in *Celsr1*$^{Crsh/Crsh}$ and *Vangl2*$^{Lp/Lp}$ mutant lungs, an assessment of the actin-myosin cytoskeleton and adherens junctions was undertaken.

E14.5 and E18.5 cryosections were stained with phalloidin to highlight F-actin (Fig 3.9 A-C, D-F). In wildtype sections cortical actin could be observed surrounding individual epithelial and mesenchymal cells. Phalloidin staining could also be detected at high levels along the apical surfaces of epithelial cells at E14.5 surrounding the airway lumen (Fig 3.9 A). In contrast the cortical F-actin appeared more discontinuous and diffuse both around individual cells and along the apical/luminal surface of the narrower *Ceslr1*$^{Crsh/Crsh}$ and *Vangl2*$^{Lp/Lp}$ mutant airways (Fig 3.9 B-C). Disruption to F-actin localisation was also observed at E18.5 in both mutants, with a loss of focal enrichment of F-actin particularly in those cells adjacent

to airways, compared with wildtype tissue (Fig 3.9 E,F compared to D). Non-muscle myosin II, another critical component of the cytoskeleton that directly links Rho kinase signalling with cytoskeletal organisation, was also disrupted in lungs of both mutants compared to wildtype littermates (Fig 3.9 H,I compared to G). The actin-myosin cytoskeletal disruption appeared more severe in *Celsr1*$^{Crsh/Crsh}$ lung tissue than in *Vangl2*$^{Lp/Lp}$ tissue, consistent with previous observations (see section 3.2.1). However immunostaining with anti-β-catenin revealed no defects in cell adherens junctions in either mutant compared with littermate controls (Fig 3.9 K,L compared to J). Therefore suggesting in *Celsr1*$^{Crsh/Crsh}$ and *Vangl2*$^{Lp/Lp}$ mutants the defects in cell organisation and branching arise not from disruption to individual cell adhesion, but are as a result of groups of cells being unable to move in a co-ordinated manner and therefore unable to give rise to new branches because of cytoskeletal disruption.

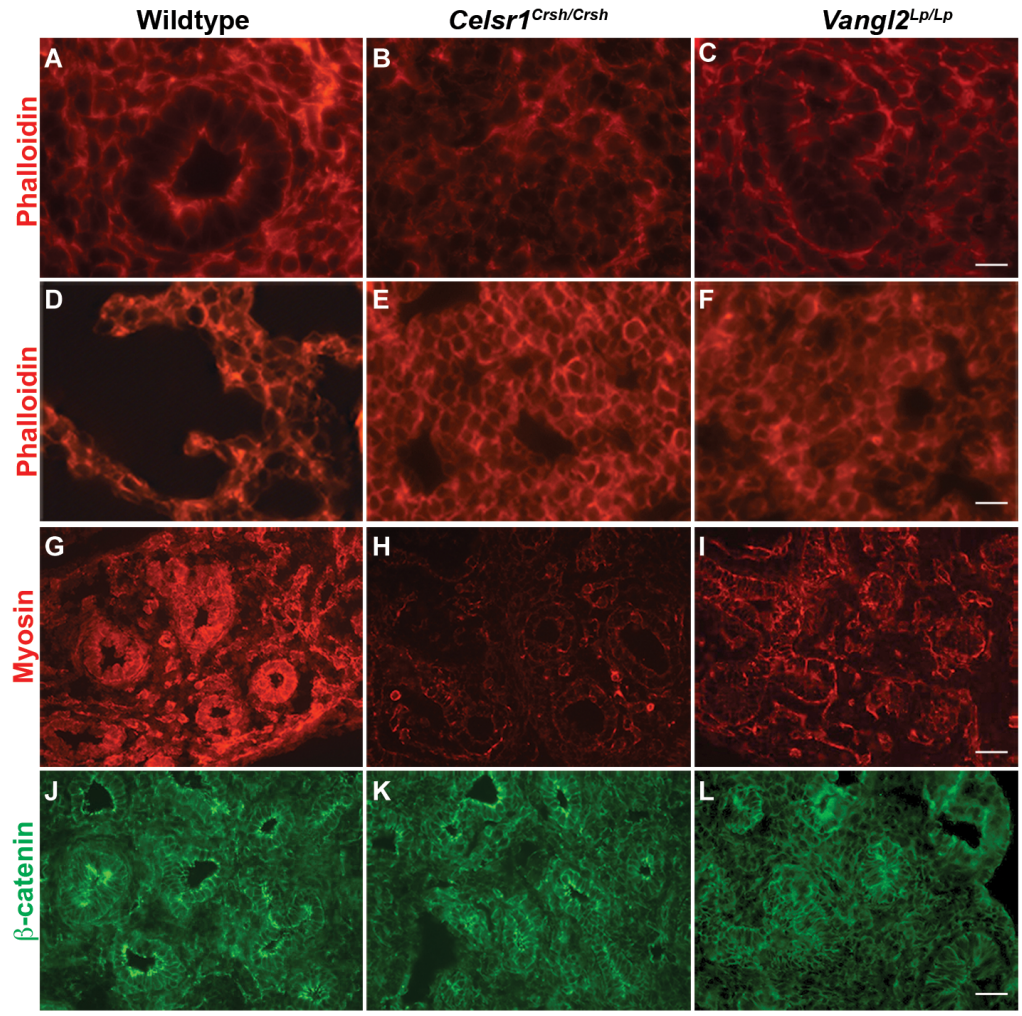


Figure 3.9 Mutant lungs display aberrant cell architecture. Cryosections of E14.5 wildtype (A,D,G,J) *Celsr1*$^{Crsh/Crsh}$ (B,E,H,K) and *Vangl2*$^{Lp/Lp}$ (C,F,I,L). Rhodamine phalloidin staining of F-actin reveals cytoskeletal defects in mutants at E14.5 (B,C) and E18.5 (E,F) compared to wildtype (A,D), as does staining with antibodies to non-muscle myosin IIA in mutants (H,I), compared to wildtype (G). Anti-β-catenin staining appears normal in *Celsr1*$^{Crsh/Crsh}$ (K) and *Vangl2*$^{Lp/Lp}$ (L), compared to wildtype (J). Scale bars: A-F 5μM, G-L 25μM, G-L 25μM.

3.2.8 Apical-basal polarity remains intact in *Celsr1*$^{Crsh/Crsh}$ and *Vangl2*$^{Lp/Lp}$ mutants

Apical-basal polarity is a requirement for epithelial tubes to form; because of the disruption in epithelial tube formation observed in both *Ceslr1*$^{Crsh/Crsh}$ and *Vangl2*$^{Lp/Lp}$ airways, an assessment of apical-basal polarity was carried out. Double immunostaining with ZO-2 (Fig 3.10 B,C compared to A), a tight junction protein located towards the apical surface or aPKCζ (Fig 3.10 D,E compared to D) a component of the apical membrane with the basement membrane protein laminin revealed no obvious changes in apical-basal polarity in either mutant airways compared to wildtypes. Some differences in the precise pattern of expression of the apical markers could be seen, but this is likely as a result of misaligned epithelial cells within the narrow lumina of the mutant airways, rather than disrupted apical-basal polarity.

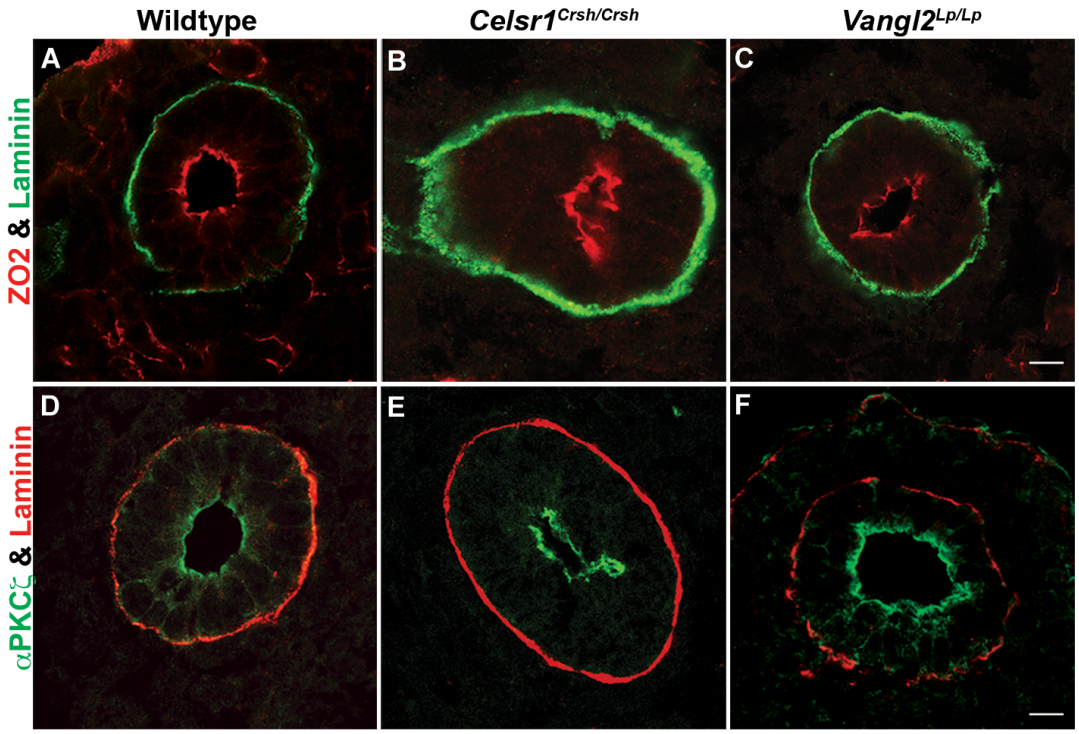


Figure 3.10 *Celsr1*$^{Crsh/Crsh}$ and *Vangl2*$^{Lp/Lp}$ mutant lungs display normal apical-basal polarity. Apical-basal polarity in lung is shown by double-labelling of wildtype (A), *Celsr1*$^{Crsh/Crsh}$ (B) and *Vangl2*$^{Lp/Lp}$ (C) airways with ZO-2 (red) and laminin (green in A-C and red in D-F) and by double-labelling of wildtype (D) *Celsr1*$^{Crsh/Crsh}$ (E) and *Vangl2*$^{Lp/Lp}$ (F) with aPKCς (green). Scale bars: A-F 12.5μM plus 3x zoom.

3.2.9 Lung endoderm from *Celsr1*$^{Crsh/Crsh}$ and *Vangl2*$^{Lp/Lp}$ mutants responds to the chemoattractant FGF10 but is unable to branch

In order to further investigate the tissue morphogenesis defects observed in *Ceslr1*$^{Crsh/Crsh}$ and *Vangl2*$^{Lp/Lp}$ lungs, their ability to respond to a key chemoattractant, FGF10, was tested. E11.5 lung epithelium denuded of mesenchyme was cultured in a 3-dimensional matrix for 48h in the presence of FGF10. In *vivo* FGF10 signals from the mesenchyme to its receptor FGFR2 in the epithelium to direct lung branching. As expected, wildtype epithelium responded to FGF10 signalling by the forming multiple buds (Fig 3.11 A,B), whereas mutant epithelium grew in size but in most cases did not branch at all in response to the chemoattractant (Fig 3.11 C,D). Quantification of the number of phospho-ERK1/2 positive cells (Fig 3.11 E) along with western blot analysis in the lungs of either *Ceslr1*$^{Crsh/Crsh}$ or *Vangl2*$^{Lp/Lp}$ compared with wildtype littermates, showed no difference in the levels of phospho-ERK1/2 (Fig 3.11 F), which is up regulated in response to FGF10 signalling. Thus indicating that the morphological defects observed in *Ceslr1*$^{Crsh/Crsh}$ and *Vangl2*$^{Lp/Lp}$ lungs prevent them from responding to a key branching signal, despite the FGF signalling pathway, at least that mediated by ERK1/2 remaining intact in mutant lungs.

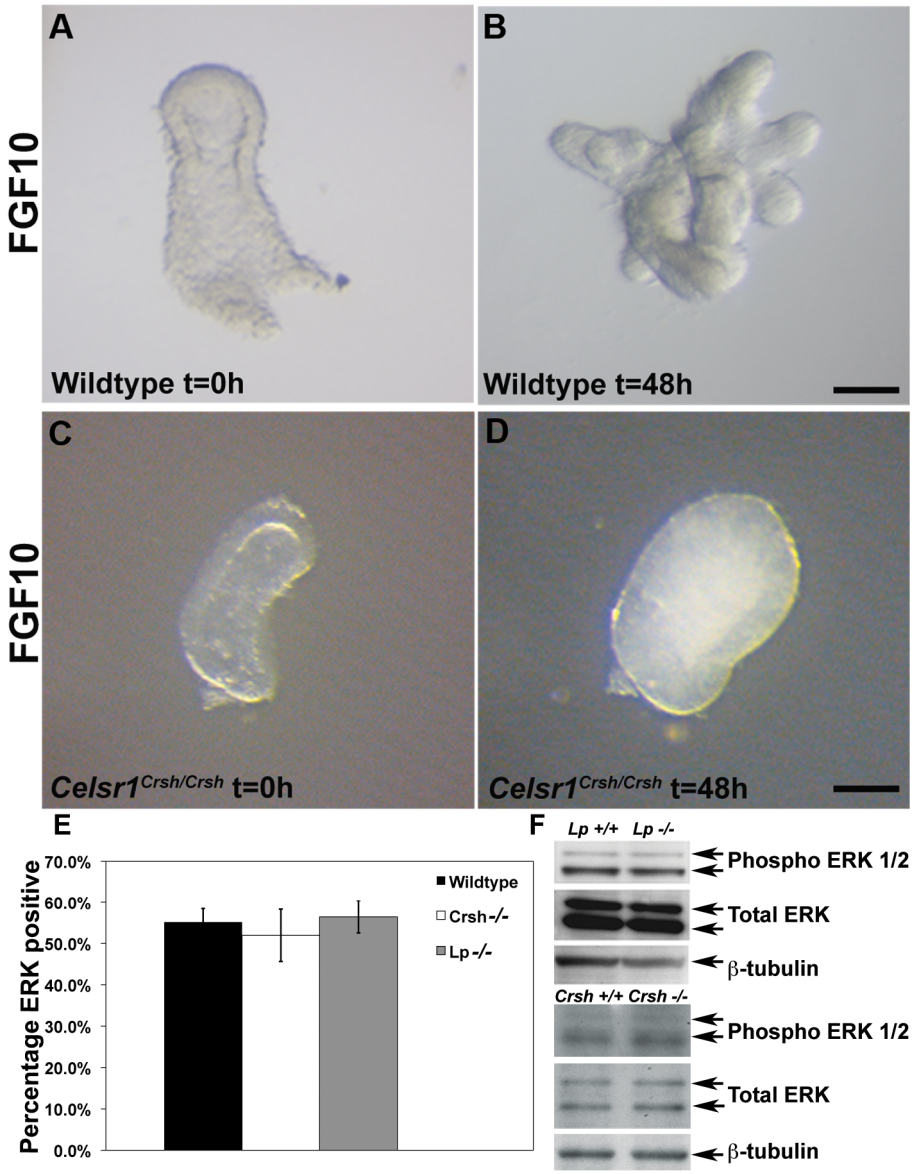


Figure 3.11 Mutant lung endoderm responds to FGF10 but is unable to undergo branching. (A,B) Wildtype lung endoderm branches in response to 400 ng/ml FGF10 (mean bud number=11 n=6). (C-D) mutant lungs do not branch in response to FGF10 (mean bud number *Crsh,* =0.9 n=6). P-ERK1/2 staining of E14.5 lung, shows no significant difference in percentage of P-ERK1/2 positive cells in the epithelium of mutants compared to wildtype controls (E): wildtype 55.17%, ±3, n=10; *Crsh* 51.97%, ±6.3, n=7, P=0.6074; *Lp* 56.45%, ±3.9, n=9, P=0.7939. Data from three embryos for each genotype. Western blotting reveals no change in the relative levels of P-ERK1/2 in wildtype and *Lp/Lp* or *Crsh/Crsh* littermates (F). Scale bars: A-D 5μM.

3.2.10 Celsr1 and Vangl2 proteins are spatially restricted and differentially expressed in lung epithelia

In order to gain insight into the functional role for Celsr1 and Vangl2 in regulating normal lung branching morphogenesis, wildtype E11.5 and E14.5 transverse sections were immunostained for anti-Celsr1 or anti-Vangl2 (Fig 3.12 A, B and C, E). Previous studies in other organisms and tissues have shown Celsr1 and Vangl2 contribute to a multi-protein complex and co-localise at cell membranes (Devenport and Fuchs, 2008; Jenny and Mlodzik, 2006). Whilst Celsr1 and Vangl2 do co-localise in some areas within lung epithelia, differences in the spatial expression patterns were also observed in the lung.

At E11.5, Celsr1 is highly expressed in the airway epithelium with the strongest expression restricted to the basal membranes as well as towards the apical surfaces of the airways at E11.5 (Fig 3.12 A). At E11.5 Vangl2 is expressed in the mesenchyme with higher levels of expression in the airway epithelium. Unlike Celsr1, Vangl2 staining appears more punctate and evenly distributed around cell membranes, but like Celsr1, Vangl2 is also enriched along the apical membranes surrounding the airway lumen, which is consistent with a previous study (Torban et al., 2007). Thus, while some overlap in expression patterns is observed, Celsr1 and Vangl2 appear to localise into seperate spatial domains within the lung epithelium.

The localisation of both Celsr1 and Vangl2 remains mostly the same at E14.5, but enrichment of Celsr1 towards the apical surface is more pronounced (Fig 3.12 C,E). *Celsr1*$^{Crsh/Crsh}$ sections immunostained with anti-Celsr1 showed a dramatic reduction in the level of expression compared to wildtype littermates, (Fig 3.12 D compared to C) as did *Vangl2*$^{Lp/Lp}$ sections immunostained with anti-Vangl2 compared to wildtype littermates (Fig 3.12 F compared to E). Thus confirming that

the mutation in Crash and Looptail result in loss of function in the lung. In addition, this data confirms the specificity of the Celsr1 and Vangl2 antibodies used in these studies.

The surprising differences in spatial and temporal distribution of Celsr1 and Vangl2 within the lung is very interesting as it suggests they have differing roles in some aspects of lung development, a novel concept for these proteins that were previously thought to always act together, within a complex. To understand the relationship between Celsr1 and Vangl2 in the lung, the localisation of Celsr1 in *Vangl2*$^{Lp/Lp}$ E14.5 sections (Fig 3.12 G) and visa versa, the localisation of Vangl2 in *Celsr1*$^{Crsh/Crsh}$ sections (Fig 3.12 H) was assessed. Ceslr1 localisation did not appear disrupted in *Vangl2*^{Lp} E14.5 transverse sections, (Fig 3.12 H compare with C), however Vangl2 localisation at the apical surface was lost in *Celsr1*$^{Crsh/Crsh}$ sections (Fig 3.12 G compare with E). This suggests Celsr1 is required for the correct localisation of Vangl2 at the apical surface in airway epithelia. However, Vangl2 is not required for the correct localisation of Celsr1. This finding is consistent with previous studies that place Celsr1 upstream of Vangl2 in the PCP signalling pathway (Seifert and Mlodzik, 2007; Strutt, 2001).

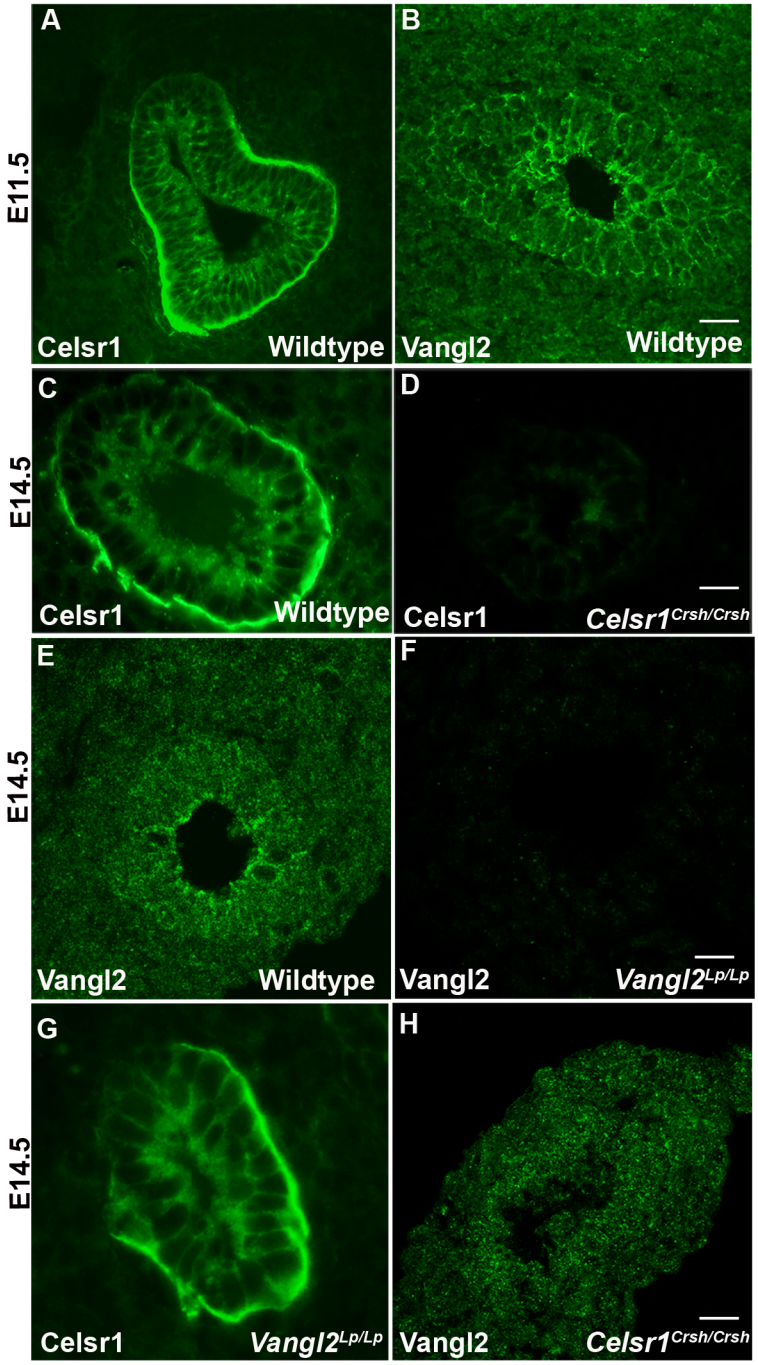


Figure 3.12 Celsr1 and Vangl2 proteins are spatially restricted and differentially expressed in lung epithelia. (A,B) E11.5 transverse cryosections of lungs immunostained with antibodies against Celsr1 (A), and Vangl2 (B). (C-F) Immunostaining of transverse cryosections of E14.5 wildtype (C,E) with anti-Celsr1 (C) and anti-Vangl2 (E) antibodies. Corresponding protein levels are dramatically decreased in lung tissue of mutants; anti-Celsr1 in *Celsr1*$^{Crsh/Crsh}$ (D) and anti-Vangl2 in *Vangl2*$^{Lp/Lp}$ (F) compared to wildtype (C,E). Immunostaining of Celsr1 protein in *Vangl2*$^{Lp/Lp}$ (G) reveals no change in spatial localisation. Enrichment of Vangl2 protein adjacent to the lumen is lost in *Celsr1*$^{Crsh/Crsh}$ (H) mutant lung sections. Scale bars: A,B 125mM plus x1.9 zoom, C 125mM plus x2.5 zoom, D 125mM plus x1 zoom, E,H 125mM plus x2 zoom, F,G 125μM plus x3 zoom.

3.2.11 Celsr1 co-localises with the basement membrane component laminin

The strong localisation of Celsr1 around the basal side of airways was an intriguing and novel finding as Celsr1 like most PCP proteins are thought to act in complexes localised mainly towards the apical surface of cells. Celsr1 staining was present in a thick band, reminiscent of basement membrane staining. To confirm this hypothesis E14.5 wildtype sections were double labelled with anti-Celsr1 (Fig 3.13 A) and anti-laminin (Fig 3.13 B) and these proteins were subsequently shown to co-localise, by sequential confocal imaging (Fig 3.13 C, D-F). The basement membrane is the fusion of two lamina, the basal lamina and the reticular lamina (or lamina reticularis) and functions primarily to anchor down the epithelium to its loose connective tissue underneath while acting as a mechanical barrier. The basal lamina layer can further be divided into two layers. The clear layer closer to the epithelium is called the lamina lucida, while the dense layer closer to the connective tissue is called the lamina densa. Laminin and therefore Celsr1 reside in the Lamina Lucida. As a control experiment, double labelling of Laminin with β-catenin showed no overlapping of expression as these proteins exist in two separate compartments. β-catenin localises to the plasma membrane around the circumference of the cells (Fig 3.13 G-I).

Celsr1 expression is frequently unevenly distributed in the basement membrane around airways in a similar pattern to laminin, with stronger expression on one side of an airway compared to the other. Areas of reduced basement membrane or laminin staining indicates areas of cell movement such as new bud outgrowth, whereas areas with stronger thicker basement membrane staining where Celsr1 and laminin colocalise indicates areas of restricted growth such as cleft regions. This novel finding that Celsr1 localises to the basement membrane in the lung suggests a novel, role for this protein in lung branching. Interestingly, this data is consistent with

a recent study that shows Celsr1 localises to the extreme basal domain of neuroepithelial cells both within the early neural tube and in a population of cells at the dorsal ventral midline of the developing spinal cord (Formstone et al., 2010b).

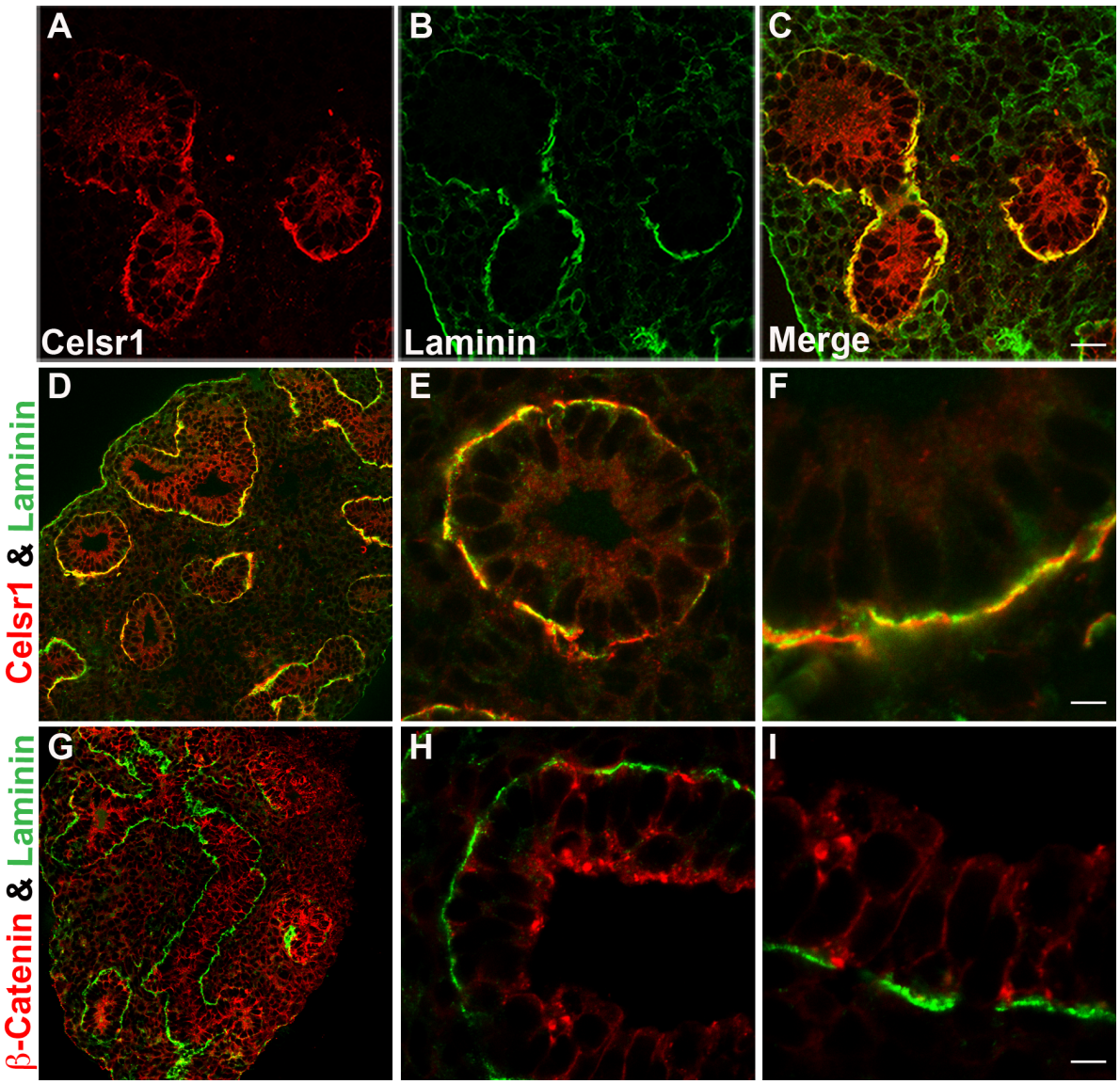


Figure 3.13 Celsr1 colocalises with laminin a component of the basement membrane. Double labelling of wildtype E14.5 cryosections with Celsr1 (red) A,C-F and laminin (green) B, C-F reveals co-localisation of these proteins in wildtype basement membrane surrounding lung epithelium. Double labelling with β-catenin (red) and laminin (green) G-I shows no co-localisation in wildtype lung. Scale bars; A-C 125μM x2 zoom; D,G 125μM; E,H 125μM x3 zoom;F,I 125μM x4 zoom.

3.2.12 Celsr1 and Vangl2 expression is enriched in highly specific regions of the branching lung epithelium

To determine the localisation of Celsr1 and Vangl2 in an active 3D model of lung branching, wildtype lung endoderm was denuded of mesenchyme and cultured in the presence of FGF10 to promote branching. The explants were then post stained with either anti-Celsr1 (Fig 3.14 A, B) or anti-Vangl2 (Fig 3.14 C, D) and phalloidin (Fig 3.14 E-H) to highlight cortical actin. Regions enriched with cortical actin are likely undergoing cytoskeletal remodelling that allows cell rearrangement and/or movement. Both Celsr1 and Vangl2 were observed around epithelial cell membranes, while z-stack images through explants reveal that Vangl2 is enriched at the apical surface of epithelial buds (Fig 3.14 C,D). Consistent with the section data, Celsr1 localises to the basement membrane and is highly enriched at regions of restricted growth, e.g. at sites immediately adjacent to the outgrowth of new buds (Fig 3.14 A,B). This data strengthens the idea that Celsr1 and Vangl2 have differential roles in lung branching morphogenesis.

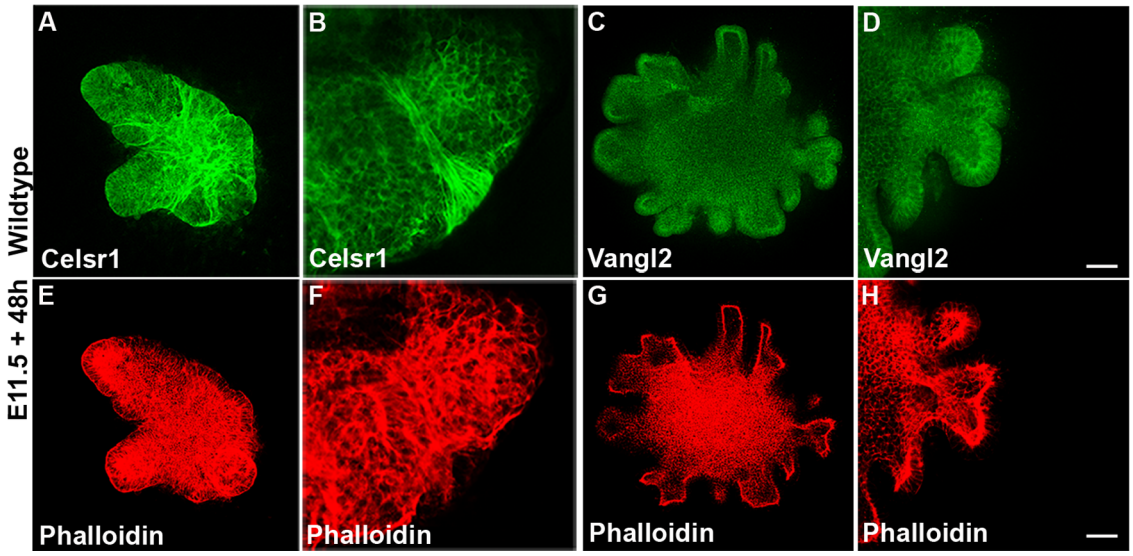


Figure 3.14 Differential expression of Celsr1 and Vangl2 is observed in branching lung endoderm explants E11.5 lung endoderm explants cultured for 48h in 400ng/ml FGF10 and double labelled with phalloidin (H-K) and Celsr1 (D,E) or Vangl2 (F,G) antibodies. High levels of Celsr1 expression are present in regions of restricted tissue growth such as points of bifurcation (D,E,H,I). Vangl2 is most highly expressed at the luminal surface of outgrowing buds (F,G,J,K). Scale bars: A,C,E,G 125μM x2.7 zoom, B,F 125μM x 10 zoom D,H 125μM x8 zoom.

3.2.13 Loss of *Vangl2$^{Lp/Lp}$* results in kidney branching defects

As describe in section 3.2.1 mutations in Celsr1 and Vangl2 also perturbs kidney branching morphogenesis. Macroscopic analysis of *Celsr1$^{Crsh/Crsh}$* and *Vangl2$^{Lp/Lp}$* kidneys at E18.5 revealed them to be smaller, abnormally shaped and with a shortened proximal distal axis (Fig. 3.2 D,E). To further investigate the role of the core PCP gene *Vangl2* in branching morphogenesis, analysis of the kidney phenotype in *Vangl2$^{Lp/Lp}$* mutants was carried out.

E11.5 transverse sections through whole wildtype (Fig 3.15 A) and *Vangl2$^{Lp/Lp}$* (Fig. 3.15 B) embryos revealed no obvious defects in paired metanephric rudiments. Both wildtype and *Vangl2$^{Lp/Lp}$* displayed a ureteric bud (ub, Fig 3.15 A,B) surrounded by mesenchymal cells (m, Fig 3.15 A,B). Thus suggesting Vangl2 is not required for the initial invagination of this epithelial branch into the metenephric mesenchyme.

However, by E13.5 when the ureteric bud has branched several times (Costantini and Kopan, 2010), a defect was observed in both *Vangl2^{Lp}* homozygous (Fig 3.15 D,E) and heterozygous (Fig. 3.15 E) kidneys compared to wildtype littermates (Fig. 3.15 C,E). Whole mount immunostaining for anti-pan cytokeratin to highlight both branching tips and collecting duct stalks (Kobayashi et al., 2008) revealed a significant reduction in the number of kidney tubules observed in both *Vangl2$^{Lp/Lp}$* and *Vangl2$^{Lp/+}$* kidneys compared to wildtype littermates. Thus suggesting that while Vangl2 is not required for early ureteric bud formation, is it required for subsequent branching and determining the number of kidney tubules later in development.

Assesment of proliferation by immunostaining E14.5 and E18.5 sections with anti-phospho histone H3 and apoptosis by immunostaining for anti-cleaved caspase

revealed no obvious defects in proliferation or apoptosis in *Vangl2*$^{Lp/Lp}$ kidneys consistent with the lung data presented above (Yates et al., 2010a). Also consistent with findings in the lung, differentiation appeared unaffected in *Vangl2*$^{Lp/Lp}$ kidneys as assessed by immunostaining whole E12.5 kidneys cultured *ex vivo* for 5 days with anti-WT1 to highlight glomerular podocytes (Guo et al., 2002; Yates et al., 2010a).

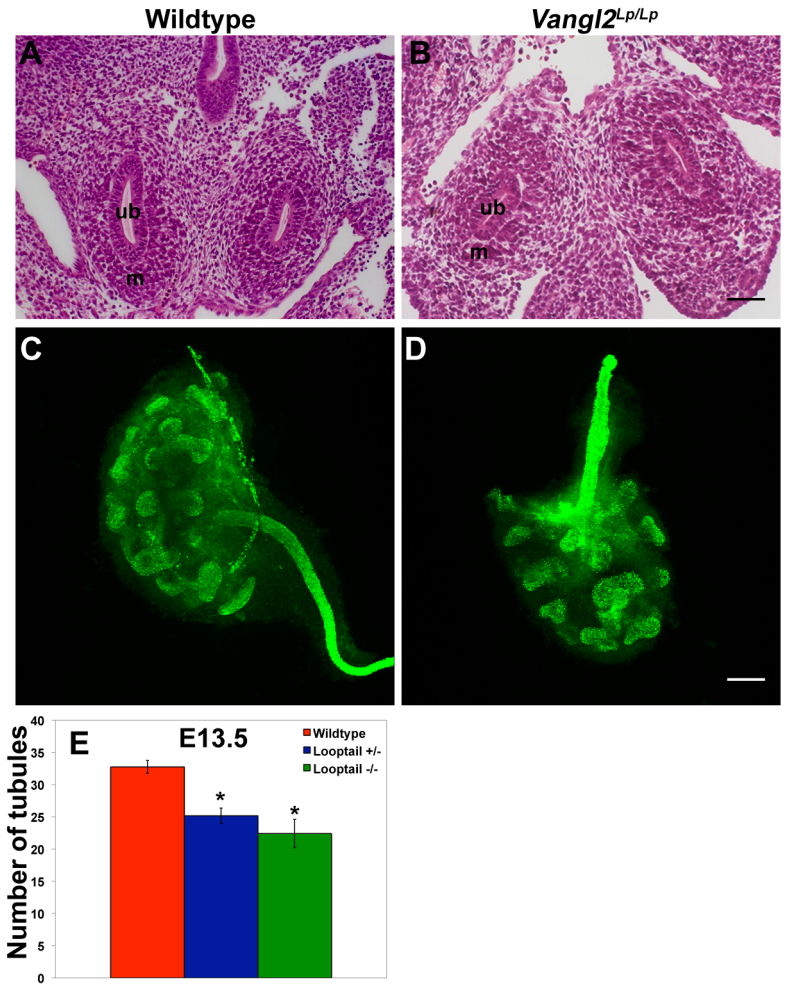


Figure 3.15 Loss of Vangl2 leads to defects in kidney branching morphogenesis

E11.5 H&E stained sections through whole UGR's revealed no obvious differences in the development of *Vangl2*$^{Lp/Lp}$ ureteric buds (B) when compared to wildtype littermates (A). E13.5 whole z-stack images of wildtype kidneys (C) and *Vangl2*$^{Lp/Lp}$ (D) kidneys were immunostained with anti-pan cytokeratin to highlight epithelial tubules. A significant reduction in the number of epithelial tubules was observed in *Vangl2*$^{Lp/Lp}$ and *Vangl2*$^{Lp/+}$ kidneys when compared to wildtype littermates (E), wildtype 32.75 ± 0.98 n=4, *Lp*/+ 25.17 ± 1.18 n=12, *Lp/Lp* 22.4 ± 2.2 n=5. Wt:Het P=0.002, WT:Hom P= 0.003. (ub) ureteric bud, (m) meteneprhic mesenchyme. Scale bars: A-B 25μM, C-D 125μM x 1.3 zoom.

3.2.14 The late gestation *Vangl2*$^{Lp/Lp}$ kidney has poor cortico-medullary definition, a hypoplastic medulla and mildly dysmorphic tubules

By E18.5 wildtype kidneys have acquired their characteristic "kidney bean shape" with its centre occupied by a slit-like renal pelvis, the cavity that rceives urine from the collecting duct system (Fig 3.16 A). Analysis of E18.5 paraffin wax sections through whole *Vangl2*^{Lp} heterozygous kidneys revealed them to be similar to wildtype littermates whereas *Vangl2*$^{Lp/Lp}$ kidneys lacked the characteristic "kidney bean shape" and the renal pelvis resembled a hole rather than the normal elongated cavity (compare outline of organ in Fig 3.16 C with A).

Wildtype kidneys at E18.5 contained a well-defined cortex and medulla (Fig. 3.16 D). Ureteric bud branch tips comprise the outer cortex with S-shaped bodies within the cortex below, which are immature nephrons beginning to segment into glomerular and proximal tubule epithelia, as well as proximal tubules and glomeruli (Fig 3.16 D and G). The border between the cortex and medulla was unclear in *Vangl2*$^{Lp/Lp}$ kidneys (Fig 3.16 F) with heterozygous kidneys (Fig 3.16 E) having an intermediate appearance between null mutant and wildtype littermates. Proximal tubules and glomeruli however showed no difference between *Vangl2*$^{Lp/+}$ kidneys compared to wildtype controls (compare Fig 3.16 H with G). Whereas homozygous mutant kidneys contained subsets of glomeruli which were small or distorted and some tubules contained attenuated brush borders as visualised by periodic acid Schiff staining (Fig 3.16 I). Proximal tubules contain a brush border consiting of microvilli on the apical surface of proximal tubules cells, which are rich in actin (Ashworth et al., 2001; Ashworth et al., 2003). Using phalloidin staining to visualise the f-actin cytoskeleton, some proximal tubule cells in E18.5 *Vangl2*$^{Lp/Lp}$ kidneys had an irregular and

discontinuous actin pattern versus proximal tubules in wildtype littermates (compare Fig 3.16 K with J). The crenelated or indented pattern of F-actin in wildtype glomerular tufts, likely represents actin in both the basal zone of podocytes and in closely adjacent endothelia in forming capillary tufts (Goto and Ishikawa, 1998), appeared less prominent in *Vangl2*$^{Lp/Lp}$ glomeruli (Fig 3.16 compare M to L).

Disruption to the cortical actin cytoskeleton in *Vangl2*$^{Lp/Lp}$ kidneys was similar to the disruption observed in the lung (see section 3.2.7), indicating *Vangl2* operates via a similar mechanism in the kidney as in the lung to modulate branching. Although some tubules in *Vangl2*$^{Lp/Lp}$ mutant kidneys appeared dilated (Fig 3.16 I), an early indication of cyst formation an overt polycystic phenotype was not seen in Vangl2 mutant kidneys.

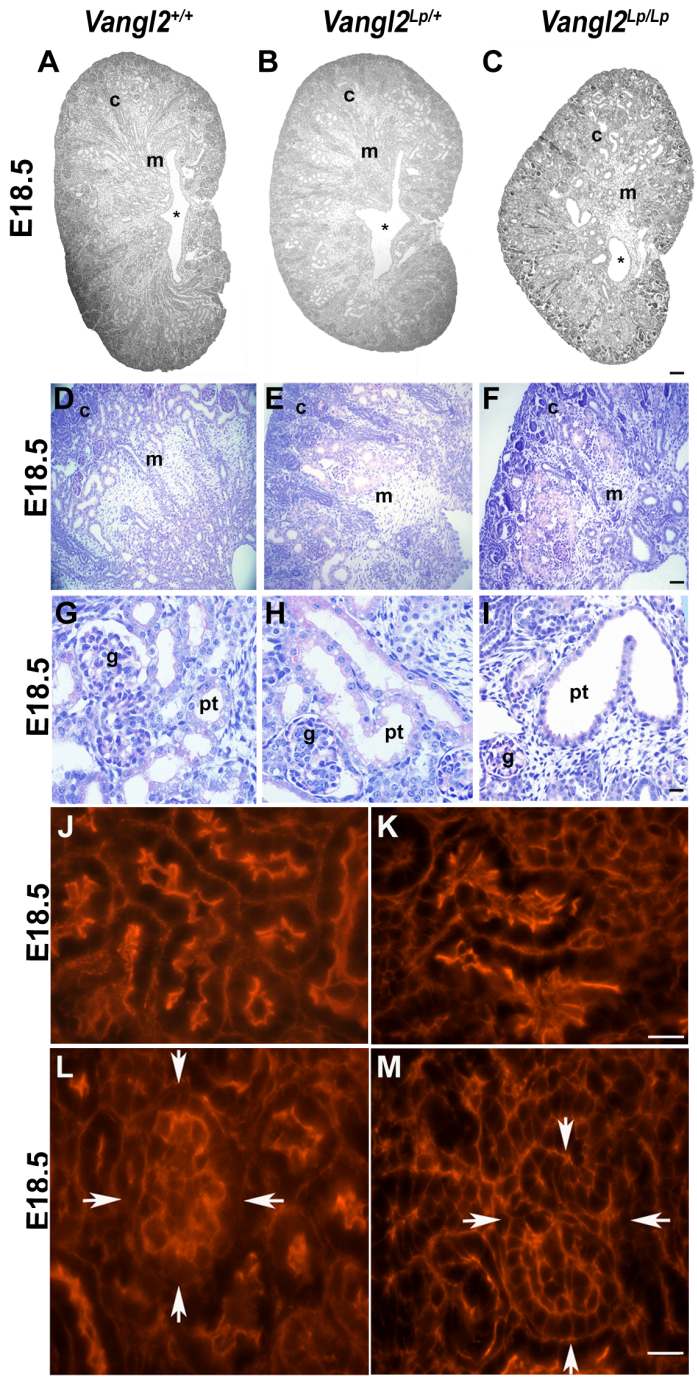


Figure 3.16 Histology of E18.5 looptail kidney sections. At E18.5, *Lp/+* (B) and *Lp/Lp* (C) kidneys are smaller than wildtype littermate kidneys (A). *Vangl2*$^{Lp/Lp}$ kidneys are visibly misshaped, with a hypoplastic medulla (compare F to D) and without the slit-like pelvis (*) seen in the wild type and *Vangl2*$^{Lp/+}$ kidneys. Occasional enlarged and distorted proximal tubules were observed in *Vangl2*$^{Lp/Lp}$ mice (I) but no overt cystic phenotype. Phalloidin staining highlights disruption to the organisation of the actin cytoskeleton in *Vangl2*$^{Lp/Lp}$ proximal tubules; particularly at the apical surface (K), in comparison to the ordered cytoskeletal arrangement in *Vangl2*$^{+/+}$ (J). Phalloidin staining highlighted the typical indented or crenelated pattern of f-actin in wildtype glomerulus (arrowed in L) which appeared less apparent in a *Vangl2*$^{Lp/Lp}$ glomerulus (arrowed in M). Images are representative of at least 3 animals in each category. (c) cortex, (g) glomerulus, (m) medulla, (pt) proximal tubule. Scale bars: A-C;200μm, D-I;25μm, J-M;5μm.

3.2.15 Looptail heterozygous kidneys have fewer glomeruli but do not display functional defects when compared to wildtype littermates

Previous studies have shown Vangl2 protein to be expressed in developing murine kidneys, in ureteric bud branch tips, collecting ducts, nephron vesicles and forming glomeruli (S-shaped bodies and podocyte epithelia) (Babayeva et al., 2010; Torban et al., 2007). In addition analysis of E18.5 parrafin sections (3.2.14) revealed the morphology of glomeruli in *Vangl2*$^{Lp/Lp}$ to be disrupted. This prompted further analysis of glomeruli in *Vangl2*$^{Lp/Lp}$ mutants as dysfunction of the glomerulus is the most common cause of renal failure. *Vangl2*$^{Lp/Lp}$ kidneys displayed malformed glomeruli, with a distorted glomerular tuft. Less than 90% of all glomeruli contained two or more capillary lumens and, more strikingly, only half of these had more than two lumens. Whereas in wildtype kidneys over 95% of glomerular cross-sections displayed two or more capillary lumens (a marker of maturity), and most had more than two such lumens (data not shown, (Yates et al., 2010a) *Vangl2*$^{Lp/+}$ glomeruli displayed an intermediate phenotype between wildtypes and null mutants (data not shown, (Yates et al., 2010a)).

Due to the morphology defects observed in *Vangl2*$^{Lp/+}$ mutants, an assessment of the number and function of glomeruli was carried out in adult mice. Due to embryonic lethality this could not be tested in adult homozygous mutants. One month old *Vangl2*$^{Lp/+}$ kidneys were found to have a modest but significant reduction in glomerular numbers (Fig. 3.17 A) although immunostaining for synaptopodin and nephrin were normal, and there was no sign of glomerulosclerosis (scarring) as assessed by periodic acid Schiff staining (data not shown, (Yates et al., 2010a)). Tubules also revealed no cyst formation, an early sign of polycystic kidney disease.

No variation in urinary albumin concentration was observed in 4 month old *Vangl2*$^{Lp/+}$ mice compared to wildtype littermates, indicating the glomerular permeability barrier (i.e. a podocyte function) in mutants remains intact (Fig 3.17 B). Retinol binding protein excretion was also measured in 4 month old *Vangl2*$^{Lp/+}$ to determine whether proximal tubule uptake of small molecules was impaired in these mutants, however no significant impairment was observed compared to wildtype littermates (Fig 3.17 C). So despite the morphological and histological defects observed in *Vangl2*$^{Lp/+}$ mutants these are not severe enough to impact on adult kidney function under normal conditions.

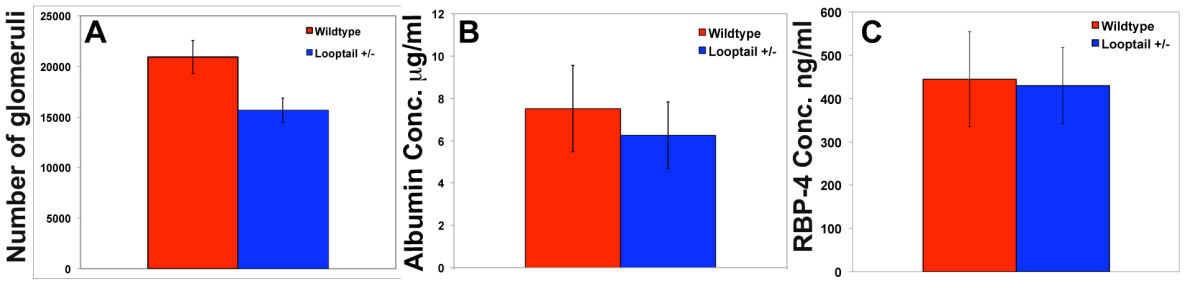


Figure 3.17 Vangl2 heterozygote kidneys have fewer glomeruli but have normal renal function. 4 week old adult wildtype and *Vangl2*$^{Lp/+}$ kidneys were dissected, acid dissociated and the number of glomeruli counted, a reduction in the number of glomeruli was observed in *Vangl2*$^{Lp/+}$ kidneys compared to littermate controls (A) (wildtype 20,937.5 ± 1636.1 n=4, *Vangl2*$^{Lp/+}$ 15,694.4 ± 1185.5 n= 4). 4 month old wildtype and *Vangl2*$^{Lp/+}$ mice were housed in metabolic cages for 24 hours and urine collected over this time period. The concentration of both urine albumin (normalised to creatine) (B) and RBP-4 (C) were determined by ELISA and no significant difference in levels was observed for either between genotypes (Albumin; wildtype 7.52 mg/ml, ± 1.65 n=11 *Vangl2*$^{Lp/+}$ 6.26mg/ml, ± 1.99 n=8, P=0.63. RBP-4; wildtype 444.95ng/ml ± 109.63 n=11 *Vangl2*$^{Lp/+}$ 430.17ng/ml ± 175.3 n=8 P=0.927).

3.3 Discussion

Defects in lung or kidney epithelial tube formation results in a number of common disorders such as cystadenomatoid malformations, hypertension and agenesis or hypoplasia of the lung or kidney, which represent a significant clinical burden (Jancelewicz et al., 2008; Thebaud and Abman, 2007; Whitsett et al., 2004). Disruption of lung or kidney development can have significant repercussions on the post-natal function of these organs. Efficient post-natal function requires the generation of normal cell and tissue architecture in utero (Whitsett et al., 2004). One of the dominant features of diseases such as Idiopathic pulmonary fibrosis and adult respiratory distress syndrome is fibrosis; which results in abnormal tissue structure leading to impaired gas/air exchange and respiratory dysfunction (Chapman, 2004).

In the post-natal kidney, disruption to orientated cell division during the development of kidney tubules leads to dilation of tubules and formation of cysts, a major cause of ciliary disease (Fischer et al., 2006; Ross et al., 2005; Simons et al., 2005). It is crucial therefore to understand in more detail the molecular mechanisms and underlying signalling pathways that direct development of these branched organs if we are to improve treatment regimes for these diseases.

3.3.1 Mutations in PCP genes disrupt lung branching morphogenesis and cytoskeletal organisation

The results presented in this chapter demonstrate a novel role for Celsr1 and Vangl2, two core PCP genes in the control of normal lung branching morphogenesis. Mutations in *Celsr1* and *Vangl2* result in reduced epithelial bud branching and disrupted epithelial cell arrangements likely a consequence of cytoskeletal defects which, result in narrower airways and tissue hypoplasia. Disruption to Celsr1 or

Vangl2 does not completely abolish epithelial branching, instead these mutations result in fewer epithelial branches that have structural malformations which are likely severe enough to impact on lung function. The observation that Celsr1 and Vangl2 do not completely abolish branching in the lung is consistent with studies of mouse mutants of other genes required for branching morphogenesis, (De Langhe et al., 2005; Gontan et al., 2008; Kaartinen et al., 1995; Miettinen et al., 1997; Quaggin et al., 1999), disruption to Celsr1 or Vangl2. Unfortunately this was not possible to demonstrate due to perinatal lethality caused by neural tube defects.

Ex Vivo culture of Celsr1 and Vangl2 homozygous lungs reveals broader, but not shorter, epithelial buds compared to wildtype. This finding was interesting as in vertebrates, PCP signalling regulates convergent extension movements whereby intercalation of cells enables elongation and narrowing of tissues, including rearrangement of the neural plate during neurulation (Ybot-Gonzalez et al., 2007). In addition, recent studies in the kidney have shown that convergent extension occurs during kidney tubule formation and that this process is mediated via the PCP pathway (Karner et al., 2009).What about involvement of orientated cell division?, From the phenotypes observed in Ceslr1 and Vangl2, mouse mutants i.e. broader but not shorter buds, it appears these genes do not affect elongation of lung buds. However, since elongation of epithelial tubes is less dramatic in the lung compared to that in the kidney this finding is perhaps not surprising. The PCP signalling pathway has additionally been shown to be required for proper morphogenesis of tissue in a number of other distinct sites including heart, formation of the female reproductive tract and directed cell migration *in vitro* (Dow et al., 2007; Henderson et al., 2006; Kalabis et al., 2006; Phillips et al., 2007b; Vandenberg and Sassoon, 2009; Zhou et al.,

2007b). Future studies will be required to determine whether any of these cellular behaviours are disrupted in *Celsr1*$^{Crsh/Crsh}$ and *Vangl2*$^{Lp/Lp}$ lungs.

By inhibiting Rho Kinase, a known downstream effector of PCP and key regulator of the cytoskeleton (Habas et al., 2001; Marlow et al., 2002; Strutt et al., 1997) the Celsr1 and Vangl2 mutant branching phenotype is recapitulated in wildtype lung explants. This phenotype can be partially rescued in mutant lung explants by CNF-1 induced Rho activation. It is likely that the defects in the actin-myosin cytoskeleton observed in Celsr1 and Vangl2 mutant lungs prevent normal tissue movement such that they cannot branch in response to the chemoattractant FGF10; despite the FGF signalling pathway remaining intact. Crucially, apical basal polarity, a key requirement for normal epithelial tube formation, does not appear affected in mutant lungs.

3.3.2 The expression patterns of Celsr1 and Vangl2 suggest both common and differential roles for these proteins in lung branching morphogenesis

Previous studies in other tissues and organisms have shown the PCP proteins often co-localise at cell membranes and are thought to form a multi-protein complex (Devenport and Fuchs, 2008; Jenny and Mlodzik, 2006). Whereas, interetesingly in the lung, Celsr1 and Vangl2 display novel differential expression patterns suggesting differing functions. Celsr1 is highly expressed between buds as well as at sites where bifurcation occurs. In contrast, Vangl2 is not enriched at sites of tissue indentation or bifurcation and instead, the highest levels of Vangl2 are in cells surrounding the lumen. Further evidence for the differing roles of these two proteins comes from Morpholino knockdown and Real time imaging experiments carried out by Yates et al. (Yates et al., 2010b). Consistent with the localisation data presented in this chapter, Celsr1 MO knockdown in lung explant culture also revals an independent function for

Celsr1 in some aspects of lung branching morphogenesis. Whilst it is possible that these differences may be a consequence of additional roles of these genes outside the PCP pathway, to date, no such additional roles have been attributed to Vangl2 or Celsr1 making this possibility less likely. Therefore, histological, molecular marker and macroscopic analysis of *Celsr1* and *Vangl2* mouse mutants, reveals that while both are obligatory for normal lung development, these proteins regulate some distinct steps in airway formation.

In addition to their differing roles, Celsr1 and Vangl2 do display regions of overlapping expression, in particular, Celsr1 and Vangl2 are asymmetrically enriched towards luminal airway surface. Both mutants show loss of or reduced diameter of lung lumina, suggesting like other apically enriched proteins, Celsr1 and Vangl2 may have an important role in establishing a proper lumen i.e. they may help to modulate co-ordinated cellular movement via regulation of the cytoskeleton that is necessary for the formation of a normal lumen.

Previous studies have suggested Celsr1 may act at the top of a hierarchy of PCP proteins, helping to recruit other PCP proteins to the cell membranes. Analysis of Vangl2 expression in *Crsh* mutants showed a distinct loss of Vangl2 enrichment adjacent to the lumen, indicating that Celsr1 is required to correctly localise Vangl2 and this is consistent with these previous studies. In addition, the $Celsr1^{Crsh/Crsh}$ mutant phenotype was consistently more severe than that of $Vangl2^{Lp/Lp}$ again suggesting that in lung, Celsr1 may operate upstream of Vangl2.

3.3.3 Celsr1 is required for bud bifurcation

A previously propsed mechanism of bud bifurcation describes newly synthesised extracellular matrix being deposited transiently and focally in forming cleft regions

(Rebustini et al., 2007; Sakai et al., 2003). At these points, the extracellular matrix is thought to act as a "rock in the river" by which the middle of the expanded bud is constrained in position and the bud then bifurcates and flows around this rock to form two new buds. Immunohistochemistry reveals that Celsr1 localises to regions where bud growth is constrained, resembling a "rope" which tethers the cells at the constriction point or "rock". In the lung therefore it appears that Celsr1 is required for bud bifurcation; this idea is supported by defects in bifurcation observed following morpholino knockdown of Celsr1 (Yates et al., 2010b). Further support for this hypothesis comes from studies of salivary gland branching that suggests laminin may also be a component of the constriction point and its expression shows an intriguing similarity to the Celsr1 "rope" that we observe in the lung endoderm cultures (Rebustini et al., 2007). Celsr1 may play an active role in constraining the bifurcation event or may function as a scaffold protein to localize other proteins to sites of constriction during branching. The finding that Celsr1 is expressed in the basal lamina surrounding the lung epithelium is surprising, given that it is known as a transmembrane protein: however, the protein contains a number of laminin G repeats which may enable interaction with the basement membrane. These new data expand a molecular explanation for the "rock in the river" model as a mechanism to split the expanded bud into two.

3.3.4 Vangl2 is required for normal kidney development

Mutations in *Vangl2* result in branching defects of the ureteric tree and impaired glomerular maturation. This finding that a core component of the PCP pahway is required for normal branching of the urerteric bud and metenephric mesenchyme-derived structures is novel. Vangl2 has been shown to be expressed in both the

ureteric bud and developing glomeruli consistent with a probable function in these structures (Babayeva et al., 2010; Torban et al., 2007). Parallels exist between the defective branching observed in *Vangl2*$^{Lp/Lp}$ embryonic kidneys and *Vangl2*$^{Lp/Lp}$ embryonic lung branching. Both exhibit cytoskeletal disruption which can result in impaired tissue morphogenesis that disrupts normal branching of the organ. It is likely that Vangl2 mediates branching in both the lung and kidney in a cell-autonomous manner acting, as it does in neural tube closure (Ybot-Gonzalez et al., 2007) through Rho kinase (ROCK) mediated cytoskeletal remodelling. ROCK indirectly inhibits actin filament (Olson, 2008) depolymerisation and when disrupted, actin monomers that are required to continue actin polymerization for migration and cell movement become limited over time. As discussed above defects in *Vangl2*$^{Lp/Lp}$ lungs can be mimicked by chemical inhibition of Rho kinase in organ culture and previous studies have shown branching morphogenesis in the metenephros is sensitive to Rho kinase activity (Korostylev et al., 2008; Meyer et al., 2006; Michael et al., 2005). Although no distinctive alterations in the pattern of f-actin was observed in ureteric bud branch tips (data not shown), apical f-actin within proximal-like tubules appeared irregular in mutant sections compare to wildtype controls.

Analysis of glomeruli in E18.5 *Vangl2*$^{Lp/Lp}$ kidneys were smaller than their wildtype littermates (Yates et al., 2010a) and previous studies have shown endothelia in developing glomeruli to express *Vangl2* transcripts (Genito-Urinary Development Molecular Anatomy Project database GUDMAP 2010)). Podocytes, the highly specialised epithelial cells of the glomeruli are extremely plastic cells and as such they are able to alter their shape *via* molecular regulation of their intracellular cytoskeleton. Cytoskeletal disruption caused by injury or genetic disorders of glomerular function leads to misshaping or absence of foot processes (Faul et al.,

2007; Patrakka and Tryggvason, 2010). Thus resulting in leakage of protein into the glomerular filtrate, glomerular scarring and eventually, chronic renal failure. An understanding of the molecular mechanisms regulating podocyte architecture is likely therefore to be valuable in designing treatment of glomerular dysfunction. A recent study showed siRNA knockdown of Vangl2 in podocytes reduced the number of cell projections, decreased actin stress fibers and impaired cell motility (Babayeva et al., 2010). How this result relates to the glomerular phenotype observed in *Vangl2*$^{Lp/Lp}$ kidneys is not clear although it provides proof of principle that Vangl2 plays an active role in podocyte biology.

In mice, new nephrons continue to be generated during the first week after birth (Yuan et al., 2000). Due to the embryonic lethality of homozygous *Vangl2* mice as a result of severe NTDs post natal analyses of their kidneys was impossible. The next available option was to analyse *Vangl2*$^{Lp/+}$ mice, which displayed a modest decrease in neprhon number four weeks after birth. Glomeruli were counted using the acid-medicated dissociation of the kidney method (Welham et al., 2005). While it is possible this method may be less accurate than stereology (Cullen-McEwen et al., 2003; Keller et al., 2003), any directional bias would be equal in wildtype and *Vangl2*$^{Lp/+}$ samples because the latter displayed no tissue abnormalities such as cyst formation which might affect the efficiency of dissociation. As both *Vangl2* heterozygous and homozygous *Vangl2* mice have a branching defect, the reduction in final glomerular numbers (Keller et al., 2003) may be caused by a relative lack of branch tips available to induce mesenchymal cells to differentiate into nephrons.

Within the human population healthy individuals have a range of glomeruli numbers (approximately 1-2 million) per kidney (Keller et al., 2003). Both animal (Cullen-McEwen et al., 2003; Welham et al., 2005) and human studies (Zhang et al., 2008)

suggest both environmental factors such as the diet a mother eats when pregnant and genetic factors such as polymorphisms of genes expressed in the developing kidney, together determine the final nephron number. Despite the variability of nephron number in healthy individuals studies in humans suggest a congenital nephron deficit likely results in essential hypertension (Keller et al., 2003). This is consistent with studies in animals, that indicate those born with too few nephrons are more likely to develop arterial hypertension later in life (Cullen-McEwen et al., 2003). It will be interesting in the future to investigate whether *Looptail* mice are prone to hypertension or susceptible to glomerular scarring as they age.

Interestingly renal failure is the most common cause of death in individuals born with NTDs. Renal failure was thought to arise as a result of excessive back-pressure on the kidneys from impaired urine flow combined with bacterial infection ascending from urine pooled in poor-emptying urinary bladders. However in some cases individuals with NTDs also displayed congenital kidney malformations including agenesis (unilateral absent kidney), gross defects in renal shape (horsehoe kidney) and ureteric duplication (duplex kidneys) (Hunt and Whitaker, 1987; Mandell et al., 1996; Robson et al., 1991). These findings suggest both the reanl abnormalities and the NTDs occur as a result of common genetic and/or environmental causes. Based on the analysis of *Looptail* mice in this chapter its possible that the subset of individuals with NTDs who also have kidney malformation may have mutations in Vangl2 or other PCP genes.

Despite studies linking components of the PCP pathway to the development of cystic kidneys; mutations in *Wnt9b* disrupt the normal CE-like rearrangement of exisiting epithelial cells during tube elongation and narrowing resulting in cystic kidneys (Karner et al., 2009), no cystic phenotype was observed in either *Vangl2* homozygous or heterozygous fetal kidneys or in one month old *Vangl2* heterozygous kidneys. This was fairly surprising as Saburi et al. showed the cystic phenotype observed in the Fat4 mutants was accentuated when mice were haploinsufficicent for Vangl2 (Saburi et al., 2008). Fat4 mutants display defects in oriented cell divisions and tubule elongation, processes which require the function of primary cilia (Fischer et al., 2006).

Fat4 was also shown to be expressed in primary cilia (Saburi et al., 2008), which are organelles that protrude from the apical epithelial surface and transduce signals thought to be triggered by tubular fluid flow and perhaps also by yet-to-be defined components in the fluid (McNeill, 2009). Another link between PCP and the development of renal cysts came from Simons et al. who showed inversin mutants develop cystic kidneys. Inversin can mediate the switch from canonical to non-canonical Wnt signalling and is upregulated by fluid flow (Simons et al., 2005). Despite these findings analysis of *Vangl2*$^{Lp/Lp}$ fetal kidney tubules by immunostaining for acetylated α-tubulin and IFT88 (Ferrante et al., 2009; Jones et al., 2008) found them to contain primary cilia (data not shown), however their orientation or numbers were not formally assessed in detail. Although no cystic phenotype was observed in Vangl2 mutants it does not rule out the possibility a more profound and prolonged Vangl2 deficiency could lead to kidney cysts later in life.

3.4 Conclusion

In conclusion, the data presented in this chapter show for the first time that PCP signalling pathway components, Ceslr1 and Vangl2, are required for normal branching morphogenesis. Further analysis of *Celsr1*$^{Crsh/Crsh}$ and *Vangl2*$^{Lp/Lp}$ mutant mice revealed disrupted lung development and cytoskeletal defects, which in combination with protein localisation data lead to the conclusion that the PCP pathway is required for formation of normal epithelial branches in the lung. Celsr1 and Vangl2 appear to regulate the morphogenetic movement of epithelial tissue required for normal branching morphogenesis, at least in part via Rho kinase-mediated regulation of the cytoskeleton.

Interestingly it also appears that Vangl2 and Celsr1 have some different roles within the lung , for example, Cesr1 may have a role in bud bifurcation.

In addition to its role in lung epithelial tube formation Vangl2 also appears to regulate branching in the Kidney in a similar manner to that in the lung, i.e. via cytoskeletal organisation. Vangl2 is expressed in glomeruli and an absence of one copy is enough to cause a reduction in the number of glomeruli, though this is not sufficient to cause a significant functional defect under normal conditions. However, it is likely that a more prolonged deficit of Vangl2 or if *Looptail* mice were challenged, for example by injury or environmental insults, the reduced glomerular numbers may have detrimental affects on kidney function later in life.

The novel finding that *Celsr1* and *Vangl2* are required for epithelial tube formation opens up a new avenue of research that will likely increase our understanding of human diseases; particularly those involving defects in lung and kidney architecture such as fibrosis and also those caused as a result of branching defects such as hypertension and cystic diseases.

4 Chapter Four: Scribble is required to maintain the airway lumen

4.1 Introduction

In addition to the lung defects, described in chapter three, that arise from mutations in the core PCP genes *CELSR1* and *VANGL2*, mutations in two other PCP genes, *SCRIBBLE* and *PTK7*, also cause similar lung defects. Both *SCRIBBLE* and *PTK7* mouse mutants have small lungs with irregular shaped lobes (Yates et al., manuscript in preparation; (Paudyal et al., 2010).

Scribble (*Scrib* in *Drosophila* and *Scrib1* in mammals) was first identified in *Drosophila* where homozygous null mutants in *Scrib* displayed loss of apico-basal polarity and neoplastic tissue overgrowth (Bilder and Perrimon, 2000; Mechler et al., 1985; Woods and Bryant, 1989). Two *Scrib* protein isoforms exist in *Drosophila,* resulting from alternative splicing during *Scrib* transcription (Li et al., 2001). *Scrib* operates within one of three key A/B polarity complexes in *Drosophila* along with Discs Large (Dlg) and Lethal giant larvae (Lgl). The Crumbs and Par complexes comprise the two remaining A/B polarity modules. The Crumbs (Crb) complex is comprised of Crb, Stardust (Sdt) and Patj; the Par3/Bazooka (Baz) complex is comprised of Baz, Par6 and atypical protein kinase C (aPKC) (Assemat et al., 2008; Humbert et al., 2008). Work in *Drosophila* has shown the Crumbs complex to be most apically localised, followed by the Par3/Baz complex, which is associated with the apical junctional areas. The Scribble complex is localised to the septate junctions just basal to the adherens junction. Many of the proteins that comprise these complexes contain PSD-95, ZO-1 and Discs large (PDZ) protein-protein interaction domains, including Sdt, dPatj, Baz Dlg and Scribble, which has multiple PDZ domains. The Par complex plays a role in polarity and spatial organisation in almost all metazoan cells whereas the Crumbs complex appears more specific to epithelial cells. The three

complexes interact to define the apical and basolateral surfaces of epithelial cells in *Drosophila* (Bilder et al., 2003; Tanentzapf and Tepass, 2003). Interplay between these three complexes is crucial for establishing A/B polarity in *Drosophila* (Bilder et al., 2003; Tanentzapf and Tepass, 2003) and some components of these complexes have also been shown to be required for A/B polarity in mammals; for example, mammalian Par3 is localised to tight junctions at the apical/lateral boundary (Izumi et al., 1998) and functions in their assembly (Chen and Macara, 2005), while Par6/aPKC are required to maintain the integrity of the apical membrane (Martin-Belmonte et al., 2007).

In *Drosophila*, no direct role in establishing planar polarity has been attributed to *Scrib*, however, a recent publication revealed *Scrib* interacts genetically and physically with Stbm/Vang (mammalian homolog Vangl2) (Courbard et al., 2009). Courbard et al., showed Scrib binds Stbm/Vang through its third PDZ domain and cooperates with Stbm/Vang in establishing PCP in the *Drosophila* eye and wing (Courbard et al., 2009).

The mouse mutant Circletail (*Crc*) contains a single base insertion that creates a frame shift leading to truncation of the Scrib1 protein. The mutant protein lacks two of its four PDZ domains (Murdoch et al., 2003). *Crc* homozygous mice show typical PCP defects such as craniorachischisis and disruption to the outer hair cells of the cochlea. In addition, *Scribble*^{Crc} mice have been shown to genetically interact with *Vangl2*^{Lp} mice, since double heterozygotes also exhibit craniorachischisis, a phenotype not observed in single heterozygotes (Murdoch et al., 2003).

Only one Scribble gene (*Scrib1*) exists in mammals (Nakagawa and Huibregtse, 2000; Santoni et al., 2002). *Scrib1* is a LAP protein (Kallay et al., 2006) and contains 16 leucine rich-repeats (LRR) and four PDZ domains (reviewed by (Bryant and Huwe,

2000; Santoni et al., 2002). In *Drosophila* epithelial cells, pre-gastrulation, Scrib localises to the cortex, basal to the adherens junctions, at the septate junctions that are located on the basolateral membrane (Bilder and Perrimon, 2000). However, during gastrulation Scrib relocates to a more apical position along the lateral cell membrane and remains here into late embryogenesis, where it then localises further into a narrow subapical region, that corresponds to the location of the septate junctions. These data indicate that Scrib is an early marker for the site of the future septate junction, at the apical boundary of the basolateral compartment in *Drosophila* (Bilder and Perrimon, 2000). In mammalian epithelial cells, human Scribble (hScrib) has been shown to localise to the basolateral membranes and displays overlapping expression with the adherens junctions (Dow et al., 2003; Navarro et al., 2005). The localisation of hScrib at, and basal to, adherens junctions and its colocalisation with mammalian Dlg in epithelial cells (Dow et al., 2003) suggests a high degree of conservation in the polarised localisation of Scribble between the *Drosophila* and mammalian epithelium.

Lung development involves the production of a network of epithelial tubes, each of which contains a lumen at its centre to enable gaseous exchange. Correct lumen formation and maintenance of lumen diameter are critical for proper lung function. Despite this, the molecular mechanisms underlying mammalian lumen formation and maintenance are poorly understood. Disruption of lumen diameter is a feature of a number of human diseases affecting diverse organs including polycystic kidney disease, hypertension and ischemic injury. In the lung, understanding the mechanisms behind lumen formation and maintenance may be important for understanding lung diseases such as pulmonary hypertension, cystadenomatoid malformations and even asthma, all of which involve aberrant lumen diameter.

In vitro studies have shown cell polarity, cell-cell adhesion and the establishment of an apical membrane are pre-requisites for lumen formation in both *Drosophila* and mammalian cells. Mammalian Scribble has been shown to directly bind to the C-terminal motif of the tight junction protein ZO-2 (Metais et al., 2005), which in turn interacts with other components of the tight junctions, including ZO-1, Occludin, Cingulin and Claudins (Cordenonsi et al., 1999; Gumbiner et al., 1991; Itoh et al., 1999). The interaction between Scribble and ZO-2 likely takes place at the cell junctions before ZO-2 becomes segregated into the tight junctions (Metais et al., 2005). Scribble and E-Cadherin are mutually dependent for their proper targeting to adherens junctions (Navarro et al., 2005; Qin et al., 2005). Finally, if Scribble is suppressed by siRNA knockdown in MDCK cells, a delay in tight junction assembly can occur, though no overt disruption to apical-basal polarity is observed (Qin et al., 2005).

Lumen formation in the lung occurs via a process known as budding, whereby cells within an epithelium invaginate through apical restriction and subsequently extend in a direction that is orthogonal to the plane of the original epithelium (Hogan and Kolodziej, 2002; Lubarsky and Krasnow, 2003). The orthogonal extension necessary for the new tube to 'grow' can occur through additional cell recruitment, cell division and/or cell elongation and is most likely a mix of all three. In a similar manner to the epithelium itself, when new buds form from existing branches, it is thought that the new lumen remains contiguous with the original lumen.

As outlined above, studies in both *Drosophila* and vertebrates have shown Scribble to play a role in both the planar and apical-basal polarity pathways. This evidence suggested that Scrib1 might play a role in lung development/tubulogenesis. Therefore, the overall aim of this chapter was to determine whether loss of Scrib1

would lead to defects in lung development, particularly in lumen architecture; and if so, whether this was due to perturbed apical-basal and/or planar polarity. To assess the role of Scrib1 in the lung, an in-depth analysis of the mouse mutant, *Circletail* (*Crc*), was carried out, along with morpholino knockdown of Scribble protein *in vitro*.

4.1.1 Aims

- To understand the role of Scribble in normal lung branching morphogenesis
- To determine whether loss of Scribble affects apical-basal and/or planar polarity within the lung
- To determine the role of Scribble in maintaining the airway lumen

4.2 Results

4.2.1 Scribble is required for normal lung development

Analysis of E14.5 (Fig 4.1 B) and E18.5 (Fig 4.1 D) whole *Scribble*$^{Crc/Crc}$ lungs revealed them to be smaller, with fewer branches and abnormally shaped lobes in comparison to wildtype littermates (Fig 4.1 A,C). E14.5 *Scribble*$^{Crc/Crc}$ epithelial airway cells were misaligned and disorganised, often occupying the luminal space. In contrast, wildtype epithelial cells were well-ordered and surrounded a clearly visible lumen (Fig 4.1 E,F). The total number of airways was significantly reduced in *Scribble*$^{Crc/Crc}$ lungs at both E14.5 and E18.5 (Fig 4.1 O,P). In addition, the percentage of "organised" epithelial airways was calculated by counting the number of "organised" airways in a single frame, in both wildtype and *Scribble*$^{Crc/Crc}$ E14.5 sections. An "organised" airway was classified as a single layer of well-ordered epithelial cells surrounding an open lumen. A significant reduction in the number of "organised" airways was observed in *Scribble*$^{Crc/Crc}$ compared to wildtype littermates (Fig 4.1 M). The width of *Scribble*$^{Crc/Crc}$

airways at E14.5 was also significantly reduced compared to wildtype controls (Fig 4.1 N) suggesting a defect. By E18.5, *Scribble*$^{Crc/Crc}$ lung architecture was highly disrupted and there was clear evidence of hypoplasia and a distinct lack of septation (Fig 4.1 G,H). It is likely these defects would be inconsistent with post-natal life, however, like *Vangl2*$^{Lp/Lp}$ and *Ceslr1*$^{Crsh/Crsh}$ mouse mutants (see chapter 3), homozygous *Circletail* mice die at birth, and so this could not be confirmed. Immunostaining for the epithelial marker anti-pan-cytokeratin, which highlights the epithelial cell disorganisation showed that in *Crc* homozygotes, cells frequently appeared to occupy the luminal space (Fig 4.1 I,K) (Fig 4.1 J,L). By Dapi staining alone, it was almost impossible to distinguish the epithelial airways in *Scribble*$^{Crc/Crc}$ sections, whereas in wildtype sections, distinctive organised epithelial cells surrounding a clear lumen can be seen. Similarities in the lung phenotypes of *Celsr1*$^{Crsh/Crsh}$, *Vangl2*$^{Lp/Lp}$ and *Scribble*$^{Crc/Crc}$ mouse mutants were observed, however, *Scribble*$^{Crc/Crc}$ were consistently the most severely affected.

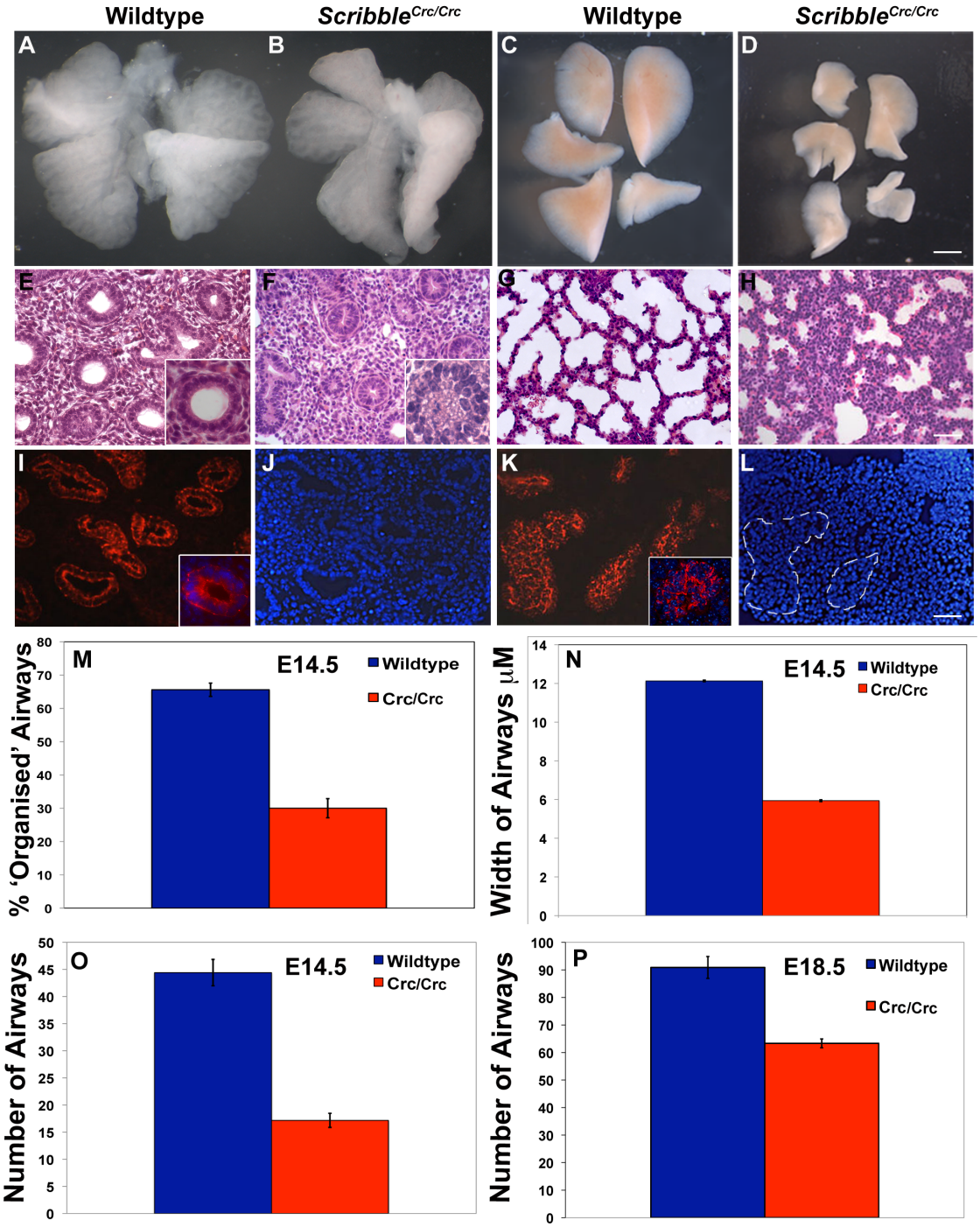


Figure 4.1 Scrib1 is required for normal lung development. Analysis of E14.5 and E18.5 whole *Scribble*$^{Crc/Crc}$ lungs (B,D) revealed them to be smaller, with misshapen lobes and fewer branches than wildtype littermates (A,C). Histological analysis of E14.5 H&E stained sections show fewer, less organised, epithelial airways in *Scribble*$^{Crc/Crc}$ lungs (E,M,N,O) compared with wildtype littermates (F,M,N,O). By E18.5 severe hypoplasia is evident, with a significant reduction in the number of airways in *Scribble*$^{Crc/Crc}$ lungs (H,P) compared to wildtype controls (G,P). Immunostaining of E14.5 transverse cryosections with anti-pan-cytokeratin highlights the disorganisation of epithelial cells in *Scribble*$^{Crc/Crc}$ lungs (K) compared to littermate controls (I). Epithleial cells are difficult to distinguish from surrounding mesenchyme by DAPI staining in *Scribble*$^{Crc/Crc}$ sections (L) but are easily distinguished in wildtype sections (J). Scale bars; A-D 62.5µM, E-L 25µM.

4.2.2 Differentiation, proliferation and apoptosis are unaffected in *Scribble*$^{Crc/Crc}$ lungs

To begin to understand how loss of Scrib1 function affects lung development at the molecular level, E18.5 paraffin wax sections of *Scribble*$^{Crc/Crc}$ lungs were immunostained with antibodies to a number of cell-type-specific differentiation markers: the distal airway markers Aqp5 (Fig 4.2 G,H), which marks a water channel located on the apical membranes of type I distal epithelial cells, and Pro-SpC to highlight alveolar type II distal airway cells (Fig 4.2 C,D); the proximal cell markers α-SMA, that highlights smooth muscle actin around the proximal airways (Fig 4.2 A,B), and CC10, which marks non-ciliated proximal airway epithelial cells (Fig 4.2 E,F). No differences in levels or numbers of cells expressing these markers were observed between *Scribble*$^{Crc/Crc}$ and wildtype lung. Thus, the defects observed in *Scribble*$^{Crc/Crc}$ lungs do not appear to result from altered cell fate determination or differentiation, consistent with the findings in *Celsr1*$^{Crsh/Crsh}$ and *Vangl2*$^{Lp/Lp}$ lungs .

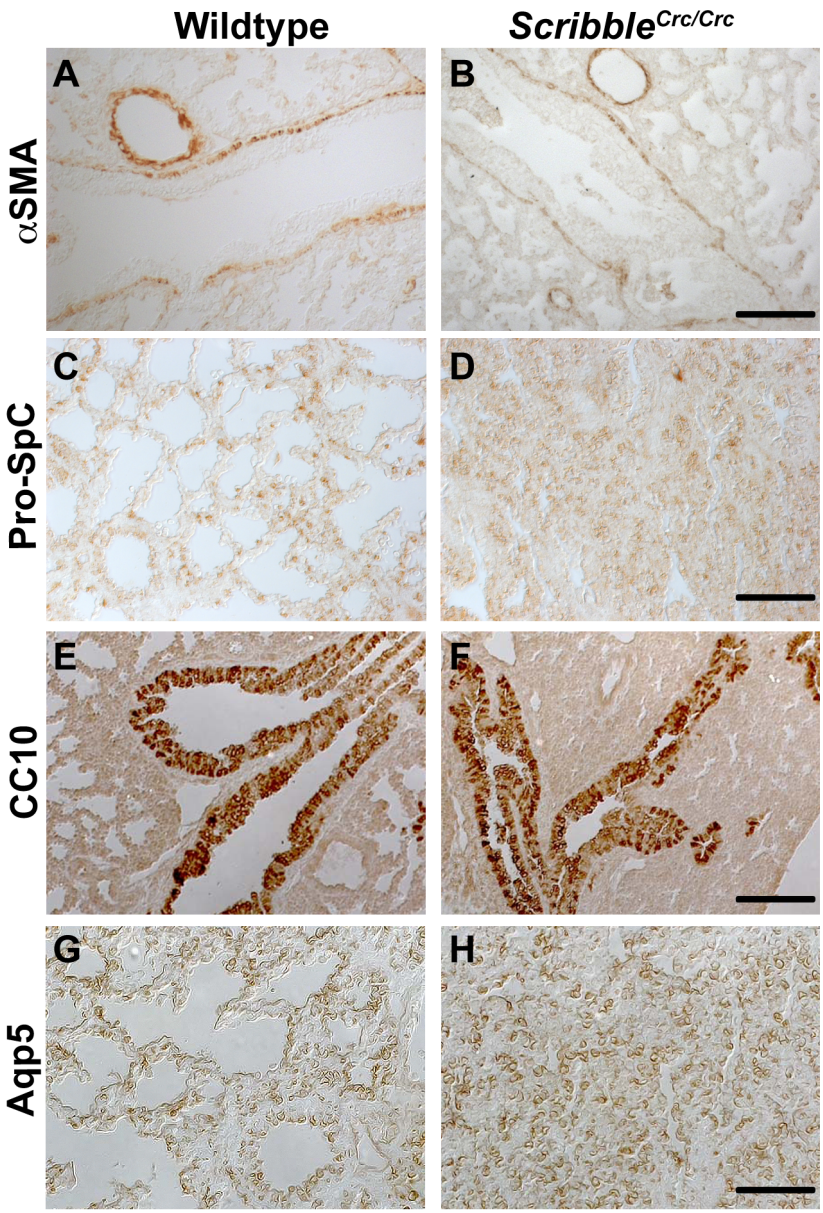


Figure 4.2 Differentiation is unaffected in *Scribble*$^{Crc/Crc}$ lungs. Analysis of two proximal airway markers, αSMA (A,B) and Clara cell-10 (E,F), and two distal airway markers, Pro-SpC (C,D) and Aqp5 (G,H), by immunohistochemistry revealed no obvious differences in differentiation in *Scribble*$^{Crc/Crc}$ lungs (B,D,F,H) compared to wildtype littermates (A,C,E,G). Scale bars; A-H 12.5μM.

Scribble$^{Crc/Crc}$ lungs are much smaller than wildtype controls and the tissue appears highly compact with cells crowded together. In *Drosophila,* Scrib is known as a *Drosophila* neoplastic tumor suppressor gene (nTSG) along with lgl and Dlg. All three genes act as key regulators of apico-basal polarity by restricting apical proteins from the basolateral surface. Epithelia in mutants of these genes have mislocalised apical proteins and adherens junctions that are ectopically expressed at basolateral sites. In addition, the mispolarized imaginal discs of *Drosophila* Scrib mutants are dramatically overgrown (Brumby and Richardson, 2003; Gateff, 1978; Pagliarini and Xu, 2003), therefore it was important to determine if apoptosis or proliferation was affected in *Scribble*$^{Crc/Crc}$ lungs. To address these questions, proliferation was assessed by immunostaining for anti-phospho histone H3 antibody which detects endogenous levels of histone H3 when phosphorylated at Ser28, which only occurs when cells are undergoing mitosis (Goto et al., 1999). Immunostaining was carried out on both E11.5 and E14.5 cryosections. No difference in the percentage of proliferating cells in either epithelium or mesenchyme was found between Scribble homozygous mutant lungs and wildtype littermates. This important result indicates that the reduced size of *Crc/Crc* lungs is not as a result of reduced proliferation.

To assess apoptosis, E11.5 and E14.5 cryosections of both *Scribble*$^{Crc/Crc}$ and wildtype lungs were immunostained for anti-cleaved caspase-3. Caspase-3 is a critical mediator of apoptosis, as it is either partially or totally responsible for the proteolytic cleavage of many key proteins (CPP-32, Apoptain, Yama, SCA-1). Cleaved caspase-3 (Asp175) antibody detects endogenous levels of the large fragment (17/19 kDa) of activated caspase-3 resulting from cleavage adjacent to Asp175, and therefore is a useful maker of apoptosis. No significant difference was observed in apoptosis between wildtype and *Scribble*$^{Crc/Crc}$ lungs at either E11.5 or E14.5 (Fig. 4.3),

indicating the reduction in lung size observed in *Scribble*$^{Crc/Crc}$ lungs is not a result of excessive apoptosis.

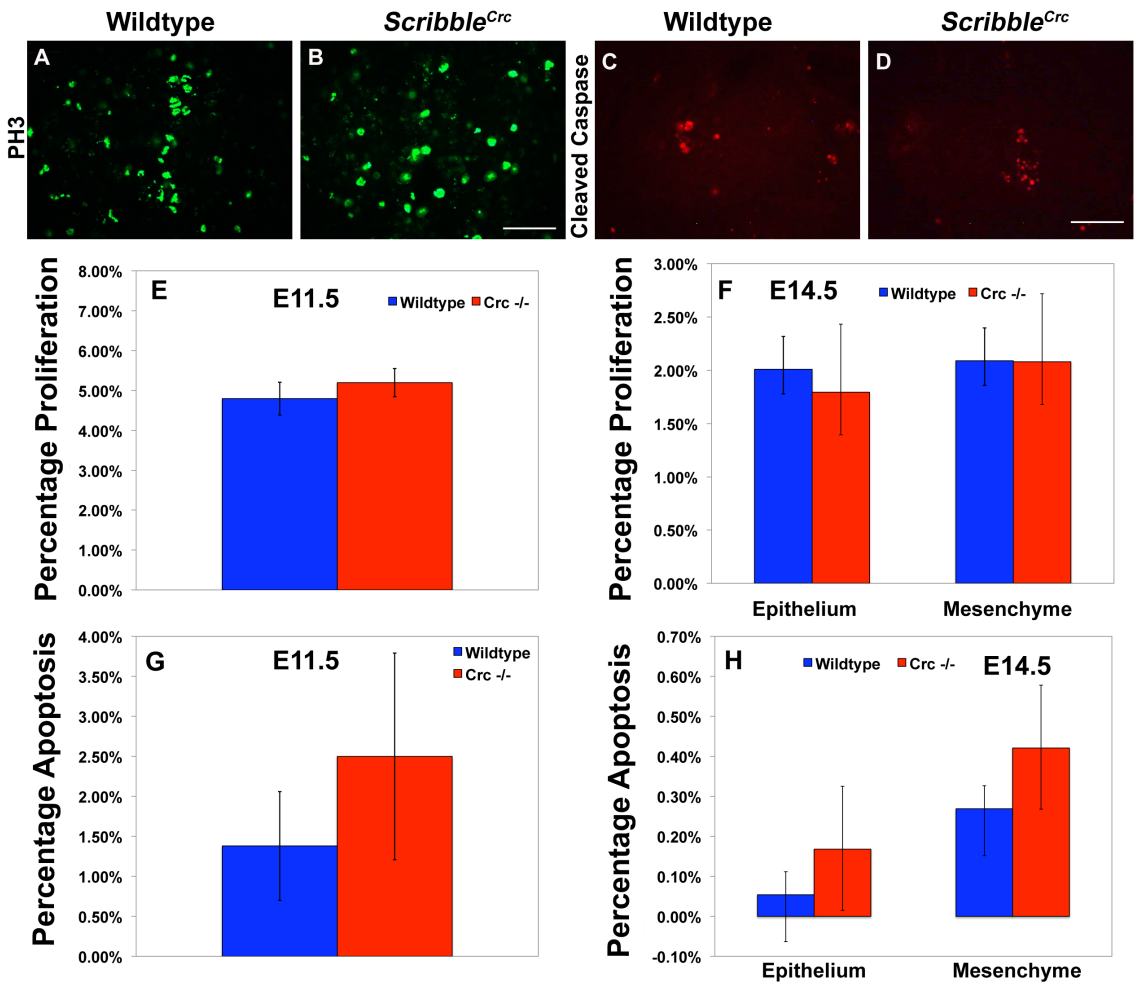


Figure 4.3 Proliferation and apoptosis are unaffected in *Scribble*$^{Crc/Crc}$ lungs.

E14.5 Wildtype (A,C) and *Scribble*$^{Crc/Crc}$ (B,D) sections were immunostained with anti-PH3 (A,B) to assess proliferation or anti-cleaved caspase-3 (C,D) to assess apoptosis. No difference in proliferation or apoptosis was observed between *Scribble*$^{Crc/Crc}$ and wildtype littermates. This was confirmed by quantification of the % number of proliferating cells (E,F) or the % number of cells undergoing organised cell death (G,H) at both E11.5 (E,G) and E14.5 (F,H) . Scale bars; A-D 12.5μM.

4.2.3 Epithelial tube formation is perturbed in Scribble$^{Crc/Crc}$ mutants

All PCP mouse mutants, including *Circletail*, have a shortened proximal-distal axis as a result of convergence extension defects. This axial shortening likely leads to reduced intrathoracic space, which can itself perturb embryonic lung development and cause pulmonary hyperplasia (Laudy and Wladimiroff, 2000). To determine whether the *in vivo* lung phenotype observed in *Scribble$^{Crc/Crc}$* lungs was due to reduced intrathoracic space, E11.5 left *Scribble$^{Crc/Crc}$* and wildtype lung lobes were cultured *ex vivo* for 48h, after which the total number of terminal end buds in each explant were counted. At T0, *Scribble$^{Crc/Crc}$* and wildtype left lobes appeared similar (Fig 4.4 A,C); however, 48h after culture wildtype lungs had branched extensively (Fig 4.4 B), whereas significantly fewer terminal buds were observed in *Scribble$^{Crc/Crc}$ lungs* (Fig 4.4 D).

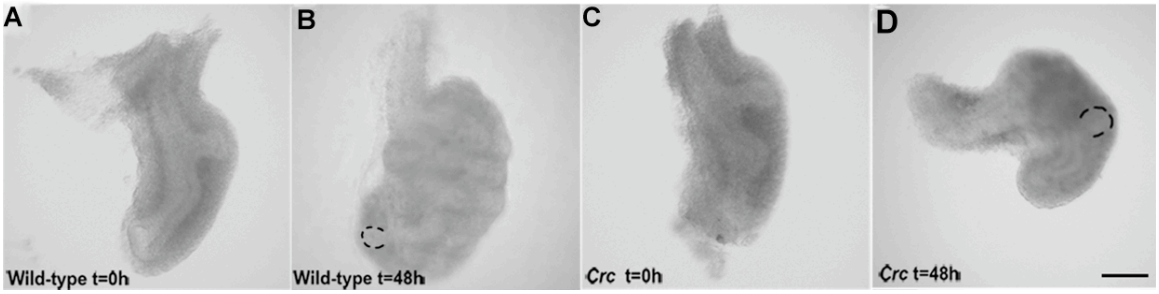


Figure 4.4 *Ex vivo* cultures of *Scribble*$^{Crc/Crc}$ lungs have fewer buds that appear broader and far denser than wildtype littermates. E11.5 left lung lobes were dissected and cultured for 48h. At T0 the number of buds was identical in *Scribble*$^{Crc/Crc}$ (C) and wildtype littermate lungs (A). 48h later, however, wildtype lungs branched extensively to produce multiple new epithelial buds (B dotted line), whereas *Scribble*$^{Crc/Crc}$ lungs developed far fewer terminal buds (D dotted line). Scale bars; A-D 63μM.

4.2.4 Scrib1 is expressed in tight junctions

In order to further understand the role of Scrib1 in lung development, it was important to determine where in the lung this protein was expressed. To do this, E11.5 and E14.5 transverse lung sections were immunostained for anti-Scrib1 (Fig 4.5 A, C). Scrib1 was found to localise to the cell membranes of mesenchymal and epithelial cells. Strongest expression, however, was observed towards the apical/luminal surface of epithelial cells. It was noted that this pattern of expression was similar to that of the tight junction protein ZO-2 and double-labelling of E11.5 sections with anti-Scrib1 and anti-ZO2 antibodies, followed by confocal imaging, revealed Scrib1 and ZO-2 to co-localise in the lung (Fig 4.5 A-C).

Scrib1 staining was almost completely absent in E14.5 *Crc/Crc* cryosections (Fig 4.5 F), indicating that this is a loss of function mutation.

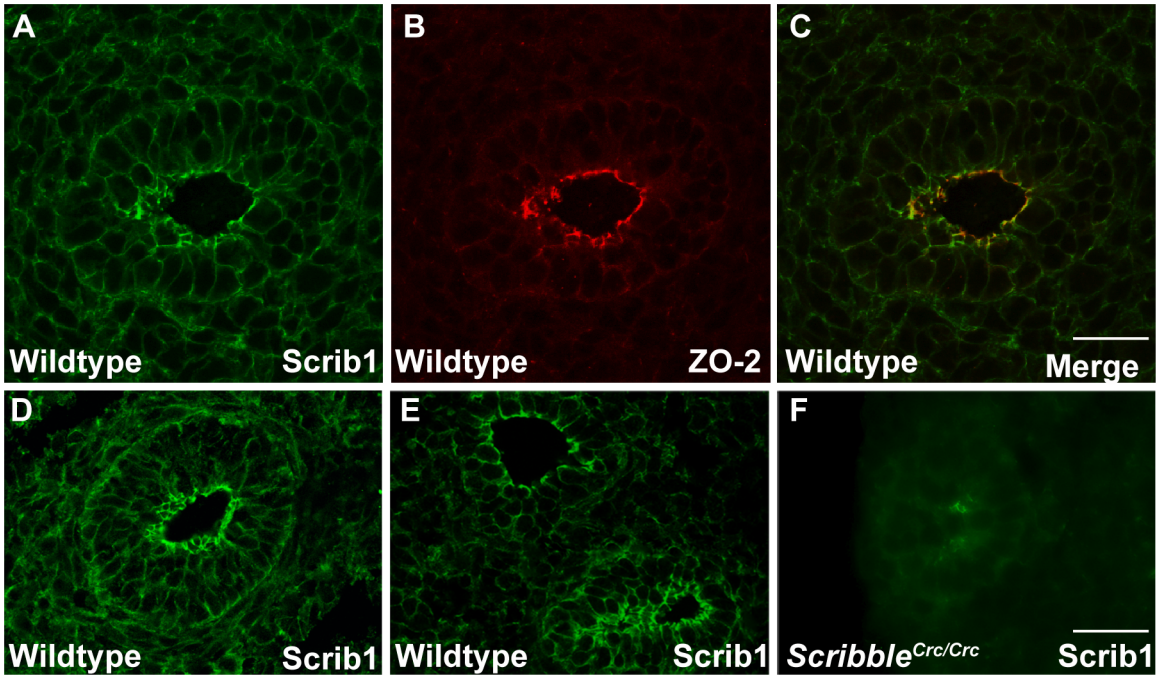


Figure 4.5 Scrib1 is expressed in tight junctions. E11.5 wildtype, transverse sections immunostained for Scrib1 (A,C) reveal Scrib1 to be localised to the membranes of epithelial and mesenchymal cells; strongest staining is observed apically, towards the luminal surface, where it colocalises with the tight junction protein ZO-2 (B,C). Scrib1 is also highly localised towards the apical surface at E14.5 as shown by immunostaining of E14.5 transverse sections (D,E). Scrib1 expression is absent in E14.5 *Scribble*$^{Crc/Crc}$ lungs (F). Scale bars; A-D, F 125μM plus x3 zoom. E 125μM plus x2 zoom.

4.2.5 Loss of Scrib1 leads to specific tight junction disruption

The finding that Scrib1 localises with ZO-2 in the lungs, along with the observed disruption to epithelial airways and reduced luminal space in *Scribble*$^{Crc/Crc}$ lungs, prompted examination of other tight and adherens junction markers in the lungs of *Scribble*$^{Crc/Crc}$ mice.

Loss of Scrib1 leads to the mislocalisation of the tight junction protein ZO-2 (Fig 4.6 B, compared to A) but not ZO-1 (Fig 4.6 D compared to C); this finding is not surprising as Scrib1 is known to directly bind ZO-2 and shows overlapping expression with ZO-2 in the lung. Tight junctions are comprised of a stable multiprotein complex with both integral and peripheral membrane proteins (Steed et al., 2010). The zonula occludins (ZO-1, ZO-2 and ZO-3) form part of the peripheral membrane proteins that connect the integral membrane proteins, claudins and occludin, to the underlying actin cytoskeleton as well as to different types of signalling proteins (Steed et al., 2010). Detailed examination revealed that loss of Scrib1 also results in mislocalisation of two integral membrane proteins: occludin (Fig 4.6 F, compared to E) and claudin-18 (Fig 4.6 H compared G). In mammalian epithelial cells, tight junctions comprise the most apical component of the cell junctional complex with adherens junctions localised more basally. In wildtype E14.5 sections occludin and claudin-18 are more strongly expressed in epithelial cells towards the apical surface; however, in *Scribble*$^{Crc/Crc}$ sections the expression appears more diffuse with increasing levels in the mesenchyme sections. This is surprising, as mesechymal cells do not maintain strong cell-cell contacts, such as tight junctions, thus allowing them to migrate and move independently. It is only when mesenchymal cells undergoing mesenchymal-epithelial transition (MET) that they form tight and adherens junctions. There is no

evidence as yet of MET occurring in the lung, however it has been widely studied during kidney development (Chaffer et al., 2007).

Analysis of the adherens junctions by immunostaining for β-catenin (Fig 4.6 I,J) also revealed a mild disruption in *Scribble*$^{Crc/Crc}$ lungs. β-catenin is less evenly distributed around mutant epithelial cells compared to the thin continuous, narrow line of expression around wildtype epithelial cells. Interestingly, E-cadherin, an essential component of the adherens junction that is required for both adhesive contacts between epithelial cells and, in vertebrates, for the assembly of tight junctions (Gumbiner, 2000, 2005), appears unaffected in *Scribble*$^{Crc/Crc}$ lungs (Fig 4.6 K,L). Previous mammalian *in vitro* studies have shown that Scrib1 can regulate E-cadherin adhesive activity in MDCK epithelial cells; however, as observed in lung, reduction of Scrib1 levels in MDCK cells by shRNAs had no effect on the expression of E-cadherin (Qin et al., 2005).

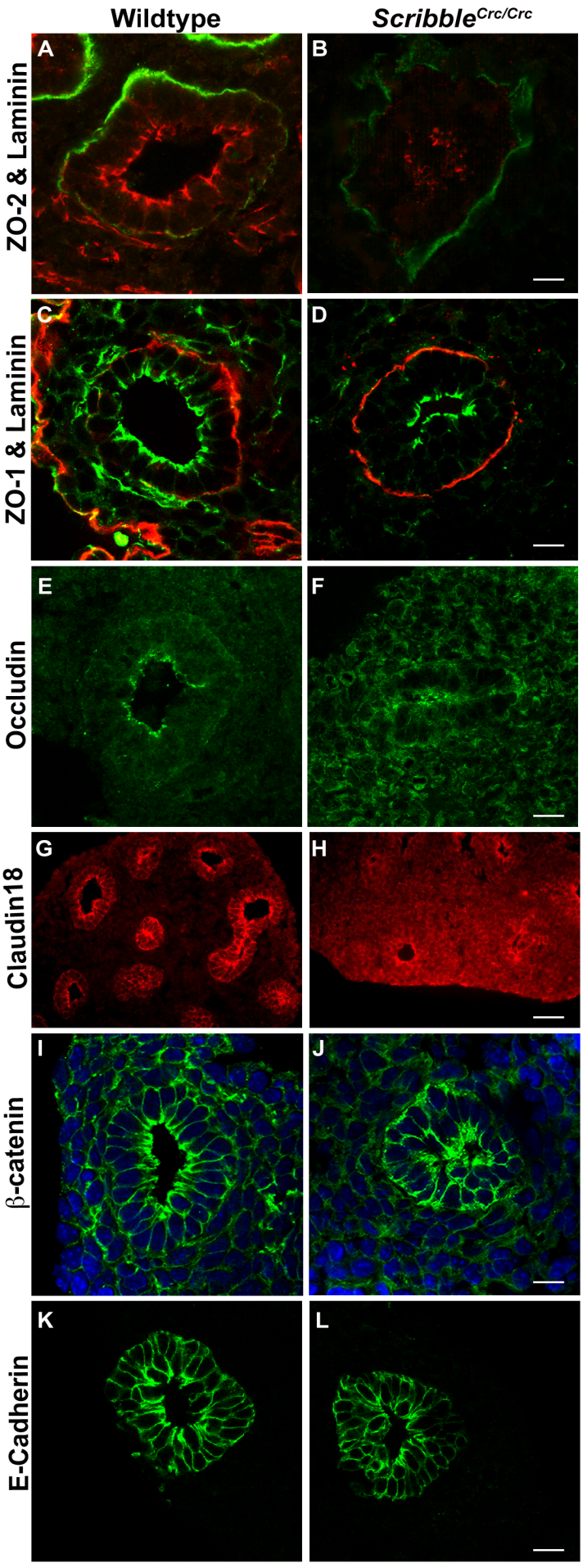


Figure 4.6 Specific tight junction proteins are disrupted in *Scribble*$^{Crc/Crc}$ lungs. E14.5 transverse *Scribble*$^{Crc/Crc}$ (B,D,F,H,J,L) and wildtype (A,C,E,G,I,K) lung sections were immunostained for a number of tight and adherens junction markers. Despite the apical localisation of ZO-2 being maintained in *Scribble*$^{Crc/crc}$ lungs (B), the pattern of expression is disrupted in comparison to wildtype (A) sections. ZO-1 appears normal in *Scribble*$^{Crc/Crc}$ lungs (D) compared to wildtype (C). Both Occludin (E,F) and Claudin-18 staining (G,H) appear more diffuse and less restricted towards the apical surface of epithelial cells and expression is higher in the mesenchyme in *Scribble*$^{Crc/Crc}$ (F,H) compared with wildtype sections (E,G). β-catenin (I,J) is less evenly distributed around mutant epithelial cells compared to wildtype epithelial cells. Finally E-cadherin (K,L) appears normal in *Scribble*$^{Crc/Crc}$ sections (J,L) compared to littermate controls (I,K). Scale bars; A-F 125μM plus x3 zoom, G-H 12.5μM, I-L 125μM plus x3 zoom.

4.2.6 Scribble is expressed towards the luminal surface in a 3D model of active branching

To determine the localisation of Scrib1 in a 3D model of active lung branching, wildtype lung endoderm was denuded of mesenchyme and cultured in the presence of FGF10 to promote branching. Explants were post stained with anti-Scrib1 (Fig 4.7 A,C) and Phalloidin (Fig 4.7 B,C) to highlight the cortical F-actin. Regions enriched with cortical actin are likely those undergoing cell rearrangement and/or movement mediated by cytoskeletal remodelling. Scrib1 expression was observed around epithelial cell membranes, while z-stack images through explants revealed Scrib1 more strongly localised towards the apical surface, consistent with the section data above (Fig 4.5). Scrib1 localisation towards the apical membrane was consistent with the idea that it may play a role in maintaining the airway lumen.

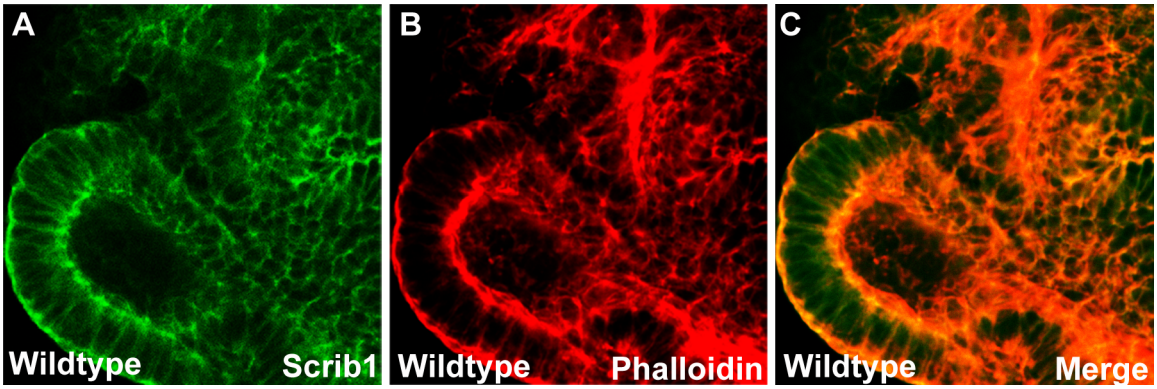


Figure 4.7 Immunostaining of an active 3D model of branching with Scribble and Phalloidin. E11.5 wildtype lung endoderm explants cultured for 48h in 400ng/ml FGF10 and double labelled with anti-Scrib1 (A,C) and phalloidin (B,C). Scribble is most highly expressed towards the luminal surface of outgrowing buds (A,C). Scale bars: A-C 125μM x 10 zoom.

4.2.7 Scribble signals via the PCP pathway downstream effector, Rho kinase

Rho kinase is a downstream effector of the PCP pathway that can modulate cytoskeletal dynamics. In the previous chapter it was shown that *Celsr1* and *Vangl2* signal via Rho kinases to direct cytoskeletal organisation and thereby drive branching morphogenesis in the lung.

Previous studies, where E11.5 wildtype left lung lobes were cultured *ex vivo* in the presence of a Rho kinase inhibitor (Y27632) (Uehata et al., 1997; Ybot-Gonzalez et al., 2007) for 48h, showed a dose-dependent inhibition of branching along with enlarged terminal buds (Fig 3.7 A,D). Interestingly, *Scribble*$^{Crc/Crc}$ lungs, both *in vivo* (Fig. 4.4 D) and *in vitro,* are morphologically reminiscent of lungs treated with the Rho kinase inhibitor, suggesting Scrib1 may operate via Rho GTPases and Rho kinase in the PCP pathway to modulate lung branching, as has been previously shown for *Celsr1* and *Vangl2* (Yates et al., 2010b).

The phenotypic similarities between *Scribble*$^{Crc/Crc}$ lungs and those from Vangl2 and Celsr1 homozygous mouse mutants suggested that Scribble operates within the PCP pathway to regulate branching morphogenesis. To further determine whether Scribble signals via the PCP pathway, the levels of active and total RhoA protein in E13.5 *Scribble*$^{Crc/Crc}$ and wildtype lungs were compared by Western blotting. A reduction in the level of active RhoA was evident in mutants compared to wildtype lungs (Fig 4.8), with no alteration in the level of total RhoA between wildtype and *Crc/Crc* lungs. These data are consistent with Scribble operating via the PCP pathway in the lung.

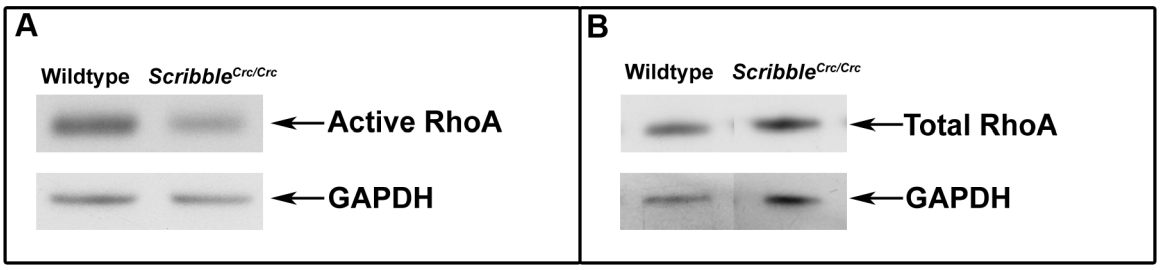


Figure 4.8 Levels of Total and Active RhoA are reduced in *Scribble*$^{Crc/Crc}$ lungs.
Western blotting (A) reveals a 40% reduction in the relative levels of active RhoA in E13.5 *Scribble*$^{Crc/Crc}$ lungs compared to wildtype littermates (relative expression levels wildtype: 100, *Scribble*$^{Crc/Crc}$: 60.68, n=3 for each genotype). No alteration in the levels of total RhoA was observed between *Scribble*$^{Crc/Crc}$ and wildtype controls (B). GAPDH was used as a loading control, levels of Active RhoA were normalised to GAPDH levels.

4.2.8 Scribble$^{Crc/Crc}$ lung epithelia displayed cytoskeletal defects

One of the affects of Rho activation is the assembly of contractile actin-myosin filaments that drive cytoskeletal dynamics. Since a reduction in the level of active RhoA was observed in *Crc/Crc* lungs, an assessment of the cytoskeleton was conducted to determine if a similar disruption to the actin-myosin cytoskeleton observed in both *Vangl2*$^{Lp/Lp}$ and *Celsr1*$^{Crsh/Crsh}$ mutants exists in *Scribble*$^{Crc/Crc}$ lungs. An assessment of the actin-myosin cytoskeleton was carried out by immunostaining with Phalloidin to highlight F-actin and anti-non-muscle myosin II (Fig 4.9).

The F-actin cytoskeleton was severely disrupted in *Scribble*$^{Crc/Crc}$ lungs at both E14.5 (Fig 4.9 A,B) and E18.5 (Fig 4.9 C,D). At E14.5, wildtype airways displayed a continuous line/band of evenly distributed actin around individual epithelial cells as well as along the apical and basal surfaces of the airway; this band is the cortical actin, which is located just below the plasma membrane that surrounds each cell (Fig 4.9 A, C). In *Scribble*$^{Crc/Crc}$ airways, cortical actin is no longer evenly distributed around epithelial cells and instead appears discontinuous (Fig 4.9 B,D). Non-muscle myosin II, another critical component of the cytoskeleton that directly links Rho kinase signalling with cytoskeletal organisation, was also disrupted in *Scribble*$^{Crc/Crc}$ lungs, with staining appearing more diffuse and disjointed compared to wildtype littermates (Fig 4.9 E,F).

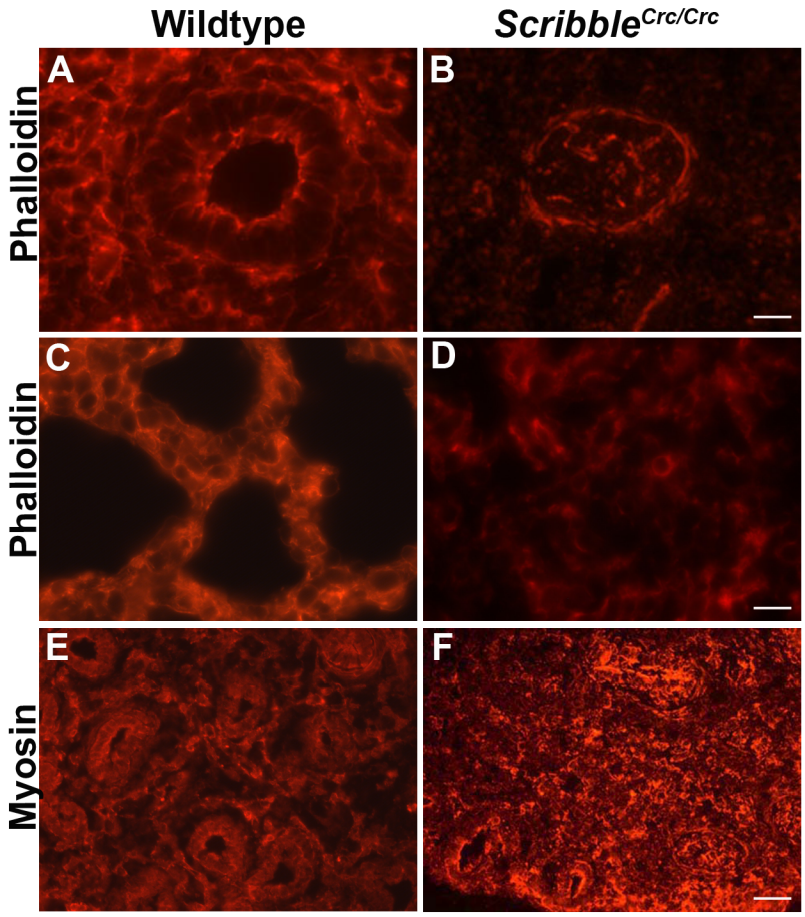


Figure 4.9 Actin-myosin cytoskeleton is disrupted in *Scribble*$^{Crc/Crc}$ lungs. E14.5 (A, B) and E18.5 (C, D) Phalloidin-stained cryosections reveal severe disruption to the actin cytoskeleton in *Scribble*$^{Crc/Crc}$ (B, D) lungs compared to wildtype littermates (A, C). Immunostaining with anti-non muscle myosin II antibody (E,F) also revealed defects in non-muscle myosin in *Scribble*$^{Crc/Crc}$ (F) lungs compared to wildtype littermates (E). Scale bars; A-D 5μM, E-F 25μM.

4.2.9 Apical-basal polarity appears unaffected in Scribble$^{Crc/Crc}$ lungs

In *Drosophila*, a number of groups have highlighted a role for Scrib in determining and maintaining apical-basal polarity*;* yet in mammals, despite extensive studies, only one report has indicated a role for Scrib1 in apical-basal polarity (Zhan et al., 2008). This study, however, relies purely on *in vitro* data and only examines one aspect of apical-basal polarity: the location of the Golgi in relation to the nucleus, which displays only a "modest but reproducible disruption in orientation" (Zhan et al., 2008).

As apical-basal polarity is necessary for both lumen and tube formation, we assessed apical-basal polarity in *Scribble*$^{Crc/Crc}$ lungs by immunohistochemistry (Fig 4.10). aPKCς, a component of the apical surface (Fig 4.10 A-D), remains apically located in *Scribble*$^{Crc/Crc}$ lungs and the basal marker laminin (Fig 4.10 A,B), a component of the basement membrane, remains basally located in *Scribble*$^{Crc/Crc}$ lungs suggesting apical-basal polarity is not affected in *Scribble*$^{Crc/Crc}$ lungs. In addition, immunostaining for the Golgi marker GM130 (Fig 4.10 C,D), and DAPI to highlight cell nuclei, showed the Golgi were located on the apical side of the nuclei in *Scribble*$^{Crc/Crc}$ lungs as in wildtype. Taken together these data show that apical-basal is not visibly affected in *Scribble*$^{Crc/Crc}$ lungs.

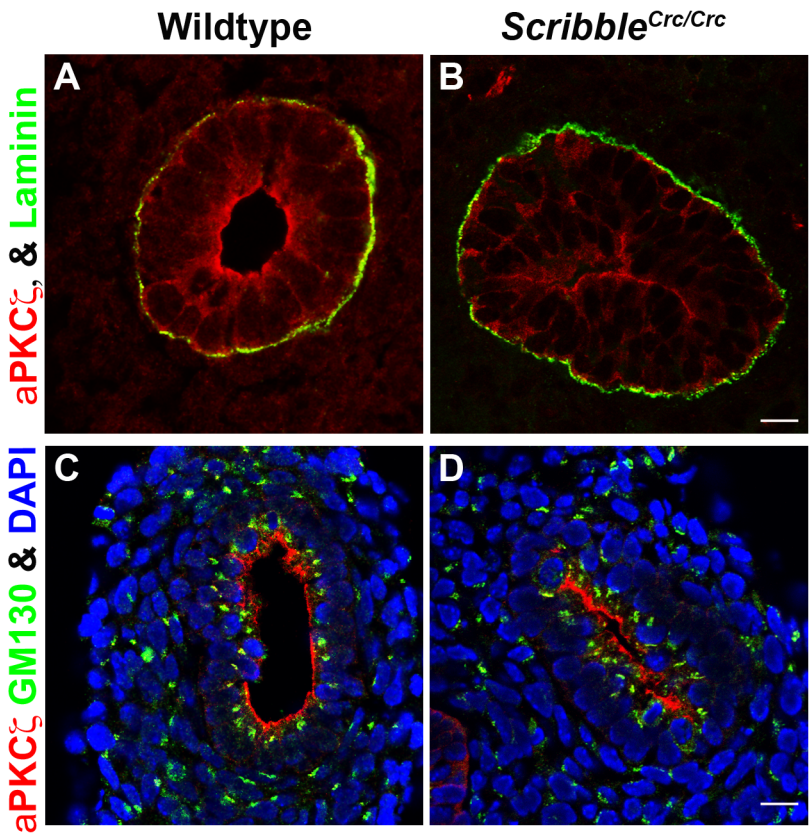


Figure 4.10 Apical-basal polarity appears unaffected in *Scribble*$^{Crc/Crc}$ lungs.

No obvious defects in apical basal polarity were observed between *Scribble*$^{Crc/Crc}$ and wildtype littermates as assessed by immunostaining E11.5 transverse lung cryosections. aPKCζ, a component of the apical surface, is expressed on the luminal surface in both *Scribble*$^{Crc/Crc}$ (red B,D) and wildtype sections (red A,C). Laminin, a component of the basement membrane, localises to the basal side of the airways in both *Scribble*$^{Crc/Crc}$ (green B) and wildtype sections (green A). GM130 (green C,D) marks the Golgi apparatus, which is present on the apical side of DAPI-stained (blue C,D) nuclei in both *Scribble*$^{Crc/Crc}$ (D) and wildtype sections (C). Scale bars; 125μM plus x3 zoom.

4.2.10 Scribble is required for epithelial cell organisation necessary for the formation of new airways

The disruption to tight and adherens junction proteins in *Scribble*$^{Crc/Crc}$ mutant lungs, along with the phenotype showing that epithelial cells are disordered around a small or absent lumen, lead to the hypothesis that loss of Scrib1 prevents the correct associations between epithelial cells within an airway, that are necessary for the formation and/or maintenance of airway lumina. To test this hypothesis, wildtype E12.5 lungs were disassociated into a single cell suspension consisting of both epithelial and mesenchymal cells and cultured in a 3-D matrix for 48h in the presence of either Scribble (Fig 4.11 C,D,G-L) or control morpholino (Fig 4.11 A,B,E,F) antisense oligos. In the presence of control morpholino, the epithelial cells associated into organised epithelial cysts (a 2-dimensional cylinder of epithelial cells) that formed a structured lumen, as observed by staining with Phalloidin to highlight F-actin and DAPI to highlight cell nuclei. In the presence of Scribble morpholino, some cysts did form but far fewer than in control cultures. Strikingly, Scribble knockdown lead to highly disrupted epithelial organisation in those cysts that did form; specifically these cysts rarely contained a lumen, and when they did, the lumen was small and not centrally located. These data support the hypothesis that Scribble is required for normal epithelial cell association and organisation that are necessary to form and/or maintain an airway lumen.

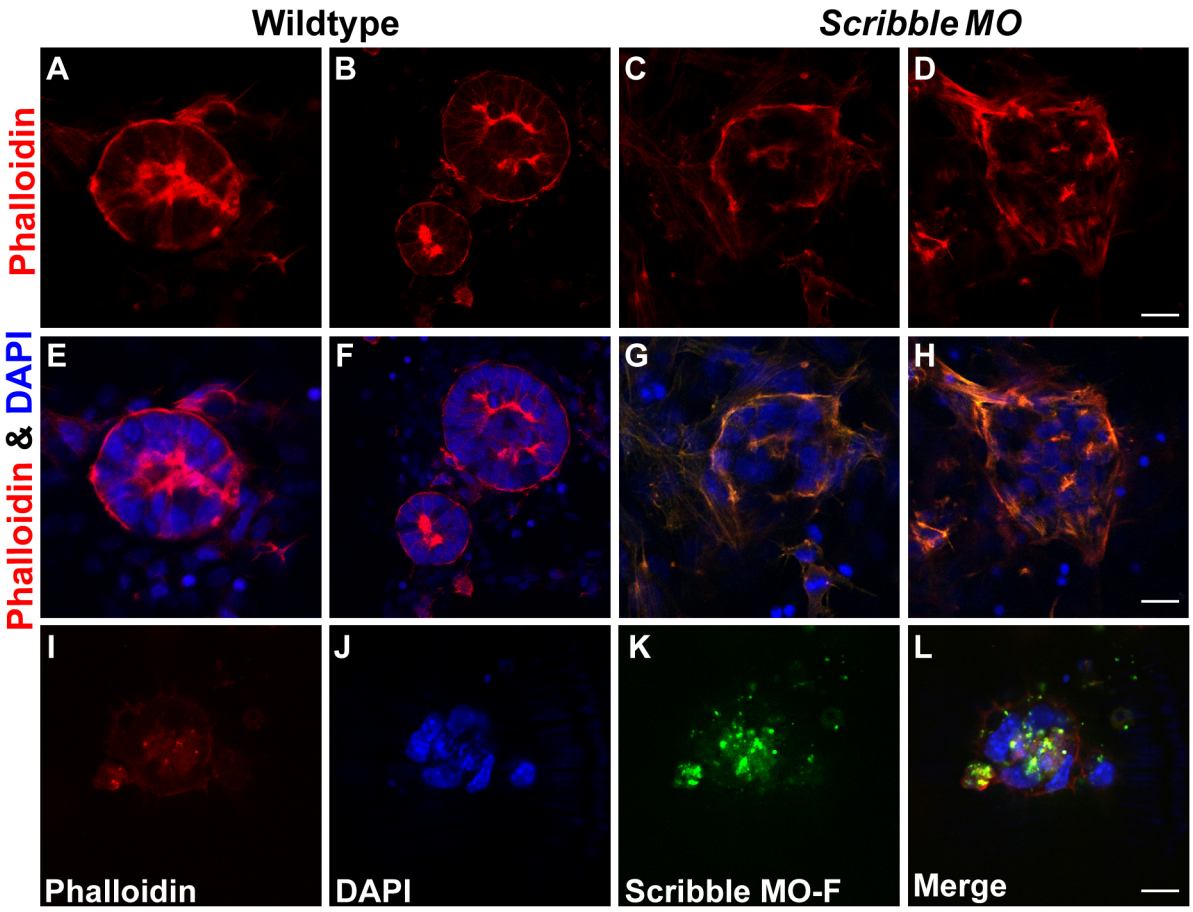


Figure 4.11 Morpholino knockdown of Scribble prevents normal epithelial cyst formation in organotypic culture.

Morpholino knockdown of Scribble in organotypic cultures prevented the re-association of epithelial cells into organised 2D cysts with a centrally located lumen, reminiscent of an *in vivo* *Scribble*$^{Crc/Crc}$ airway. Phalloidin (A-H, I,L) and DAPI (E-H, J,L) staining reveal the organised structure of cysts forming when cultured in the presence of a control morpholino. Epithelial cells surround either a partially forming or open lumen (A,B,E,F), whereas in the presence of a Scribble morpholino the cysts comprise misaligned epithelial cells frequently without any sign of a lumen (C,D,G,H-L). K-L shows Scribble morpholino with a fluorescent tag within the epithelial cells in a single cyst. Scale bars; A-L 125μM x4 zoom.

4.2.11 Scribble modulates localisation of the core PCP proteins Celsr1 and Vangl2 in lung epithelium

One of the hallmarks of the so-called 'core' PCP proteins is that they are capable of modulating the localisation of other core PCP proteins. Therefore, to look for

evidence of Scrib1 associating with other PCP proteins and thereby operating via this pathway in the lung, immunostaining experiments were carried out on E14.5 transverse cryosections.

In wildtype sections, Celsr1 is expressed in epithelial cells around the cell membranes but is enriched towards the apical surface and is strongly expressed around the basal side of airways, in what has been shown to be the basement membrane (see chapter 3.2.11 and Fig 4.12 A). In *Scribble*$^{Crc/Crc}$ lungs, both the strong basal expression and the enrichment of Celsr1 towards the apical surface is lost (Fig 4.12 B) indicating that Scrib1 is required for the correct localisation of Celsr1 in the lung. Conversely, Scrib1 expression appears only mildly affected in *Celsr1*$^{Crsh/Crsh}$ lungs, such that the normal enrichment of Scrib1 expression towards the apical surface (in the tight junctions) is slightly reduced (Fig 4.12 C).

In wildtype lung, Vangl2 shows strong expression around epithelial cell membranes in a punctate pattern and expression is notably enriched in wildtype sections towards the apical surface (Fig 4.12 D and see section 3.2.10). However, in *Scribble*$^{Crc/Crc}$ lungs, this enrichment towards the apical surface is much reduced (Fig 4.12 E), again suggesting Scrib1 is required for correct Vangl2 localisation. Scrib1 expression is unaffected in *Vangl2*$^{Lp/Lp}$ lungs (Fig 4.12 F).

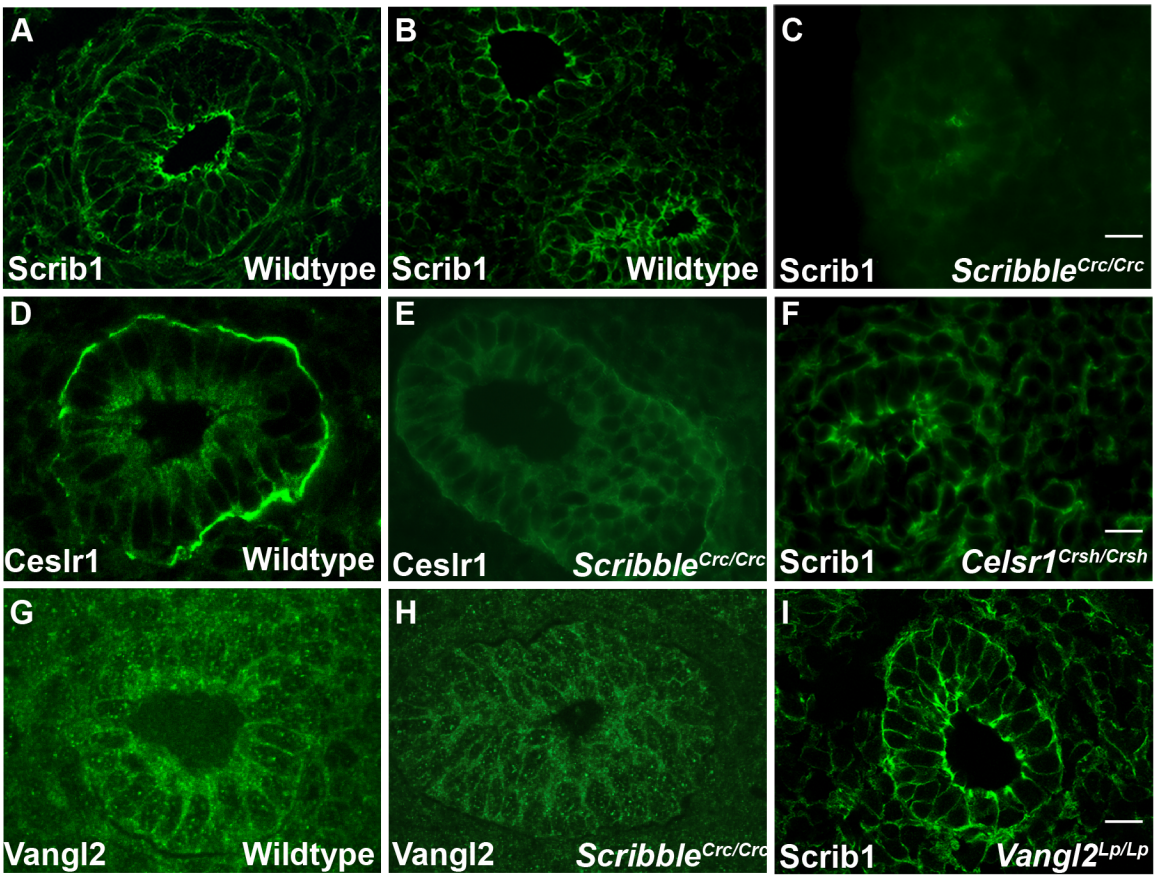


Figure 4.12 Scrib1 is required for Celsr1 localisation in the basement membrane Scrib1 localises strongly towards the apical surface at E14.5 as shown by immunostaining of E14.5 transverse sections (A,B). Scrib1 expression is almost absent in E14.5 *Scribble*$^{Crc/Crc}$ lungs (C). E14.5 wildtype transverse cryosections immunostained with anti-Celsr1 show Celsr1 localises predominantly to the basement membrane (D). However in *Scribble*$^{Crc/Crc}$ sections, loss of this strong basement membrane expression is observed (E). Scrib1 expression is also disrupted in the absence of Celsr1; Scrib1 staining is weaker around epithelial membranes and appears more diffuse (F). Vangl2 is enriched towards the apical surface in wildtype sections (G), however this enrichment appears weaker in *Scribble*$^{Crc/Crc}$ sections (H). In *Vangl2*$^{Lp/Lp}$, Scrib1 expression is unaffected (I). Scale bars; A,C-H 125μM plus x3 zoom, B 125μM plus x2 zoom, I 125μM plus x2.5 zoom.

4.3 Discussion

4.3.1 Scribble$^{Crc/Crc}$ lungs display branching morphogenesis and cytoskeletal defects

Scribble$^{Crc/Crc}$ lungs were smaller and misshapen in comparison to wildtype littermates, and showed a significant reduction in airway number, width and, importantly, in the number of organised airways compared to wildtype littermates. This reduction in size is not a result of defects in proliferation, apoptosis or differentiation. In *ex vivo* culture, where *Scribble*$^{Crc/Crc}$ lungs were able to grow in the absence of *in vivo* space restriction, a severe reduction in branch formation was still observed, indicating that space restriction is not the cause of the phenotype.

Western blot analysis suggested Scrib1 operates via Rho signalling in the lung as a significant reduction in active RhoA (Rho GDP) was observed in *Scribble*$^{Crc/Crc}$ lungs. In addition, severe disruption to the actin-myosin cytoskeleton in *Scribble*$^{Crc/Crc}$ lungs suggests Scrib1 operates in the lung via a similar mechanism to *Celsr1* and *Vangl2* i.e. it modulates branching via Rho kinase-mediated organisation of the cytoskeleton to enable organised and co-ordinated movement of groups of cells (morphogenesis) and thereby give rise to new branches.

4.3.2 Scribble appears to operate via the PCP pathway

From the results presented in this chapter, Scrib1 appears to operate via the PCP pathway to mediate Rho activation of the cytoskeleton, which in turn drives branching morphogenesis of the lung. This conclusion is based on the following evidence: 1) the phenotype observed in *Crc/Crc* mutants is strikingly similar to that observed in lungs of other PCP mutants: *Celsr1*, *Vangl2* and *PTK7* (see chapter 3 and (Paudyal et al., 2010). 2) as presented above, *Crc/Crc* mutants show a significant

reduction in active RhoA and disruption to the cytoskeleton which is the target of the PCP signalling pathway. 3) immunohistochemistry reveals that disruption to Scrib1 can affect the localisation of other core PCP proteins, suggesting that these proteins may directly interact in a complex. Specifically, Scrib1 is required for the correct localisation of Vangl2 in the lung, a result that is consistent with published data describing an interaction between *Scrib* and *Vangl2* in *Drosophila* (Courbard et al., 2009) as well as a genetic interaction between *Vangl2* and *Scrib1* in regulating PCP in the mammalian cochlea (Montcouquiol et al., 2003). Loss of *Vangl2,* however, has no affect on Scrib1 expression. Scrib1 also appears to be required for the correct localisation of Celsr1 in the lung and, conversely, Celsr1 has a mild affect on Scrib1 localisation, indicating an interplay between these two proteins in the lung.

4.3.3 Scrib1 is not required for apical basal polarity in the lung

Establishment of apical basal polarity is a key requirement for the correct formation of an epithelial tube (Affolter and Zeller, 2009; Andrew and Ewald, 2010; Morrisey and Hogan, 2010). Several studies in *Drosophila* and a single study in mammals have indicated a role for Scrib1 in maintaining apical-basal polarity. However, assessment of apical-basal polarity in *Scribble*$^{Crc/Crc}$ lungs by immunohistochemistry revealed no obvious defects. These data suggest that, at least in the lung, Scrib1 is operating via a different pathway, the PCP pathway, to promote the formation of the lung epithelial tubes and maintain the airway lumina.

4.3.4 Scrib1 is required to maintain airway lumina

Close cell-cell association of epithelial cells, maintained by tight and adherens junctions, is a key requirement for a correctly sized and positioned lumen at the centre of an airway (Affolter and Zeller, 2009; Andrew and Ewald, 2010; Morrisey

and Hogan, 2010). Therefore, disruption to tight or adherens junctions will likely lead to disruption of lumina. In *Scribble*$^{Crc/Crc}$ lungs, the normal spatial expression of some tight and adherens junction proteins is perturbed and this may lead to destabilisation of epithelial cells, causing them to collapse into the luminal space. Interestingly, Scrib1 colocalises with ZO-2 in the lung and ZO-2 expression is severely affected in *Scribble*$^{Crc/Crc}$ lungs, while no obvious defects are observed in ZO-1. Previous studies by Metais et al., have shown that human Scribble (hScrib) directly binds to ZO-2 and that this interaction relies on the PDZ3 and PDZ4 domains of hScrib; these domains are absent in *Crc/Crc* mice. Scribble shows overlapping expression with ZO-1 and occludin in human colonic epithelial cell lines T84 and SK-CO15; while no disruption to ZO-1 expression or protein levels was observed in *Crc/Crc* lungs, disruption to both occludin and claudin tight junctions was observed in *Scribble*$^{Crc/Crc}$ lungs, consistent with the human studies (Metais et al., 2005).

The misorganisation of epithelial cells around the airway lumen in *Scribble*$^{Crc/Crc}$ lungs, along with disruption to cell associations required for correct lumen formation and Scrib1's localisation towards the apical surface, suggests a role for Scrib1 in maintaining the airway lumen. Further confirmation of this comes from knockdown of Scribble using a specific morpholino in a 3D culture system. In the presence of specific Scribble antisense morpholinos, epithelial cells were unable to reorganise into cysts with a structured lumen unlike control cultures, which formed many more cysts with organised and uniformly aligned epithelial cells surrounding an open lumen.

Taken together, the results of this chapter describe a role for Scribble in normal lung development by maintaining the airway lumina, which are essential for lung function. As the molecular mechanisms of mammalian lumen formation are

poorly understood this finding is an important step towards understanding the biology of this key process in tubulogenesis and diseases such as polycystic kidney disease, hypertension and ischemic injury, which arise as a result of disruption to lumen formation and/or maintenance.

4.3.5 Cross talk between PCP and A/B polarity pathways

The majority of epithelial tissues require both apical-basal polarisation and planar polarisation for optimal organisation and function. Indeed, it is likely that these two pathways are closely linked at the molecular level, and that crosstalk will exist between them. In *Drosophila*, there is now considerable evidence of such crosstalk between the PCP and A/B polarity pathways. Djiane et al., have shown that in the *Drosophila* eye, the activity of the PCP factor Frizzled is regulated by phosphorylation, which is mediated by aPKC and antagonised by Bazooka, two apical-basal determinants (Djiane et al., 2005). A recent study by Courbard et al., has shown the core PCP component Strabismus (Stbm)/Van Gogh (Vang) and the *Drosophila* apical-basal determinant Scrib interact both genetically and physically. Scrib binds Stbm/Vang through its PDZ domain 3 and it cooperates with Stbm/Vang in PCP establishment, therefore showing that in the *Drosophila* eye and wing, Scrib does play a role in aiding the establishment of PCP (Courbard et al., 2009). This study is the first to show that Scrib can function in the PCP pathway in *Drosophila* in addition to its established role in apical-basal polarity. In mammals, Scrib1 has an recognized role in PCP, as shown by analysis of the *Scribble*$^{Crc/Crc}$ mouse mutant, which displays the open neural tube defect craniorachischisis, along with defects in stereociliary polarisation (Montcouquiol et al., 2003), both of which are well-known PCP phenotypes. From the literature it is clear that cross-talk does exist between these two polarity pathways

and, since Scribble has a role in both pathways, it may act as a linker between the two by binding different apical-basal and PCP determinants via its multiple PDZ and LRR domains (Courbard et al., 2009; Kallay et al., 2006). However, to date most data showing Scribble is required for apical-basal polarity comes from *Drosophila,* with the majority of mammalian studies revealing a role for Scribble in the PCP pathway. Indeed, data from this chapter show that in the lung, apical-basal polarity is not visibly perturbed in *Scribble*$^{Crc/Crc}$ and instead there is strong evidence that it is acting in the PCP pathway. This demonstration is interesting given the critical and predominant role for Scrib in apical-basal polarity in *Drosophila*. However, Courbard et al., used a Stbm/Vang hypomorphic (*stbm*^{153}) allele that displays mild defects in PCP combined with heterozygous conditions for Scrib. This Scrib allele is largely PCP-specific, and interestingly is molecularly very similar to Circletail. It is therefore possible that the mutation in *Crc/Crc* is not severe enough or specific enough to cause defects in apical-basal polarity and therefore it is possible that further studies utilising different Scribble alleles may yet reveal that this gene is required for mammalian apical-basal polarity.

4.3.6 A more severe phenotype is observed in Scribble$^{Crc/Crc}$ lungs compared to those of either Celsr1$^{Crsh/Crsh}$ or Vangl2$^{Lp/Lp}$ mouse mutants

Scribble$^{Crc/Crc}$ lungs are more severely affected than *Vangl2*$^{Lp/Lp}$ and *Celsr1*$^{Crsh/Crsh}$ lungs. Macroscopically, *Scribble*$^{Crc/Crc}$ lungs are smaller, epithelial cell organisation around the airways is severely disrupted and many airways lack a lumen as the space is occupied by cells. All three of these mouse mutants display disruption to the actin-myosin cytoskeleton within the lung that is required to maintain the overall structure and morphogenesis of epithelial cells. In addition, however, *Scribble*$^{Crc/Crc}$ lungs also

display defects in epithelial cell-cell association that are not observed in *Celsr1* or *Vangl2* mutants. It is these additional defects that appear to increase the severity of the phenotype in *Scribble*$^{Crc/Crc}$ lungs by resulting in collapsed lumina.

However, an alternative explanation for the severe phenotype observed in *Crc/Crc* lungs is that, in mammals, there is only one *SCRIB* gene, whereas there are three *CELSR* genes and two *VANGL* genes. Simultaneous disruption of all three murine *CELSR,* or of both *VANGL* family members, may result in a similarly severe phenotype to that seen in Circletail.

5 Chapter Five: Preliminary analysis of lung phenotype and function in *Vangl2*$^{Lp/+}$ mice

5.1 Introduction

The adult lung is capable of some repair after injury, however neonatal deficiencies such as those caused by premature birth, cannot be rescued by postnatal regeneration, thereby resulting in lifelong respiratory problems and further clinical burdens (Greenough, 2009). This highlights the requirement for a more in depth understanding of the mechanisms driving embryonic lung development as a means to improve the outcome of adult lung diseases such as COPD and asthma.

Pressure is required for the breathing process to work. When a volume of air moves from outside the body (high pressure) into the body (low pressure) this creates a pressure gradient. In a spontaneously breathing subject at rest, these pressures are provided by the respiratory muscles during inspiration, and by the tendency of stretched respiratory tissues to recoil to their resting configurations during expiration. Measurement of lung mechanics reflects the physical properties of the components of the lung. It is a general term used to describe all things that determine the relationships between pressures, airflows and air volumes in the lung. Measurements of respiratory mechanics and lung function are crucial and invaluable tools for many areas of basic and pre-clinical pharmacological pulmonary research as they provide a method of directly measuring acute or chronic, disease-related changes to the lungs. For example, in a disease scenario, such as during an asthma attack, the airways become narrow so greater pressure than normal is required to force the air through. In emphysematous lungs that have enlarged airspaces, the lungs are more easily inflated than normal, so less pressure is required.

Unrestrained plethysmography (UP) has been widely used to measure airway reactivity in conscious mice. It was first investigated in 1868 and further developed

in 1955 by Drorbaugh and Fenn (Drorbaugh and Fenn, 1955) as a method for assessing lung function in infants. It is non-invasive, easy to use and in animals, this method is invaluable as it allows a large throughput of animals for screening purposes. Mice are placed, unrestrained into one chamber of a whole body plethysmograph (WBP), and airway responsiveness is ascertained by exposure to aerosols generated from increasingly concentrated solutions of a bronchoconstrictor such as methacholine. There are two types of WBP: the sealed plethysmograph or pressure plethysmograph (PWBP); and a plethysmograph with a pneumotachograph in its wall or flow plethysmograph (FWBP). The flow plethysmograph was used in this study and is therefore discussed below. FWBP measures the rate of which a change in volume occurs in the chamber as a result of the movement of air from chamber to body and back again i.e. the rate of change of thoracic displacement and the nasal flow.

Penh is a dimensionless parameter derived from chamber pressure and therefore from the respiratory pattern of the animal within the chamber. Increases in Penh are related to an increase in pulmonary resistance (airway resistance is the opposition to flow) (Bates and Irvin, 2003). Figure 5.1 shows how Penh is calculated from the pressure changes occurring inside a chamber from a spontaneously breathing animal.

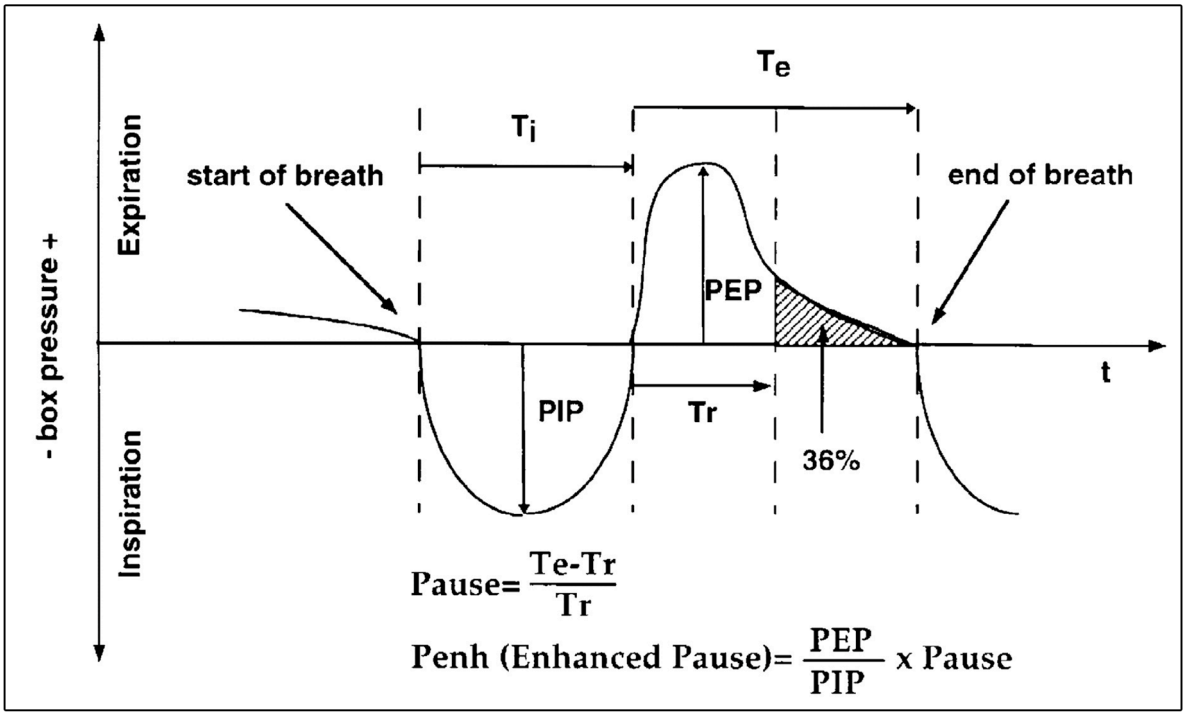


Figure 5.1 Calculation of enhanced pause (Penh). Penh is calculated as follows = (P1/P2) x (T1xT2), where P is pressure and T is time. The schematic diagram shows how pressure is measured inside the plethysmograph in which the mouse was placed. The pressure within the WBP (box/chamber) varies cyclically as the mouse breathes. The inspiratory and expiratory durations (T1 and T2 respectively) are defined on the basis of the upper and lower portions of the pressure curve and do not necessarily correspond to actual inspiration expiration. PEP, peak expiratory pressure; PIP, peak inspiratory pressure; t, time; Tr, time to expire 74% of the tidal volume. (Adapted from (Bates and Irvin, 2003).

Penh reflects changes in the waveform of the chamber pressure signal from both inspiration and expiration (PIP, PEP) and combines it with the timing comparison of early and late expiration referred to as Pause. An example of the chamber pressure waveform from a normal mouse before and after challenge with aerosolized methacholine is shown in Fig 5.2, demonstrating the changes in the waveform as well as in Pause and Penh after agonist inhalation.

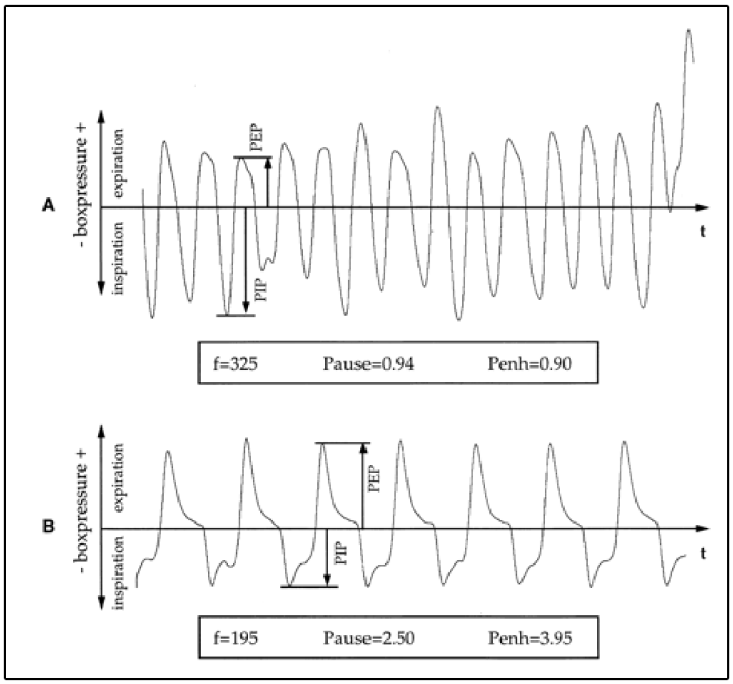


Figure 5.2 Changes in chamber pressure waveform after methacholine challenge. Waveform of the chamber pressure signal derived from a normal mouse after 3 min of nebulisation with aerosolized PBS (A) or aerosolized methacholine (50 mg/ml in PBS) (B). Methacholine causes the airways to constrict making it harder for the mouse to breath; therefore Penh reflects a deficit in the ability of the lung to function normally. f = respiratory rate (breaths/min); Pause, Penh (enhanced pause), PEP, peak expiratory pressure; PIP, peak inspiratory pressure. (Adapted from (Hamelmann et al., 1997).

Due to the embryonic lethality of *Celsr1 Vangl2* and *Scribble* homozygotes, it was not possible to establish whether mutations in these genes would affect adult lung function. The Vangl2 mutation in *Looptail* had previously been shown to cause phenotypes in heterozygotes, however, these mice are viable. Therefore analysis of *Vangl2*$^{Lp/+}$ lungs was carried out to determine if loss of one copy of Vangl2 was sufficient to cause similar embryonic defects to those observed in *Vangl2 homozygotes* (see Chapter Three) and if so, whether these abnormalities affected adult lung function.

5.1.1 Aims

- To ascertain whether *Vangl2* heterozygous mice display an embryonic and/or adult lung phenotype
- To determine whether loss of one copy of *Vangl2* causes a functional defect in the adult mammalian lung

5.2 Results

5.2.1 Vangl2 heterozygotes have reduced numbers of airways and display localised tissue disruption in the lung.

To first determine whether loss of a single copy of *Vangl2* resulted in embryonic lung defects, E14.5 and E18.5 wildtype and *Vangl2*$^{Lp/+}$ paraffin wax sections were stained with H&E (Fig 5.3 A-C). At E14.5 *Vangl2*$^{Lp/+}$ airways showed mild disruption to epithelial organisation with material frequently occupying the luminal space (Fig 5.3 B).

At E18.5 disruption to *Vangl2*$^{Lp/+}$ mutant lungs appeared patchy, with some areas reminiscent of the normal, honeycomb-like structure of wildtype lungs and evidence of septation (the process by which epithelial cells migrate across existing

sacculae to form new airways) (arrows in Fig 5.3 D), whilst other areas displayed thickened tissue with multiple cell layers, fewer airway spaces and evidence of septation (boxed area in Fig 5.3 D) compared to wildtype littermates (Fig 5.3 C). This heterogeneous phenotype is consistent with a similar albeit milder phenotype to that observed in homozygous lungs (see Chapter Three). Quantification of the number of epithelial airways at both E14.5 and E18.5, revealed a significant reduction compared to wildtype littermates (Fig 5.3 E-F). However the reduced number of airways and mild histological defects in the lungs did not affect viability of these mice.

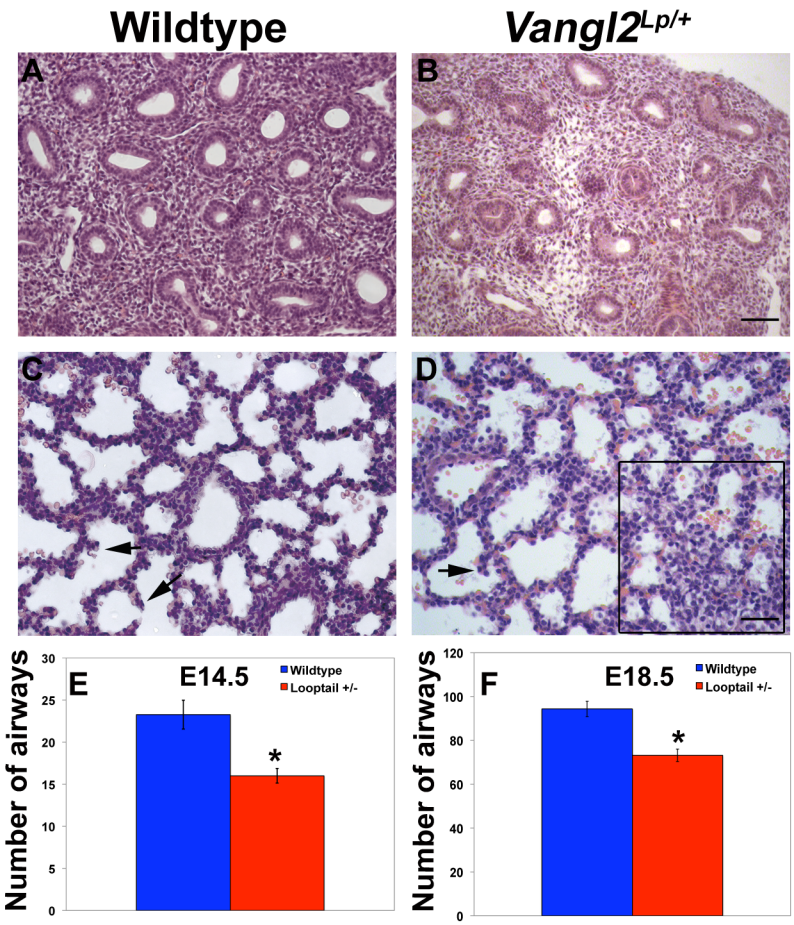


Figure 5.3 *Vangl2*$^{Lp/+}$ mice have mild histological lung defects with reduced branching. E14.5 wildtype lung sections stained with H&E revealed clearly visible lumina surrounded by a single layer of organised epithelial cells (A). E14.5 *Vangl2*$^{Lp/+}$ lungs displayed a mild disruption to the organisation of epithelial cells surrounding partially open lumina, which were often filled with material (B). E18.5 *Vangl2*$^{Lp/+}$ (D) sections showed a variation in histology, some areas were reminiscent of wildtype sections, (C) with an organised honeycomb-like structure and clear evidence of septation (arrows), whereas tissue appeared thickened in other areas, having multiple cell layers with no evidence of septation (boxed region in D). A significant reduction in the number of epithelial airways in *Vangl2*$^{Lp/+}$ at both E14.5 (E) (wildtype 23.26, ±1.71, n=3; *Vangl2*$^{Lp/+}$ 16, ±0.87, n =3), and E18.5 (F) (wildtype 94.36, ±3.48, n=3; *Vangl2*$^{Lp/+}$ 73.18, ±2.84, n =3) was observed compared to wildtype controls. Scale bars: A-B 50μM, C-D 12.5μM.

5.2.2 Differentiation, proliferation and apoptosis are unaffected in Vangl2$^{Lp/+}$ lungs

While no difference in differentiation, proliferation or apoptosis was observed between *Vangl2*$^{Lp/Lp}$ lungs and wildtype controls, it was necessary to ensure that these processes were equally unaffected in *Vangl2* heterozygote animals. To do this, E14.5 *Vangl2*$^{Lp/+}$ and wildtype paraffin sections were immunostained for the distal airway marker Pro-SpC (Fig 5.4 A-B), and the two proximal airway markers CC-10, (Clara cell marker) (Fig 5.4 C-D) and α-SMA (Fig 5.4 E-F). No difference was observed in the expression patterns of Pro-Spc, CC10 or α-SMA between *Vangl2*$^{Lp/+}$ and wildtype lungs (Fig 5.4 compare B,D,F with A,C,E).

Proliferation was assessed by immunostaining E14.5 *Vangl2*$^{Lp/+}$ and wildtype cryosections with anti-Phospho histone H3 (Fig 5.4 G-H). No difference in the levels of proliferation was observed between Vangl2 heterozygote and wildtype lungs (Fig 5.4 compare H with G). Apoptosis was assessed by immunostaining E14.5 *Vangl2*$^{Lp/+}$ and wildtype cryosections with anti-cleaved caspase-3 (Fig 5.4 I-J), and again no difference in the levels of apoptosis was observed between *Vangl2* heterozygote and wildtype lungs (Fig 5.4 compare J with I). Thus, neither abnormalities in cell proliferation nor apoptosis lead to the *Vangl2*$^{Lp/+}$ lung phenotype.

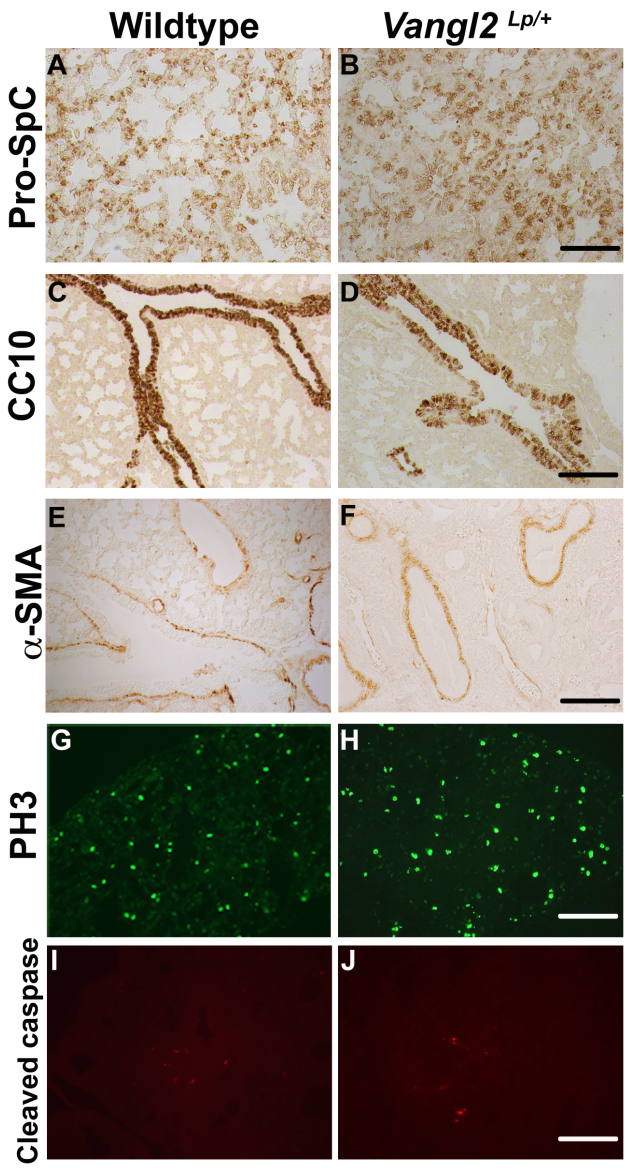


Figure 5.4 Differentiation, proliferation nor apoptosis were affected in *Vangl2*$^{Lp/+}$ lungs compared to wildtype controls. E14.5 wildtype (A,C,E) and *Vangl2*$^{Lp/+}$ (B,D,F) paraffin wax sections were immunostained with the distal airway marker anti-Pro Spc (A,B) and the two proximal airway markers anti-CC-10 (C,D) and anti-α-SMA (E,F). No difference in any of the differentiation markers was observed between *Vangl2*$^{Lp/+}$ and wildtype littermates. E14.5 wildtype (G,I) and *Vangl2*$^{Lp/+}$ (H,J) cryosections were immunostained with either anti-phospho histone H3 (G,H) to assess proliferation or anti-cleaved caspase-3 (I,J) to assess apoptosis. No difference was observed in the levels of either proliferation or apoptosis in *Vangl2*$^{Lp/+}$ lungs compared to controls. Scale bars: A-B 12.5μM, C-J 25μM.

5.2.3 Mild disruption to actin-myosin cytoskeleton is observed in Vangl2$^{Lp/+}$ lungs

As described in Chapter 3 (section 3.2.7), perturbation of the actin-myosin cytoskeleton results in abnormal lung morphogenesis in *Vangl2*$^{Lp/Lp}$ mice. To establish whether defects in the actin-myosin cytoskeleton could also be the cause of the tissue defects observed *Vangl2*$^{Lp/+}$ mutant lungs, an assessment of the actin-myosin cytoskeleton was undertaken.

E14.5 and E18.5 cryosections were stained with phalloidin to highlight the cortical F-actin (Fig 5.5 A-D). Cortical actin was observed surrounding individual epithelial and mesenchymal cells in wildtype sections. High levels of Phalloidin staining were also observed along the apical surfaces of epithelial cells at E14.5, adjacent to the airway lumina (Fig 5.5 A). In some *Vangl2*$^{Lp/+}$ airways the cortical actin remained continuous around individual epithelial cells reminiscent of wildtype airways, however some *Vangl2*$^{Lp/+}$ airways displayed a more discontinuous and diffuse pattern of cortical actin both around individual cells and along the apical/luminal surface of the *Vangl2*$^{Lp/+}$ mutant airways (Fig 5.5 compare B with A). Mild disruption to F-actin localisation was also observed at E18.5 in *Vangl2* heterozygotes, with less enrichment of F-actin particularly in those cells immediately adjacent to airways, compared with wildtype tissue (Fig 5.5 D compared to C). Non-muscle myosin II, another critical component of the cytoskeleton, was also mildly disrupted in *Vangl2*$^{Lp/+}$ lungs (Fig 5.5 F compared to E). Taking in to account all these data, it therefore appears likely that the defects in cell organisation and branching observed in *Vangl2*$^{Lp/+}$ embryonic lung result from groups of cells being incapable of moving in a co-ordinated manner because of cytoskeletal disruption. As a result, cells are unable to give rise to normally structured and organised branches

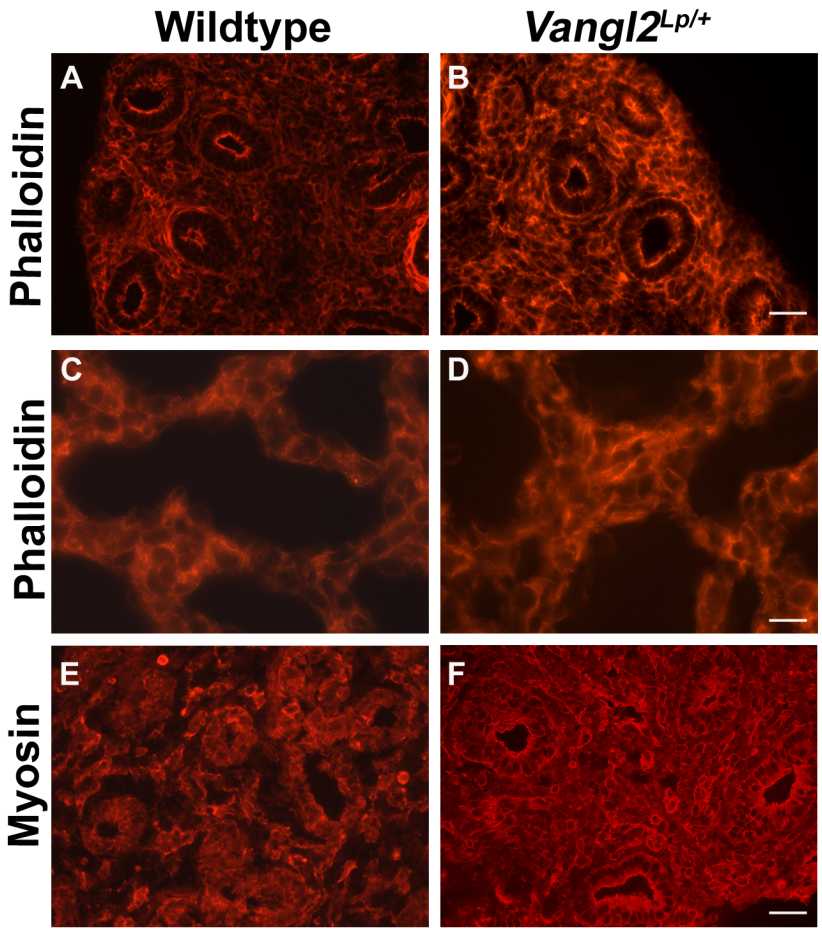


Figure 5.5 *Vangl2*$^{Lp/+}$ lungs displayed mild disruption to the actin-myosin cytoskeleton. Rhodamine phalloidin staining of F-actin reveals mild cytoskeletal defects in *Vangl2*$^{Lp/+}$ mutants at E14.5 (B) and E18.5 (D) compared to wildtype (A,C), as does staining with antibodies to non-muscle myosin IIA in mutants (F), compared to wildtype (E). Scale bars: A-B,E-F 25μM, C-D 5μM.

5.2.4 Adult Vangl2$^{Lp/+}$ display histological defects

To determine whether the cellular disruption and branching defects observed during *Vangl2*$^{Lp/+}$ embryonic lung development, persisted into adulthood, an assessment of adult lung histology was conducted. Macroscopically, adult *Vangl2*$^{Lp/+}$ lungs were consistently smaller and shorter than wildtype lungs (Fig 5.6 A,B). However crude measurement of terminal and lung weights did not reveal any significant difference between genotypes (Fig 5.6 C,D), neither did the body:lung weight ratio (data not shown).

Histological analysis of 10-week-old wildtype and *Vangl2*$^{Lp/+}$ lungs stained with M.S.B (Fig 5.6 E-H) revealed variable defects within isolated regions of the lung. Consistent with the embryonic lung defects, adult *Vangl2*$^{Lp/+}$ lungs, displayed small regions that appeared normal and reminiscent of wildtype lungs. However, large areas of the lungs showed severely enlarged airspaces and disruption to the airway walls, reminiscent of an emphysema-like phenotype.

Analysis of immune cell populations within bronchioalveolar fluid (BALF) from both 10 week old wildtype and *Vangl2*$^{Lp/+}$ lungs (Fig 5.6 I, J), revealed the presence of activated immune cells in BALF from *Vangl2* heterozygote lungs compared to controls. Naive mutant and control lungs were lavaged via a tracheal tube with PBS, and the cellular content was analyzed following cytospin and histological staining. Interestingly, macrophages in BALF from *Vangl2*$^{Lp/+}$ lungs appeared activated or “foamy” with multiple nuclei and a higher number of neutrophils were present, all of which are signs of an active immune response in the lungs. In contrast, wildtype BALF cells were in a “rested” or non-activated state. A

significant increase in both activated macrophages and neutrophils was observed in *Vangl2*$^{Lp/+}$ BALF in comparison to wildtype BALF (Fig 5.6 K-L).

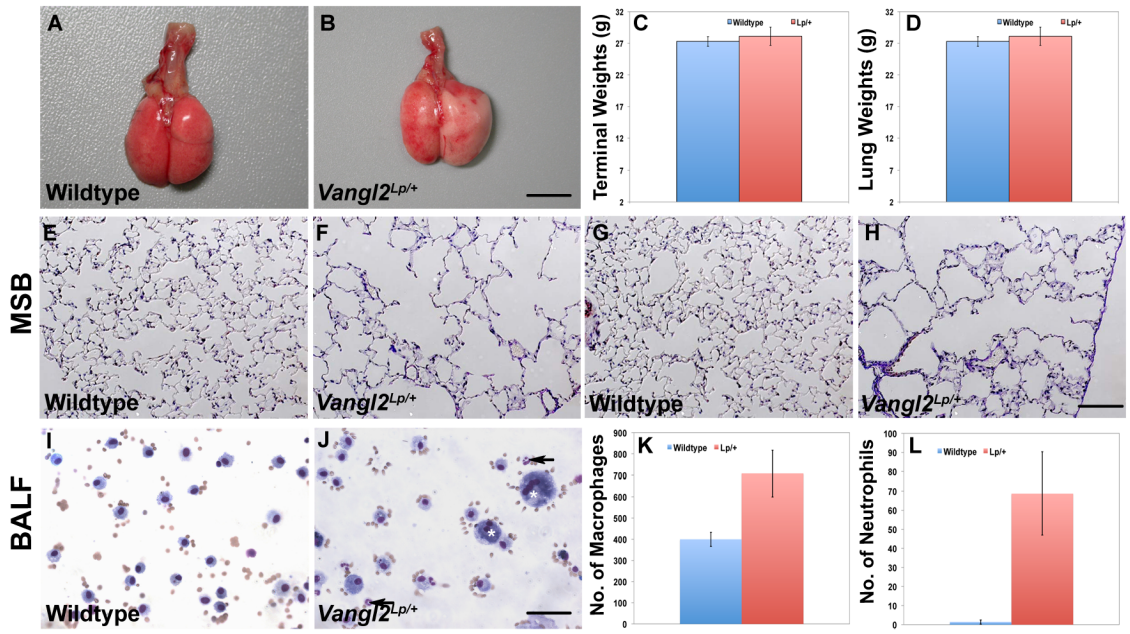


Figure 5.6. Histological Analysis of 10 week old Adult *Vangl2*$^{Lp/+}$ lungs. Analysis of whole 10-week-old lungs from both wildtype (A) and *Vangl2*$^{Lp/+}$ (B) mice revealed no significant variation in their overall morphology. No significant difference was observed in either terminal (C) or lung weights (D) between 10 week old *Vangl2*$^{Lp/+}$ and wildtype mice (Terminal Weights; wildtype mean = 27.29g ± 0.77 n=3, *Vangl2*$^{Lp/+}$ mean = 28.10g ± 1.44 n=3 p=0.575. Lung Weights; wildtype mean = 0.26g ± 0.02 n=3, *Vangl2*$^{Lp/+}$ mean = 0.28g ± 0.01 n=3 p=0.327.) Histological analysis of paraffin wax sections (E-H) revealed a variable defect in *Vangl2*$^{Lp/+}$ (F, H) lungs compared to wildtype controls (E, G). Some areas were reminiscent of wildtype lungs, however large regions of *Vangl2*$^{Lp/+}$ lungs displayed an enlargement of the airspaces. Analysis of immune cells within BALF collected from wildtype (I) and *Vangl2*$^{Lp/+}$ (J) lungs revealed activated or "foamy" macrophages (white asterisk in F) and an infiltration of neutrophils (arrows in F) in *Vangl2*$^{Lp/+}$ (H) lungs compared to wildtype (G), indicative of an immune response. Both the number of macrophages (K) and neutrophils (L) in *Vangl2*$^{Lp/+}$ BALF was elevated compared to wildtype BALF. Scale bars; A-B μM, C-D 25μM, E-F 12.5μM.

5.2.5 Adult heterozygotes have an intrinsic lung function defect

To determine whether the histological and cytoskeletal defects mentioned above would affect lung function in *Vangl2*$^{Lp/+}$ mice, an initial assessment was conducted by measuring Penh. 12 wildtype and 12 *Vangl2*$^{Lp/+}$ 10 week old mice were assessed for lung function defects using an unrestrained whole body plethysmograph (uWBP) system. Four chambers were used simultaneously, allowing recordings of both wildtype and *Vangl2*$^{Lp/+}$ lung function to be collected at the same time. No significant difference in Penh was observed following dosing with increasing concentrations of methacholine, at any point during lung function analysis between *Vangl2*$^{Lp/+}$ and wildtype mice (Fig 5.7). However, a consistent elevation in Penh was observed at baseline in *Vangl2*$^{Lp/+}$ mice compared with controls, suggesting an intrinsic lung deficiency is present. This elevation was not statistically significant however it does suggest that there is a functional defect in *Vangl2*$^{Lp/+}$ mice that results from the histological and cytoskeletal defects mentioned above. In addition only 33% of *Vangl2 heterozygote* mice could be challenged with the highest dose of methacholine as either their Penh spiked to 6 or above, or the animal appeared too distressed, whereas 67% of wildtype mice were dosed with 50mg/ml methacholine.

The baseline functional defect that we observed, is consistent with the results from analysis of immune cell populations which showed an activated immune response in BALF taken from *Vangl2*$^{Lp/+}$ lungs.

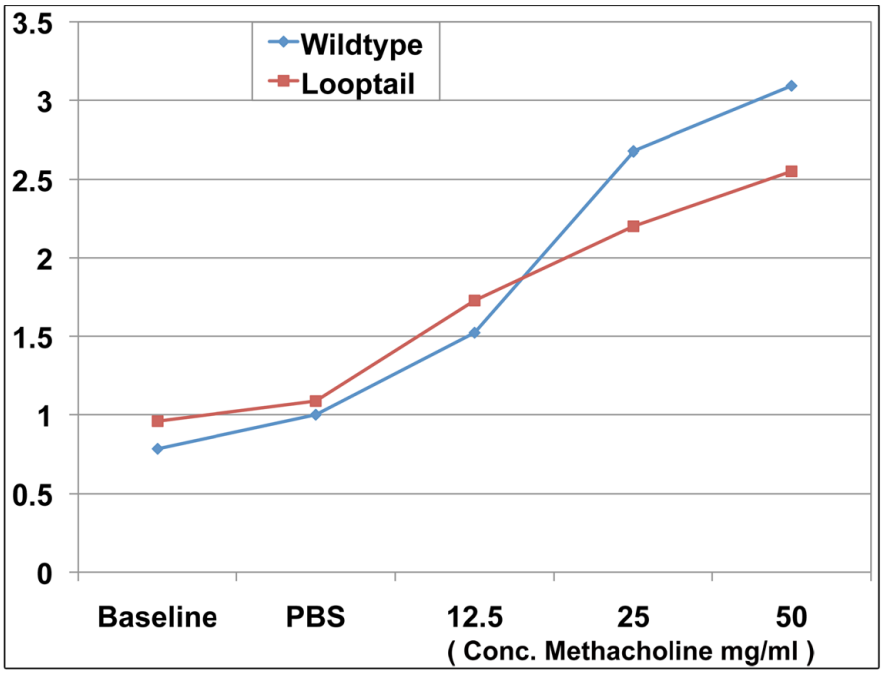


Figure 5.7 No significant difference in Penh was observed between *Vangl2*$^{Lp/+}$ and wildtype mice. Mice were placed into one of four uWBP chambers and baseline readings collected for 2mins. Mice were then nebulized first with PBS, followed by increasing doses (12.5, 25 and 50 mg/ml) of methacholine for 2 min for each nebulization, followed by readings of breathing parameters for a further 3 min after each nebulization, with Penh values determined. No significant difference in Penh was observed between *Vangl2*$^{Lp/+}$ and wildtype controls at any point. However elevation in Penh in *Vangl2*$^{Lp/+}$ at baseline was consistent throughout, suggesting an intrinsic lung deficiency in *Vangl2*$^{Lp/+}$ mice compared to controls. Penh was averaged for each subject group at each point and these values were plotted on the graph. (Wildtype average Penh: Baseline; 0.782, PBS; 0.999, 12.5mg/ml; 1.522, 25mg/ml; 2.676, 50mg/ml; 3.09. *Vangl2*$^{Lp/+}$ average Penh: Baseline; 0.958, PBS; 1.087, 12.5mg/ml; 1.728, 25mg/ml; 2.201 50mg/ml; 2.551).

5.3 Discussion

5.3.1 Vangl2 heterozygous mice display embryonic lung defects

Branching morphogenesis is affected in *Vangl2*$^{Lp/+}$ lungs, as evidenced by the reduction in the number of airways present at E14.5 and E18.5. Just prior to birth, at E18.5, the lungs appear hypoplastic and regions of 'normal' tissue are interspersed with focally restricted areas of abberent tissue morphology where thickened interstitium is evident and in these areas septation is not observed. At E14.5 some airways appear normal with a single layer of organised epithelial cells surrounding an open lumina, whereas in other airways epithelial cells appear more disorganised and cellular material often occupies the luminal space. By E18.5 whilst some regions appear normal again, other regions display multiple cell layers surrounding airways, The multiple cell layers observed around airways and the increased tissue thickness observed is reminiscent of a fibrotic-like phenotype in the lungs of *Vangl2 heterozygote* mutants.

Embryonic analyses of *Vangl2 heterozygote* lungs reveals a similar but milder phenotype to *Vangl2 homozygous* mice (see Chapter Three). The tissue disruption in the heterozygote lungs mimics the more severe disruption observed in the homozygoutes lungs consistent with the loss of only one copy of Vangl2. Proliferation, apoptosis and differentiation are unaffected in both Vangl2 heterozygotes and homozygotes. Finally, analysis of the actin-myosin cytoskeleton reveals yet again a similar but milder phenotype in *Vangl2* heterozygote lungs compared to *Vangl2* homozygote lungs. Thus concluding that the milder histological and branching defects observed in *Vangl2*$^{Lp/+}$ lungs are likely due to defects in cytoskeletal organisation

required for normal branching morphogenesis consistent with the mechanism described in *Vangl2*$^{Lp/Lp}$ lungs (see Chapter Three).

5.3.2 Adult Vangl2$^{Lp/+}$ mice have histological defects

An assessment of 10-week-old *Vangl2*$^{Lp/+}$ lungs revealed that overall lung topology was affected so that heterozygote lungs were smaller and notably shorter than wildtypes. However neither lung nor whole body terminal weights were significantly different between wildtype and *Vangl2L*$^{p/+}$ mice. A relatively crude method was used to measure both terminal and lung weights of *Vangl2 heterozygote* and wildtype mice, therefore subtle differences between the two genotypes might not have been detected. A more accurate way to measure the lungs would be to determine the volume of the lungs as apposed to their weight, as this would an indication of lung capacity which is more closely related to lung function.

Histological analysis revealed severely enlarged distal airways, and disruption of some airway walls in *Vangl2*$^{Lp/+}$ lungs compared to controls. Noteably, this phenotype is similar to that seen in emphysema, a condition of the lung characterized by abnormal permanent enlargement of the airspaces distal to the terminal bronchiole, accompanied by destruction of their walls without obvious fibrosis. This discovery was interesting as during embryogenesis regions of Vangl2 heterozygote lung tissue appears thickened with a fibrotic-like phenotype, yet by 10-weeks of age airspaces appear larger than wildtype controls adopting a more emphysema-like phenotype. One explanation for this could be that lack of septation resulting in a reduction in the number of airways during embryonic development could result in larger airspaces in adulthood. It is also important to note that mouse models that

develop emphysema do not display airspace enlargement until approx. 3 weeks of age, which then becomes progressively worse with advancing age (Wert et al., 2000).

5.3.3 *Vangl2*$^{Lp/+}$ mice have an activated immune system with a consistent increase in Penh at baseline, but no significant elevation in Penh is observed following administration of methacholine.

Analysis of BAL cells from both *Vangl2*$^{Lp/+}$ and wildtype lungs revealed both an increase number of macrophages and neutrophils (polymorphonuclear leukocytes; PMN) in *Vangl2*$^{Lp/+}$ BALF. In addition macrophages appeared in a more active state, such they were large in size "foamy" and contained multiple nuclei. Resident macrophages are central in defending the lungs against the assaults of particles and pathogens in inspired air, play a critical role in homeostasis, and tissue remodeling (Lambrecht, 2006). The lungs are especially sensitive and prone to damage, thus to avoid damage to lung tissue, alveolar macrophages are kept in a quiescent state producing little inflammatory cytokines. Neutrophil infiltration into the lung is also an important component of the inflammatory response in acute lung injury (Abraham, 2003). Together this suggests that even in the absence of an environmental insult or allergen challenge, the immune system of *Vangl2*$^{Lp/+}$ mice is in an active state. Indicating that *Vangl2*$^{Lp/+}$ lungs are stressed or mildly injured in some way and this may be as a direct result of the cellular disruption and reduced number of airways.

The above results strongly implied that *Vangl2*$^{Lp/+}$ mice may have impaired lung function however, no significant difference in Penh was observed between wildtype and *Vangl2*$^{Lp/+}$ mice. One explanation of the apparent lack of functional defect in *Vangl2*$^{Lp/+}$ lungs is that the histological and cytoskeletal defects observed in

both embryonic and adult *Vangl2*$^{Lp/+}$ lungs is not severe enough to result in a significant functional impairment. However, the Penh of *Vangl2*$^{Lp/+}$ mice at baseline, was consistently elevated in comparison to controls. This suggests that even without the challenge of a bronchoconstrictor, such as methacholine, *Vangl2*$^{Lp/+}$ lungs have intrinsically impaired lung function, that would be consistent with the histological phenotype observed.

5.3.4 Advantages and disadvantages of using Penh to determine lung function

Mouse models are widely used in lung research today as a result of the numerous advantages of this species: they have a short reproductive cycle, a well characterized genome, there is a wide variety of tools and reagents available to aid investigations in mouse and they are fairly economical to keep.

One of the main obstacles when studying lung function is finding the balance between achieving accurate measurements whilst maintaining "natural" conditions. This is also true when considering the use of *in vitro* vs. *in vivo* methods for answering a biological question. In lung physiology, this is referred to as the "phenotyping uncertainty principle" (See Fig 5.8). This is the compromise between the achievement of studying an animal's lung function under natural conditions whilst recording measurements with detailed precision.

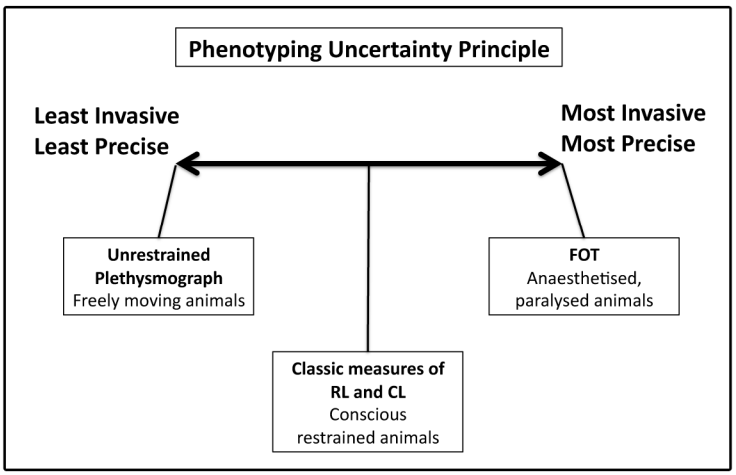


Figure 5.8 The Phenotyping uncertainty principle. The compromise one has to make when measuring lung function; maintaining natural conditions, whilst recording the most accurate data.

One extreme, classed as “controlling nothing” is an assessment of lung function by unrestrained plethysmography. Assessing lung function in an unrestrained chamber such as the uWBP system, does have its advantages, for example, it does not require the use of anesthetic agents or surgical preparation, the same mouse can be studied on a number of occasions and it is relatively quick and easy to use. Many labs have shown its use to be a good, albeit crude, parameter to gain initial insight into lung function (Dohi et al., 1999; Finotto et al., 2001; Hamelmann et al., 1997). However, when using a system that allows mice to move freely, no direct measures of the pressures driving ventilation are obtained, making the conclusions with respect to lung mechanics less robust than those made with techniques that utilize direct pressure measurements. In addition, because the airway is not instrumented (e.g. no direct access to the lung via a trachea tube is available), changes in the resistance of the nasal passages to air-flow (the mouse being an obligate nose breather) are registered as changes in respiratory resistance (Drazen et al., 1999).

Using Penh as a measurement of lung function is controversial. Some studies have shown a good correlation between Penh and other measures of lung function (Dohi et al., 1999; Finotto et al., 2001; Hamelmann et al., 1997), while others suggest Penh does not correlate well with morphometric changes in mice (Lundblad et al., 2002; Petak et al., 2001).

Additionally the parameter measured, Penh, as a measurement of lung function is controversial. Some studies have shown a good correlation between Penh and other measures of lung function (Dohi et al., 1999; Finotto et al., 2001; Hamelmann et al., 1997), while others suggest Penh does not correlate well with morphometric changes in mice (Lundblad et al., 2002; Petak et al., 2001). Penh, is not derived from first physical principles but rather is an empirical derivative of the variations in chamber

pressure. This makes it a less reliable read-out of lung mechanics. During induced bronchoconstriction, Penh can also change without real airway obstruction or dilation occurring (Drazen et al., 1999). Therefore, ideally, Penh should be used as an initial indicator of lung mechanics but should be followed up by use of a more invasive approach that enables more reliable measurement of lung mechanics.

One such approach is to measure dynamic lung resistance (RL) (airway resistance is the opposition to flow) and compliance (CL) (the ability of the lungs to stretch as a result of change in pulmonary volume relative to an applied change in pressure) (Irvin and Bates, 2003). Determination of RL and CL involves the measurement of flow and pressure, which can be done using a restrained plethysmograph chamber. Pressure can be measured with an external transducer or a telemetry implant. Studies can be performed on spontaneously breathing, and on conscious subjects using an implanted pressure sensor. Thus making this a halfway point: animals can be conscious but are restrained, therefore experience elevated levels of stress compared to the unrestrained system but the measurements recorded are far more accurate. An increase in RL suggests narrowing of the conducting airways and alterations in the lung periphery (heterogeneous narrowing or closure of distal airways together with changes in the intrinsic mechanical properties of the parenchyma). A decrease in CL will only reflect events occurring in the periphery of the lung, particularly airway closure (Bates and Irvin, 2002). Administration of bronchoconstrictors can also be used to challenge mice, therefore this is technique is often used to confirm Penh results.

At the other end of the phenotyping uncertainty principle is 'controlling everything', this ensures the greatest degree of accuracy and specificity of *in vivo* lung function measurements. Here, breathing frequency, tidal volume, mean lung volume

and volume history are all under control, and the influence of the upper airways (the nose and mouth) has been. The disadvantages of this technique however is that it requires both surgical and pharmacological stresses to the animal that can themselves affect lung mechanics, through release of mediators such as catecholamines and the modulation of neural responses. An example of this is the forced oscillation technique (FOT) which requires animals to be anesthetized and paralyzed. Mice are tracheostomised to bypass the uppermost airways (the nose and mouth) and mechanical ventilation allows the control of breathing frequency, tidal volume and volume history. This technique measures the complex input impedance (Z) of the lungs. This is directly related to the resistance of the lungs at a specific frequency. FOT such as the commonly used flexivent system, therefore allows both RL and CL to be measured but with more accuracy, since it measures these factors at each frequency contained in the flow signal applied to the lungs (e.g a computer controlled piston that modulates the flow of air into the lungs (Shalaby et al., 2010; Tomioka et al., 2002).

In conclusion, the use of the whole body plethysmograph and determination of Penh in *Lp* mice was a suitable method to initially investigate lung function in *Vangl2*$^{Lp/+}$ heterozygous mice. It allowed rapid analysis of a cohort of mice within a short time frame. The increase in Penh at baseline is a very interesting finding particularly when taken together with the histological and BALF data. Future studies will be undertaken to confirm any functional defects using the flexivent FOT system. This analysis will provide us with an in depth understating of lung function and mechanics in *Vangl2*$^{Lp/+}$ mutant mice.

6 Discussion

6.1 Overall findings of this study

The overall aim of this thesis was to determine the role of the PCP pathway in branching morphogenesis. To do this, analysis of mouse mutants that contain loss of function mutations in three core PCP genes Celsr1, Vangl2 and Scribble was carried out primarily in the lung. The results presented in this thesis describe Celsr1, Vangl2 and Scribble are all required for normal lung branching morphogenesis such that they operate via rho kinase signalling to modulate cytoskeletal dynamics crucial for the formation and growth of new branches. In addition Vangl2 is required for kidney tubule formation and glomeruli maturation. Vangl2 heterozygotes show a reduction in the number of glomeruli, but no overt functional defects under normal conditions. However these defects may predispose individuals when exposed to environmental factors to kidney disorders later in life.

A single point mutation in the A/B and PCP component Scribble revealed defects in lung branching that are more severe than those observed in *Vangl2*$^{Lp/Lp}$ and *Celsr1*$^{Crsh/Crsh}$ mouse mutants. Scribble also operates via rho kinase signalling to modulate cytoskeletal dynamics required for the formation of new branches. In addition tight junction and adherens junctions appeared disrupted and lumen formation was subsequently impaired in mutant lungs. Interestingly, assessment of apical basal polarity reveals it to be largely unaffected in *Scribble*$^{Crc/Crc}$ lungs

suggesting that while Scribble can function in both the A/B and PCP pathways, in the lung it appears to operate primarily via the PCP pathway and is shown to be required for the correct localisation of both Celsr1 and Vangl2.

Finally, an assessment of *Vangl2*$^{Lp/+}$ mice revealed that loss of a single copy of Vangl2 is enough to cause defects in embryonic lung development that persist into adult life, potentially affecting lung function.

6.2 Future work

This project has identified a new molecular pathway that is required for branching morphogenesis, a crucial process essential for the correct formation of many branched organs including the lung and kidney. Thus providing many different and interesting avenues to continue this project further.

6.2.1 Embryonic analysis

6.2.1.1 Real-time confocal imaging

Real-time confocal imaging could be used to further understand the roles of Celsr1, Vangl2 and Scribble in embryonic lung branching morphogenesis. This will enable detailed information at the cellular level to be collected that will give more insight into the function of these three proteins within the lung. By intecrossing heterozygous PCP mouse mutants with a novel transgenic line (memb-TdTomato/H2B-GFP (Tg)) which carries a red fluorescent reporter linked to a membrane protein and a green fluorescent reporter linked to histone H2B in the nucleus (memb-TdTomato/H2B-GFP (Tg)) will enable visualisation of both the plasma membranes and nuclei of cells, in time-lapse studies of *ex-vivo* lung cultures to follow individual cell movements during development. It will allow us to follow both the cellular mechanisms of branching morphogenesis, how individual cells move with

respect to each other as well as their orientation. This may even give insight into whether convergent extension, which involves the polarized rearrangement of cells within a single cell type (e.g. epithelia), such that cell intercalation results in elongated growth by narrowing and lengthening of the tissue along perpendicular axes, occurs in the lung. This process, mediated by the PCP pathway, is critical for gastrulation movements in *Xenopus* and *Zebrafish* and for neural tube closure in mouse (Jones and Chen, 2007). The lungs of *Crsh/Crsh*, *Lp/Lp* and *Crc/Crc* mice both *in vivo* and *ex vivo* appear broader and shorter suggesting convergent extension may play a role in normal branching of the lung and an absence of these PCP genes may affect this process. As these genes occupy seperate spatial domains within the lung and appear to have divergent functions, this experiment will also allow us to determine if differences in cellular behaviour contribute to the phenotypic differences, by direct comparison of each heterozygote mouse mutant crossed to Tg, in comparison to wildtype controls.

6.2.1.2 Recombination cultures

Branching morphogenesis relies on reciprocal interactions between the epithelium and mesenchyme (Shah et al., 2004; Warburton et al., 2000). Celsr1, Vangl2 and Scribble whilst predominantly expressed in the epithelium, is expressed at a lower level in the lung mesenchyme. To assess whether one or both cell types contribute to the phenotype in lung epithelium, lung recombination cultures, a methodology used extensively to study branching systems (Lin et al., 2001; Shannon, 1994) could be carried out. E11.5 lung endoderm denuded of mesenchyme from *Lp*/*Lp*, will be cultured in matrigel and recombined with wildtype mesenchyme. If only endoderm contributes to the phenotype, defects will be observed in branching with this

combination of tissues. If only mesenchyme contributes, endoderm branching will be normal but disrupted when the reverse experiment; recombining mutant mesenchyme with wildtype endoderm, is carried out. If both tissues contribute, defects will be present in both combinations.

6.2.1.3 Does the PCP pathway operate via JNK signalling in branched organs?

The results presented in this thesis describe Celsr1, Vangl2 and Scribble are likely to operate via rho kinase mediated organisation of the cytoskeleton. However studies have shown that the JNK pathway functions downstream of Dishevelled to mediate the PCP pathway in *Drosophila (Boutros et al., 1998).* In addition, studies in *Xenopus* have shown Wnt5a can activate JNK and the JNK pathway can mediate the action of Wnt5a to regulate convergent extension movements (Yamanaka et al., 2002). Therefore an important next experiment would be to determine if Celsr1, Vangl2 and Scribble operate only via Rho kinase signaling or can also operate via JNK signaling in branched organs.

6.2.1.4 Simultaneous knockdown of Vangl1/2 or Celsr1/2/3

Only one Scribble gene exists in mammals whereas there are three Celsr genes Celsr1, Celsr2 and Celsr3 and two Vangl genes, Vangl1 and Vangl2. *Scribble*$^{Crc/Crc}$ lungs display the most severest phenotype compared with *Celsr1*$^{Crsh/Crsh}$ and *Vangl2*$^{Lp/Lp}$. This maybe as a result of compensation from Vangl2 in *Lp/Lp* and Celsr2 and/or Celsr3 in *Crsh/Crsh*. It would be interesting therefore to simultaneously knockdown Vangl1/2 and all three Celsr genes to determine if the overall lung phenotype becomes more severe and whether compensation does exist for these genes.

6.2.1.5 Investigation of other branched organs in Crsh/Crsh and Crc/Crc embryos

It is clear from the evidence presented in chapeter 3, that loss of either Celsr1, Vangl2 or Scribble results in disrupted kidney, salivary gland and lacrimal gland branching morphogenesis. Organs from all three homozygous mouse mutants display an altered morphology and have a reduction in the number of epithelial branches or tubules. In addition it has been shown Vangl2 is required for kidney tubule formation and glomeruli maturation (Chapter 3 and (Yates et al., 2010a). Therefore it would be interesting to determine the role of both Celsr1 and Scribble in kidney, salivary and lacrimal branching, and to determine if like in the lung they have differing spatial expression patterns or have overlapping expression patterns that may potentially impact on their function both embryonically and postnatally.

6.2.2 Adult analysis

Homozygous Celsr1, Vangl2 and Scribble mouse mutants are all embryonically lethal, making an assessment of adult lung function impossible. Preliminary data suggests an intrinsic defect in *Vangl2*$^{Lp/+}$ lung function (Chapter 5). The recent availability of conditional mouse mutants for all three PCP genes will allow a complete analysis of the adult histological and functional defects that may arise in adult homozygous mutants for Celsr1, Vangl2 and Scribble. In a similar manner to which the *Vangl2*$^{Lp/+}$ mice were tested for lung functional defects, conditional knockdown of Celsr1, Vangl2 and Scribble in the lung followed by an initial determination of Penh after exposure to increasing doses of the bronchoconstrictor methacholine could be carried out. If in a similar manner to *Vangl2*$^{Lp/+}$ heterozygotes mice, an indication of lung function defects can be observed, a more in depth and sensitive analysis could be carried out

to determine if these genes have a functional role in lung mechanics during adulthood, by use of the forced oscillitation technique (described in section 5.3.3).
In addition further in depth analysis of the functional defects observed in *Vangl2*$^{Lp/+}$ mice would more definitively confirm whether loss of one copy of Vangl2 is enough to result in lung function abnormalities. Finally assessment of the heterozygote lung phenotype of both Scribble and Celsr1 mouse mutants will also determine if these genes have a functional role in adult lung mechanics. Heterozygosity for mutations in all three genes may be an important mechanism for congenital lung defects and adult lung disease in humans.

6.3 Conclusion

Extensive work has shown the PCP pathway to regulate the establishment of polarity within the plane of an epithelium and to control convergent extension and neural tube closure in vertebrates (Kibar et al., 2007; Montcouquiol et al., 2006; Torban et al., 2007; Ybot-Gonzalez et al., 2007). In addition to regulating the patterning of external epidermal structures such as wing hair cells in *Drosophila* (Adler, 2002), the PCP pathway is more widely utilised for modifying cellular direction and movement (Barrow, 2006; Jenny and Mlodzik, 2006; Seifert and Mlodzik, 2007). The end result of this pathway is polarisation of the cytoskeleton, which, in turn drives cellular morphogenesis and/or morphogenetic movement such as convergent extension.

Recent studies are now identifying new and more complex roles for this pathway such as mediating the directed movement of groups of cells, it is required for female reproductive tract development (Vandenberg and Sassoon, 2009), normal heart development (Henderson et al., 2006; Phillips et al., 2007a) and kidney tubule formation (Karner et al., 2009). This thesis has highlighted a role for three

components of the PCP pathway Celsr1, Vangl2 and Scribble to be required for branching morphogenesis. A more indepth analysis of all three genes in the lung and Vangl2 in the kidney has provided more insight into the developmental mechanisms that drive both lung and kidney branching, that will also enhance our understanding of both congenital and adult diseases that affect all branched organs, potentially leading to novel therapeutic strategies in the future.

7 References

Abraham, E. (2003). Neutrophils and acute lung injury. Crit Care Med *31*, S195-199.

Adler, P.N. (2002). Planar signaling and morphogenesis in Drosophila. Dev Cell *2*, 525-535.

Affolter, M., and Zeller, R. (2009). From cells to organs: new insight into organ morphogenesis. Curr Opin Genet Dev *19*, 421-423.

Affolter, M., Zeller, R., and Caussinus, E. (2009). Tissue remodelling through branching morphogenesis. Nat Rev Mol Cell Biol *10*, 831-842.

Albertson, R., Chabu, C., Sheehan, A., and Doe, C.Q. (2004). Scribble protein domain mapping reveals a multistep localization mechanism and domains necessary for establishing cortical polarity. J Cell Sci *117*, 6061-6070.

Andrew, D.J., and Ewald, A.J. (2009). Morphogenesis of epithelial tubes: Insights into tube formation, elongation, and elaboration. Dev Biol.

Andrew, D.J., and Ewald, A.J. (2010). Morphogenesis of epithelial tubes: Insights into tube formation, elongation, and elaboration. Dev Biol *341*, 34-55.

Asanuma, K., Kim, K., Oh, J., Giardino, L., Chabanis, S., Faul, C., Reiser, J., and Mundel, P. (2005). Synaptopodin regulates the actin-bundling activity of alpha-actinin in an isoform-specific manner. J Clin Invest *115*, 1188-1198.

Asanuma, K., Yanagida-Asanuma, E., Faul, C., Tomino, Y., Kim, K., and Mundel, P. (2006). Synaptopodin orchestrates actin organization and cell motility via regulation of RhoA signalling. Nat Cell Biol *8*, 485-491.

Ashworth, S.L., Sandoval, R.M., Hosford, M., Bamburg, J.R., and Molitoris, B.A. (2001). Ischemic injury induces ADF relocalization to the apical domain of rat proximal tubule cells. Am J Physiol Renal Physiol *280*, F886-894.

Ashworth, S.L., Southgate, E.L., Sandoval, R.M., Meberg, P.J., Bamburg, J.R., and Molitoris, B.A. (2003). ADF/cofilin mediates actin cytoskeletal alterations in LLC-PK cells during ATP depletion. Am J Physiol Renal Physiol *284*, F852-862.

Assemat, E., Bazellieres, E., Pallesi-Pocachard, E., Le Bivic, A., and Massey-Harroche, D. (2008). Polarity complex proteins. Biochim Biophys Acta *1778*, 614-630.

Atwood, S.X., Chabu, C., Penkert, R.R., Doe, C.Q., and Prehoda, K.E. (2007). Cdc42 acts downstream of Bazooka to regulate neuroblast polarity through Par-6 aPKC. J Cell Sci *120*, 3200-3206.

Axelrod, J.D. (2001). Unipolar membrane association of Dishevelled mediates Frizzled planar cell polarity signaling. Genes Dev *15*, 1182-1187.

Axelrod, J.D. (2009). Progress and challenges in understanding planar cell polarity signaling. Semin Cell Dev Biol *20*, 964-971.

Babayeva, S., Zilber, Y., and Torban, E. (2010). Planar cell polarity pathway regulates actin rearrangement,cell shape, motility and nephrin distribution in podocytes. Am J Physiol Renal Physiol.

Bacallao, R.L., and McNeill, H. (2009). Cystic kidney diseases and planar cell polarity signaling. Clin Genet *75*, 107-117.

Baena-Lopez, L.A., Baonza, A., and Garcia-Bellido, A. (2005). The orientation of cell divisions determines the shape of Drosophila organs. Curr Biol *15*, 1640-1644.

Bagnat, M., Cheung, I.D., Mostov, K.E., and Stainier, D.Y. (2007). Genetic control of single lumen formation in the zebrafish gut. Nat Cell Biol *9*, 954-960.

Barrett, K., Leptin, M., and Settleman, J. (1997). The Rho GTPase and a putative RhoGEF mediate a signaling pathway for the cell shape changes in Drosophila gastrulation. Cell *91*, 905-915.

Barrow, J.R. (2006). Wnt/PCP signaling: a veritable polar star in establishing patterns of polarity in embryonic tissues. Semin Cell Dev Biol *17*, 185-193.

Bastock, R., and Strutt, D. (2007). The planar polarity pathway promotes coordinated cell migration during Drosophila oogenesis. Development *134*, 3055-3064.

Bastock, R., Strutt, H., and Strutt, D. (2003). Strabismus is asymmetrically localised and binds to Prickle and Dishevelled during Drosophila planar polarity patterning. Development *130*, 3007-3014.

Bates, C.M. (2007). Role of fibroblast growth factor receptor signaling in kidney development. Pediatr Nephrol *22*, 343-349.

Bates, J.H., and Irvin, C.G. (2002). Time dependence of recruitment and derecruitment in the lung: a theoretical model. J Appl Physiol *93*, 705-713.

Bates, J.H., and Irvin, C.G. (2003). Measuring lung function in mice: the phenotyping uncertainty principle. J Appl Physiol *94*, 1297-1306.

Behr, M., Riedel, D., and Schuh, R. (2003). The claudin-like megatrachea is essential in septate junctions for the epithelial barrier function in Drosophila. Dev Cell *5*, 611-620.

Bellaiche, Y., Gho, M., Kaltschmidt, J.A., Brand, A.H., and Schweisguth, F. (2001). Frizzled regulates localization of cell-fate determinants and mitotic spindle rotation during asymmetric cell division. Nat Cell Biol *3*, 50-57.

Bellusci, S., Grindley, J., Emoto, H., Itoh, N., and Hogan, B.L. (1997). Fibroblast growth factor 10 (FGF10) and branching morphogenesis in the embryonic mouse lung. Development *124*, 4867-4878.

Betschinger, J., Eisenhaber, F., and Knoblich, J.A. (2005). Phosphorylation-induced autoinhibition regulates the cytoskeletal protein Lethal (2) giant larvae. Curr Biol *15*, 276-282.

Bilder, D., Li, M., and Perrimon, N. (2000). Cooperative regulation of cell polarity and growth by Drosophila tumor suppressors. Science *289*, 113-116.

Bilder, D., and Perrimon, N. (2000). Localization of apical epithelial determinants by the basolateral PDZ protein Scribble. Nature *403*, 676-680.

Bilder, D., Schober, M., and Perrimon, N. (2003). Integrated activity of PDZ protein complexes regulates epithelial polarity. Nat Cell Biol *5*, 53-58.

Blum, Y., Belting, H.G., Ellertsdottir, E., Herwig, L., Luders, F., and Affolter, M. (2008). Complex cell rearrangements during intersegmental vessel sprouting and vessel fusion in the zebrafish embryo. Dev Biol *316*, 312-322.

Bourbon, J.R., Boucherat, O., Boczkowski, J., Crestani, B., and Delacourt, C. (2009). Bronchopulmonary dysplasia and emphysema: in search of common therapeutic targets. Trends Mol Med *15*, 169-179.

Boute, N., Gribouval, O., Roselli, S., Benessy, F., Lee, H., Fuchshuber, A., Dahan, K., Gubler, M.C., Niaudet, P., and Antignac, C. (2000). NPHS2, encoding the glomerular protein podocin, is mutated in autosomal recessive steroid-resistant nephrotic syndrome. Nat Genet *24*, 349-354.

Boutros, M., Paricio, N., Strutt, D.I., and Mlodzik, M. (1998). Dishevelled activates JNK and discriminates between JNK pathways in planar polarity and wingless signaling. Cell *94*, 109-118.

Brumby, A.M., and Richardson, H.E. (2003). scribble mutants cooperate with oncogenic Ras or Notch to cause neoplastic overgrowth in Drosophila. EMBO J *22*, 5769-5779.

Bryant, P.J., and Huwe, A. (2000). LAP proteins: what's up with epithelia? Nat Cell Biol *2*, E141-143.

Buechner, M. (2002). Tubes and the single C. elegans excretory cell. Trends Cell Biol *12*, 479-484.

Caruana, G., Young, R.J., and Bertram, J.F. (2006). Imaging the embryonic kidney. Nephron Exp Nephrol *103*, e62-68.

Casal, J., Lawrence, P.A., and Struhl, G. (2006). Two separate molecular systems, Dachsous/Fat and Starry night/Frizzled, act independently to confer planar cell polarity. Development *133*, 4561-4572.

Casal, J., Struhl, G., and Lawrence, P.A. (2002). Developmental compartments and planar polarity in Drosophila. Curr Biol *12*, 1189-1198.

Chae, J., Kim, M.J., Goo, J.H., Collier, S., Gubb, D., Charlton, J., Adler, P.N., and Park, W.J. (1999). The Drosophila tissue polarity gene starry night encodes a member of the protocadherin family. Development *126*, 5421-5429.

Chaffer, C.L., Thompson, E.W., and Williams, E.D. (2007). Mesenchymal to epithelial transition in development and disease. Cells Tissues Organs *185*, 7-19.

Chapman, H.A. (2004). Disorders of lung matrix remodeling. J Clin Invest *113*, 148-157.

Chen, W.S., Antic, D., Matis, M., Logan, C.Y., Povelones, M., Anderson, G.A., Nusse, R., and Axelrod, J.D. (2008). Asymmetric homotypic interactions of the atypical cadherin flamingo mediate intercellular polarity signaling. Cell *133*, 1093-1105.

Chen, X., and Macara, I.G. (2005). Par-3 controls tight junction assembly through the Rac exchange factor Tiam1. Nat Cell Biol *7*, 262-269.

Cheng, H.T., Kim, M., Valerius, M.T., Surendran, K., Schuster-Gossler, K., Gossler, A., McMahon, A.P., and Kopan, R. (2007). Notch2, but not Notch1, is required for proximal fate acquisition in the mammalian nephron. Development *134*, 801-811.

Chi, X., Michos, O., Shakya, R., Riccio, P., Enomoto, H., Licht, J.D., Asai, N., Takahashi, M., Ohgami, N., Kato, M.*, et al.* (2009). Ret-dependent cell rearrangements in the Wolffian duct epithelium initiate ureteric bud morphogenesis. Dev Cell *17*, 199-209.

Chong, B.T., Agrawal, D.K., Romero, F.A., and Townley, R.G. (1998). Measurement of bronchoconstriction using whole-body plethysmograph: comparison of freely moving versus restrained guinea pigs. J Pharmacol Toxicol Methods *39*, 163-168.

Chung, S., and Andrew, D.J. (2008). The formation of epithelial tubes. J Cell Sci *121*, 3501-3504.

Copp, A.J., Greene, N.D., and Murdoch, J.N. (2003). Dishevelled: linking convergent extension with neural tube closure. Trends Neurosci *26*, 453-455.

Corbit, K.C., Aanstad, P., Singla, V., Norman, A.R., Stainier, D.Y., and Reiter, J.F. (2005). Vertebrate Smoothened functions at the primary cilium. Nature *437*, 1018-1021.

Cordenonsi, M., D'Atri, F., Hammar, E., Parry, D.A., Kendrick-Jones, J., Shore, D., and Citi, S. (1999). Cingulin contains globular and coiled-coil domains and interacts with ZO-1, ZO-2, ZO-3, and myosin. J Cell Biol *147*, 1569-1582.

Costantini, F. (2006). Renal branching morphogenesis: concepts, questions, and recent advances. Differentiation *74*, 402-421.

Costantini, F., and Kopan, R. (2010). Patterning a complex organ: branching morphogenesis and nephron segmentation in kidney development. Dev Cell *18*, 698-712.

Courbard, J.R., Djiane, A., Wu, J., and Mlodzik, M. (2009). The apical/basal-polarity determinant Scribble cooperates with the PCP core factor Stbm/Vang and functions as one of its effectors. Dev Biol *333*, 67-77.

Crompton, L.A., Du Roure, C., and Rodriguez, T.A. (2007). Early embryonic expression patterns of the mouse Flamingo and Prickle orthologues. Dev Dyn *236*, 3137-3143.

Cullen-McEwen, L.A., Kett, M.M., Dowling, J., Anderson, W.P., and Bertram, J.F. (2003). Nephron number, renal function, and arterial pressure in aged GDNF heterozygous mice. Hypertension *41*, 335-340.

Curtin, J.A., Quint, E., Tsipouri, V., Arkell, R.M., Cattanach, B., Copp, A.J., Henderson, D.J., Spurr, N., Stanier, P., Fisher, E.M*., et al.* (2003). Mutation of Celsr1 disrupts planar polarity of inner ear hair cells and causes severe neural tube defects in the mouse. Curr Biol *13*, 1129-1133.

Das, G., Jenny, A., Klein, T.J., Eaton, S., and Mlodzik, M. (2004). Diego interacts with Prickle and Strabismus/Van Gogh to localize planar cell polarity complexes. Development *131*, 4467-4476.

Davies, A., Formstone, C., Mason, I., and Lewis, J. (2005). Planar polarity of hair cells in the chick inner ear is correlated with polarized distribution of c-flamingo-1 protein. Dev Dyn *233*, 998-1005.

Davis, C.G. (1990). The many faces of epidermal growth factor repeats. New Biol *2*, 410-419.

Dawes-Hoang, R.E., Parmar, K.M., Christiansen, A.E., Phelps, C.B., Brand, A.H., and Wieschaus, E.F. (2005). folded gastrulation, cell shape change and the control of myosin localization. Development *132*, 4165-4178.

De Langhe, S.P., Sala, F.G., Del Moral, P.M., Fairbanks, T.J., Yamada, K.M., Warburton, D., Burns, R.C., and Bellusci, S. (2005). Dickkopf-1 (DKK1) reveals that fibronectin is a major target of Wnt signaling in branching morphogenesis of the mouse embryonic lung. Dev Biol *277*, 316-331.

De Moerlooze, L., Spencer-Dene, B., Revest, J.M., Hajihosseini, M., Rosewell, I., and Dickson, C. (2000). An important role for the IIIb isoform of fibroblast growth factor receptor 2 (FGFR2) in mesenchymal-epithelial signalling during mouse organogenesis. Development *127*, 483-492.

Dean, C.H., Miller, L.A., Smith, A.N., Dufort, D., Lang, R.A., and Niswander, L.A. (2005). Canonical Wnt signaling negatively regulates branching morphogenesis of the lung and lacrimal gland. Dev Biol *286*, 270-286.

Debnath, J., Mills, K.R., Collins, N.L., Reginato, M.J., Muthuswamy, S.K., and Brugge, J.S. (2002). The role of apoptosis in creating and maintaining luminal space within normal and oncogene-expressing mammary acini. Cell *111*, 29-40.

DeLorme, M.P., and Moss, O.R. (2002). Pulmonary function assessment by whole-body plethysmography in restrained versus unrestrained mice. J Pharmacol Toxicol Methods *47*, 1-10.

deMello, D.E., Sawyer, D., Galvin, N., and Reid, L.M. (1997). Early fetal development of lung vasculature. Am J Respir Cell Mol Biol *16*, 568-581.

Devenport, D., and Fuchs, E. (2008). Planar polarization in embryonic epidermis orchestrates global asymmetric morphogenesis of hair follicles. Nat Cell Biol *10*, 1257-1268.

Di Paolo, G., and De Camilli, P. (2006). Phosphoinositides in cell regulation and membrane dynamics. Nature *443*, 651-657.

Djiane, A., Riou, J., Umbhauer, M., Boucaut, J., and Shi, D. (2000). Role of frizzled 7 in the regulation of convergent extension movements during gastrulation in Xenopus laevis. Development *127*, 3091-3100.

Djiane, A., Yogev, S., and Mlodzik, M. (2005). The apical determinants aPKC and dPatj regulate Frizzled-dependent planar cell polarity in the Drosophila eye. Cell *121*, 621-631.

Dohi, M., Tsukamoto, S., Nagahori, T., Shinagawa, K., Saitoh, K., Tanaka, Y., Kobayashi, S., Tanaka, R., To, Y., and Yamamoto, K. (1999). Noninvasive system for evaluating the allergen-specific airway response in a murine model of asthma. Lab Invest *79*, 1559-1571.

Dow, L.E., Brumby, A.M., Muratore, R., Coombe, M.L., Sedelies, K.A., Trapani, J.A., Russell, S.M., Richardson, H.E., and Humbert, P.O. (2003). hScrib is a functional homologue of the Drosophila tumour suppressor Scribble. Oncogene *22*, 9225-9230.

Dow, L.E., Kauffman, J.S., Caddy, J., Zarbalis, K., Peterson, A.S., Jane, S.M., Russell, S.M., and Humbert, P.O. (2007). The tumour-suppressor Scribble dictates cell polarity during directed epithelial migration: regulation of Rho GTPase recruitment to the leading edge. Oncogene *26*, 2272-2282.

Drazen, J.M., Finn, P.W., and De Sanctis, G.T. (1999). Mouse models of airway responsiveness: physiological basis of observed outcomes and analysis of selected examples using these outcome indicators. Annu Rev Physiol *61*, 593-625.

Dressler, G.R. (2009). Advances in early kidney specification, development and patterning. Development *136*, 3863-3874.

Drorbaugh, J.E., and Fenn, W.O. (1955). A barometric method for measuring ventilation in newborn infants. Pediatrics *16*, 81-87.

Duan, D., Yue, Y., Zhou, W., Labed, B., Ritchie, T.C., Grosschedl, R., and Engelhardt, J.F. (1999). Submucosal gland development in the airway is controlled by lymphoid enhancer binding factor 1 (LEF1). Development *126*, 4441-4453.

Etienne-Manneville, S., and Hall, A. (2002). Rho GTPases in cell biology. Nature *420*, 629-635.

Fanto, M., Clayton, L., Meredith, J., Hardiman, K., Charroux, B., Kerridge, S., and McNeill, H. (2003). The tumor-suppressor and cell adhesion molecule Fat controls planar polarity via physical interactions with Atrophin, a transcriptional co-repressor. Development *130*, 763-774.

Fanto, M., Weber, U., Strutt, D.I., and Mlodzik, M. (2000). Nuclear signaling by Rac and Rho GTPases is required in the establishment of epithelial planar polarity in the Drosophila eye. Curr Biol *10*, 979-988.

Farquhar, M.G., and Palade, G.E. (1963). Junctional complexes in various epithelia. J Cell Biol *17*, 375-412.

Faul, C., Asanuma, K., Yanagida-Asanuma, E., Kim, K., and Mundel, P. (2007). Actin up: regulation of podocyte structure and function by components of the actin cytoskeleton. Trends Cell Biol *17*, 428-437.

Feiguin, F., Hannus, M., Mlodzik, M., and Eaton, S. (2001). The ankyrin repeat protein Diego mediates Frizzled-dependent planar polarization. Dev Cell *1*, 93-101.

Ferrante, M.I., Romio, L., Castro, S., Collins, J.E., Goulding, D.A., Stemple, D.L., Woolf, A.S., and Wilson, S.W. (2009). Convergent extension movements and ciliary function are mediated by ofd1, a zebrafish orthologue of the human oral-facial-digital type 1 syndrome gene. Hum Mol Genet *18*, 289-303.

Finotto, S., De Sanctis, G.T., Lehr, H.A., Herz, U., Buerke, M., Schipp, M., Bartsch, B., Atreya, R., Schmitt, E., Galle, P.R., *et al.* (2001). Treatment of allergic airway inflammation and hyperresponsiveness by antisense-induced local blockade of GATA-3 expression. J Exp Med *193*, 1247-1260.

Fischer, E., Legue, E., Doyen, A., Nato, F., Nicolas, J.F., Torres, V., Yaniv, M., and Pontoglio, M. (2006). Defective planar cell polarity in polycystic kidney disease. Nat Genet *38*, 21-23.

Formstone, C.J., and Little, P.F. (2001). The flamingo-related mouse Celsr family (Celsr1-3) genes exhibit distinct patterns of expression during embryonic development. Mech Dev *109*, 91-94.

Formstone, C.J., Moxon, C., Murdoch, J., Little, P., and Mason, I. (2010a). Basal enrichment within neuroepithelia suggests novel function(s) for Celsr1 protein. Mol Cell Neurosci *44*, 210-222.

Formstone, C.J., Moxon, C., Murdoch, J., Little, P., and Mason, I. (2010b). Basal enrichment within neuroepithelia suggests novel function(s) for Celsr1 protein. Mol Cell Neurosci *44*, 210-222.

Garoia, F., Guerra, D., Pezzoli, M.C., Lopez-Varea, A., Cavicchi, S., and Garcia-Bellido, A. (2000). Cell behaviour of Drosophila fat cadherin mutations in wing development. Mech Dev *94*, 95-109.

Gassama-Diagne, A., Yu, W., ter Beest, M., Martin-Belmonte, F., Kierbel, A., Engel, J., and Mostov, K. (2006). Phosphatidylinositol-3,4,5-trisphosphate regulates the formation of the basolateral plasma membrane in epithelial cells. Nat Cell Biol *8*, 963-970.

Gateff, E. (1978). Malignant neoplasms of genetic origin in Drosophila melanogaster. Science *200*, 1448-1459.

Gho, M., and Schweisguth, F. (1998). Frizzled signalling controls orientation of asymmetric sense organ precursor cell divisions in Drosophila. Nature *393*, 178-181.

Goldberg, S., Harvey, S.J., Cunningham, J., Tryggvason, K., and Miner, J.H. (2009). Glomerular filtration is normal in the absence of both agrin and perlecan-heparan sulfate from the glomerular basement membrane. Nephrol Dial Transplant *24*, 2044-2051.

Gontan, C., de Munck, A., Vermeij, M., Grosveld, F., Tibboel, D., and Rottier, R. (2008). Sox2 is important for two crucial processes in lung development: branching morphogenesis and epithelial cell differentiation. Dev Biol *317*, 296-309.

Goto, H., Tomono, Y., Ajiro, K., Kosako, H., Fujita, M., Sakurai, M., Okawa, K., Iwamatsu, A., Okigaki, T., Takahashi, T.*, et al.* (1999). Identification of a novel phosphorylation site on histone H3 coupled with mitotic chromosome condensation. J Biol Chem *274*, 25543-25549.

Goto, K., and Ishikawa, H. (1998). Differential distribution of actin and cytokeratin in isolated full-length rabbit renal tubules. Cell Struct Funct *23*, 73-84.

Goto, T., and Keller, R. (2002). The planar cell polarity gene strabismus regulates convergence and extension and neural fold closure in Xenopus. Dev Biol *247*, 165-181.

Greenough, A. (2009). Does low birth weight confer a lifelong respiratory disadvantage? Am J Respir Crit Care Med *180*, 107-108.

Gubb, D., and Garcia-Bellido, A. (1982). A genetic analysis of the determination of cuticular polarity during development in Drosophila melanogaster. J Embryol Exp Morphol *68*, 37-57.

Guillemin, K., Groppe, J., Ducker, K., Treisman, R., Hafen, E., Affolter, M., and Krasnow, M.A. (1996). The pruned gene encodes the Drosophila serum response factor and regulates cytoplasmic outgrowth during terminal branching of the tracheal system. Development *122*, 1353-1362.

Gumbiner, B., Lowenkopf, T., and Apatira, D. (1991). Identification of a 160-kDa polypeptide that binds to the tight junction protein ZO-1. Proc Natl Acad Sci U S A *88*, 3460-3464.

Gumbiner, B.M. (2000). Regulation of cadherin adhesive activity. J Cell Biol *148*, 399-404.

Gumbiner, B.M. (2005). Regulation of cadherin-mediated adhesion in morphogenesis. Nat Rev Mol Cell Biol *6*, 622-634.

Guo, J.K., Menke, A.L., Gubler, M.C., Clarke, A.R., Harrison, D., Hammes, A., Hastie, N.D., and Schedl, A. (2002). WT1 is a key regulator of podocyte function: reduced expression levels cause crescentic glomerulonephritis and mesangial sclerosis. Hum Mol Genet *11*, 651-659.

Guo, N., Hawkins, C., and Nathans, J. (2004). Frizzled6 controls hair patterning in mice. Proc Natl Acad Sci U S A *101*, 9277-9281.

Habas, R., Kato, Y., and He, X. (2001). Wnt/Frizzled activation of Rho regulates vertebrate gastrulation and requires a novel Formin homology protein Daam1. Cell *107*, 843-854.

Hacker, U., and Perrimon, N. (1998). DRhoGEF2 encodes a member of the Dbl family of oncogenes and controls cell shape changes during gastrulation in Drosophila. Genes Dev *12*, 274-284.

Haigo, S.L., Hildebrand, J.D., Harland, R.M., and Wallingford, J.B. (2003). Shroom induces apical constriction and is required for hingepoint formation during neural tube closure. Curr Biol *13*, 2125-2137.

Hall, A. (1998). Rho GTPases and the actin cytoskeleton. Science *279*, 509-514.

Hamelmann, E., Schwarze, J., Takeda, K., Oshiba, A., Larsen, G.L., Irvin, C.G., and Gelfand, E.W. (1997). Noninvasive measurement of airway responsiveness in allergic mice using barometric plethysmography. Am J Respir Crit Care Med *156*, 766-775.

Haraldsson, B., Nystrom, J., and Deen, W.M. (2008). Properties of the glomerular barrier and mechanisms of proteinuria. Physiol Rev *88*, 451-487.

Harvey, S.J., Jarad, G., Cunningham, J., Rops, A.L., van der Vlag, J., Berden, J.H., Moeller, M.J., Holzman, L.B., Burgess, R.W., and Miner, J.H. (2007). Disruption of glomerular basement membrane charge through podocyte-specific mutation of agrin does not alter glomerular permselectivity. Am J Pathol *171*, 139-152.

Heisenberg, C.P., Tada, M., Rauch, G.J., Saude, L., Concha, M.L., Geisler, R., Stemple, D.L., Smith, J.C., and Wilson, S.W. (2000). Silberblick/Wnt11 mediates convergent extension movements during zebrafish gastrulation. Nature *405*, 76-81.

Henderson, D.J., Phillips, H.M., and Chaudhry, B. (2006). Vang-like 2 and noncanonical Wnt signaling in outflow tract development. Trends Cardiovasc Med *16*, 38-45.

Hikasa, H., Shibata, M., Hiratani, I., and Taira, M. (2002). The Xenopus receptor tyrosine kinase Xror2 modulates morphogenetic movements of the axial mesoderm and neuroectoderm via Wnt signaling. Development *129*, 5227-5239.

Hildebrand, J.D. (2005). Shroom regulates epithelial cell shape via the apical positioning of an actomyosin network. J Cell Sci *118*, 5191-5203.

Hinkes, B., Wiggins, R.C., Gbadegesin, R., Vlangos, C.N., Seelow, D., Nurnberg, G., Garg, P., Verma, R., Chaib, H., Hoskins, B.E.*, et al.* (2006). Positional cloning uncovers mutations in PLCE1 responsible for a nephrotic syndrome variant that may be reversible. Nat Genet *38*, 1397-1405.

Hogan, B.L., and Kolodziej, P.A. (2002). Organogenesis: molecular mechanisms of tubulogenesis. Nat Rev Genet *3*, 513-523.

Hough, T.A., Nolan, P.M., Tsipouri, V., Toye, A.A., Gray, I.C., Goldsworthy, M., Moir, L., Cox, R.D., Clements, S., Glenister, P.H.*, et al.* (2002). Novel phenotypes identified by plasma biochemical screening in the mouse. Mamm Genome *13*, 595-602.

Humbert, P.O., Dow, L.E., and Russell, S.M. (2006). The Scribble and Par complexes in polarity and migration: friends or foes? Trends Cell Biol *16*, 622-630.

Humbert, P.O., Grzeschik, N.A., Brumby, A.M., Galea, R., Elsum, I., and Richardson, H.E. (2008). Control of tumourigenesis by the Scribble/Dlg/Lgl polarity module. Oncogene *27*, 6888-6907.

Humphreys, R.C., Krajewska, M., Krnacik, S., Jaeger, R., Weiher, H., Krajewski, S., Reed, J.C., and Rosen, J.M. (1996). Apoptosis in the terminal endbud of the murine mammary gland: a mechanism of ductal morphogenesis. Development *122*, 4013-4022.

Hunt, G.M., and Whitaker, R.H. (1987). The pattern of congenital renal anomalies associated with neural-tube defects. Dev Med Child Neurol *29*, 91-95.

Hurd, T.W., Gao, L., Roh, M.H., Macara, I.G., and Margolis, B. (2003). Direct interaction of two polarity complexes implicated in epithelial tight junction assembly. Nat Cell Biol *5*, 137-142.

Hutterer, A., Betschinger, J., Petronczki, M., and Knoblich, J.A. (2004). Sequential roles of Cdc42, Par-6, aPKC, and Lgl in the establishment of epithelial polarity during Drosophila embryogenesis. Dev Cell *6*, 845-854.

Irvin, C.G., and Bates, J.H. (2003). Measuring the lung function in the mouse: the challenge of size. Respir Res *4*, 4.

Ishibe, S., Haydu, J.E., Togawa, A., Marlier, A., and Cantley, L.G. (2006). Cell confluence regulates hepatocyte growth factor-stimulated cell morphogenesis in a beta-catenin-dependent manner. Mol Cell Biol *26*, 9232-9243.

Ishibe, S., Joly, D., Liu, Z.X., and Cantley, L.G. (2004). Paxillin serves as an ERK-regulated scaffold for coordinating FAK and Rac activation in epithelial morphogenesis. Mol Cell *16*, 257-267.

Ishibe, S., Joly, D., Zhu, X., and Cantley, L.G. (2003). Phosphorylation-dependent paxillin-ERK association mediates hepatocyte growth factor-stimulated epithelial morphogenesis. Mol Cell *12*, 1275-1285.

Ishibe, S., Karihaloo, A., Ma, H., Zhang, J., Marlier, A., Mitobe, M., Togawa, A., Schmitt, R., Czyczk, J., Kashgarian, M.*, et al.* (2009). Met and the epidermal growth factor receptor act cooperatively to regulate final nephron number and maintain collecting duct morphology. Development *136*, 337-345.

Itoh, M., Furuse, M., Morita, K., Kubota, K., Saitou, M., and Tsukita, S. (1999). Direct binding of three tight junction-associated MAGUKs, ZO-1, ZO-2, and ZO-3, with the COOH termini of claudins. J Cell Biol *147*, 1351-1363.

Izumi, Y., Hirose, T., Tamai, Y., Hirai, S., Nagashima, Y., Fujimoto, T., Tabuse, Y., Kemphues, K.J., and Ohno, S. (1998). An atypical PKC directly associates and colocalizes at the epithelial tight junction with ASIP, a mammalian homologue of Caenorhabditis elegans polarity protein PAR-3. J Cell Biol *143*, 95-106.

Jancelewicz, T., Nobuhara, K., and Hawgood, S. (2008). Laser microdissection allows detection of abnormal gene expression in cystic adenomatoid malformation of the lung. J Pediatr Surg *43*, 1044-1051.

Jaskoll, T., and Melnick, M. (1999). Submandibular gland morphogenesis: stage-specific expression of TGF-alpha/EGF, IGF, TGF-beta, TNF, and IL-6 signal transduction in normal embryonic mice and the phenotypic effects of TGF-beta2, TGF-beta3, and EGF-r null mutations. Anat Rec *256*, 252-268.

Jenny, A., Darken, R.S., Wilson, P.A., and Mlodzik, M. (2003). Prickle and Strabismus form a functional complex to generate a correct axis during planar cell polarity signaling. EMBO J *22*, 4409-4420.

Jenny, A., and Mlodzik, M. (2006). Planar cell polarity signaling: a common mechanism for cellular polarization. Mt Sinai J Med *73*, 738-750.

Jones, C., and Chen, P. (2007). Planar cell polarity signaling in vertebrates. Bioessays *29*, 120-132.

Jones, C., Roper, V.C., Foucher, I., Qian, D., Banizs, B., Petit, C., Yoder, B.K., and Chen, P. (2008). Ciliary proteins link basal body polarization to planar cell polarity regulation. Nat Genet *40*, 69-77.

Kaartinen, V., Voncken, J.W., Shuler, C., Warburton, D., Bu, D., Heisterkamp, N., and Groffen, J. (1995). Abnormal lung development and cleft palate in mice lacking TGF-beta 3 indicates defects of epithelial-mesenchymal interaction. Nat Genet *11*, 415-421.

Kalabis, J., Rosenberg, I., and Podolsky, D.K. (2006). Vangl1 protein acts as a downstream effector of intestinal trefoil factor (ITF)/TFF3 signaling and regulates wound healing of intestinal epithelium. J Biol Chem *281*, 6434-6441.

Kallay, L.M., McNickle, A., Brennwald, P.J., Hubbard, A.L., and Braiterman, L.T. (2006). Scribble associates with two polarity proteins, Lgl2 and Vangl2, via distinct molecular domains. J Cell Biochem *99*, 647-664.

Kamei, M., Saunders, W.B., Bayless, K.J., Dye, L., Davis, G.E., and Weinstein, B.M. (2006). Endothelial tubes assemble from intracellular vacuoles in vivo. Nature *442*, 453-456.

Kaplan, J.M., Kim, S.H., North, K.N., Rennke, H., Correia, L.A., Tong, H.Q., Mathis, B.J., Rodriguez-Perez, J.C., Allen, P.G., Beggs, A.H.*, et al.* (2000). Mutations in ACTN4, encoding alpha-actinin-4, cause familial focal segmental glomerulosclerosis. Nat Genet *24*, 251-256.

Karihaloo, A., Nickel, C., and Cantley, L.G. (2005). Signals which build a tubule. Nephron Exp Nephrol *100*, e40-45.

Karner, C., Wharton, K.A., Jr., and Carroll, T.J. (2006). Planar cell polarity and vertebrate organogenesis. Semin Cell Dev Biol *17*, 194-203.

Karner, C.M., Chirumamilla, R., Aoki, S., Igarashi, P., Wallingford, J.B., and Carroll, T.J. (2009). Wnt9b signaling regulates planar cell polarity and kidney tubule morphogenesis. Nat Genet *41*, 793-799.

Kauffman, S.L. (1980). Cell proliferation in the mammalian lung. Int Rev Exp Pathol *22*, 131-191.

Keller, G., Zimmer, G., Mall, G., Ritz, E., and Amann, K. (2003). Nephron number in patients with primary hypertension. N Engl J Med *348*, 101-108.

Kestila, M., Lenkkeri, U., Mannikko, M., Lamerdin, J., McCready, P., Putaala, H., Ruotsalainen, V., Morita, T., Nissinen, M., Herva, R.*, et al.* (1998). Positionally cloned gene for a novel glomerular protein--nephrin--is mutated in congenital nephrotic syndrome. Mol Cell *1*, 575-582.

Kibar, Z., Bosoi, C.M., Kooistra, M., Salem, S., Finnell, R.H., De Marco, P., Merello, E., Bassuk, A.G., Capra, V., and Gros, P. (2009). Novel mutations in VANGL1 in neural tube defects. Hum Mutat *30*, E706-715.

Kibar, Z., Capra, V., and Gros, P. (2007). Toward understanding the genetic basis of neural tube defects. Clin Genet *71*, 295-310.

Kibar, Z., Underhill, D.A., Canonne-Hergaux, F., Gauthier, S., Justice, M.J., and Gros, P. (2001a). Identification of a new chemically induced allele (Lp(m1Jus)) at the loop-tail locus: morphology, histology, and genetic mapping. Genomics *72*, 331-337.

Kibar, Z., Vogan, K.J., Groulx, N., Justice, M.J., Underhill, D.A., and Gros, P. (2001b). Ltap, a mammalian homolog of Drosophila Strabismus/Van Gogh, is altered in the mouse neural tube mutant Loop-tail. Nat Genet *28*, 251-255.

Kilian, B., Mansukoski, H., Barbosa, F.C., Ulrich, F., Tada, M., and Heisenberg, C.P. (2003). The role of Ppt/Wnt5 in regulating cell shape and movement during zebrafish gastrulation. Mech Dev *120*, 467-476.

Klein, T.J., and Mlodzik, M. (2005). Planar cell polarization: an emerging model points in the right direction. Annu Rev Cell Dev Biol *21*, 155-176.

Knust, E., and Bossinger, O. (2002). Composition and formation of intercellular junctions in epithelial cells. Science *298*, 1955-1959.

Kobayashi, A., Valerius, M.T., Mugford, J.W., Carroll, T.J., Self, M., Oliver, G., and McMahon, A.P. (2008). Six2 defines and regulates a multipotent self-renewing nephron progenitor population throughout mammalian kidney development. Cell Stem Cell *3*, 169-181.

Kolsch, V., Seher, T., Fernandez-Ballester, G.J., Serrano, L., and Leptin, M. (2007). Control of Drosophila gastrulation by apical localization of adherens junctions and RhoGEF2. Science *315*, 384-386.

Komiya, Y., and Habas, R. (2008). Wnt signal transduction pathways. Organogenesis *4*, 68-75.

Korostylev, A., Worzfeld, T., Deng, S., Friedel, R.H., Swiercz, J.M., Vodrazka, P., Maier, V., Hirschberg, A., Ohoka, Y., Inagaki, S*., et al.* (2008). A functional role for semaphorin 4D/plexin B1 interactions in epithelial branching morphogenesis during organogenesis. Development *135*, 3333-3343.

Lambrecht, B.N. (2006). Alveolar macrophage in the driver's seat. Immunity *24*, 366-368.

Laudy, J.A., and Wladimiroff, J.W. (2000). The fetal lung. 1: Developmental aspects. Ultrasound Obstet Gynecol *16*, 284-290.

Lawrence, P.A., Casal, J., and Struhl, G. (2004). Cell interactions and planar polarity in the abdominal epidermis of Drosophila. Development *131*, 4651-4664.

Legouis, R., Jaulin-Bastard, F., Schott, S., Navarro, C., Borg, J.P., and Labouesse, M. (2003). Basolateral targeting by leucine-rich repeat domains in epithelial cells. EMBO Rep *4*, 1096-1102.

Lei, Y.P., Zhang, T., Li, H., Wu, B.L., Jin, L., and Wang, H.Y. (2010). VANGL2 mutations in human cranial neural-tube defects. N Engl J Med *362*, 2232-2235.

Lemmers, C., Michel, D., Lane-Guermonprez, L., Delgrossi, M.H., Medina, E., Arsanto, J.P., and Le Bivic, A. (2004). CRB3 binds directly to Par6 and regulates the morphogenesis of the tight junctions in mammalian epithelial cells. Mol Biol Cell *15*, 1324-1333.

Lerm, M., Schmidt, G., Goehring, U.M., Schirmer, J., and Aktories, K. (1999). Identification of the region of rho involved in substrate recognition by Escherichia coli cytotoxic necrotizing factor 1 (CNF1). J Biol Chem *274*, 28999-29004.

Li, M., Marhold, J., Gatos, A., Torok, I., and Mechler, B.M. (2001). Differential expression of two scribble isoforms during Drosophila embryogenesis. Mech Dev *108*, 185-190.

Lin, Y., Liu, A., Zhang, S., Ruusunen, T., Kreidberg, J.A., Peltoketo, H., Drummond, I., and Vainio, S. (2001). Induction of ureter branching as a response to Wnt-2b signaling during early kidney organogenesis. Dev Dyn *222*, 26-39.

Litingtung, Y., Lei, L., Westphal, H., and Chiang, C. (1998). Sonic hedgehog is essential to foregut development. Nat Genet *20*, 58-61.

Liu, F., Schaphorst, K.L., Verin, A.D., Jacobs, K., Birukova, A., Day, R.M., Bogatcheva, N., Bottaro, D.P., and Garcia, J.G. (2002). Hepatocyte growth factor enhances endothelial

cell barrier function and cortical cytoskeletal rearrangement: potential role of glycogen synthase kinase-3beta. FASEB J *16*, 950-962.

Lu, X., Borchers, A.G., Jolicoeur, C., Rayburn, H., Baker, J.C., and Tessier-Lavigne, M. (2004). PTK7/CCK-4 is a novel regulator of planar cell polarity in vertebrates. Nature *430*, 93-98.

Lubarsky, B., and Krasnow, M.A. (2003). Tube morphogenesis: making and shaping biological tubes. Cell *112*, 19-28.

Lundblad, L.K., Irvin, C.G., Adler, A., and Bates, J.H. (2002). A reevaluation of the validity of unrestrained plethysmography in mice. J Appl Physiol *93*, 1198-1207.

Ma, D., Yang, C.H., McNeill, H., Simon, M.A., and Axelrod, J.D. (2003). Fidelity in planar cell polarity signalling. Nature *421*, 543-547.

Maddala, R., Reddy, V.N., Epstein, D.L., and Rao, V. (2003). Growth factor induced activation of Rho and Rac GTPases and actin cytoskeletal reorganization in human lens epithelial cells. Mol Vis *9*, 329-336.

Maeda, Y., Dave, V., and Whitsett, J.A. (2007). Transcriptional control of lung morphogenesis. Physiol Rev *87*, 219-244.

Mandell, G.A., Maloney, K., Sherman, N.H., and Filmer, B. (1996). The renal axes in spina bifida: issues of confusion and fusion. Abdom Imaging *21*, 541-545.

Marlow, F., Topczewski, J., Sepich, D., and Solnica-Krezel, L. (2002). Zebrafish Rho kinase 2 acts downstream of Wnt11 to mediate cell polarity and effective convergence and extension movements. Curr Biol *12*, 876-884.

Marose, T.D., Merkel, C.E., McMahon, A.P., and Carroll, T.J. (2008). Beta-catenin is necessary to keep cells of ureteric bud/Wolffian duct epithelium in a precursor state. Dev Biol *314*, 112-126.

Martin, A.C., Kaschube, M., and Wieschaus, E.F. (2009). Pulsed contractions of an actin-myosin network drive apical constriction. Nature *457*, 495-499.

Martin-Belmonte, F., Gassama, A., Datta, A., Yu, W., Rescher, U., Gerke, V., and Mostov, K. (2007). PTEN-mediated apical segregation of phosphoinositides controls epithelial morphogenesis through Cdc42. Cell *128*, 383-397.

Martin-Belmonte, F., and Mostov, K. (2007). Phosphoinositides control epithelial development. Cell Cycle *6*, 1957-1961.

Martin-Belmonte, F., and Mostov, K. (2008). Regulation of cell polarity during epithelial morphogenesis. Curr Opin Cell Biol *20*, 227-234.

Martin-Belmonte, F., Yu, W., Rodriguez-Fraticelli, A.E., Ewald, A.J., Werb, Z., Alonso, M.A., and Mostov, K. (2008). Cell-polarity dynamics controls the mechanism of lumen formation in epithelial morphogenesis. Curr Biol *18*, 507-513.

Matakatsu, H., and Blair, S.S. (2004). Interactions between Fat and Dachsous and the regulation of planar cell polarity in the Drosophila wing. Development *131*, 3785-3794.

Matter, K., and Balda, M.S. (2003). Signalling to and from tight junctions. Nat Rev Mol Cell Biol *4*, 225-236.

McNeill, H. Planar cell polarity: keeping hairs straight is not so simple. Cold Spring Harb Perspect Biol *2*, a003376.

McNeill, H. (2009). Planar cell polarity and the kidney. J Am Soc Nephrol *20*, 2104-2111.

Mechler, B.M., McGinnis, W., and Gehring, W.J. (1985). Molecular cloning of lethal(2)giant larvae, a recessive oncogene of Drosophila melanogaster. EMBO J *4*, 1551-1557.

Mendelsohn, C., Lohnes, D., Decimo, D., Lufkin, T., LeMeur, M., Chambon, P., and Mark, M. (1994). Function of the retinoic acid receptors (RARs) during development (II). Multiple abnormalities at various stages of organogenesis in RAR double mutants. Development *120*, 2749-2771.

Metais, J.Y., Navarro, C., Santoni, M.J., Audebert, S., and Borg, J.P. (2005). hScrib interacts with ZO-2 at the cell-cell junctions of epithelial cells. FEBS Lett *579*, 3725-3730.

Metzger, R.J., Klein, O.D., Martin, G.R., and Krasnow, M.A. (2008). The branching programme of mouse lung development. Nature *453*, 745-750.

Meyer, T.N., Schwesinger, C., Bush, K.T., Stuart, R.O., Rose, D.W., Shah, M.M., Vaughn, D.A., Steer, D.L., and Nigam, S.K. (2004). Spatiotemporal regulation of morphogenetic molecules during in vitro branching of the isolated ureteric bud: toward a model of branching through budding in the developing kidney. Dev Biol *275*, 44-67.

Meyer, T.N., Schwesinger, C., Sampogna, R.V., Vaughn, D.A., Stuart, R.O., Steer, D.L., Bush, K.T., and Nigam, S.K. (2006). Rho kinase acts at separate steps in ureteric bud and metanephric mesenchyme morphogenesis during kidney development. Differentiation *74*, 638-647.

Michael, L., Sweeney, D.E., and Davies, J.A. (2005). A role for microfilament-based contraction in branching morphogenesis of the ureteric bud. Kidney Int *68*, 2010-2018.

Miettinen, P.J., Warburton, D., Bu, D., Zhao, J.S., Berger, J.E., Minoo, P., Koivisto, T., Allen, L., Dobbs, L., Werb, Z.*, et al.* (1997). Impaired lung branching morphogenesis in the absence of functional EGF receptor. Dev Biol *186*, 224-236.

Min, H., Danilenko, D.M., Scully, S.A., Bolon, B., Ring, B.D., Tarpley, J.E., DeRose, M., and Simonet, W.S. (1998). Fgf-10 is required for both limb and lung development and exhibits striking functional similarity to Drosophila branchless. Genes Dev *12*, 3156-3161.

Minoo, P., Hamdan, H., Bu, D., Warburton, D., Stepanik, P., and deLemos, R. (1995). TTF-1 regulates lung epithelial morphogenesis. Dev Biol *172*, 694-698.

Montcouquiol, M., Rachel, R.A., Lanford, P.J., Copeland, N.G., Jenkins, N.A., and Kelley, M.W. (2003). Identification of Vangl2 and Scrb1 as planar polarity genes in mammals. Nature *423*, 173-177.

Montcouquiol, M., Sans, N., Huss, D., Kach, J., Dickman, J.D., Forge, A., Rachel, R.A., Copeland, N.G., Jenkins, N.A., Bogani, D.*, et al.* (2006). Asymmetric localization of Vangl2 and Fz3 indicate novel mechanisms for planar cell polarity in mammals. J Neurosci *26*, 5265-5275.

Moore, K.A., Huang, S., Kong, Y., Sunday, M.E., and Ingber, D.E. (2002). Control of embryonic lung branching morphogenesis by the Rho activator, cytotoxic necrotizing factor 1. J Surg Res *104*, 95-100.

Moore, K.A., Polte, T., Huang, S., Shi, B., Alsberg, E., Sunday, M.E., and Ingber, D.E. (2005). Control of basement membrane remodeling and epithelial branching morphogenesis in embryonic lung by Rho and cytoskeletal tension. Dev Dyn *232*, 268-281.

Morrisey, E.E., and Hogan, B.L. (2010). Preparing for the first breath: genetic and cellular mechanisms in lung development. Dev Cell *18*, 8-23.

Mucenski, M.L., Nation, J.M., Thitoff, A.R., Besnard, V., Xu, Y., Wert, S.E., Harada, N., Taketo, M.M., Stahlman, M.T., and Whitsett, J.A. (2005). Beta-catenin regulates differentiation of respiratory epithelial cells in vivo. Am J Physiol Lung Cell Mol Physiol *289*, L971-979.

Munro, E.M. (2006). PAR proteins and the cytoskeleton: a marriage of equals. Curr Opin Cell Biol *18*, 86-94.

Murdoch, J.N., Doudney, K., Paternotte, C., Copp, A.J., and Stanier, P. (2001a). Severe neural tube defects in the loop-tail mouse result from mutation of Lpp1, a novel gene involved in floor plate specification. Hum Mol Genet *10*, 2593-2601.

Murdoch, J.N., Henderson, D.J., Doudney, K., Gaston-Massuet, C., Phillips, H.M., Paternotte, C., Arkell, R., Stanier, P., and Copp, A.J. (2003). Disruption of scribble (Scrb1) causes severe neural tube defects in the circletail mouse. Hum Mol Genet *12*, 87-98.

Murdoch, J.N., Rachel, R.A., Shah, S., Beermann, F., Stanier, P., Mason, C.A., and Copp, A.J. (2001b). Circletail, a new mouse mutant with severe neural tube defects: chromosomal localization and interaction with the loop-tail mutation. Genomics *78*, 55-63.

Nagasaka, K., Nakagawa, S., Yano, T., Takizawa, S., Matsumoto, Y., Tsuruga, T., Nakagawa, K., Minaguchi, T., Oda, K., Hiraike-Wada, O.*, et al.* (2006). Human homolog of Drosophila tumor suppressor Scribble negatively regulates cell-cycle progression from G1 to S phase by localizing at the basolateral membrane in epithelial cells. Cancer Sci *97*, 1217-1225.

Nakagawa, S., and Huibregtse, J.M. (2000). Human scribble (Vartul) is targeted for ubiquitin-mediated degradation by the high-risk papillomavirus E6 proteins and the E6AP ubiquitin-protein ligase. Mol Cell Biol *20*, 8244-8253.

Navarro, C., Nola, S., Audebert, S., Santoni, M.J., Arsanto, J.P., Ginestier, C., Marchetto, S., Jacquemier, J., Isnardon, D., Le Bivic, A.*, et al.* (2005). Junctional recruitment of mammalian Scribble relies on E-cadherin engagement. Oncogene *24*, 4330-4339.

Nguyen, D.X., Bos, P.D., and Massague, J. (2009). Metastasis: from dissemination to organ-specific colonization. Nat Rev Cancer *9*, 274-284.

Nguyen, D.X., and Massague, J. (2007). Genetic determinants of cancer metastasis. Nat Rev Genet *8*, 341-352.

Nishimura, T., and Takeichi, M. (2008). Shroom3-mediated recruitment of Rho kinases to the apical cell junctions regulates epithelial and neuroepithelial planar remodeling. Development *135*, 1493-1502.

Nishimura, T., and Takeichi, M. (2009). Remodeling of the adherens junctions during morphogenesis. Curr Top Dev Biol *89*, 33-54.

O'Brien, L.E., Tang, K., Kats, E.S., Schutz-Geschwender, A., Lipschutz, J.H., and Mostov, K.E. (2004). ERK and MMPs sequentially regulate distinct stages of epithelial tubule development. Dev Cell *7*, 21-32.

Okubo, T., and Hogan, B.L. (2004). Hyperactive Wnt signaling changes the developmental potential of embryonic lung endoderm. J Biol *3*, 11.

Olson, M.F. (2008). Applications for ROCK kinase inhibition. Curr Opin Cell Biol *20*, 242-248.

Otto, E.A., Schermer, B., Obara, T., O'Toole, J.F., Hiller, K.S., Mueller, A.M., Ruf, R.G., Hoefele, J., Beekmann, F., Landau, D.*, et al.* (2003). Mutations in INVS encoding inversin cause nephronophthisis type 2, linking renal cystic disease to the function of primary cilia and left-right axis determination. Nat Genet *34*, 413-420.

Pagliarini, R.A., and Xu, T. (2003). A genetic screen in Drosophila for metastatic behavior. Science *302*, 1227-1231.

Park, T.J., Haigo, S.L., and Wallingford, J.B. (2006). Ciliogenesis defects in embryos lacking inturned or fuzzy function are associated with failure of planar cell polarity and Hedgehog signaling. Nat Genet *38*, 303-311.

Patrakka, J., and Tryggvason, K. Molecular make-up of the glomerular filtration barrier. Biochem Biophys Res Commun *396*, 164-169.

Patrakka, J., and Tryggvason, K. (2009). New insights into the role of podocytes in proteinuria. Nat Rev Nephrol *5*, 463-468.

Patrakka, J., and Tryggvason, K. (2010). Molecular make-up of the glomerular filtration barrier. Biochem Biophys Res Commun *396*, 164-169.

Paudyal, A., Damrau, C., Patterson, V.L., Ermakov, A., Formstone, C., Lalanne, Z., Wells, S., Lu, X., Norris, D.P., Dean, C.H.*, et al.* (2010). The novel mouse mutant, chuzhoi, has disruption of Ptk7 protein and exhibits defects in neural tube, heart and lung development and abnormal planar cell polarity in the ear. BMC Dev Biol *10*, 87.

Pepicelli, C.V., Lewis, P.M., and McMahon, A.P. (1998). Sonic hedgehog regulates branching morphogenesis in the mammalian lung. Curr Biol *8*, 1083-1086.

Petak, F., Habre, W., Donati, Y.R., Hantos, Z., and Barazzone-Argiroffo, C. (2001). Hyperoxia-induced changes in mouse lung mechanics: forced oscillations vs. barometric plethysmography. J Appl Physiol *90*, 2221-2230.

Phillips, H.M., Rhee, H.J., Murdoch, J.N., Hildreth, V., Peat, J.D., Anderson, R.H., Copp, A.J., Chaudhry, B., and Henderson, D.J. (2007a). Disruption of planar cell polarity signaling results in congenital heart defects and cardiomyopathy attributable to early cardiomyocyte disorganization. Circ Res *101*, 137-145.

Phillips, H.M., Rhee, H.J., Murdoch, J.N., Hildreth, V., Peat, J.D., Anderson, R.H., Copp, A.J., Chaudhry, B., and Henderson, D.J. (2007b). Disruption of Planar Cell Polarity Signaling Results in Congenital Heart Defects and Cardiomyopathy Attributable to Early Cardiomyocyte Disorganization. Circ Res.

Pollack, A.L., Runyan, R.B., and Mostov, K.E. (1998). Morphogenetic mechanisms of epithelial tubulogenesis: MDCK cell polarity is transiently rearranged without loss of cell-cell contact during scatter factor/hepatocyte growth factor-induced tubulogenesis. Dev Biol *204*, 64-79.

Ponzetto, C., Bardelli, A., Zhen, Z., Maina, F., dalla Zonca, P., Giordano, S., Graziani, A., Panayotou, G., and Comoglio, P.M. (1994). A multifunctional docking site mediates signaling and transformation by the hepatocyte growth factor/scatter factor receptor family. Cell *77*, 261-271.

Qian, D., Jones, C., Rzadzinska, A., Mark, S., Zhang, X., Steel, K.P., Dai, X., and Chen, P. (2007). Wnt5a functions in planar cell polarity regulation in mice. Dev Biol *306*, 121-133.

Qin, Y., Capaldo, C., Gumbiner, B.M., and Macara, I.G. (2005). The mammalian Scribble polarity protein regulates epithelial cell adhesion and migration through E-cadherin. J Cell Biol *171*, 1061-1071.

Quaggin, S.E., and Kreidberg, J.A. (2008). Development of the renal glomerulus: good neighbors and good fences. Development *135*, 609-620.

Quaggin, S.E., Schwartz, L., Cui, S., Igarashi, P., Deimling, J., Post, M., and Rossant, J. (1999). The basic-helix-loop-helix protein pod1 is critically important for kidney and lung organogenesis. Development *126*, 5771-5783.

Rachel, R.A., Murdoch, J.N., Beermann, F., Copp, A.J., and Mason, C.A. (2000). Retinal axon misrouting at the optic chiasm in mice with neural tube closure defects. Genesis *27*, 32-47.

Rawls, A.S., Guinto, J.B., and Wolff, T. (2002). The cadherins fat and dachsous regulate dorsal/ventral signaling in the Drosophila eye. Curr Biol *12*, 1021-1026.

Rebustini, I.T., Patel, V.N., Stewart, J.S., Layvey, A., Georges-Labouesse, E., Miner, J.H., and Hoffman, M.P. (2007). Laminin alpha5 is necessary for submandibular gland epithelial morphogenesis and influences FGFR expression through beta1 integrin signaling. Dev Biol *308*, 15-29.

Robson, W.L., Leung, A.K., and Sinclair, O. (1991). Congenital urinary anomalies associated with neural tube defects. Pediatr Nephrol *5*, 369.

Rodriguez-Diaz, A., Toyama, Y., Abravanel, D.L., Wiemann, J.M., Wells, A.R., Tulu, U.S., Edwards, G.S., and Kiehart, D.P. (2008). Actomyosin purse strings: renewable resources that make morphogenesis robust and resilient. HFSP J *2*, 220-237.

Rosario, M., and Birchmeier, W. (2004). Making tubes: step by step. Dev Cell *7*, 3-5.

Ross, A.J., May-Simera, H., Eichers, E.R., Kai, M., Hill, J., Jagger, D.J., Leitch, C.C., Chapple, J.P., Munro, P.M., Fisher, S*., et al.* (2005). Disruption of Bardet-Biedl syndrome ciliary proteins perturbs planar cell polarity in vertebrates. Nat Genet *37*, 1135-1140.

Saburi, S., Hester, I., Fischer, E., Pontoglio, M., Eremina, V., Gessler, M., Quaggin, S.E., Harrison, R., Mount, R., and McNeill, H. (2008). Loss of Fat4 disrupts PCP signaling and oriented cell division and leads to cystic kidney disease. Nat Genet *40*, 1010-1015.

Sainio, K., Suvanto, P., Davies, J., Wartiovaara, J., Wartiovaara, K., Saarma, M., Arumae, U., Meng, X., Lindahl, M., Pachnis, V*., et al.* (1997). Glial-cell-line-derived neurotrophic factor is required for bud initiation from ureteric epithelium. Development *124*, 4077-4087.

Sakai, T., Larsen, M., and Yamada, K.M. (2003). Fibronectin requirement in branching morphogenesis. Nature *423*, 876-881.

Sakurai, H., Bush, K.T., and Nigam, S.K. (2001). Identification of pleiotrophin as a mesenchymal factor involved in ureteric bud branching morphogenesis. Development *128*, 3283-3293.

Sandquist, J.C., Swenson, K.I., Demali, K.A., Burridge, K., and Means, A.R. (2006). Rho kinase differentially regulates phosphorylation of nonmuscle myosin II isoforms A and B during cell rounding and migration. J Biol Chem *281*, 35873-35883.

Santoni, M.J., Pontarotti, P., Birnbaum, D., and Borg, J.P. (2002). The LAP family: a phylogenetic point of view. Trends Genet *18*, 494-497.

Sawyer, J.M., Harrell, J.R., Shemer, G., Sullivan-Brown, J., Roh-Johnson, M., and Goldstein, B. (2010). Apical constriction: a cell shape change that can drive morphogenesis. Dev Biol *341*, 5-19.

Saxen, L., and Sariola, H. (1987). Early organogenesis of the kidney. Pediatr Nephrol *1*, 385-392.

Schlessinger, K., Hall, A., and Tolwinski, N. (2009). Wnt signaling pathways meet Rho GTPases. Genes Dev *23*, 265-277.

Schoenwolf, G.C. (1984). Histological and ultrastructural studies of secondary neurulation in mouse embryos. Am J Anat *169*, 361-376.

Schoenwolf, G.C., and Delongo, J. (1980). Ultrastructure of secondary neurulation in the chick embryo. Am J Anat *158*, 43-63.

Seifert, J.R., and Mlodzik, M. (2007). Frizzled/PCP signalling: a conserved mechanism regulating cell polarity and directed motility. Nat Rev Genet *8*, 126-138.

Sekine, K., Ohuchi, H., Fujiwara, M., Yamasaki, M., Yoshizawa, T., Sato, T., Yagishita, N., Matsui, D., Koga, Y., Itoh, N.*, et al.* (1999). Fgf10 is essential for limb and lung formation. Nat Genet *21*, 138-141.

Shah, M.M., Sampogna, R.V., Sakurai, H., Bush, K.T., and Nigam, S.K. (2004). Branching morphogenesis and kidney disease. Development *131*, 1449-1462.

Shakya, R., Watanabe, T., and Costantini, F. (2005). The role of GDNF/Ret signaling in ureteric bud cell fate and branching morphogenesis. Dev Cell *8*, 65-74.

Shalaby, K.H., Gold, L.G., Schuessler, T.F., Martin, J.G., and Robichaud, A. (2010). Combined forced oscillation and forced expiration measurements in mice for the assessment of airway hyperresponsiveness. Respir Res *11*, 82.

Shannon, J.M. (1994). Induction of alveolar type II cell differentiation in fetal tracheal epithelium by grafted distal lung mesenchyme. Dev Biol *166*, 600-614.

Sharafkhaneh, A., Hanania, N.A., and Kim, V. (2008). Pathogenesis of emphysema: from the bench to the bedside. Proc Am Thorac Soc *5*, 475-477.

Shi, W., Chen, F., and Cardoso, W.V. (2009). Mechanisms of lung development: contribution to adult lung disease and relevance to chronic obstructive pulmonary disease. Proc Am Thorac Soc *6*, 558-563.

Shima, Y., Copeland, N.G., Gilbert, D.J., Jenkins, N.A., Chisaka, O., Takeichi, M., and Uemura, T. (2002). Differential expression of the seven-pass transmembrane cadherin genes Celsr1-3 and distribution of the Celsr2 protein during mouse development. Dev Dyn *223*, 321-332.

Shima, Y., Kawaguchi, S.Y., Kosaka, K., Nakayama, M., Hoshino, M., Nabeshima, Y., Hirano, T., and Uemura, T. (2007). Opposing roles in neurite growth control by two seven-pass transmembrane cadherins. Nat Neurosci *10*, 963-969.

Shima, Y., Kengaku, M., Hirano, T., Takeichi, M., and Uemura, T. (2004). Regulation of dendritic maintenance and growth by a mammalian 7-pass transmembrane cadherin. Dev Cell *7*, 205-216.

Shu, W., Guttentag, S., Wang, Z., Andl, T., Ballard, P., Lu, M.M., Piccolo, S., Birchmeier, W., Whitsett, J.A., Millar, S.E.*, et al.* (2005). Wnt/beta-catenin signaling acts upstream

of N-myc, BMP4, and FGF signaling to regulate proximal-distal patterning in the lung. Dev Biol *283*, 226-239.

Siafakas, N.M., and Tzortzaki, E.G. (2002). Few smokers develop COPD. Why? Respir Med *96*, 615-624.

Simon, M.A. (2004). Planar cell polarity in the Drosophila eye is directed by graded Four-jointed and Dachsous expression. Development *131*, 6175-6184.

Simons, M., Gloy, J., Ganner, A., Bullerkotte, A., Bashkurov, M., Kronig, C., Schermer, B., Benzing, T., Cabello, O.A., Jenny, A.*, et al.* (2005). Inversin, the gene product mutated in nephronophthisis type II, functions as a molecular switch between Wnt signaling pathways. Nat Genet *37*, 537-543.

Simons, M., and Mlodzik, M. (2008). Planar cell polarity signaling: from fly development to human disease. Annu Rev Genet *42*, 517-540.

Srinivas, S., Goldberg, M.R., Watanabe, T., D'Agati, V., al-Awqati, Q., and Costantini, F. (1999). Expression of green fluorescent protein in the ureteric bud of transgenic mice: a new tool for the analysis of ureteric bud morphogenesis. Dev Genet *24*, 241-251.

Steed, E., Balda, M.S., and Matter, K. (2010). Dynamics and functions of tight junctions. Trends Cell Biol *20*, 142-149.

Steed, E., Rodrigues, N.T., Balda, M.S., and Matter, K. (2009). Identification of MarvelD3 as a tight junction-associated transmembrane protein of the occludin family. BMC Cell Biol *10*, 95.

Strader, C.D., Fong, T.M., Graziano, M.P., and Tota, M.R. (1995). The family of G-protein-coupled receptors. FASEB J *9*, 745-754.

Strand, D., Raska, I., and Mechler, B.M. (1994). The Drosophila lethal(2)giant larvae tumor suppressor protein is a component of the cytoskeleton. J Cell Biol *127*, 1345-1360.

Strutt, D.I. (2001). Asymmetric localization of frizzled and the establishment of cell polarity in the Drosophila wing. Mol Cell *7*, 367-375.

Strutt, D.I., Weber, U., and Mlodzik, M. (1997). The role of RhoA in tissue polarity and Frizzled signalling. Nature *387*, 292-295.

Strutt, H., and Strutt, D. (2002). Nonautonomous planar polarity patterning in Drosophila: dishevelled-independent functions of frizzled. Dev Cell *3*, 851-863.

Tada, M., and Smith, J.C. (2000). Xwnt11 is a target of Xenopus Brachyury: regulation of gastrulation movements via Dishevelled, but not through the canonical Wnt pathway. Development *127*, 2227-2238.

Tanentzapf, G., and Tepass, U. (2003). Interactions between the crumbs, lethal giant larvae and bazooka pathways in epithelial polarization. Nat Cell Biol *5*, 46-52.

Taylor, J., Abramova, N., Charlton, J., and Adler, P.N. (1998). Van Gogh: a new Drosophila tissue polarity gene. Genetics *150*, 199-210.

Tebar, M., Destree, O., de Vree, W.J., and Ten Have-Opbroek, A.A. (2001). Expression of Tcf/Lef and sFrp and localization of beta-catenin in the developing mouse lung. Mech Dev *109*, 437-440.

Thebaud, B., and Abman, S.H. (2007). Bronchopulmonary dysplasia: where have all the vessels gone? Roles of angiogenic growth factors in chronic lung disease. Am J Respir Crit Care Med *175*, 978-985.

Timpl, R., Tisi, D., Talts, J.F., Andac, Z., Sasaki, T., and Hohenester, E. (2000). Structure and function of laminin LG modules. Matrix Biol *19*, 309-317.

Tissir, F., Bar, I., Goffinet, A.M., and Lambert De Rouvroit, C. (2002a). Expression of the ankyrin repeat domain 6 gene (Ankrd6) during mouse brain development. Dev Dyn *224*, 465-469.

Tissir, F., De-Backer, O., Goffinet, A.M., and Lambert de Rouvroit, C. (2002b). Developmental expression profiles of Celsr (Flamingo) genes in the mouse. Mech Dev *112*, 157-160.

Tissir, F., and Goffinet, A.M. (2006). Expression of planar cell polarity genes during development of the mouse CNS. Eur J Neurosci *23*, 597-607.

Tomioka, S., Bates, J.H., and Irvin, C.G. (2002). Airway and tissue mechanics in a murine model of asthma: alveolar capsule vs. forced oscillations. J Appl Physiol *93*, 263-270.

Torban, E., Patenaude, A.M., Leclerc, S., Rakowiecki, S., Gauthier, S., Andelfinger, G., Epstein, D.J., and Gros, P. (2008). Genetic interaction between members of the Vangl family causes neural tube defects in mice. Proc Natl Acad Sci U S A *105*, 3449-3454.

Torban, E., Wang, H.J., Groulx, N., and Gros, P. (2004). Independent mutations in mouse Vangl2 that cause neural tube defects in looptail mice impair interaction with members of the Dishevelled family. J Biol Chem *279*, 52703-52713.

Torban, E., Wang, H.J., Patenaude, A.M., Riccomagno, M., Daniels, E., Epstein, D., and Gros, P. (2007). Tissue, cellular and sub-cellular localization of the Vangl2 protein during embryonic development: effect of the Lp mutation. Gene Expr Patterns *7*, 346-354.

Tree, D.R., Shulman, J.M., Rousset, R., Scott, M.P., Gubb, D., and Axelrod, J.D. (2002). Prickle mediates feedback amplification to generate asymmetric planar cell polarity signaling. Cell *109*, 371-381.

Tufro, A., Teichman, J., Woda, C., and Villegas, G. (2008). Semaphorin3a inhibits ureteric bud branching morphogenesis. Mech Dev *125*, 558-568.

Uehata, M., Ishizaki, T., Satoh, H., Ono, T., Kawahara, T., Morishita, T., Tamakawa, H., Yamagami, K., Inui, J., Maekawa, M., *et al.* (1997). Calcium sensitization of smooth

muscle mediated by a Rho-associated protein kinase in hypertension. Nature *389*, 990-994.

Usui, T., Shima, Y., Shimada, Y., Hirano, S., Burgess, R.W., Schwarz, T.L., Takeichi, M., and Uemura, T. (1999). Flamingo, a seven-pass transmembrane cadherin, regulates planar cell polarity under the control of Frizzled. Cell *98*, 585-595.

Vandenberg, A.L., and Sassoon, D.A. (2009). Non-canonical Wnt signaling regulates cell polarity in female reproductive tract development via van gogh-like 2. Development *136*, 1559-1570.

Wallingford, J.B., Rowning, B.A., Vogeli, K.M., Rothbacher, U., Fraser, S.E., and Harland, R.M. (2000). Dishevelled controls cell polarity during Xenopus gastrulation. Nature *405*, 81-85.

Wang, J., Hamblet, N.S., Mark, S., Dickinson, M.E., Brinkman, B.C., Segil, N., Fraser, S.E., Chen, P., Wallingford, J.B., and Wynshaw-Boris, A. (2006). Dishevelled genes mediate a conserved mammalian PCP pathway to regulate convergent extension during neurulation. Development *133*, 1767-1778.

Wang, J., Mark, S., Zhang, X., Qian, D., Yoo, S.J., Radde-Gallwitz, K., Zhang, Y., Lin, X., Collazo, A., Wynshaw-Boris, A*., et al.* (2005). Regulation of polarized extension and planar cell polarity in the cochlea by the vertebrate PCP pathway. Nat Genet *37*, 980-985.

Wang, Y., and Nathans, J. (2007). Tissue/planar cell polarity in vertebrates: new insights and new questions. Development *134*, 647-658.

Warburton, D., Gauldie, J., Bellusci, S., and Shi, W. (2006). Lung development and susceptibility to chronic obstructive pulmonary disease. Proc Am Thorac Soc *3*, 668-672.

Warburton, D., Schwarz, M., Tefft, D., Flores-Delgado, G., Anderson, K.D., and Cardoso, W.V. (2000). The molecular basis of lung morphogenesis. Mech Dev *92*, 55-81.

Watanabe, D., Saijoh, Y., Nonaka, S., Sasaki, G., Ikawa, Y., Yokoyama, T., and Hamada, H. (2003). The left-right determinant Inversin is a component of node monocilia and other 9+0 cilia. Development *130*, 1725-1734.

Watanabe, T., and Costantini, F. (2004). Real-time analysis of ureteric bud branching morphogenesis in vitro. Dev Biol *271*, 98-108.

Wei, L., Roberts, W., Wang, L., Yamada, M., Zhang, S., Zhao, Z., Rivkees, S.A., Schwartz, R.J., and Imanaka-Yoshida, K. (2001). Rho kinases play an obligatory role in vertebrate embryonic organogenesis. Development *128*, 2953-2962.

Weidenfeld, J., Shu, W., Zhang, L., Millar, S.E., and Morrisey, E.E. (2002). The WNT7b promoter is regulated by TTF-1, GATA6, and Foxa2 in lung epithelium. J Biol Chem *277*, 21061-21070.

Weidner, K.M., Sachs, M., and Birchmeier, W. (1993). The Met receptor tyrosine kinase transduces motility, proliferation, and morphogenic signals of scatter factor/hepatocyte growth factor in epithelial cells. J Cell Biol *121*, 145-154.

Welham, S.J., Riley, P.R., Wade, A., Hubank, M., and Woolf, A.S. (2005). Maternal diet programs embryonic kidney gene expression. Physiol Genomics *22*, 48-56.

Welham, S.J., Wade, A., and Woolf, A.S. (2002). Protein restriction in pregnancy is associated with increased apoptosis of mesenchymal cells at the start of rat metanephrogenesis. Kidney Int *61*, 1231-1242.

Wert, S.E., Yoshida, M., LeVine, A.M., Ikegami, M., Jones, T., Ross, G.F., Fisher, J.H., Korfhagen, T.R., and Whitsett, J.A. (2000). Increased metalloproteinase activity, oxidant production, and emphysema in surfactant protein D gene-inactivated mice. Proc Natl Acad Sci U S A *97*, 5972-5977.

Whitsett, J.A., Wert, S.E., and Trapnell, B.C. (2004). Genetic disorders influencing lung formation and function at birth. Hum Mol Genet *13 Spec No 2*, R207-215.

Winberg, M.L., Tamagnone, L., Bai, J., Comoglio, P.M., Montell, D., and Goodman, C.S. (2001). The transmembrane protein Off-track associates with Plexins and functions downstream of Semaphorin signaling during axon guidance. Neuron *32*, 53-62.

Witzel, S., Zimyanin, V., Carreira-Barbosa, F., Tada, M., and Heisenberg, C.P. (2006). Wnt11 controls cell contact persistence by local accumulation of Frizzled 7 at the plasma membrane. J Cell Biol *175*, 791-802.

Woods, D.F., and Bryant, P.J. (1989). Molecular cloning of the lethal(1)discs large-1 oncogene of Drosophila. Dev Biol *134*, 222-235.

Woods, D.F., and Bryant, P.J. (1991). The discs-large tumor suppressor gene of Drosophila encodes a guanylate kinase homolog localized at septate junctions. Cell *66*, 451-464.

Woolf, A.S., Kolatsi-Joannou, M., Hardman, P., Andermarcher, E., Moorby, C., Fine, L.G., Jat, P.S., Noble, M.D., and Gherardi, E. (1995). Roles of hepatocyte growth factor/scatter factor and the met receptor in the early development of the metanephros. J Cell Biol *128*, 171-184.

Wu, J., and Mlodzik, M. (2008). The frizzled extracellular domain is a ligand for Van Gogh/Stbm during nonautonomous planar cell polarity signaling. Dev Cell *15*, 462-469.

Wu, V.M., Schulte, J., Hirschi, A., Tepass, U., and Beitel, G.J. (2004). Sinuous is a Drosophila claudin required for septate junction organization and epithelial tube size control. J Cell Biol *164*, 313-323.

Yagi, T., and Takeichi, M. (2000). Cadherin superfamily genes: functions, genomic organization, and neurologic diversity. Genes Dev *14*, 1169-1180.

Yamamoto, S., Nishimura, O., Misaki, K., Nishita, M., Minami, Y., Yonemura, S., Tarui, H., and Sasaki, H. (2008). Cthrc1 selectively activates the planar cell polarity pathway of Wnt signaling by stabilizing the Wnt-receptor complex. Dev Cell *15*, 23-36.

Yamanaka, H., Moriguchi, T., Masuyama, N., Kusakabe, M., Hanafusa, H., Takada, R., Takada, S., and Nishida, E. (2002). JNK functions in the non-canonical Wnt pathway to regulate convergent extension movements in vertebrates. EMBO Rep *3*, 69-75.

Yang, C.H., Axelrod, J.D., and Simon, M.A. (2002). Regulation of Frizzled by fat-like cadherins during planar polarity signaling in the Drosophila compound eye. Cell *108*, 675-688.

Yates, L.L., Papakrivopoulou, J., Long, D.A., Goggolidou, P., Connolly, J.O., Woolf, A.S., and Dean, C.H. (2010a). The planar cell polarity gene Vangl2 is required for mammalian kidney branching morphogenesis and glomerular maturation. Hum Mol Genet.

Yates, L.L., Schnatwinkel, C., Murdoch, J.N., Bogani, D., Formstone, C.J., Townsend, S., Greenfield, A., Niswander, L.A., and Dean, C.H. (2010b). The PCP genes Celsr1 and Vangl2 are required for normal lung branching morphogenesis. Hum Mol Genet *19*, 2251-2267.

Ybot-Gonzalez, P., Savery, D., Gerrelli, D., Signore, M., Mitchell, C.E., Faux, C.H., Greene, N.D., and Copp, A.J. (2007). Convergent extension, planar-cell-polarity signalling and initiation of mouse neural tube closure. Development *134*, 789-799.

Yin, H.L., and Janmey, P.A. (2003). Phosphoinositide regulation of the actin cytoskeleton. Annu Rev Physiol *65*, 761-789.

Yu, J., Carroll, T.J., Rajagopal, J., Kobayashi, A., Ren, Q., and McMahon, A.P. (2009). A Wnt7b-dependent pathway regulates the orientation of epithelial cell division and establishes the cortico-medullary axis of the mammalian kidney. Development *136*, 161-171.

Yuan, H.T., Suri, C., Landon, D.N., Yancopoulos, G.D., and Woolf, A.S. (2000). Angiopoietin-2 is a site-specific factor in differentiation of mouse renal vasculature. J Am Soc Nephrol *11*, 1055-1066.

Zallen, J.A. (2007). Planar polarity and tissue morphogenesis. Cell *129*, 1051-1063.

Zarbalis, K., May, S.R., Shen, Y., Ekker, M., Rubenstein, J.L., and Peterson, A.S. (2004). A focused and efficient genetic screening strategy in the mouse: identification of mutations that disrupt cortical development. PLoS Biol *2*, E219.

Zeidler, M.P., Perrimon, N., and Strutt, D.I. (1999). The four-jointed gene is required in the Drosophila eye for ommatidial polarity specification. Curr Biol *9*, 1363-1372.

Zeitler, J., Hsu, C.P., Dionne, H., and Bilder, D. (2004). Domains controlling cell polarity and proliferation in the Drosophila tumor suppressor Scribble. J Cell Biol *167*, 1137-1146.

Zhan, L., Rosenberg, A., Bergami, K.C., Yu, M., Xuan, Z., Jaffe, A.B., Allred, C., and Muthuswamy, S.K. (2008). Deregulation of scribble promotes mammary tumorigenesis and reveals a role for cell polarity in carcinoma. Cell *135*, 865-878.

Zhang, Z., Quinlan, J., Hoy, W., Hughson, M.D., Lemire, M., Hudson, T., Hueber, P.A., Benjamin, A., Roy, A., Pascuet, E.*, et al.* (2008). A common RET variant is associated with reduced newborn kidney size and function. J Am Soc Nephrol *19*, 2027-2034.

Zhou, L., Tissir, F., and Goffinet, A.M. (2007a). The atypical cadherin Celsr3 regulates the development of the axonal blueprint. Novartis Found Symp *288*, 130-134; discussion 134-140, 276-181.

Zhou, W., Lin, L., Majumdar, A., Li, X., Zhang, X., Liu, W., Etheridge, L., Shi, Y., Martin, J., Van de Ven, W.*, et al.* (2007b). Modulation of morphogenesis by noncanonical Wnt signaling requires ATF/CREB family-mediated transcriptional activation of TGFbeta2. Nat Genet *39*, 1225-1234.

8 Appendix; Publications arising from this work

1. **Yates LL**, Papakrivopoulou J, Long DA, Goggolidou P, Connolly JO, Woolf AS, Dean CH. The planar cell polarity gene *Vangl2* is required for mammalian kidney branching morphogenesis and glomerular maturation. Hum.Mol.Genet. In Press.

2. **Yates LL**, Schnatwinkel C, Murdoch JN, Bogani D, Townsend S, Greenfield A, Niswander LA, Dean CH. Celsr1 and Vangl2 are required for branching morphogenesis. (2010) Hum. Mol. Genet. 19(11):2251-67.